Investigating the recombinational response to replication fork barriers in Fission Yeast



Thesis submitted in partial fulfillment of the requirements for the degree of Doctor of Philosophy in Biochemistry to the Medical Science Division

Manisha Jalan

Department of Biochemistry
St. Peter's College
University of Oxford

Trinity Term, 2016

Declaration

I hereby declare that this thesis entitled “Investigating the recombinational response to replication fork barriers in Fission Yeast” has been originally carried out by me under the supervision of Professor Matthew Whitby, except where otherwise indicated (marked by an asterisk and described in Table 8-9). This work has not formed the basis for award of any degree or diploma previously. The particulars given in the thesis are true to the best of my knowledge.

Manisha Jalan

Dept. of Biochemistry
St. Peter’s College
University of Oxford

"If you want to shine like the sun....
first burn like the sun."

-APJ Abdul Kalam

Acknowledgements

First and foremost, I would like to thank my supervisor, Prof. Matthew Whitby for making this thesis a reality. He has always been very patient and encouraging towards all spheres of this DPhil, willing to help in any possible way.

I would also like to express my gratitude to each and every member of the Whitby Lab, specifically Dr. Alexander Lorenz, Dr. Carl Morrow, Dr. Fikret Osman, Dr. Io-Nam Wong, Andrew Fower, Claire Bryer, Jacqueline Neo, Michael Nguyen, Nadiya Ishnazarova and Sanjeeta Tamang for all their assistance, encouragement and for all the fun we have had in the last four years. They have made working towards my goals a lot more pleasant and enjoyable.

I would like to thank Prof. Ronald Chalmers for the MarBI plasmids, Micron for their help with the microscopes and the Media Glassware Sterilization Laboratory for everyday support with reagents and apparatus.

A special thank you to my parents and family members for always extending their unconditional love and support and never letting me give up. They always believed in me even when I have doubts on myself and have been my pillar of strength.

A big thank you to my friends; my lifeline. They have made these four long years pass by like a flash of lightening, ensuring I have never had to face a dull moment in my Oxford life.

Last but not the least, a special mention for all my teachers who have given me their time and guidance, providing me with the foundation to stand where I am today.

Abstract

Timely completion of DNA replication in each cell cycle is crucial for maintaining genomic integrity. This is often challenged by the presence of various replication fork barriers (RFBs). On collision with a RFB, the fate of the replication fork remains uncertain. In some cases, the integrity of the fork is maintained until the barrier is removed or the fork is rescued by merging with the incoming fork. However, fork stalling can cause dissociation of all of the associated replication proteins (fork collapse). If this occurs, the cell's recombination machinery can intervene to help restart replication in a process called recombination-dependent replication (RDR).

Programmed protein-DNA barriers like the Replication Terminator Sequence-1 (*RTS1)* have been used to demonstrate that replication fork blockage can induce recombination. However, it remains unclear how efficiently this recombination gives rise to replication restart and whether the restarted replication fork exhibits the same fidelity as an origin-derived fork. It is also unknown whether accidental replication barriers induce recombination in the same manner as programmed barriers.

In this study, I introduce recombination reporters at various sites downstream of *RTS1* to obtain information on both the fidelity and efficiency of replication restart. I find that unlike break induced replication (BIR), the restarted fork gives rise to hyper-recombination at least 75 kb downstream of the barrier. Surprisingly, fork convergence, rather than inducing recombination, acts to prevent or curtail genetic instability associated with RDR. I also investigate a number of genetic factors that have a role in either preventing or promoting genome instability associated with the progression of the restarted fork.

To compare *RTS1* with an accidental protein-DNA barrier, a novel site-specific barrier system (called MarBI) was established based on the human mariner transposase, *Hsmar1*, binding to its transposon end. Replication fork blockage at MarBI strongly induces recombination, more so than at *RTS1*. This appears to be a general feature of accidental barriers as introduction of the *E. coli* TusB-*TerB* site-specific barrier in *S. pombe* gives rise to a similar effect. Here, I compare and contrast accidental barriers with programmed barriers. I observe that there is very little replication restart, if any, at MarBI measured by direct repeat recombination downstream. This points to the fact that accidental barriers do not trigger fork collapse in the same way as programmed RFBs and that the increased recombination that they cause may be a consequence of the inability of replication forks to terminate correctly, owing to the bi-directional nature of the barrier. Several genetic factors are assessed for their impact on MarBI-induced recombination, which further highlights both similarities and differences with *RTS1*-induced recombination.

Abbreviations

AO	*RTS1* active orientation
ARS	autonomously replicating sequences
ATP	adenosine triphophate
BIR	break-induced replication
bp	base pair
BSA	bovine serum albumin
CFP	cyan fluorescent protein
Chr	Chromosome
CO	cross-over
CPT	camptothecin
D-loop	displacement loop
DDR	DNA damage response
DDT	DNA damage tolerance
dHJ	double Holliday junction
DMSO	Dimethyl sulphoxide
DNA	deoxyribonucleic acid
dNTP	deoxyribonucleotide triphosphate
DSB	double-strand break
DSBR	double-strand break repair
DTT	dithiothreitol
ECL	enhanced chemiluminescence
EDTA	ethylenediaminetetraacetic acid
EMMG	Edinburgh minimal media glutamate
EMSA	electrophoretic mobility shift assay
FACS	Fluorescence Associated Cell Sorting
FPC	fork protection complex

GCRs	gross chromosomal rearrangements
GFP	green fluorescent protein
HJ	Holliday junction
HR	homologous recombination
HRP	horseradish peroxidase
HU	hydroxyurea
ICL	inter-strand crosslink
IO	*RTS1* inactive orientation
kb	kilo base pair
LA	low adenine
LB	Luria-Bertani
Mar	Mariner protein
MarBl	Mariner Block
MCM	minichromosome maintenance
MEA	malt extract agar
MMS	methyl methanesulfonate
NCO	non cross-over
NER	nucleotide excision repair
NHEJ	non-homologous end joining
NLS	nuclear localisation signal
nmt	no message in thiamine
PCNA	proliferating cell nuclear antigen
PCR	polymerase chain reaction
Pol	DNA Polymerase
PPR	post-replicative repair
Pu-Seq	polymerase usage sequencing
rDNA	ribosomal DNA
RDR	recombination-dependent repair

RFB	replication fork barrier
RFC	replication factor C
RLC	RFC-like complex
RPM	revolutions per minute
RTS1	Replication Termination Sequence 1
SDS-PAGE	sodium dodecyl sulphate polyacrylamide gel electrophoresis
SDSA	synthesis-dependent strand annealing
SSA	single-strand annealing
SSC	saline-sodium citrate
ssDNA	single-stranded deoxyribonucleic acid
TBE	Tris-borate EDTA
TBS	Tris-buffered saline
TLS	translesion synthesis
TO1	Transposon End Orientation 1
TO2	Transposon End Orientation 2
TIR	terminal inverted repeats
tRNA	transfer ribonucleic acid
UV	ultra violet
YE	yeast extract
YES	yeast extract with supplements
YFP	yellow fluorescent protein
1D gel	one dimensional gel
2D gel	two dimensional gel

Table of Contents

Declaration ii

Acknowledgements iv

Abstract v

Abbreviations vii

Table of Contents x

Chapter 1 Introduction 1

1.1 Fundamentals of DNA replication 3

1.1.1 Replication Origins and Initiation 3

1.1.2 The Replisome 4

1.1.3 Replication Termination 6

1.2 Impediments to DNA replication 7

1.2.1 DNA lesions and strand discontinuities 8

1.2.2 Unusual DNA structures and fragile sites 9

1.2.3 Transcription-replication conflict 9

1.2.4 Programmed barriers 10

1.2.5 The cellular defence against RFBs 13

1.3 The key players in Homologous Recombination 13

1.3.1 Pre-synapsis: resection 17

1.3.2 Pre-synapsis to synapsis: Rad51 nucleoprotein filament formation and strand invasion 18

1.3.3 Post-synapsis: resolution of recombination intermediates 19

1.4 Cellular response to replication fork perturbation and the role of HR in aiding completion of DNA replication 21

1.4.1 Activation of damage tolerance pathways at single strand lesions 22

1.4.2 Stabilization of stalled forks: the role of HR proteins and the fork protection complex 27

1.4.3 Pushing past the barrier: the role of accessory DNA helicases 29

1.4.4 Deliberate and accidental breakage of replication forks and BIR 29

1.4.5 Replication restart without DNA breakage 33

1.5 Aims of the study 35

Chapter 2 Materials and Methods 37

2.1 Media 38

2.1.1 *Escherichia coli* media 38
2.1.2 *Schizosaccharomyces pombe* media 38
2.2 *S. pombe* strain construction 39
2.2.1 *S. pombe* transformation 39
2.2.2 *S. pombe* crosses 40
2.2.3 *S. pombe* colony PCR 40
2.3 Molecular and cell biology techniques 41
2.3.1 Cloning and sub-cloning DNA 41
2.3.2 *E. coli* transformation 41
2.3.3 Alkaline lysis for protein extraction from *S. pombe* 42
2.3.4 SDS-PAGE and Western Blotting 42
2.3.5 Microscopy 43
2.4 DNA analysis 44
2.4.1 *S. pombe* genomic DNA extraction 44
2.4.2 Genomic DNA extraction embedded in agarose plugs 44
2.4.3 One-dimensional (1D) gel electrophoresis – for the detection of DNA double-strand breaks. 45
2.4.4 Two-dimensional (2D) gel electrophoresis – for analysing replication intermediates 46
2.4.5 Southern blotting 47
2.5 Genetic assays 48
2.5.1 Viability spot assay 48
2.5.2 Genotoxin sensitivity spot assay 48
2.5.3 Direct repeat recombination assay 49
2.6 Data Analysis 49
2.6.1 Image Processing and analysis 49
2.6.2 Statistics 50
Chapter 3 Investigating the fidelity and genetic requirements of replication restart from a programmed protein-DNA barrier 51
3.1 Introduction 52
3.2 Results 54
3.2.1 Establishing a system for monitoring direct repeat recombination downstream of a barrier 54
3.2.2 Effect of delaying replication fork merging on direct repeat recombination downstream of a barrier 58

3.2.3 Rad51 and Rad52 are essential for direct repeat recombination downstream of *RTS1* but not cell viability. 59
3.2.4 Effect of *rad54* deletion on direct repeat recombination downstream of *RTS1* 65
3.2.5 Pfh1 promotes recombination downstream of *RTS1.* 67
3.2.6 Effect of the loss of Elg1 on direct repeat recombination downstream of *RTS1.* 71
3.2.7 Helicases that limit genetic instability associated with replication restart. 74
3.2.8 Exo1 limits direct repeat recombination associated with restarted replication. 77
3.2.9 Fen1 does not affect direct repeat recombination associated with restarted replication. 79
3.2.10 Mus81, Fml1 and Tid1 play little or no role in promoting or constraining direct repeat recombination associated with restarted replication. 80
3.2.11 Are restarted forks more susceptible to collapse at weak barriers than replication origin-derived forks? 83
3.3 Discussion 90
3.3.1 RDR induced by *RTS1* leads to genomic rearrangements as it progresses away from the site of its initiation. 90
3.3.2 Pfh1 promotes RDR and/or is needed for the progression of the restarted fork. 91
3.3.3 Loss of Elg1 delays replication restart from *RTS1*. 93
3.3.4 Srs2 constrains template switching of the restarted fork. 93
3.3.5 Loss of Rqh1 leads to increased genome instability by the restarted replication fork. 94
3.3.6 Fbh1 is essential for limiting template switching during RDR 95
3.3.7 Exo1 maintains the stability of the restarted fork. 95
3.3.8 A hypothetical model for replication restart from the barrier. 96
3.3.9 Restarted forks are more susceptible to collapse at transcriptionally active sites. 99
3.3.10 Measuring replication restart quantitatively 99
Chapter 4 Developing a novel accidental protein-DNA barrier for studying the cellular response to replication fork blockage 102
4.1 Introduction 103
4.2 Results 104
4.2.1 Constructing an accidental RFB using a reconstituted human *Tc1-mariner* transposase 104

4.2.2 Binding of Mar to a single transposon end induces direct repeat recombination 113
4.2.3 MarBI is a bi-directional RFB. 117
4.2.4 MarBI induced direct repeat recombination is partially dependent on Rad51, Rad52 and Rad54. 123
4.2.5 MarBI causes DNA breakage. 125
4.2.6 MarBI does not affect cell viability even in the absence of Rad51 and Rad52. 130
4.2.7 Studying the spatio-temporal dynamics of recruitment of recombination proteins at MarBI by live-cell imaging 132
4.3 Discussion 151

Chapter 5 Further analysis of MarBI-induced recombination and comparison to other RFBs 157
5.1 Introduction 158
5.2 Results 158
5.2.1 Does MarBI induce direct repeat recombination at sites downstream of it similar to *RTS1*? 158
5.2.2 Is the absence of replication restart due to the stabilisation of the replication fork by the fork protection complex? 161
5.2.3 Does replication past MarBI depend on Pfh1? 168
5.2.4 Elg1 promotes MarBI induced recombination. 170
5.2.5 Is Fml1 involved in processing replication forks perturbed by MarBI? 170
5.2.6 Dose Mus81 cleave replication forks stalled at MarBI? 172
5.2.7 Do other accidental RFBs induce recombination in the same manner as MarBI? 175
5.3 Discussion 181
5.3.1 There is very little measurable RDR at MarBI 181
5.3.2 The fork protection complex prevents RDR at MarBI 181
5.3.3 Pfh1's "sweepase" activity appears to be ineffective at MarBI 182
5.3.4 Elg1 promotes MarBI induced recombination. 183
5.3.5 Mus81 does not appear to cleave replication forks stalled at MarBI 184
5.3.6 TusB-*TerB* induces recombination similar to MarBI in fission yeast. 184

Chapter 6 Loss of a strong replication origin in *S. pombe* can cause genomic instability 186
6.1 Introduction 187
6.2 Results 187

6.2.1 Loss of *oriIII-1253* causes a localised zone of hyper-recombination on ChrIII 187
6.2.2 *OriIII-1253* is not the only strong origin important for maintaining genome stability in *S. pombe.* 191
6.3 Discussion 191
Chapter 7 Concluding Remarks 199
Chapter 8 Appendix 206
Chapter 9 Bibliography 263

Chapter 1

Introduction

One of the most fundamental processes in the maintenance of genome integrity is accurate DNA replication. The integrity of the genome can be said to be directly proportional to the fidelity of DNA replication. However, a serious threat to the successful completion of genome duplication is perturbation of replication fork movement along the DNA template by various obstacles ranging from protein-DNA complexes to DNA lesions like single-strand breaks (Branzei and Foiani, 2010; Carr et al., 2011; Lambert and Carr, 2013). These replication fork barriers (RFBs) can cause the replisome to stall. When a replication fork stalls, it can be protected such that either DNA synthesis can resume when the barrier is removed or it can merge with the opposing fork when it arrives to complete DNA replication. However, fork stalling can also elicit fork collapse (i.e. the dissociation of the replisome) or even fork breakage. If this occurs, the homologous recombination (HR) machinery can intervene to restore DNA integrity and restart replication, albeit with a risk of restarting at the wrong, non-contiguous sequence and causing changes to the genome if ectopic homologous sequences are recombined. Such changes include deletions, duplications, inversions, and translocations, which can lead to the development of diseases such as cancer in humans (Chen et al., 2010; Heyer et al., 2010; Lambert and Carr, 2013; Lambert et al., 2005, 2010). Thus, the use of recombination at perturbed forks is a double-edged sword; it promotes genome stability by ensuring that DNA replication is completed, but at the same time can cause catastrophic genome rearrangements.

In this study, I use the fission yeast *Schizosaccharomyces pombe* as a model system to study the recombinational response that is induced at blocked replication forks. In this first chapter, I review the process of DNA replication and the various roadblocks that challenge the successful completion of genome duplication. As a majority of the cellular strategies involve the use of HR to

overcome the impediments to replication I will also review the basic steps involved in HR and the proteins that catalyse it. Building on this, I will discuss HR's involvement in processing arrested replication forks while also reviewing the wide plethora of strategies employed by the cell to overcome impediments to DNA replication.

1.1 Fundamentals of DNA replication

1.1.1 Replication Origins and Initiation

DNA replication is initiated at specific loci called replication origins, whereby a pair of replication forks emanate and move bi-directionally away from the origin. In *E. coli*, replication starts from the origin of replication (*OriC*), moves bi-directionally and terminates at specific nucleotide sequences termed *TER* sites (Leonard and Méchali, 2013). In eukaryotes, where DNA content is much higher, replication is initiated from multiple origins along the chromosome and terminates when opposing forks meet. *Saccharomyces cerevisiae* has well defined replication origins, while in *S. pombe* and higher eukaryotes they are spread over a larger area and lack any sequence specificity (Branzei and Foiani, 2010; Errico and Costanzo, 2010). The replication origins in budding yeast are known as autonomously replicating sequences (ARS) and are comprised of about 150 bp of DNA (MacAlpine and Bell, 2005; Nieduszynski et al., 2006), however, fission yeast replication origins are much larger (500-1000 bp) and do not have a consensus sequence but are typically AT-rich (Dai et al., 2005; Hayashi et al., 2007; Heichinger et al., 2006; Segurado, 2003). Replication in metazoans starts within large initiation zones and is organized within clusters (Errico and Costanzo, 2010; Kaykov and Nurse, 2015).

In *S. cerevisiae*, origins are classified as “early” and “late” and precise control of the timing and density of origin firing is important for the accuracy of replication. Origin firing in fission yeast and mammals is more stochastic. Origins can also differ in efficiency, some being strong and some being weak (Donley and Thayer, 2013; Heichinger et al., 2006). Furthermore, all organisms seem to contain an excess of origins that may be fired when major ones are inactivated or when DNA replication is challenged to ensure complete replication of the genome (Branzei and Foiani, 2010; Ge et al., 2007; Ibarra et al., 2008; Woodward et al., 2006).

Due to the presence of multiple origins, in eukaryotes restart of interrupted replication is not as vital as it is for bacteria. Presumably in such an environment neighboring origins can take over and replicate sequences left by the stalled/collapsed replication fork. However, initiation of replication is strictly regulated to ensure that origins fire only once during each cell cycle (Diffley, 2004; Yeeles et al., 2015). Therefore, if two converging replication forks are damaged, the DNA between them will potentially remain unreplicated.

1.1.2 The Replisome

A multi-component protein complex termed the “replisome” carries out DNA replication. Replication begins when the Origin Recognition Complex (ORC), which recruits the pre-replication complex (pre-RC), binds to a replication origin in G1 and licenses it for firing. The replisome is comprised of the MCM (minichromosome maintenance) replicative helicase complex, replication elongation factors (which include the three regular DNA polymerases), the clamp loader RFC (replication factor C), the processivity clamp PCNA (proliferating cell nuclear antigen), and other factors required for fork stabilization (Branzei and Foiani, 2010). Replicative polymerases include Pol1 (α), Pol2 (ε), and Pol3 (δ) in yeast. Studies on budding yeast show that forks are stationary and that replisomes

reside within replication factories (Kitamura et al., 2006). Such a model predicts that the newly synthesized DNA is continuously extruded as replication proceeds. In contrast, in *E. coli* it has been demonstrated that independent replication forks move along chromosomal DNA (Reyes-Lamothe et al., 2008).

In budding yeast, the MCM complex, composed of Mcm2–Mcm7 subunits, serves as the replicative helicase with the help of accessory factors Cdc45 and GINS, which maintain the protein-protein interactions within the replisome (Maiorano et al., 2006). Together, Cdc45, MCM, and GINS constitute the CMG complex, which, further to its role in replication fork progression, also has a role in initiating replication at origins (Branzei and Foiani, 2010). The replisome also contains a clamp-loading complex, RFC, that recognizes ss-dsDNA junctions and loads the replicative helicase and PCNA (Majka and Burgers, 2004). PCNA forms a homotrimeric complex and acts as the DNA polymerase clamp that maintains the speed and processivity of DNA polymerases during replication. During replication, the replicative helicase, Mcm2-7, unwinds parental DNA to expose the two individual strands. DNA synthesis is initiated through the primase activity of Polα, which synthesises a short (~10 bp) RNA primer. Polα is substituted by Pol δ and Polε on the lagging and leading strand, respectively, in a manner that is regulated by RFC and PCNA (Miyabe et al., 2011). The leading strand is replicated in a 5'-3' direction continuously, whereas lagging strand synthesis is discontinuous and requires initiation by a primer and the synthesis of short DNA fragments termed Okazaki fragments. On the lagging strand, the RNA primers are displaced by Pol δ and processed by the flap endonuclease activity of FEN1 (flap endonuclease 1) and Dna2, which act on uncoated and RPA-coated flaps, respectively (Kang et al., 2000; Stewart et al., 2008, 2009). Okazaki fragments are then ligated to each other by DNA ligase I to form a continuous strand.

The classical model of DNA replication, where Pol ε and Pol δ equally distributed the load of replicating the template DNA by synthesizing the leading and lagging strand respectively, was recently challenged by work done in the Prakash lab (Johnson et al., 2015). They showed that Pol δ is the major polymerase for both strands and that Pol ε's primary role is only to proofread errors made by Pol δ during leading-strand replication. This idea is currently under debate in the field and warrants further investigation.

1.1.3 Replication Termination

Eukaryotic DNA replication terminates when replisomes from adjacent replication origins converge. Termination involves local completion of DNA synthesis, decatenation of daughter molecules and replisome disassembly. In *E. coli*, replication forks terminate at defined terminator sites (*ter*) that are positioned opposite to OriC (Hill and Marians, 1990). In eukaryotes, less is known about the precise mechanism of termination. The convergence of two forks generate catenated sister chromatids that require resolution by DNA topoisomerase II (DNA Topo II) as seen in the mammalian DNA tumor virus SV40 (Fachinetti et al., 2010; Ishimi et al., 1992). DNA decatenation can also be achieved in yeast by the Sgs1-Top3-Rmi1 complex (Cejka et al., 2012; Mundbjerg et al., 2015). Failure to decatenate sister chromatids results in the formation of DNA anaphase bridges between daughter nuclei during mitosis and may result in DNA breakage (DiNardo et al., 1984).

Recent work shows that late in S phase, the eukaryotic replicative helicase CMG is removed after the ubiquitylation of MCM7 (Maric et al., 2014; Moreno et al., 2014). While one study implied that DNA replication can go to completion in the absence of CMG unloading (Maric et al., 2014), another reported that tracts of unreplicated DNA remain in the absence of this process (Moreno et al., 2014).

Work from the Walter lab has further advanced the understanding of the events during termination and indicate that DNA synthesis does not slow detectably as forks approach each other, and that leading strands pass each other unhindered before undergoing ligation to downstream lagging strands. Dissociation of the replicative CMG helicase occurs only after the final ligation step, and is not required for completion of DNA synthesis, strongly suggesting that converging CMGs pass one another and dissociate from double-stranded DNA (Dewar et al., 2015). However, the finer details of the DNA replication finale are yet to be worked out.

1.2 Impediments to DNA replication

The progression of individual replication forks can be impeded by a wide variety of obstacles or RFBs that have the potential to cause fork stalling and even collapse. Fork stalling is defined as an arrested replication fork whose replisome components remain associated with the DNA in a configuration that may resume DNA synthesis following removal of the replication barrier (Hu et al., 2012). In contrast, fork collapse entails replisome components disassembling following fork arrest, which prevents the resumption of DNA synthesis without other factors aiding the reloading of the replisome components (Cobb et al., 2005; Katou et al., 2003; Lucca et al., 2004). A collapsed fork can become a broken fork, where there is a one-ended DNA double-strand break (DSB), but not all collapsed forks are broken and this is not a pre-requisite for replication restart (Lambert and Carr, 2013). If replication is not restarted at a stalled or collapsed fork, the fork structure still needs to be maintained in a configuration that will be capable of merging with the opposing fork. RFBs can include both damaged DNA bases (that can occur throughout the genome) as well as “inherent” RFBs that are associated with

specific chromosomal features. Discussed below are some of the commonly occurring RFBs encountered by the replication fork.

1.2.1 DNA lesions and strand discontinuities

Damaged DNA bases, which can occur as a consequence of normal physiological processes (e.g. oxidative metabolism) or through exposure to external genotoxins, are obstacles to the replicative DNA polymerases. This is because replicative polymerases cannot efficiently incorporate nucleotides opposite non-canonical bases. DNA damage thus compromises DNA synthesis, but it is not necessarily the case that DNA damage *in vivo* impedes the actual movement of the replisome and DNA fork (Branzei and Foiani, 2010). There are a number of different genotoxic agents that perturb fork progression. Methyl methanesulfonate (MMS) exposure results in the formation of 3-methyladenine (N3-MeA) adducts that block replication forks (Wyatt and Pittman, 2006). Ultraviolet light (UV) induces cyclobutane pyrimidine dimers (CPDs) that can stall the replisome. Ionizing radiation (IR) causes DNA strand breakage that can cause fork stalling and breakage. Camptothecin (CPT) poisons topoisomerase I (Top1) and inhibits the re-ligation step such that the Top1-DNA covalent intermediate becomes longer lived at the 3′ end of the ssDNA nick (Hsiang et al., 1985). Nicks on the leading strand template can lead to the formation of a one-ended DSB as the leading strand polymerase runs off the template (Kuzminov, 2001; Michel et al., 2001). Contrarily, nicks on the lagging strand template can lead to the formation of a two-ended DSB since the synthesis of the lagging strand is discontinuous (Caldecott, 2008). Hydroxyurea (HU) can temporarily pause replication forks by depleting the cellular deoxyribonucleotide triphosphate (dNTP) pool. Cisplatin induces ICLs, which prevent strand separation and impede the progression of the replicative helicase (Lambert and Carr, 2013). By perturbing the progress of the replication

fork, many of the aforementioned agents induce recombination. However, not all replication fork stalling induces recombination (Calzada et al., 2005), and even when it does, the outcome can differ. For example, UV-induced lesions strongly promote gene conversion between direct repeats, whereas CPT, at the same site, induces deletions (Ahn et al., 2005).

1.2.2 Unusual DNA structures and fragile sites

DNA repeats, such as di-nucleotide, tri-nucleotide, inverted, mirror and direct tandem repeats, can often undergo structural transitions that lead to the formation of alternative DNA structures, such as cruciform, H-DNA (triplex), G quartets, Z-DNA, and S-DNA (slipped-strand DNA), which could inhibit replication (Mirkin and Mirkin, 2007). The continuation of DNA synthesis past these elements or the abnormal replication of the repeats, most often of tri-nucleotide repeats, has been proposed to lead to their expansion, and this phenomenon is responsible for many human diseases and hereditary disorders (Budworth and McMurray, 2013; Lopez Castel et al., 2010; Mirkin, 2006). Expansion of repetitive elements has also been associated with chromosomal fragility—a cytogenetic term that describes DNA sequences that show gaps or breaks, following the partial inhibition of DNA synthesis, that are often hotspots for chromosomal rearrangements (Durkin and Glover, 2007).

1.2.3 Transcription-replication conflict

The transcription machinery constitutes a natural obstacle to replication fork progression, and collisions between both machineries are an important source of replication stress and genome instability, as shown in bacteria, yeast and mammals (Gaillard et al., 2013). Additionally, concomitant transcription and replication, whether resulting in collisions or not, generates a large amount of

torsional stress in the DNA that can lead to abundant reversed forks. Reversed forks not only contribute to delaying replication progression but can also be the target of nucleases and other enzymes that might foster genome instability (Gaillard et al., 2015; Helmrich et al., 2013). In addition, during transcription, the nascent RNA may hybridize back to the complementary DNA strand, forming an RNA–DNA hybrid and a displaced ssDNA that is termed R-loop, which has been shown to be associated with increased chromosomal fragility (Gaillard et al., 2013; Helmrich et al., 2011).

1.2.4 Programmed barriers

Interestingly, cells have also evolved programmed polar protein-DNA RFBs to ensure that replication occurs unidirectionally across certain loci for specific purposes. In most instances, these programmed RFBs are employed to prevent potentially more catastrophic problems from arising, such as DNA re-replication of chromosomes and clashes between the transcription and replication machineries. Three of the most extensively studied programmed barriers are discussed below.

1.2.4.1 Tus-*ter* barrier in *E. coli*

As prokaryotic DNA replication is initiated at only a single origin of replication with two replication forks moving bi-directionally around the circular genome, a blocked replication fork is arguably more dangerous in *E. coli* than in eukaryotes. Despite this, more than halfway in each direction there are specific termination sites, *terA*–*terF*, bound by the Tus protein that unidirectionally block replication forks by preventing the unwinding of DNA by the replicative helicase DnaB (Hill and Marians, 1990; Khatri et al., 1989). The Tus-*ter* barrier ensures that the bi-directional forks originating from the origin converge at one point to primarily prevent instances of over-replication (Hiasa and Marians, 1994). At the Tus-*ter*

barrier, replication forks remain stable, and the programmed barrier only elicits recombination if the fork from the subsequent round of replication runs into it and generates a DSB (Bidnenko et al., 2002). Surprisingly, the Tus-*ter* barrier has also recently been found to induce replication fork pausing when it is introduced into budding yeast as well as mammalian cells (Larsen et al., 2014; Willis et al., 2014).

1.2.4.2 Fob1 barrier in *S. cerevisiae*

Remarkably, yeasts also exploit RFBs for key biological functions. To avoid head-on collisions between replication and transcription complexes, *S. cerevisiae* employs a specific Fob1 protein-DNA RFB downstream of the highly transcribed and highly repetitive ribosomal DNA (rDNA) regions, which also contain a potential origin of replication, to limit replication in the direction opposite to transcription by arresting replication forks that it encounters (Brewer and Fangman, 1988). As a result, replication forks move only in the same direction as transcription. The Fob1 protein-DNA barrier is insufficient for promoting inter/intra-repeat recombination (Labib and Hodgson, 2007). Interestingly, barriers that maintain rDNA repeat copy number, such as Fob1, are evolutionarily conserved from yeast to humans (Gerber et al., 1997).

1.2.4.3 RTS1 barrier in *S. pombe*

In *S. pombe*, the Replication Terminator Sequence-1 (*RTS1)* barrier is employed for efficient mating-type switching that occurs through a replication coupled recombination event (Dalgaard and Klar, 2001). Mating-type switching in fission yeast can be considered equivalent to a type of cell differentiation where two distinct cell types express distinct sexual markers (h^+ or h^-) and the cell can efficiently switch between the two via a programmed DNA rearrangement (Egel, 2004). In order for the switching to occur, replication of the *mat1* locus has to

occur in the centromere-proximal direction so that an imprint can be laid down, which stimulates mating-type switching in the next generation. *RTS1* promotes this process as a polar replication terminator that enforces unidirectional replication of the *mat1* locus by blocking forks moving in the centromere-distal direction (Dalgaard and Klar, 1999). The switch from one sexual cell type to the other actually requires two polar fork arrest events to occur at the *mat1* locus. The second event is coordinated by another RFB that promotes imprinting on the lagging strand that subsequently results in either a paused ot broken fork that triggers a recombination-dependent replication mechanism using genetic information from one of the two silent *mat2* or *mat3* cassettes (Egel, 2004; Holmes et al., 2005; Kaykov and Arcangioli, 2004; Vengrova and Dalgaard, 2006).

RTS1 consists of four repeated 55 bp motifs named region B and an ~ 60 bp enhancer region called region A that cooperate together for efficient replication termination (Codlin and Dalgaard, 2003). The function of *RTS1* is also dependent on several intrinsic proteins, which include Rtf1 (Replication Termination Factor 1), Rtf2, Swi1, and Swi3. Rtf1 binds to the four repeated motifs as well as the enhancer region A, and self-interacts through its C-terminal tail to stabilize the interactions and, additionally, provide constraints to the unwinding of the DNA template by the approaching replicative helicase (Eydmann et al., 2008). Rtf2 stabilizes the stalled fork at *RTS1* by preventing replication fork collapse and Srs2-dependent replication restart so that DNA replication is completed by a converging replication fork that is initiated at a flanking origin arriving at the site (Inagawa et al., 2009). The remaining two factors, Swi1 and Swi3, move with the replication fork as part of the Replication Progression Complex (RPC) and serve critical roles at *RTS1* by protecting the replication fork and stabilizing stalled forks (Dalgaard and Klar, 2000; Noguchi et al., 2004). The *RTS1* barrier has been frequently used

to demonstrate that replication forks arrestted at the barrier are prone to collapse and to study their subsequent repair by HR-dependent mechanisms (Ahn et al., 2005; Lambert et al., 2005; Pryce et al., 2009).

1.2.5 The cellular defence against RFBs

Obstacles to replication fork progression destabilize the replisome and impact on the integrity of forked DNA structures. Therefore, to ensure the successful progression of a replication fork along with its associated replisome several distinct strategies have been evolved by the cell, collectively termed as DDR (DNA damage response). First, the cells have well-orchestrated mechanisms that promote continued movement of forks through potential obstacles. Second, dedicated replisome and fork DNA stabilization pathways prevent the dissociation of the replisome if its progress is halted. Third, should stabilisation fail, there are mechanisms to ensure damaged forks are accurately fused with a converging fork or, when necessary, re-associated with the replication proteins to continue replication. These responses are discussed later in this chapter.

1.3 The key players in Homologous Recombination

HR proteins play a major role in DDR and the faithful completion of DNA replication. I will therefore give a brief overview of the key factors that drive HR. HR was initially identified as a pathway that mediated genetic recombination in the context of meiosis. Apart from its role in meiosis, HR plays important roles in repairing DSBs, ssDNA gaps and damaged replication forks (Jones and Petermann, 2012). HR proteins have also been implicated in protecting stalled replication forks (Errico and Costanzo, 2012). HR typically involves the invasion of an intact duplex DNA by a 3'-ended single-stranded DNA tail from a damaged

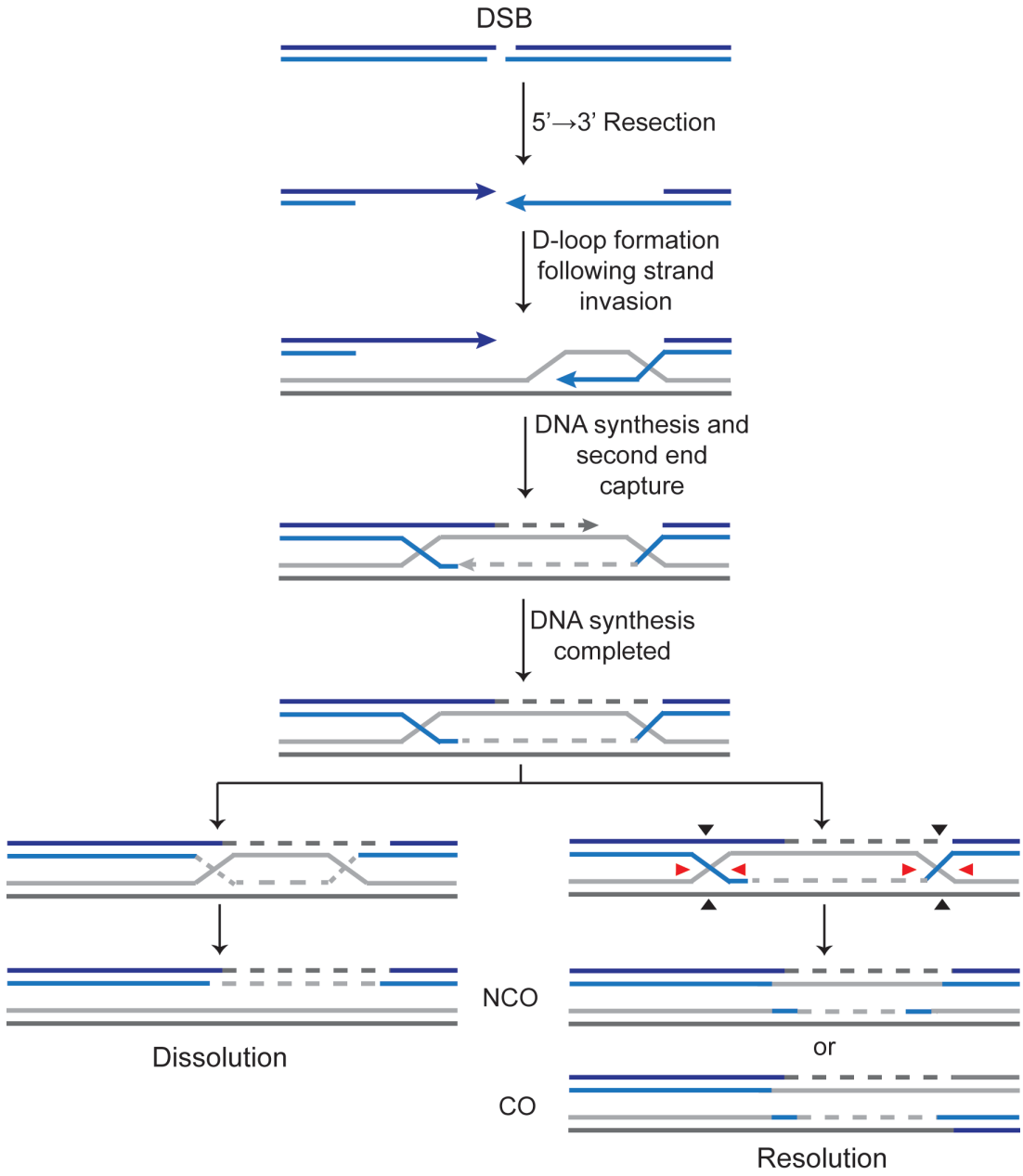


Fig. 1.i The classical double-strand break repair model.
In DSBR, the 5′ ends of the DSB are resected to generate a substrate with 3′ ssDNA tails followed by Rad51-mediated strand invasion into a homologous DNA molecule (sister chromatid or homologous chromosome), which forms a D-loop. New DNA synthesis is primed from the 3′ end of the invading strand. The D-loop then anneals to the other resected DSB end, a process termed second end capture. Filling of the gaps and ligation forms a dHJ. The dHJ is resolved by endonucleolytic cleavage of a pair of strands at each HJ to form crossover or non-crossover recombinants (cleavage points marked by red and black arrow heads). Alternatively, dHJ dissolution can occur to form non-crossover recombinants by the action of DNA helicases/translocases. Newly synthesized DNA is depicted as dashed lines in the same colour as the template; arrowheads indicate 3′ ends. Adapted from Mehta and Haber, 2014.

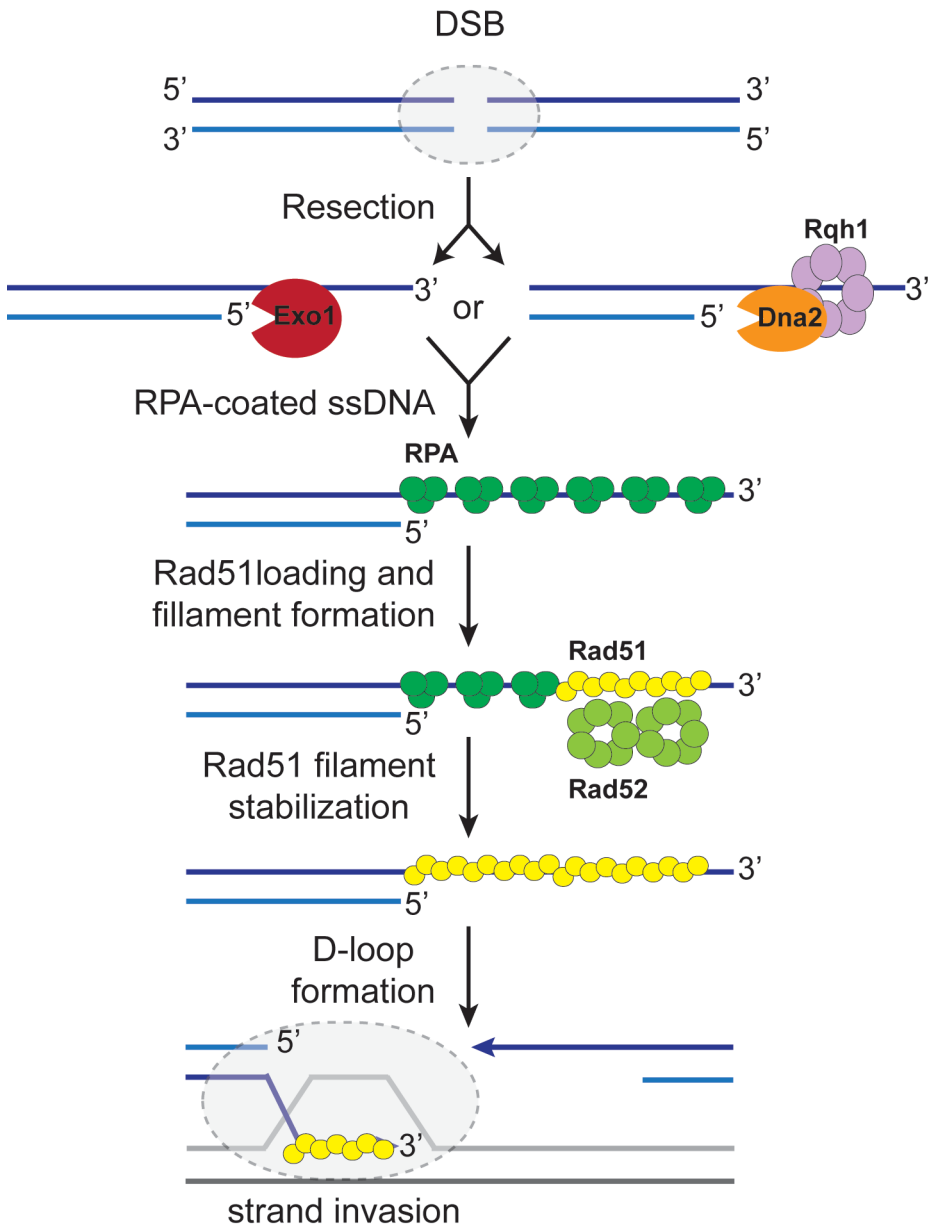


Fig. 1.ii The central reaction of homologous recombination proceeds through Rad51 nucleoprotein filament formation and strand invasion in fission yeast.

The broken end of DNA is initially resected. Long-range resection is dependent on two parallel pathways involving Rqh1-Dna2 and Exo1. RPA coats ssDNA to prevent it from forming secondary structures. Aided by Rad52, Rad51 loads on DNA to form a nucleofilament, which invades the homologous sequence on another duplex (e.g. the sister chromatid). Adapted from Renodon-Cornière et al., 2013.

Table 1-1 Key recombination proteins.

	E. coli	S. cerevisiae	S. pombe	Mammals
Pre-synapsis Processing of broken DNA ends	RecBCD			
	SbcD-SbcC	Mre11-Rad50-Nbs1	Mre11 (Rad32)-Rad50-Nbs1	MRE11-RAD50-NBS1
	-	Sae2	Ctp1	CtIP1
	RecQ	Sgs1	Rqh1	BLM
	-	Dna2	Dna2	DNA2
	RecE, RecJ	Exo1	Exo1	EXO1
	SSB	RPA	RPA	RPA
	-	-	Fbh1	FBH1
	UvrD	Srs2	Srs2	PARI
Synapsis Homologous pairing and DNA strand exchange	RecA	Rad51	Rad51 (Rhp51)	RAD51
	RecO	Rad52	Rad52 (Rhp22)	RAD52
	RecF- RecR	Rad55-Rad57	Rad55 (Rhp55)-Rad57 (Rhp57)	RAD51B, RAD51C-XRCC3
	-	Sae3-Mei5	Swi5-Sfr1	SWI5-SFR1
	-	Shu1-Shu2-Psy3-Csm2	Rlp1-Sws1-Rdl1	XRCC2-SWS1-RAD51D-SWSAP1
	-	Rad54	Rad54 (Rhp54)	RAD54
Post-synapsis Resolution of recombination intermediates	TopoIII	Top3	Top3	TopoIIIα
	RecQ	Sgs1	Rqh1	BLM, RECQ1, RECQ4, RECQ5, WRN
	-	Mph1	Fml1	FANCM
	-	-	Fbh1	FBH1
	UvrD	Srs2	Srs2	PARI
	RuvAB			
	-	Mus81-Mms4	Mus81-Eme1	MUS81-EME1
	RuvC	Yen1	-	GEN1
	-	Slx1-Slx4	Slx1-Slx4	SLX1-SLX4

Note- Homologous or functionally equivalent recombination proteins from the different species are arranged in the same row

sister chromatid or homologous chromosome. New DNA synthesis, primed from the end of the invading strand, results in the retrieval of genetic information from the undamaged homologous DNA to facilitate repair. There are different models for the HR repair of DSBs based on how they form and restore replication intermediates. However, HR has been best studied and understood in the context of classical DSB repair (DSBR), initially described by Szostak et al., 1983 [See Fig. 1.i].

One can divide DSBR by HR into three basic stages: pre-synapsis, synapsis and post-synapsis. During pre-synapsis, the DSB is resected and key recombination proteins are loaded onto the resulting ssDNA. A homologous DNA is then sought and found, paired with and invaded during synpasis. Finally, during post-synapsis, the conjoined DNA is resolved into separate DNA molecules. Each of these stages of the HR reaction is catalysed by a different subset of recombination proteins. Described below are some of these key HR proteins in yeast. Brief mention is also made of their homologues or equivalents in other species, and a list of key HR proteins in both fission and budding yeast, and their functional homologues in bacteria and mammals, is presented in Table 1-1.

1.3.1 Pre-synapsis: resection

In pre-synapsis, the initial step in the HR process, the DNA damage is processed to form an extended region of ssDNA. The Mre11-Rad50-Nbs1 (MRN) complex, or in budding yeast the Mre11-Rad50-Xrs2 (MRX) complex, is recruited to the DSB to catalyse initial DNA resection. The nuclease activity of Mre11 is essential for the preliminary processing of the DSB, and is greatly aided by Rad50. Nbs1 has DNA binding activity that helps target the complex to DNA ends (Trujillo and Sung, 2001; Trujillo et al., 2003). In budding yeast, resection is promoted by the ability of MRX to recruit another nuclease called Sae2 (a homologue of *S. pombe* Ctp1 and

mammalian CtIP). The MRX-Sae2 complex removes about 50-100 nucleotides from the 5' end of a break, thus generating short 3' ssDNA overhangs (Jasin and Rothstein, 2013; Mimitou and Symington, 2008). Resection further away from the break site is facilitated by two parallel pathways that depend on the 5'-3' exonuclease Exo1, and the 3'-5' DNA helicase Sgs1 (the budding yeast homologue of *S. pombe* Rqh1) working together with the endonuclease Dna2 (Mimitou and Symington, 2008; Zhu et al., 2008) [Fig. 1.ii].

1.3.2 Pre-synapsis to synapsis: Rad51 nucleoprotein filament formation and strand invasion

After the 3' ssDNA tails have been generated by resection, the ssDNA binding protein RPA (replication protein A) coats the tail eliminating secondary structures and protecting the DNA from nucleolytic cleavage (Sung et al., 2003). This is followed by the recruitment of the central recombinase Rad51 (RecA in bacteria) that binds to DNA forming a long polymeric nucleoprotein filament. The formation of this nucleoprotein filament is mediated by Rad52 which is thought to displace RPA from ssDNA to aid Rad51 loading (Benson et al., 1998; Kim et al., 2002; Song and Sung, 2000; Sugiyama and Kowalczykowski, 2002). The filament is then further stabilized by the Rad51 paralogues, Rad55 and Rad57 (Sung, 1997). Additionally, in fission yeast, Swi5 and Sfr1 mediators aid in Rad51 nucleation and stimulate Rad51-mediated strand exchange by snugly binding within the helical groove of the Rad51 filament (Akamatsu et al., 2003; Haruta et al., 2008). The Rad55-Rad57 and Swi5-Sfr1 complexes are proposed to work in parallel pathways promoting Rad51 activity (Akamatsu et al., 2007; Haruta et al., 2008).

Once bound to the ssDNA, Rad51 catalyzes a homology search and, once a homologous double-stranded DNA sequence has been located, recombines the 3'-overhang into it to form a displacement loop (D-loop) (Baumann et al., 1996).

This is followed by DNA synthesis, primed from the end of the invading DNA strand, and using the intact homologous sequence as a template. Recent single-molecule experiments have shown that Rad51 does its homology search by identifying units of microhomology, rejecting any DNA with less than 8 nucleotides of homology (Qi et al., 2015).

In addition to Rad55 and Rad57, fission yeast has two more highly divergent Rad51 paralogues, Rlp1 and Rdl1. These are members of the so-called Shu complex, which functions alongside Rad55-Rad57 (Khasanov et al., 2004; Martín et al., 2006). Recent work in budding yeast indicates that the Shu complex potentially has a role in antagonising Srs2's anti-recombinase activity in disassembling Rad51 filaments (Bernstein et al., 2011). Another protein that aids Rad51 nucleoprotein formation and function is Rad54, a member of the Swi2/Snf2 family of DNA-dependent ATPases/DNA translocases. In addition to aiding Rad51 in catalyzing strand invasion and D-loop formation, Rad54 also plays an important role in the dissociation of Rad51 from DNA. This latter function gives the DNA polymerase access to the 3' end of the invading DNA strand for DNA synthesis and enables Rad51 to be recycled for new rounds of recombination (Heyer et al., 2006; Li and Heyer, 2009; Solinger et al., 2002).

1.3.3 Post-synapsis: resolution of recombination intermediates

Following strand invasion, the 3' end at the D-loop is typically extended by a DNA polymerase. The key factors that determine the fate of the D-loop are typically DNA helicases or translocases. These enzymes can variously stabilize the D-loop by helping to extend the region of heteroduplex DNA by catalyzing branch migration of the four-way junction at one end of the D-loop or unwinding the three-way junction at its other end. Conversely, by working in the opposite direction on these DNA junctions, DNA helicases/translocases can also dissociate D-loops.

Indeed, in some cases the same enzyme may be able to perform both D-loop promoting and dissociating functions, with other factors determining which of these activities is deployed in any given circumstance. In eukaryotes, the FANCM-like helicases (Fml1 in *S. pombe*, Mph1 in *S. cerevisiae* and FANCM in mammals), Srs2, Fbh1 and RecQ-type helicases (Rqh1 in *S. pombe*, Sgs1 in *S. cerevisiae* and BLM, WRN, RECQ1, RECQ4 and RECQ5 in humans) have been implicated in processing D-loops (Bachrati et al., 2006; Bernstein et al., 2010; Dupaigne et al., 2008; Lorenz et al., 2009, 2012; Prakash et al., 2009; Sharma et al., 2005; Sun et al., 2008). In most cases they are thought to disrupt the D-loop to either abort recombination or to promote DSBR via synthesis dependent strand annealing (SDSA).

BLM and RECQ5 have been shown to strip Rad51 off ssDNA *in vitro*, which is similar to the mode of action of the Srs2 helicase in yeast (see below) (Bugreev et al., 2007; Hu et al., 2007). Mutations in the human RecQ homologues BLM, WRN and RECQ4 cause Bloom, Werner and Rothmund-Thomson syndromes respectively, all of which are characterized by cancer predisposition due to genome instability arising from inappropriate recombination (Hickson, 2003).

Srs2 is an SF1 family 3'-5' helicase that suppresses recombination by disassembling Rad51 nucleofilaments (Doe and Whitby, 2004; Krejci et al., 2003; Veaute et al., 2003). Srs2 is thought to promote SDSA by dislodging Rad51 from ssDNA tails, preventing second-end capture and dissociating D-loops (Dupaigne et al., 2008; Ira et al., 2003). Loss of Srs2 results in increased Rad51 and Rad54 focus formation and hyper-recombination at a site-specific RFB, supporting its anti-recombinase activity *in vivo* (Burgess et al., 2009; Lorenz et al., 2009). Mammals and fission yeast have another anti-recombinase, Fbh1 (F-box helicase 1), which is absent in *S. cerevisiae*. Like Srs2, Fbh1 can also actively dislodge

Rad51 from ssDNA using its helicase/translocase activity and in doing so seems to work in opposition to the mediator Rad52 (Lorenz et al., 2009; Osman et al., 2005; Simandlova et al., 2013).

If the D-loop is not disrupted, then second end capture can occur and the recombination intermediate can eventually mature into a double Holliday junction (dHJ). Alternatively, strand invasion events can occur at both ends of the DSB, followed by DNA synthesis and annealing, which also leads to the formation of a dHJ. From this point, the recombination reaction can proceed down several different paths that variously lead to either a non-crossover (NCO) or crossover (CO) outcome based on how the dHJ is processed. The classical method of processing dHJs is by DNA structure-specific nucleases that target four-way DNA junctions. These so-called HJ resolvases include RuvC in *E. coli* and Yen1/GEN1, Mus81-Eme1, and Slx1-Slx4 in eukaryotes. These enzymes resolve HJs by cutting pairs of DNA strands at or adjacent to the junction point. In the case of RuvC, Yen1 and GEN1 the cuts are symmetrical, whereas, Mus81-Eme1, either on its own or with Slx1-Slx4, introduces cuts that are asymmetric (Hickson, 2014). HJ resolvases can deliver either COs or NCOs depending on the orientation with which they cleave each junction. dHJs can also be “dissolved” without cleavage to give rise to NCOs (Jasin and Rothstein, 2013). This reaction is catalysed by the combined action of a RecQ-type helicase and Topoisomerase III (Top3) [Fig. 1.i] (Ira et al., 2003; Wu and Hickson, 2003).

1.4 Cellular response to replication fork perturbation and the role of HR in aiding completion of DNA replication

As seen in Section 1.2, replication fork progression is continuously challenged by a wide plethora of obstacles. Replication forks are vulnerable to stalling or collapse as they encounter these obstacles on the template DNA, potentially leading to a

failure to complete DNA replication. Stretches of unreplicated DNA persisting into mitosis can lead to the formation of ultrafine anaphase bridges and ultimately to DNA breakage (Chan et al., 2007, 2009; Jacome and Fernandez-Capetillo, 2011).

Importantly, chromosome fragments resulting from breakage of anaphase bridges can give rise to micronuclei, which can persist through several cell cycles. The DNA within micronuclei appears to experience high rates of damage and rearrangement resulting from elevated levels of replication stress. Upon reassimilation into the main nucleus such derivative chromosomes could drive tumorigenesis. Indeed the phenomenon of chromothripsis, which is associated with some cancers, is thought to occur by such a mechanism of micronuclei formation and reassimilation (Crasta et al., 2012; Hoffelder et al., 2004; Stephens et al., 2011; Zhang et al., 2015).

It is becoming abundantly clear that the faithful and complete replication of chromosomes is essential to maintain genetic stability and prevent the accumulation of cancer-promoting mutations. To counter the threat that RFBs pose, cells have evolved mechanisms to aid replication forks in overcoming barriers and to restart replication if the fork collapses. These mechanisms are discussed below.

1.4.1 Activation of damage tolerance pathways at single strand lesions

Perturbation of replication fork movement by lesions in either one of the template DNA strands activates the DNA damage tolerance (DDT) pathways that are crucial in aiding replication past the lesion and preventing replication fork breakage. There are two basic DDT pathways that are conserved across all eukaryotes: the error-prone trans-lesion synthesis (TLS) pathway that uses a polymerase to read past

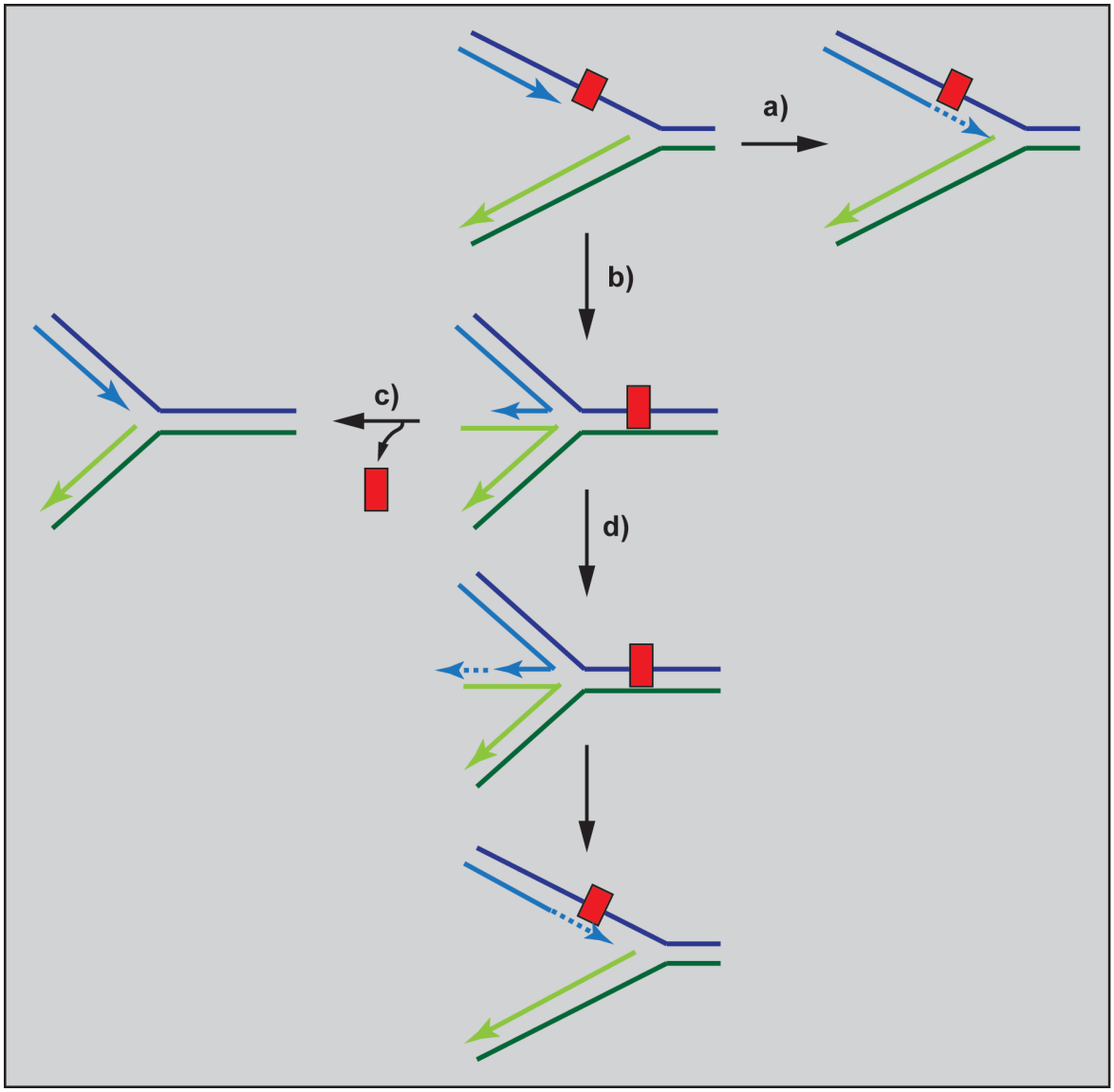


Fig. 1.iii. DNA damage tolerance pathways employed by the replication fork on encountering a single strand lesion.

a) TLS: Replication past the obstacle using TLS polymerases. b) Reversed fork formation by annealing of the two nascent strands. c) Branch migration or the action of a nuclease can reset the replication fork once the lesion is removed. d) Template switching: The protruding strand is used as a template to replicate past the sequence affected by the lesion. Newly synthesized DNA is depicted in the same colour as the template but a shade lighter; arrowheads indicate 3′ ends. The red box represents the lesion. The dashed lines represent DNA synthesis past the barrier that can be error-prone or error-free.

the obstacle; and the error-free template-switching pathway that employs HR proteins (Branzei and Szakal, 2016) [Fig. 1.iii]. These mechanisms can be deployed when the replication fork first encounters the lesion. Alternatively, if the replication fork "skips" the lesion, then they can operate on the resulting lesion-containing ssDNA gap that is left in the wake of the fork.

1.4.1.1 Trans-lesion synthesis

The cell can read past the damaged base and complete DNA replication without causing the fork to stall or collapse using specialized TLS polymerases [Fig. 1.iii.a]. Experiments in *E. coli* showed that UV-induced cyclobutane pyrimidine dimers could persist through generations in Nucleotide Excision Repair (NER)-deficient strains, indicating that the damage is not removed but "tolerated". This prompted the use of the term DNA damage tolerance (DDT) mechanism (Bridges et al., 1968; Ganesan, 1974; Rupp and Howard-Flanders, 1968). All TLS polymerases are specialized enzymes which lack 3'-5' proofreading exonuclease activity and have non-restrictive active sites that poorly discriminate between correct and incorrect incoming nucleotides (Andersen et al., 2008; Yang and Woodgate, 2007). Although TLS can aid replication to progress past DNA lesions, it does so at the risk of causing mutations and hence is known as the error-prone DDT pathway.

1.4.1.2 Template switching

Fork blocking lesions in the leading strand template can be tolerated via a mechanism known as template switching. This involves the transient uncoupling of leading and lagging strand polymerases so that the lagging strand polymerase can proceed beyond the position at which the leading strand polymerase is blocked (Higuchi et al., 2003). In this way, the extended lagging strand can serve as a

template for the prematurely terminated leading strand via a fork regression process. The lesion on the leading strand template can, therefore, be bypassed by employing the nascent lagging strand as a template. Theoretically, no mutations are introduced during template switching as the lagging strand contains the same information as the “original” template strand of the leading strand. The regressed fork can then be resolved either by its re-setting [Fig. 1.iii.d] or by a strand invasion based mechanism in which the 3′ end of the newly synthesized leading strand invades the parental template at a point downstream of the lesion (Branzei and Szakal, 2016; McGlynn and Lloyd, 2002). In budding yeast, error-free DDT is mediated by the E2-E3 ubiquitin complex Mms2-Ubc13-Rad5 (Hofmann and Pickart, 1999; Ulrich et al., 2000), and it is thought that Rad5, which is a DNA helicase, directly promotes fork reversal (Blastyák et al., 2007).

1.4.1.3 Post replicative repair

As mentioned above, when either the leading or the lagging strand polymerase is impeded it can potentially “skip” the barrier on its template strand and reinitiate synthesis downstream of the barrier. Due to the discontinuous nature of lagging strand synthesis, lesions on the lagging strand may stop extension of a single Okazaki fragment, but should not stop replication as new Okazaki fragments can continue to be synthesized (Branzei and Psakhye, 2016). In contrast, lesions on the leading strand were believed to stop DNA synthesis since synthesis is naturally continuous on the leading strand. However, it was later shown that leading strand synthesis can tolerate some lesions, such as pyrimidine dimers, via a mechanism of discontinuous DNA synthesis, which does not involve replisome disassembly and is independent of known replication-restart proteins (Lopes et al., 2006; Yeeles and Marians, 2011). The lesion-containing ssDNA gap that is left

behind by the replication fork is later filled in by post-replicative TLS or HR-mediated template switching (Lopes et al., 2006).

1.4.1.4 Factors affecting the pathway choice

In eukaryotes, the switch between error-prone and error-free DDT is largely dependent on posttranslational modification of PCNA, which in budding yeast is mediated by the Rad6-Rad18 complex. Rad6 is an E2-Ubiquitin conjugating enzyme, which together with the E3-ligase Rad18 has been shown to promote DNA synthesis through UV-induced ssDNA gaps in the absence of NER (Hoege et al., 2002; Jentsch et al., 1987; Prakash, 1981).

Rad6-Rad18 mono-ubiquitinates PCNA on residue Lys164 in response to DNA damage and this may only happen at stalled replication forks (Garg and Burgers, 2005; Hoege et al., 2002). Mms2-Ubc13-Rad5 can further poly-ubiquitinate PCNA at the same residue (Hoege et al., 2002). Therefore, while mono-ubiquitinated PCNA has been implicated in modulating error-prone DDT (Stelter and Ulrich, 2003), poly-ubiquitinated PCNA promotes error-free damage bypass (Branzei et al., 2008; Torres-Ramos et al., 2002). PCNA is also sumoylated and this modification modulates error-free bypass and increases PCNA affinity for Srs2 (Branzei et al., 2008; Haracska et al., 2004; Papouli et al., 2005; Pfander et al., 2005). The PCNA-Srs2 interaction down regulates HR, suggesting that Srs2 may be a molecular switch between DDT and HR.

In addition to PCNA, TLS is promoted by checkpoint proteins, such as Mec1, whose phosphorylation induces TLS polymerase re-localisation to sites of damage (Hirano and Sugimoto, 2006). The checkpoint can also promote error-free repair; for example in *S. pombe* the checkpoint kinase Rad3 phosphorylates the

checkpoint clamp protein Rad9 and this is important to limit TLS and promote Rad6-dependent error-free repair (Kai et al., 2007).

1.4.2 Stabilization of stalled forks: the role of HR proteins and the fork protection complex

An essential function of the DNA replication checkpoint is to maintain replication fork integrity (Lindsay et al., 1998; Tercero et al., 2003). In fact, in many cases it appears that the primary response to replication fork stalling is to protect the fork and prevent the replisome from disassembling. This enables DNA replication to resume following removal of the block or ensures that canonical replication termination occurs when the opposing fork arrives. Checkpoint proteins phosphorylate replisome components to keep the replication fork competent and to prevent accumulation of abnormal structures. In budding yeast, Mec1 (ATR in mammals and Rad3 in *S. pombe*) and Rad53 (CHK2 in mammals and Cds1 in fission yeast) have been shown to prevent replisome disassembly and collapse (Cobb et al., 2003, 2005; Lucca et al., 2004).

Additionally, HR proteins play a crucial role in maintaining stability of the replication fork by protecting the newly synthesized strands from extensive resection by nucleases. Rad51 loading onto the newly replicated strands protects them from the action of the MRN complex and prevents chromosome fragmentation (Hashimoto et al., 2010). This has been demonstrated both in bacteria and eukaryotes (Chow and Courcelle, 2004; Schlacher et al., 2011). For example, Rad51-mediated fork reversal appears to be the universal response to fork arrest on encountering genotoxic stress in mammalian cells (Zellweger et al., 2015). Furthermore, it has been observed that forks arrested at barriers are more susceptible to breakage in the absence of HR proteins (Lomonosov et al., 2003). Conversely, it is also thought that reversed forks are structures that protect stalled

forks from cleavage by Mus81 (Neelsen and Lopes, 2015). The repair of stalled or regressed replication forks by cleavage runs the risk of having inappropriate recombination between the broken end of the fork and a homologous sequence somewhere else in the genome. The likelihood of that happening is high given the large proportion of repetitive sequences in eukaryotic genomes. It is hence unsurprising that nucleases, like Mus81, which have the ability to cleave stalled or regressed replication forks are strictly regulated (Froget et al., 2008). Thus HR proteins might play a role in maintaining stalled fork integrity so that merging of the arrested fork with the converging fork occurs without mishap (Carr and Lambert, 2013).

Another key element of fork preservation is the so-called Fork Protection Complex (FPC). Loss of components of the FPC results in uncoupling of the replication apparatus from the site of nucleotide incorporation following HU treatment (Katou et al., 2003).The FPC is comprised of two proteins: Timeless and Tipin in metazoans, Swi1 and Swi3 in *S. pombe*, and Tof1 and Csm3 in *S. cerevisiae.* It has been shown that the FPC associates with replication forks at the origins when replication is initiated and travels with the fork during replication, interacting with both chromatin and various replisome components (Leman and Noguchi, 2012; Noguchi et al., 2004). The FPC plays a vital role in normal DNA replication, as well as in helping replicate difficult-to-replicate genomic loci and aiding in replication fork pausing/stalling. One way the FPC is thought to aid fork stability is by coupling the DNA polymerases to the replicative helicase and thereby preventing excessive DNA unwinding in the absence of DNA synthesis which would result in extensive ssDNA formation (Jones and Petermann, 2012; Leman and Noguchi, 2012). Additionally, the FPC in fission yeast has been shown to have a role in inhibiting late-origin firing in response to DNA damage by

interacting with the Hsk1-Dfp1 complex (Matsumoto et al., 2005; Sommariva et al., 2005).

1.4.3 Pushing past the barrier: the role of accessory DNA helicases

In addition to the MCM2-7 helicase, the replisome contains other DNA helicases that have a critical role in displacing tightly bound non-histone DNA-protein complexes that might otherwise impede the advancing replication fork. In budding yeast, the 5'-3' helicase, Rrm3, which physically associates with the replisome through the leading strand DNA polymerase and/or PCNA, globally promotes replication of protein-bound DNA, particularly at difficult-to-replicate sites, such as the rDNA, centromere, and telomere (Azvolinsky et al., 2006; Ivessa et al., 2002, 2003; Schmidt et al., 2002). In fact, Rrm3 is required for preventing replication forks from pausing and/or breaking at an estimated 1,400 sites containing natural RFBs (including rDNA and tRNA genes, centromeres, telomeres, inactive replication origins, and transcriptional silencers) in the budding yeast genome (Ivessa et al., 2003). Beyond minimizing the frequency and/or duration of fork pausing, the importance of accessory helicases is underscored by their role in repressing the need for recombination-dependent restart of blocked replication forks, which could result in gross chromosomal rearrangements (Ivessa et al., 2003; Torres et al., 2004). The Rrm3 homolog in fission yeast is Pfh1, which has a similar role in promoting DNA replication through hard-to-replicate sites and suppressing genome instability (Sabouri et al., 2012; Steinacher et al., 2012).

1.4.4 Deliberate and accidental breakage of replication forks and BIR

DSBs can arise through replication fork run-offs at ssDNA nicks in the template DNA when they are encountered during leading strand synthesis (Harper et al., 2010). Alternatively, the structure-specific endonuclease Mus81-Eme1 can act on

a stalled or collapsed replication fork structure by cleaving it at the junction point to deliberately cause a one-sided DSB (Doe et al., 2002; Forment et al., 2011; Froget et al., 2008; Hanada et al., 2007; Regairaz et al., 2011). DNA damage like ICLs also arrest forks, which can be processed by nucleases (Long et al., 2011; Moriel-Carretero and Aguilera, 2010).

The accidentally or deliberately broken fork is repaired by HR, which is able to rebuild the replisome to allow the resumption of DNA synthesis, in a process termed Break Induced Replication (BIR), which has been studied most extensively in *S. cerevisiae* [Fig. 1.iv]. BIR was first identified as leading to the formation of long gene conversion tracts spanning hundreds of kilobases (kb) along a chromosome arm (Anand et al., 2013). The mechanism of BIR has been mostly dissected using systems in which a site-specific DSB is introduced by an inducible endonuclease such as HO or I-SceI (Bosco and Haber, 1998; Morrow et al., 1997). However, in most cases it has been studied outside the context of S-phase and, therefore, the majority of experiments do not directly address the problem of repair of a stalled or broken replication fork where there is a broken chromosome end and an intact sister chromatid.

Like canonical DSB repair, BIR begins with resection of the break to generate a 3’ ssDNA tail onto which RPA loads, followed by Rad52. Rad52 subsequently mediates the loading of Rad51, which catalyses homologous pairing and strand invasion, generating a D-loop. The 3’ end of the invading DNA can then prime DNA synthesis (Anand et al., 2013). Unlike canonical DSB repair, in BIR only one end of the chromosomal DSB shares homology with a template and, therefore, repair cannot proceed via SDSA or second end capture leading to the formation of a dHJ. Instead the strand invasion establishes a ‘replication fork’, consisting of a migrating D-loop that can duplicate large chromosomal regions by proceeding for

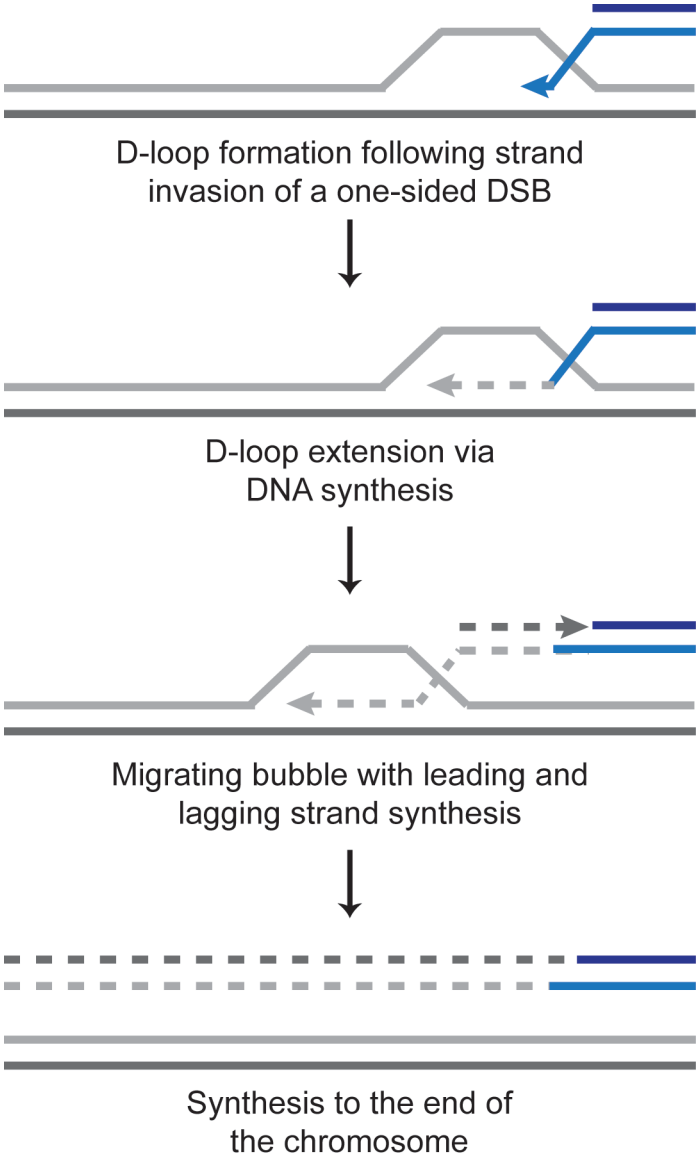


Fig. 1.iv The break-induced replication model.
BIR ensues when a one-ended DSB invades into a homologous DNA sequence. This leads to a migrating bubble that persists for potentially hundreds of kilobases down the length of the chromosome and to the end of the telomere. It results in conservative inheritance of the newly synthesized DNA. Newly synthesized DNA is depicted as dashed lines in the same colour as the template but a shade lighter; arrowheads indicate 3′ ends. Adapted from Mehta and Haber, 2014.

potentially hundreds of kilobases even to the end of a chromosome arm. Unlike, canonical DNA replication, BIR leads to conservative inheritance of newly synthesized DNA (Bosco and Haber, 1998; Donnianni and Symington, 2013; Morrow et al., 1997; Saini et al., 2013; Wilson et al., 2013). Repair by BIR results in loss of the chromosome arm distal to the break and its replacement with sequences downstream of the region of homology with the DSB site (Anand et al., 2013; Bosco and Haber, 1998). This can lead to loss of heterozygosity (e.g. loss of a wild type allele and expression of a recessive one), and chromosomal rearrangements, if the invading strand pairs with non-allelic sequences (Morrow et al., 1997).

Initiation of BIR synthesis requires Cdc45, loading of Mcm2-7 by Cdt1, the GINS complex, plus the initiation and elongation factors Mcm10, Ctf4, and Dpb11-Sld3 (Lydeard et al., 2010). BIR also requires both the leading and lagging strand replication machinery and the Pol32 subunit of Pol δ, which is not necessary for origin-derived replication (Lydeard et al., 2007, 2010). Unlike normal replication fork, progression of the migrating D-loop is dependent on the Pif1 helicase (Saini et al., 2013; Wilson et al., 2013).

While BIR and canonical DNA replication share a requirement for the key replisome components, and proceed with the same rate of DNA synthesis, there are some key differences between them. Unlike canonical replication, BIR is highly recombinogenic, at least for the first 10 kb following its initiation, owing to frequent template switching (Anand et al., 2013; Malkova et al., 2005; Smith et al., 2007). Moreover, the mutation rate during BIR is deemed to be 2800 times higher than that which occurs during canonical DNA replication. However, the “fork” eventually seems to mature as it moves along and template-switch associated mutations are not observed 10kb downstream of the point of initiation of BIR (Deem et al., 2011;

Smith et al., 2007). Potentially, Mus81 may play an important role in limiting template switching and “stabilizing” BIR by resolving the migrating D-loop into a “normal” replication fork (Mayle et al., 2015; Roseaulin et al., 2008). BIR events are initiated with a delay of about 4-6 hours. This delay reflects the cell’s attempt to mend the break by alternate means before embarking upon BIR (Jain et al., 2009).

1.4.5 Replication restart without DNA breakage

BIR is not the only method deployed by the cell to restart DNA replication. When a replication fork collapses but does not break, HR proteins can be engaged to restart replication in a process called recombination-dependent restart (RDR). The best studied example of break-independent replication restart in eukaryotes is the fission yeast protein-DNA barrier, *RTS1* (described in Section 1.2.4.3) (Ahn et al., 2005; Lambert et al., 2005). It is important to define how break-induced and break-independent replication restart compare.

Studies of the *RTS1* barrier have clearly demonstrated involvement of recombination proteins in the events induced by the block. Direct repeat recombination induced by *RTS1* placed at an ectopic locus between two *ade6* heteroalleles is dependent on both Rad51 and Rad52 (Ahn et al., 2005). Since most recombination events result in conservative gene conversion, breakage is unlikely to be responsible for them. Recruitment of Rad52 and Rad51 to *RTS1* has been demonstrated directly by ChIP analysis in the so-called *RuraR* system developed by Lambert and colleagues (Lambert et al., 2005). Here, induction of replication fork blockage resulted in increased Rad52 and Rad51 localization at the barrier and RTS1-induced recombination was fully dependent on Rad52. Replication restart at RTS1 has been shown to be semi-conservative, unlike BIR,

and requires Pol δ (Miyabe et al., 2015). Additionally, RDR is initiated during S-phase, approximately within 10 minutes of the fork being arrested, which is in stark contrast to BIR (Nguyen et al., 2015).

One often touted mechanism of RDR postulates that the collapsed fork is regressed or reversed and thereby converted into a chicken foot structure. A chicken foot is a four-way DNA junction that resembles a HJ where the two nascent strands are unwound from their templates and annealed to each other, whilst the parental DNA strands re-anneal (Higgins et al., 1976; Postow et al., 2001; Sogo et al., 2002). Resection of the reversed fork by the MRN complex or Exo1 is thought to generate a 3' ssDNA tail onto which Rad51 loads and catalyses the formation of a D-loop structure that provides a platform onto which replication proteins can reload and restart replication. DNA helicases/translocases, like Fml1, Rqh1, Fbh1 and Rad54, in vitro have been shown to promote fork regression and hence could promote RDR at *RTS1* (Atkinson and McGlynn, 2009; Bugreev et al., 2011; Fugger et al., 2015; Gari et al., 2008; Ralf et al., 2006; Sun et al., 2008; Whitby, 2010; Zheng et al., 2011). However, Rqh1, Srs2 and Fbh1 are involved in preventing ectopic recombination at the stalled fork (Ahn et al., 2005; Lorenz et al., 2009).

Recent studies have demonstrated that RDR caused by fork arrest is a "double-edged sword", which promotes cell viability at the expense of genome instability. Similar to BIR, forks restarted by HR are less stable and can lead to gross chromosomal rearrangements due to compromised fidelity. Firstly, there is an increase in non-allelic HR during the restart process and once restarted, the new "fork" is associated with heightened genome rearrangements and template switching within inverted repeats, at least within the first 2.4kb downstream of the

barrier (Iraqui et al., 2012; Mizuno et al., 2013). The source of this instability remains undetermined and will be discussed further in later chapters.

1.5 Aims of the study

It has been shown that forks blocked by protein-DNA barriers, like *RTS1,* result in 'fork collapse' and to induce DSB-independent RDR to rescue the replication fork, similar to BIR (Ahn et al., 2005; Lambert et al., 2005). However, recent work has shown that forks restarted by HR at *RTS1* are less stable and can lead to gross chromosomal rearrangements due to compromised fidelity, as measured within the first 2.4kb downstream of the barrier (Iraqui et al., 2012; Mizuno et al., 2013). The precise source of this instability has not been determined. It is also unclear whether the RDR-initiated fork suffers from the same tendency of D-loop dissociation as observed in BIR or whether it matures into a stable replication fork as it moves along.

The primary aim of my project was to characterise the error-prone nature of RDR induced by replication fork blockage at *RTS1*. I wanted to determine how far along the genomic instability induced by the restarted fork extends. I also wanted to identify factors that influence the genomic instability that is caused by restarted replication (see Chapter 3).

Much of our knowledge of how cells respond to replication fork collision with barriers comes from studies using *RTS1*. However, it is unclear whether the cell's response to *RTS1* is representative of what happens at accidental protein-DNA barriers. I address this question in the second major aim of my project, which is to compare what happens at *RTS1* with that at an accidental protein-DNA barrier. For this, I developed a novel site-specific barrier system (called MarBI) based on the human mariner transposase, *Hsmar1*, binding to its transposon end (see Chapters 4 and 5)

While studying the progression of restarted replication, and the role of fork convergence in curtailing the instability associated with it, I observed that deleting a single replication origin can lead to a localised region of genomic instability. The generality of this observation and possible explanations for it are explored and discussed in Chapter 6.

Chapter 2

Materials and Methods

2.1 Media

2.1.1 *Escherichia coli* media

E. coli was grown in Luria-Bertani (LB) (10g Tryptone, 5g yeast extract (YE), 5g NaCl per liter) broth or on LB-agar (15g/l agar) at 37°C unless otherwise stated. Media were supplemented with antibiotics where appropriate, namely ampicillin (final concentration 50µg/ml), kanamycin (final concentration 50µg/ml) and chloramphenicol (final concentration 20µg/ml) (Sambrook et al., 1989). Antibiotics were filtered (0.2µm Millipore syringe filters) and stored as 1000X stocks at 4°C (Sambrook et al., 1989).

2.1.2 *Schizosaccharomyces pombe* media

YE and YE supplemented with all the amino acids (YES) were used as complete media. Edinburgh Minimal Media with 3.7mg/ml L-glutamic acid monosodium salt (EMMG) (20ml 50X salts, 1ml 1000X vitamins, 0.1ml 10000X minerals, 30g D-Glucose, 3.7g sodium glutamate, 2.2g anhydrous Na_2HPO_4, 3g potassium hydrogen phthalate in 1liter water) was used as minimal media and supplemented with amino acids as appropriate at a concentration of 225mg/l (Sabatinos and Forsburg, 2010). When needed, 18g/l Difco™ agar was added to the media. *S. pombe* were grown at 30°C unless otherwise stated.

Strains that are auxotrophic for one or more of the following: uracil, leucine, lysine, histidine, arginine and/or adenine, require the respective supplements at 225mg/l for growth on minimal media. For selection of strains carrying antibiotic resistance, media was supplemented with geneticin (G418, final concentration 100mg/l), nourseothricin (clonNat, final concentration 100mg/l) or hygromycin B (final concentration 200mg/l).

To differentiate between *ade*$^+$ and *ade*$^-$ colonies, cells were plated onto low adenine (LA) medium containing 10mg/l adenine, which allows *ade*$^+$ colonies to appear white and *ade*$^-$ colonies red. In the recombination assays, *ade*$^+$ recombinants were selected for on YE media lacking adenine and supplemented with 200mg/l guanine, dissolved in 1M NaOH, to prevent uptake of residual adenine (Osman and Whitby, 2009).

To repress expression from the *nmt* promoter, 5nM to 4μM thiamine was added to EMMG as indicated. In order to obtain complete de-repression of the *nmt* promoter, cells were grown in EMMG with 0μM thiamine for a minimum of 50 hours at 30°C.

2.2 *S. pombe* strain construction

General molecular genetic techniques for *S. pombe* are based on established protocols (Sabatinos and Forsburg, 2010). The *S. pombe* strains used in this study and a brief description of their method of construction is described in Table 8-6.

2.2.1 *S. pombe* transformation

To integrate linear DNA constructs or expression plasmids, *S. pombe* was transformed by the established lithium acetate transformation protocol (Okazaki et al., 1990). Cells were washed three times with sterile Milli-Q water and resuspended in an equal volume of 0.1mM lithium acetate (pH 7.5) with TE (10mM Tris-HCl (pH7.5), 1mM EDTA (ethylenediaminetetraacetic acid)) in a 1:1 ratio. Between 1 to 10μg of linearised or plasmid DNA was mixed with 100μl of cells and incubated at room temperature for 10 minutes. 260μl of 0.1mM lithium acetate-TE and 40% polyethylene glycol (PEG) were then added to the mixture, which was then incubated at 30°C for 2 hours. 43μl of dimethylsulfoxide (DMSO) was added before the cells were heat-shocked at 42°C for 5 minutes. The transformed cells

were plated in 1:1, 1:10 and 1:100 dilutions, either directly onto selective media (for nourseothricin selection and/or auxotrophic markers) or plated onto complete media without antibiotics and incubated at 30°C for 48 hours before replica plating the transformants onto selective media (for geneticin and hygromycin B). Colonies were screened for correct integration of the DNA construct by colony polymerase chain reaction (PCR) (described in Section 2.2.3).

2.2.2 *S. pombe* crosses

Cells with opposite mating types (h^+/h^-) were mixed and grown on Malt Extract Agar (MEA) (30g malt extract, 20g agar in 1liter water (pH>5.5)) at 25°C for 2-5 days until asci formation was observed. The spores were released by overnight Glusulase (PerkinElmer) digestion at 30°C. The spores were washed in sterile Milli-Q water and plated onto the appropriate selection plate. Progeny were screened for appropriate genetic markers and genotoxin sensitivities, and their mating type was determined.

2.2.3 *S. pombe* colony PCR

Colony PCRs were performed to confirm accurate integration of linear DNA fragments into the *S. pombe* genome. Where possible, PCR primers were designed such that one primer anneals to the parental chromosome sequence flanking the target site while the second primer anneals within the inserted DNA.

Colony PCRs were performed by boiling a single colony of yeast, at 100°C for 2 minutes, to release the chromosomal DNA in a final reaction volume of 50µl. This was followed by amplification of specific DNA fragments, with Taq polymerase (New England Biolabs, Ipswich, MA) using the Hybaid (OmniGene, Woburn, MA) thermocycler. All colony PCRs were carried out alongside a wild-type negative control. Where necessary, the PCR products were sequenced to

confirm the presence or absence of point mutations. At least 6 independent transformants were subsequently tested for growth and genotoxin sensitivity to determine the reproducibility of the phenotype.

2.3 Molecular and cell biology techniques

2.3.1 Cloning and sub-cloning DNA

All restriction enzymes used in this study were supplied by New England Biolabs. Custom-made oligonucleotides for PCR amplification were supplied by Sigma-Aldrich (Dorset, England) and are listed in Table 8-8. PCR reactions were performed using a Biometra (Goettingen, Germany) thermocycler.

For plasmid construction, the appropriate DNA fragment was excised, or PCR-amplified with Phusion High-Fidelity DNA Polymerase (Thermo Scientific, Loughborough, UK), from the appropriate parental plasmid construct. Such DNA fragments were purified by 0.8-1.2% agarose gel eletrophoresis, followed by extraction from the gel using a QIAquick Gel Extraction Kit (Qiagen, Hiden, Germany). Fragments were ligated with suitably digested plasmid DNA using T4 DNA ligase (New England Biolabs), incubating at room temperature for a minimum of 2 hours or at 4°C overnight. Correctly constructed plasmids were verified by restriction digests and sequencing. The plasmids used in this study, together with a brief description of their method of construction, are described in Table 8-7.

2.3.2 *E. coli* transformation

Competent *E.coli* cells (DH5α or MACH1) were transformed with a minimum of 50 to 100ng plasmid DNA using a standard 42°C heat shock treatment for bacterial transformation (Sambrook et al., 1989). Cells were plated on LB medium with 50μg/ml ampicillin and grown at 37°C overnight. For mini and midi-scale plasmid

preps, the QIAScreen Miniprep protocol and QIAprep Spin Midiprep Kits (Qiagen) were used, respectively, following the manufacturer's instructions.

2.3.3 Alkaline lysis for protein extraction from *S. pombe*

Whole-cell extracts were prepared by the established protocol of protein extraction from fission yeast (Matsuo et al., 2006). Overnight logarithmically growing cultures were harvested, washed and resuspended in STOP buffer (5% 1MNaF, 3% 5M NaCl, 5% 0.2M EDTA (pH 8.0) and 0.01% sodium azide in sterile water). Following centrifugation at 3000 RPM for 3 minutes, the cells were resuspended in 0.3ml sterile water plus 0.3ml 0.6M NaOH and incubated at room temperature for 10 minutes. The cells were then pelleted at 1300 RPM for 30 seconds and washed with sterile water. The cells were then resuspended in SDS-PAGE loading buffer (60mM Tris-HCl (pH6.8), 4% β-Mercaptoethenol, 4% Sodium Dodecyl Sulphate (SDS), 0.01% Bromophenol Blue and 5% Glycerol) and lysed by boiling at 100°C for 3 minutes.

2.3.4 SDS-PAGE and Western Blotting

Cell lysates were prepared as described in Section 2.3.3. The lysate was resolved on 10% SDS-polyacrylamide gels (Mini-PROTEAN 3 Cell, Bio-Rad Laboratories, Hercules, CA), alongside a pre-stained protein marker (ColourPlus Prestained Protein Marker, Broad Range, New England Biolabs). The gels were run at a constant voltage of 60V for approximately 1 hour and subsequently processed for western blotting.

The protein gels were electro-blotted onto Trans-Blot transfer medium membranes (Bio-Rad Laboratories) using the Bio-Rad mini trans blot system (Mini-PROTEAN 3 Cell, Bio-Rad) at a 100V for 1 hour. The blots were blocked at room temperature in TBST-blocking buffer (5% milk powder, 2.5% Bovine Serum

Albumin (BSA), 1.8% lysine in Tris-buffered saline with 1% Tween20) for 1 hour. They were probed with an anti-GFP antibody (G6539-Sigma; dilution 1:2000 in TBST-blocking buffer) or with anti-tubulin (T9026-Sigma; dilution 1:2000 in TBST-blocking buffer) as a loading control. Primary antibodies were incubated overnight at 4°C with gentle rocking. The blots were subsequently incubated with an appropriate secondary antibody conjugated to horseradish peroxidase at a dilution of 1:20,000 in TBST-blocking buffer for 1 hour at room temperature. Following both primary and secondary antibody incubations, the membrane was washed three times (10 minutes each) with 1XTBST. The proteins were detected using Amersham ECL Western Blotting Detection Reagents (GE Healthcare UK Ltd., Little Chalfont, UK). Membranes were then exposed to Super RX medical X-ray film (Fujifilm, Tokyo, Japan).

2.3.5 Microscopy

For time-lapse imaging, the cells were grown at 30°C in EMMG lacking histidine (0μM thiamine) for a minimum of 54 hours to ensure complete de-repression of the *nmt* promoter. Cells were mounted with soybean lectin (Sigma-Aldrich) in a glass bottom culture dish (MatTek Corp., Ashland, MA) and observed in the appropriate medium in a thermally insulated temperature-controlled chamber at 30°C. Live cells were imaged on an inverted Olympus IX71 microscope controlled by a DV Elite Core using DeltaVision SoftWoRx 5.5.0 software (Applied Precision Inc., Issaquah, WA). Images were taken using either the CFP/YFP/mCherry or GFP/mCherry filters with an Evolve^{TM} 512 EMCCD camera (Photometrics, Tuscon, AZ) using an oil-immersed Olympus 100X UPlanSApo objective with a NA of 1.40. A stack of 16 focal planes at a step-size of 0.3μm was taken at an interval of 5 minutes for 4 hours. Brightfield images of the cells were imaged with a 100ms exposure time and 10% neutral density filter. LacI-tdKatushka2, Rad52-YFP and

Rad54-GFP were imaged with a 100ms exposure time and 5% neutral density filter.

2.4 DNA analysis

2.4.1 *S. pombe* genomic DNA extraction

Small-scale preparations for PCR or southern blot analyses were made from 10ml overnight *S. pombe* cultures. Harvested cells were spheroplasted by incubating in 1ml of Citrate Phosphate buffer (40mM EDTA, 50mM Na_2HPO_4, 55mM citric acid and 1.2M sorbitol) containing 2.5mg of Zymolyase 20T (MP Biomedical) for 1 hour at 37°C. The efficiency of spheroplasting was assessed by microscopic examination of cells mounted in 2% SDS. Spheroplasts were resuspended in 550µl TE (10mM Tris-HCl (pH 8.0), 1mM EDTA) with 1% SDS and incubated at 65°C for 1 hour. 175µl of 5M potassium acetate was then added and the sample was centrifuged at 13000 RPM for 15 minutes at 4°C. 450µl of the supernatant was retained and the DNA was precipitated by adding 200µl of 5M ammonium-acetate and 1ml isopropanol. After pelleting the DNA by centrifugation at 13000 RPM for 30 minutes at 4°C, the DNA was resuspended in 90 µl 1XTE containing 1µg/µl RNase A and incubated at 37°C for 1 hour. The DNA precipitation step was repeated and the DNA was washed with 70% ice-cold ethanol. The DNA was resuspended in 1XTE and stored at -20°C.

2.4.2 Genomic DNA extraction embedded in agarose plugs

To isolate intact chromosomal DNA for running 1D and 2D gels, 500ml asynchronous cultures of *S. pombe* were grown overnight at 30°C to a concentration of 1 X 10^7 cells/ml. In the case of strains containing MarBI, cells were grown for a minimum of 50 hours to ensure complete de-repression of the *nmt* promoter. Cells were then killed by the addition of 0.1% sodium azide (Sigma-

Aldrich) and washed with sterile Milli-Q water. The cells were stored at -80°C at this point.

Subsequently, the cells were spheroplasted in an equal volume of CPES buffer (40mM EDTA, 120mM Na_2HPO_4, 40mM citric acid, 1.2M sorbitol, 5mM DTT) containing 10mg/ml *Trichoderma harzianum* lysing enzymes (L-1412, Sigm-Aldrich) and 0.625mg/ml *Arthrobacter luteus* lyticase (L-4025, Sigma-Aldrich) for 1 hour at 37°C. The spheroplasted cells were embedded in 1.2% agarose plugs as described by Hyppa & Smith (2009), using Bio-Rad Low Melt Agarose (Bio-Rad). To degrade the proteins, the plugs were incubated for two days in 3ml NDS buffer (495 mM EDTA, 10 mM Tris-HCl (pH 7.5), 1% N-lauroylsarcosine) containing 1mg/ml Proteinase K at 50°C. To inactivate residual Proteinase K activity, the plugs were incubated in 10ml 1XTE with 0.5mM PMSF on a rocking platform for 1 hour at room temperature. They were then subsequently washed three times in 15ml 1X TE for 1 hour each on a rocking platform before being stored in 1X TE at 4°C.

2.4.3 One-dimensional (1D) gel electrophoresis – for the detection of DNA double-strand breaks.

Following genomic DNA extraction in agarose plugs (as described in Section 2.4.2), plugs containing equivalent of 0.5 X 10^9 cells (approximately $1/3^{rd}$ of the total number of plugs made) were washed three times with copious amounts of sterile Milli-Q water to get rid of the 1X TE buffer used for storage. Next, the plugs were washed three times with 1X CutSmart Buffer (New England Biolabs), melted at 65°C for 10-15 minutes and then incubated with 2.5µl of β-agarase I (New England Biolabs) for 2 hours at 42°C for complete digestion of the agarose. The genomic DNA was then incubated with 5µl (100 units) of NdeI and 5µl of RNaseA (10mg/ml) overnight at 37°C. The next day, the incubation mixture was

supplemented with 2µl (40 units) of NdeI and further incubated overnight at 37°C. The following day, the reaction was then centrifuged at 4000 RPM for 15 minutes at room temperature to get rid of the agarose. The supernatant containing the digested genomic DNA was stripped of residual proteins by passing it through one round of phenol:chloroform:isoamyl alcohol (25:24:1) extraction. The DNA was then precipitated by the addition of one volume of isopropanol and 1/10th volume of 3M sodium-acetate overnight at -20°C. After pelleting the DNA by centrifugation at 13000 RPM for 30 minutes at 4°C, the DNA was washed twice with 70% ice-cold ethanol. The DNA was resuspended in 25µl of 1X TE at 4°C over a period of 2 days.

Following this, ~10µg of digested DNA was loaded onto a 1% agarose gel and run in 1X TBE for ~18 to 20 hours at 50V at room temperature. The gel was stained with 0.3µg/ml ethidium bromide for 1 hour to visualize the DNA and then southern blotted (as described in Section 2.4.5).

2.4.4 Two-dimensional (2D) gel electrophoresis – for analysing replication intermediates

The method of DNA preparation and the neutral-neutral 2D gel electrophoresis has been previously established (Brewer and Fangman, 1987). Digestion of the genomic DNA in plugs was carried out in a similar manner as described in 2.4.3 except that plugs containing equivalent of 1.5 to 2 X 10^9 cells were used. The DNA was digested with 200 units of the respective restriction enzyme and 10µl of RNaseA (10mg/ml) overnight and supplemented with 50 units of the enzyme on the following day. The DNA was resuspended in 40µl of 1X TE at 4°C over a period of 2 days.

In the first dimension, DNA fragments were separated on the basis of their size by running on a 0.4% agarose gel in 1X TBE without ethidium bromide to

ensure uninterrupted migration. The first dimension was run for ~48 hours at 25V at room temperature. The gel was stained with 0.3µg/ml ethidium bromide for 1 hour to visualize the DNA. The slice containing the DNA fragments of interest was excised and DNA from this slice was then run in the second dimension in a 1.2% agarose gel in 1X TBE with 0.3µg/ml ethidium bromide under continuous buffer (1X TBE with 0.3µg/ml ethidium bromide) recirculation at 4°C to separate the intermediates on the basis of their shape. The second dimension was run for ~18 hours at 120V, until the dye front had migrated at least 8cm. This was followed by Southern blotting as described below (Section 2.4.5).

2.4.5 Southern blotting

Before blotting, gels were gently shaken at room temperature in 0.25M HCl for 15 to 20 minutes to depurinate the DNA and then in transfer buffer (0.5M NaOH, 1.5M NaCl) for 10 minutes. DNA was transferred from the gels onto positively-charged nylon membranes (Hybond^{TM}-XL, GE Healthcare) by capillary transfer (Sambrook et al., 1989). After dismantling the blot, membranes were briefly washed with 2x saline sodium citrate (SSC) (0.3M sodium citrate, 0.03M NaCl buffer) and stored at -20°C. Pre-hybridization was done at 55°C for 60 minutes in modified Church and Gilbert Buffer (0.5M Phosphate buffer (pH 7.2), 7% SDS, 10mM EDTA). Hybridization was performed at 55°C overnight as described in Sambrook & Russell (2001) in a Grant Boekel hybridization oven (HIR10M). Bands of interest were detected by radiolabeling the appropriate probe with [α-^{32}P]dCTP (PerkinElmer) using an Amersham^{TM} Rediprime II Random Prime Labeling System kit following the manufacturer's instructions. Probe A is an EcoNI-XbaI restriction fragment from pFOX2 (Ahn et al., 2005). Probe D is a DNA fragment amplified from genomic DNA by PCR using primers oMW706 and oMW707 (Ahn et al., 2005). Probe E is an BlpI-NdeI restriction fragment from pFOX2 (Osman et al.,

2016). Following one wash with 1X SSC and 0.1% SDS and another wash with 0.5X SSC and 0.1% SDS, both at 55°C for 20 minutes, probed membranes were exposed to phosphor-screens for up to one week, which were then scanned using a Fuji FLA-3000 phosphorimager (FujiFilm) and analysed using Image Gauge software (FujiFilm).

2.5 Genetic assays

2.5.1 Viability spot assay

For the viability spot assay, cells were grown in EMMG at 30°C to mid-exponential phase and were then harvested, washed and resuspended in sterile Milli-Q water to an initial concentration of 1 X 10^7 cells/ml. The suspension was serially diluted in five-fold steps to 1 X 10^3 cells/ml and 10µl aliquots of each suspension was spotted onto an EMMG plate. The cells were photographed after 4 days of growth at 30°C. In the case of MarBl-containing strains, cells were plated onto EMMG plus and minus 4µM thiamine to compare growth with and without Mar expression.

2.5.2 Genotoxin sensitivity spot assay

Exponentially growing cells from liquid culture were harvested, washed and resuspended in sterile Milli-Q water to an initial concentration of 1 X 10^7 cells/ml. Subsequent 10-fold dilutions were performed from 1 X 10^6 to 1 X 10^4 cells/ml. Aliquots (10µl) of the cell suspensions were spotted onto YES plates containing appropriate concentrations of chemical genotoxins (MMS, HU, CPT) or onto YES plates that were then irradiated with various doses of UV light using a Stratalinker (Stratagene). Plates were typically incubated at 30°C for up to 4-5 days, with growth being recorded daily by taking photographs of the plate. The spot assays reveal relative differences in survival and growth following a single (acute) exposure to UV or prolonged (chronic) exposure to MMS, HU and CPT, which

generate DNA lesions that can variously cause replication fork stalling, blockage and breakage.

2.5.3 Direct repeat recombination assay

The mitotic direct-repeat recombination assay was performed according to the previously established protocol (Osman and Whitby, 2009). The cells were initially grown on YES or appropriately supplemented EMMG, lacking thiamine (for MarBI-containing strains), plates for 5 to 6 days at 30°C. 10-20 single colonies from these were then resuspended in sterile Milli-Q water. Approximately 10^4-10^6 cells were plated onto YE plates lacking adenine to score for *ade*$^+$ recombinants and 10^2-10^3 cells were plated onto non-selective plates of YE to assess cell viability. The frequency of the recombinants was calculated by counting the colonies after growth for 4 to 6 days at 30°C. Plates with *ade*$^+$ recombinants were then replica-plated onto minimal media lacking both histidine and adenine to estimate the proportion of gene conversions. For strains with the direct-repeat reporter at Site II (12.4 kb away from the endogenous *ade6* locus), where expression of adenine in recombinants with a gene deletion is poor, YE plates lacking adenine were incubated for 8 to 10 days at 30°C to ensure that *ade*$^+$ colonies had sufficient time to grow.

2.6 Data Analysis

2.6.1 Image Processing and analysis

Raw images collected on the DV Elite Core were subsequently denoised with Priism with the dimensionality set to “3D: xyz” for three iterations (Kervrann and Boulanger, 2006). Denoised images were then deconvolved with softWoRx 5.5.0 software with the “additive” method for 12 cycles (Applied Precision). Foci were scored manually and separately for each of the fluorescent channels. Foci were

distinguished from background as being at least three to five times brighter in intensity and having a minimum volume of 2X2 pixels. Perfect co-localisation was manually assessed and scored as foci in separate channels overlapping in xyz by a minimum of 2 pixels. Another class of co-localisation was defined as ‘adjacent’ if there was a maximum of 1pixel distance between the foci.

2.6.2 Statistics

All statistical tests were performed using GraphPad Prism version 6.0 for Macintosh (GraphPad Software, La Jolla California, USA). Data were tested for normal distribution by the Shapiro-Wilk normality test. In accordance with the distribution of data, means were compared by the appropriate independent-sample two-tailed T-test. *P* values below 0.05 (5% significance interval) were considered significant and below 0.01 (1% significance interval) were highly significant

Chapter 3

Investigating the fidelity and genetic requirements of replication restart from a programmed protein-DNA barrier

3.1 Introduction

Our lab has previously shown that replication fork blockage at *RTS1* induces HR between direct repeats of *ade6*$^{-}$ heteroalleles positioned at the endogenous *ade6* locus (Site I) on ChrIII in *S. pombe* [Fig. 3.i.b] (Ahn et al., 2005). The direct repeat reporter consists of two loss-of function *ade6*$^{-}$ heteroalleles, with a single point mutation in each (*ade6-M375* and *ade6-L469*), and an intervening *his3*$^{+}$ gene. An Ade^{+} cell can arise if there is ectopic recombination between the *ade6*$^{-}$ alleles that restores wild-type function to at least one of them, and this can be scored using a plating assay (see Section 2.5.3). There are two classes of recombinants, gene conversions (Ade^{+} His^{+}) and deletions (Ade^{+} His^{-}) [Fig. 3.i.a]. As this assay only scores for functional Ade^{+} recombinants it does not measure all recombination events, many of which will be genetically silent. Nonetheless, it provides a robust readout for a proportion of recombination events from which the prevalence of overall recombination activity at the site can be inferred (Osman and Whitby, 2009).

RTS1 is a unidirectional programmed RFB that consists of cis-acting DNA sequence elements and trans-acting factors that interact with it creating the barrier, including the myb domain-containing protein Rtf1 (Codlin and Dalgaard, 2003; Eydmann et al., 2008). Replication across the *ade6* locus is virtually unidirectional due to the presence of a cluster of early firing strong replication origins located on its telomere proximal side [Fig. 3.i.a]. As a consequence, only one orientation of *RTS1* induces replication fork blockage at this site, which is referred to as the active orientation (AO). The opposite orientation, which is permissive to the uninterrupted passage of replication forks, is called the inactive orientation (IO). At site I, when *RTS1-AO* is positioned between the direct repeats, there is ~98 fold stimulation in gene conversions and ~30 fold increase in deletions

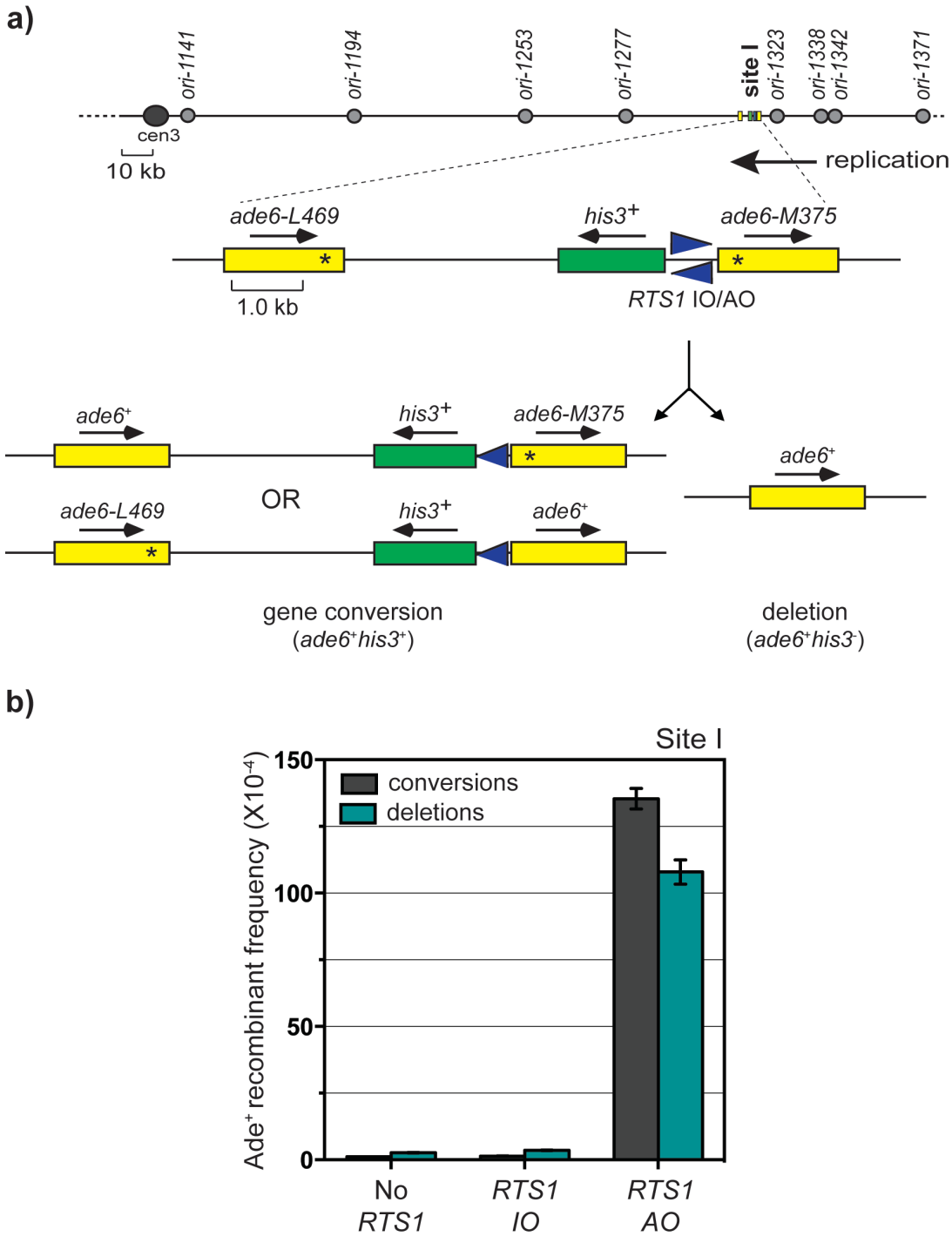


Fig. 3.i Effect of replication fork blockage by *RTS1* on direct repeat recombination at the endogenous *ade6* locus on ChrIII.

a) Schematic showing the relative position of the *ade6*$^-$ intra-chromosomal recombination substrate flanking the *his3*$^+$ gene and the polar *RTS1* RFB in relation to nearby replication origins (grey circles) on ChrIII. The genomic locations of the origins are according to OriDB, a DNA replication origin database (Nieduszynski et al., 2007). Asterisks indicate the position of the point mutations in *ade6-L469* and *ade6-M375*. Replication across the *ade6* locus occurs in the telomere to centromere direction as indicated by the arrow. Possible *ade6*$^+$ recombinant products that may arise spontaneously, or be induced by blockage of the replication fork, are either gene conversions or deletions. b) Bar chart showing the frequency of Ade$^+$ recombinants in strains with no *RTS1*, *RTS1-IO* (permissive orientation) and *RTS1-AO* (blocking orientation) at the endogenous *ade6* locus (site I). The strains are MCW429*, MCW4712* and MCW4713*. Error bars represent ± standard error of the mean.

as compared to *RTS1-IO* [Fig. 3.i.b & Table 8-1] (Ahn et al., 2005). Native 2D gel electrophoresis analysis of replication intermediates in an EcoNI fragment containing *RTS1* confirms that *RTS1-AO* strongly blocks the passage of replication forks [See Chapter 4, Fig. 4.viii.a & b]. It also shows that the forks are blocked long enough at the barrier for replication to be completed by the opposing fork resulting in fork merging, indicated by the accumulation of double Y-shaped DNA molecules [See Chapter 4, Fig. 4.viii.b & c]. The presence of large Y-shaped molecules indicate that a portion of forks restart and replicate past the barrier [See Chapter 4, Fig. 4.viii.b & c]. Based on this 2D gel analysis, it has been estimated that approximately half the forks blocked at *RTS1* restart before fork convergence can occur (Nguyen et al., 2015).

Thus, replication fork blockage at *RTS1* has been shown to elicit DSB-independent RDR seemingly as a default response, even though it is not critical for cell viability (Ahn et al., 2005; Lambert et al., 2005, 2010; Nguyen et al., 2015). However, RDR appears to be a double-edged sword. Like BIR, *RTS1*-induced RDR has been shown to be error-prone, inducing genome instability by performing U-turns at small inverted repeats positioned within the first 2.4 kb downstream of the barrier (Mizuno et al., 2013). The aim of this study was to further investigate whether this property of the restarted fork was due to a tendency for it to collapse and undergo further rounds of recombination.

3.2 Results

3.2.1 Establishing a system for monitoring direct repeat recombination downstream of a barrier

To determine whether restarted DNA replication can cause elevated levels of direct repeat recombination, the *RTS1* barrier was re-positioned 0.2 kb upstream of the *ade6*$^{-}$ heteroalleles such that the replication fork would be blocked by *RTS1*-

AO before it enters the region of homology. The frequency of Ade$^+$ recombinants was measured at this site [Fig. 3.iii.a : site I]. With *RTS1-IO*, the recombinants were similar to the background level of spontaneous recombination; however, when *RTS1-AO* is present, the total recombinants increase by ~134 fold and ~3.3 fold more than when the barrier is positioned between the *ade6*$^-$ repeats [Fig. 3.iii.b & Table 8-1] (Nguyen et al., 2015). More than 80% of these are deletion events but there is also a substantial increase (~89 fold) in gene conversions over the spontaneous level. Unlike deletions, which can be formed in a Rad51-independent manner, gene conversions require Rad51 to catalyse the strand invasion of the donor duplex DNA by a homologous ssDNA tail (Doe and Whitby, 2004; Lorenz et al., 2009). Thus, the increase in gene conversions observed indicates that the restarted fork must suffer disengagement of the newly synthesised strand to facilitate HR. This is similar to BIR which has been shown to be prone to template-switching within the first 10 kb from a DSB (Smith et al., 2007).

To determine if the restarted fork remains prone to recombination as it moves away from *RTS1*, a series of strains were made in which the *ade6*$^-$ reporter was re-positioned at sites downstream of the endogenous *ade6* locus [Fig. 3.ii.a : 12.4 kb (site II); 35 kb (site III); 75 kb (site IV); and 140 kb (site V)]. The correct integration of the reporters was confirmed by Southern blot analysis [See Appendix Fig. 8.i] and their spontaneous level of recombination was determined to confirm whether local chromatin architecture influenced recombinant frequency [Fig. 3.ii.b & Table 8-1]. The total recombinant frequency was similar at each site, and also comparable to that at site I (the endogenous *ade6* locus). However, the ratio of gene conversions to deletions was markedly different at site II and III

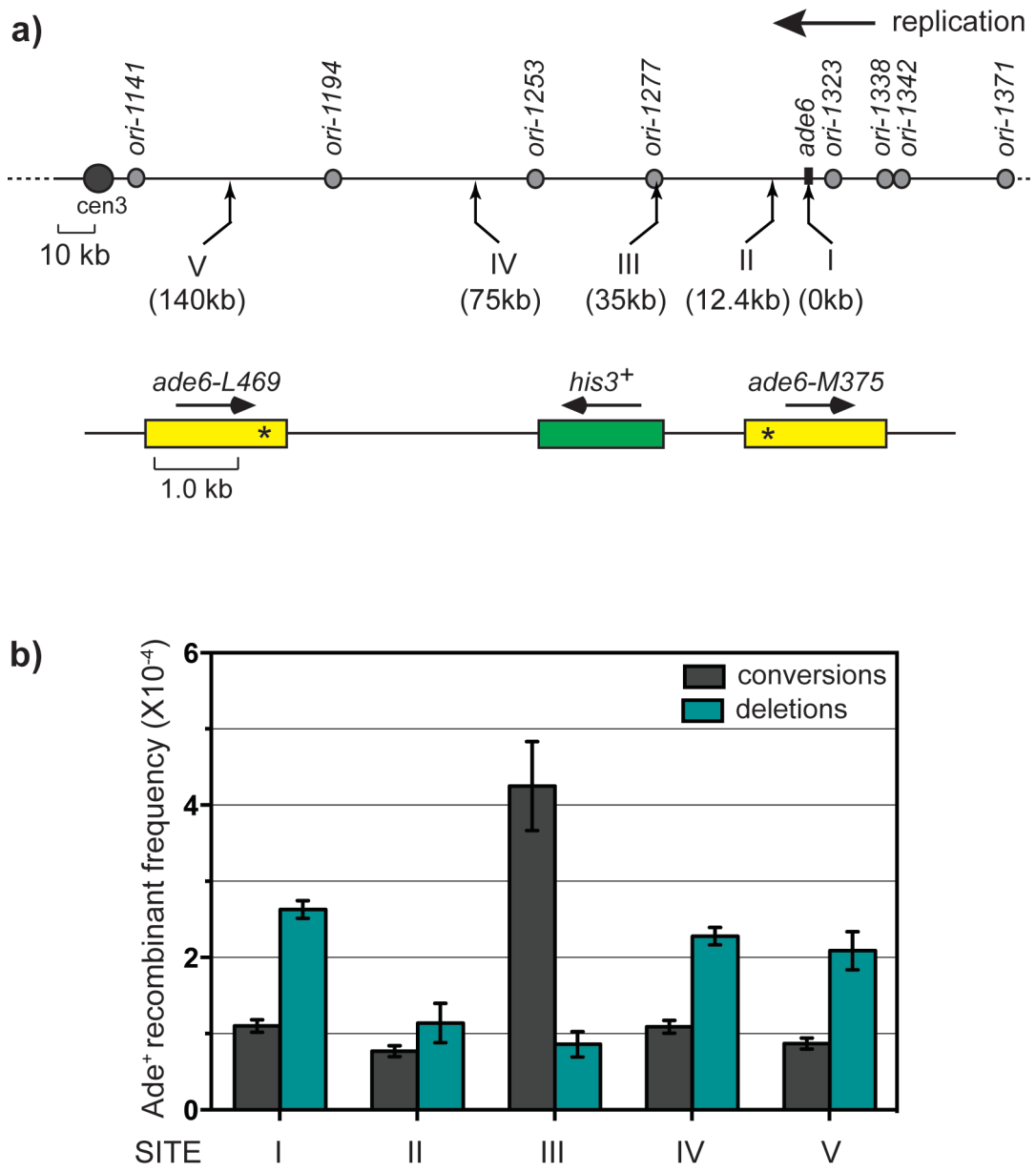


Fig. 3.ii Spontaneous direct repeat recombination measured at different positions on ChrIII.

a) Schematic showing the relative positions on ChrIII where the *ade6*- reporter (shown in the bottom panel) is inserted at and downstream of the *ade*6 gene at its endogenous locus. The sites I to V are marked on the chromosome arm and their relative distance from the endogenous *ade6* locus is indicated. The genomic locations of the origins are according to OriDB, a DNA replication origin database (Nieduszynski et al., 2007). b) Bar chart showing the spontaneous frequency of Ade+ recombinants at these sites. The strains are MCW429*, MCW7229, MCW7429, MCW7430 and MCW7297. Error bars represent ± standard error of the mean.

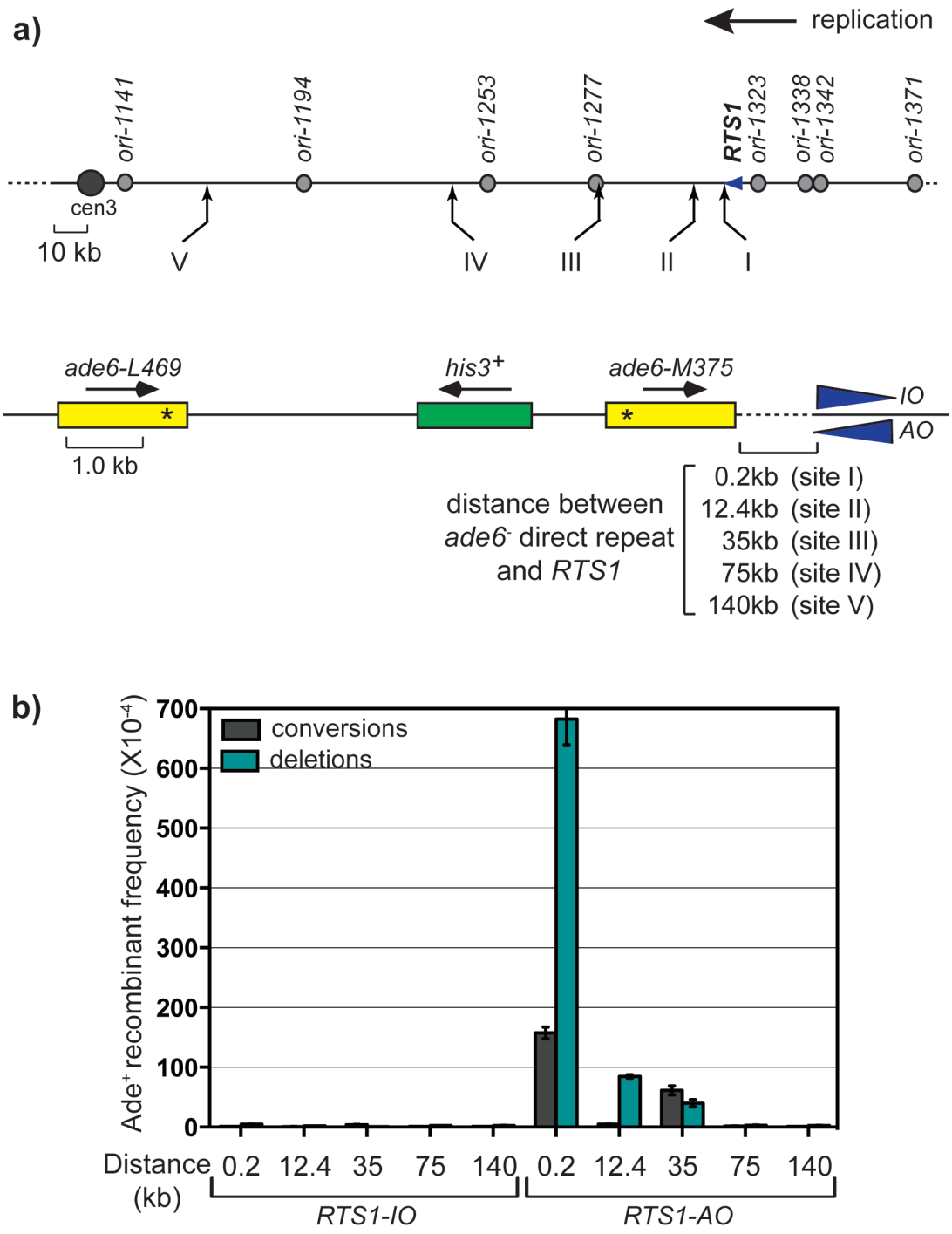


Fig. 3.iii Direct repeat recombination downstream of *RTS1*.
a) Schematic showing the relative positions on ChrIII where the *ade6*- reporter (shown in the lower panel) is inserted downstream of the *ade*6 gene at its endogenous locus. The endogenous *ade6* gene is deleted and *RTS1* is inserted either before the reporter (site I) or replaces the *ade6* gene at its endogenous locus (site II-V). The genomic locations of the origins are according to OriDB, a DNA replication origin database (Nieduszynski et al., 2007). b) Bar chart showing the frequency of Ade+ recombinants in strains MCW7131 (site I), MCW7257 (site II), MCW7565 (site III), MCW7614 (site IV), MCW7326 (site V), MCW7133 (site I), MCW7259 (site II), MCW7567 (site III), MCW7616 (site IV) and MCW7328 (site V). Error bars represent ± standard error of the mean.

compared to other sites. Presumably these differences are due to local chromatin architecture, which is known to influence recombination outcomes (Bethke and Golin, 1994; Lang and Murray, 2011; Smith and Aladjem, 2014).

Having established strains with the *ade6*$^{-}$ reporter downstream of the site of the endogenous *ade6* locus, I next positioned the *RTS1* element in place of the endogenous *ade6* gene and determined what effect this would have on direct repeat recombination at the various downstream sites [Fig. 3.iii.a]. At site II (12.4 kb distance between *ade6*$^{-}$ repeats and *RTS1*), while the frequency of recombination with *RTS1-IO* was comparable to the spontaneous level, with *RTS1-AO* there was an increase of ~31 fold over the spontaneous level [Fig. 3.iii.b & Table 8-1] (Nguyen et al., 2015). The majority of recombinants at this site (~95%) were deletions, similar to what was observed at site I with *RTS1*-AO positioned 0.2 kb upstream. However, there was a noticeable increase (~6-fold) in gene conversions, which is indicative of Rad51-dependent recombination. A similar trend was seen at site III (35 kb distance between *ade6*$^{-}$ repeats and *RTS1*), with *RTS1-AO* inducing a ~23 fold increase in recombination over the spontaneous level [Fig. 3.iii.b & Table 8-1]. At site IV (75 kb distance between *ade6*$^{-}$ repeats and *RTS1*) and site V (140 kb distance between *ade6*$^{-}$ repeats and *RTS1*) spontaneous levels of recombination were observed even in the presence of *RTS1-AO*, and this is likely due to the fact that these regions get replicated by canonical replication forks initiated from near-by origins (i.e. *oriIII-1194* and *oriIII-1253*) before the restarted replication fork reaches them [Fig. 3.iii.b & Table 8-1].

3.2.2 Effect of delaying replication fork merging on direct repeat recombination downstream of a barrier

Template switching that is associated with restarted replication appears to decrease as the fork moves away from the point of initiation (Mizuno et al., 2013;

Smith et al., 2007). Hence, the decrease in recombination observed as the reporter was moved from site I to site IV could be explained by the restarted fork undergoing some kind of maturation as it progresses away from the barrier, rendering it less error-prone. Alternatively, the reduction in recombination could be a consequence of replication fork convergence curtailing restarted replication and, therefore, preventing the restarted fork from reaching these distant sites.

To investigate this, the strongest origin in this chromosomal region (*oriIII-1253*) was deleted and recombination at site II was re-measured [Fig. 3.iv.a]. Intriguingly, with *RTS1-AO* present, the frequency of gene conversions increased by ~57 fold and deletions by ~236 fold, which is ~12 fold higher than in the comparable strain containing *oriIII-1253* [Fig. 3.iv.b & Table 8-1]. This indicates that it is replication fork convergence that is limiting the frequency with which restarted forks reach site II and, therefore, the amount of direct repeat recombination that is induced. To provide further support for this notion, I next assessed whether deleting *oriIII-1253* would result in heightened levels of recombination at site IV when *RTS1-AO* was present [Fig. 3.iv.a]. Indeed, in a strain with *oriIII-1253* deleted and *RTS1-AO* present, a ~5 fold increase in recombination at site IV was measured compared to when *RTS1* was absent [Fig. 3.iv.b & Table 8-1]. This suggests that the restarted fork may remain liable to stimulating recombination indefinitely, only being curtailed by fork convergence.

3.2.3 Rad51 and Rad52 are essential for direct repeat recombination downstream of *RTS1* but not cell viability.

Our lab has previously shown that the induction of recombination between the direct repeats, when they flank *RTS1* at site I, is dependent upon Rad51 and Rad52 [Fig. 3.v.b & Table 8-1] (Ahn et al., 2005). Recent work, based on 2D gel

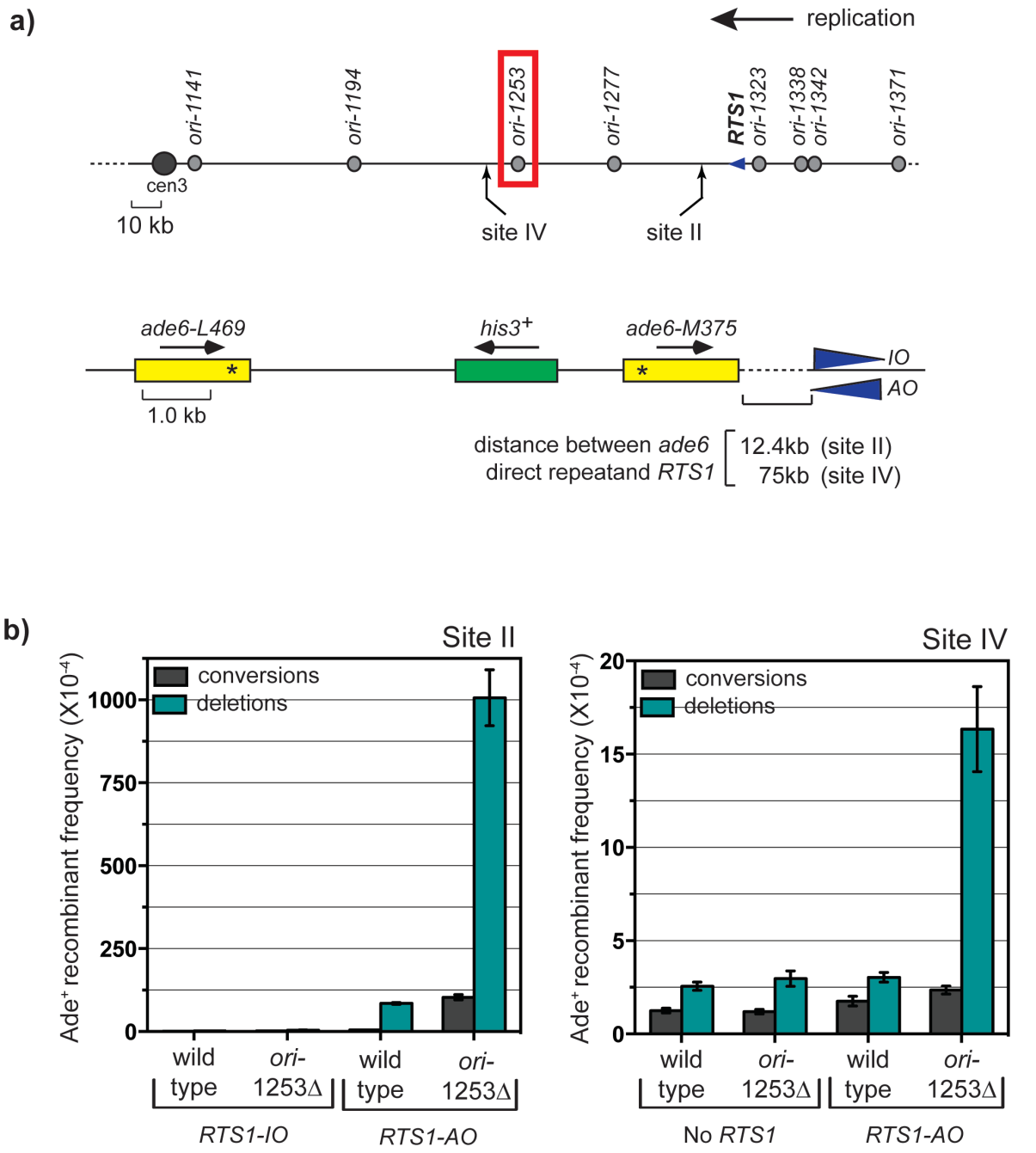


Fig. 3.iv The incoming replication fork curtails recombination downstream of *RTS1*.

a) Schematic showing the relative positions on ChrIII where the *ade6*$^-$ reporter (shown in the bottom panel) is inserted downstream of *RTS1* which replaces the *ade6* gene at its endogenous locus. b) Bar chart showing the frequency of Ade$^+$ recombinants in strains with and without *oriIII-1253* at site II and site IV. The strains used are MCW7257, MCW72293, MCW7259, MCW7295, MCW7614, MCW7987, MCW7616 and MCW7620. Error bars represent ± standard error of the mean.

analysis, has also implicated Rad52 in promoting restart past *RTS1* both with and independent of Rad51 (Lambert et al., 2010; Nguyen et al., 2015). From the recombination frequencies observed so far, it is also evident that at least some of the recombination downstream of the barrier is due to Rad51 [Fig. 3.iv & Table 8-1].

To verify that the observed direct repeat recombination downstream of *RTS1-AO* is dependent on Rad51 and Rad52, the recombination frequency at site II was measured in both *rad51Δ* and *rad51Δrad52Δ* mutants [Fig. 3.v.a]. As expected, virtually all gene conversions were dependent on Rad51 [Fig. 3.v.b & Table 8-1]. Deletions were also largely abolished in a *rad51*Δ mutant. Importantly, the residual levels of deletions in a *rad51*Δ mutant are essentially the same with either *RTS1-AO* or *RTS1-IO* [Fig. 3.v.b & Table 8-1]. This is consistent with the known spontaneous hyper-recombination of a *rad51*Δ mutant, which is dependent on Rad52 (Ahn et al., 2005; Doe et al., 2004). Together these data show that Rad51 is needed for essentially all of the increased direct repeat recombination associated with restarted replication at site II. Its requirement indicates that it promotes one or more of the following processes: 1) the initial restart past the barrier; 2) progression of the restarted fork; and 3) template switching of the restarted fork.

Previous studies have shown that both Rad51 and Rad52 are needed to maintain cell viability following fork blockage at *RTS1* when positioned at the *ura4* locus on ChrIII (Lambert et al., 2005, 2010). To see if the same is true for *RTS1* positioned at the *ade6* locus, the growth/viability of wild-type and *rad51*Δ and *rad51Δrad52Δ* mutant strains, containing either *RTS1-AO* or *RTS1-IO* positioned at the endogenous *ade6* locus, was compared [Fig. 3.vi]. Neither the wild-type nor

Fig. 3.v Rad51 and Rad52 are essential for direct repeat recombination downstream of *RTS1.*

a) Schematic showing the relative positions on ChrIII where the *ade6*$^{-}$ reporter (shown in the bottom panel) is inserted downstream of *RTS1* which replaces the *ade6* gene at its endogenous locus. b) Bar chart showing the frequency of Ade^{+} recombinants in MCW 4712*, MCW1691*, MCW1695*, MCW7257, MCW7812, MCW7816, MCW4713*, MCW1692*, MCW1696*, MCW7259, MCW7814 and MCW7818. Error bars represent ± standard error of the mean.

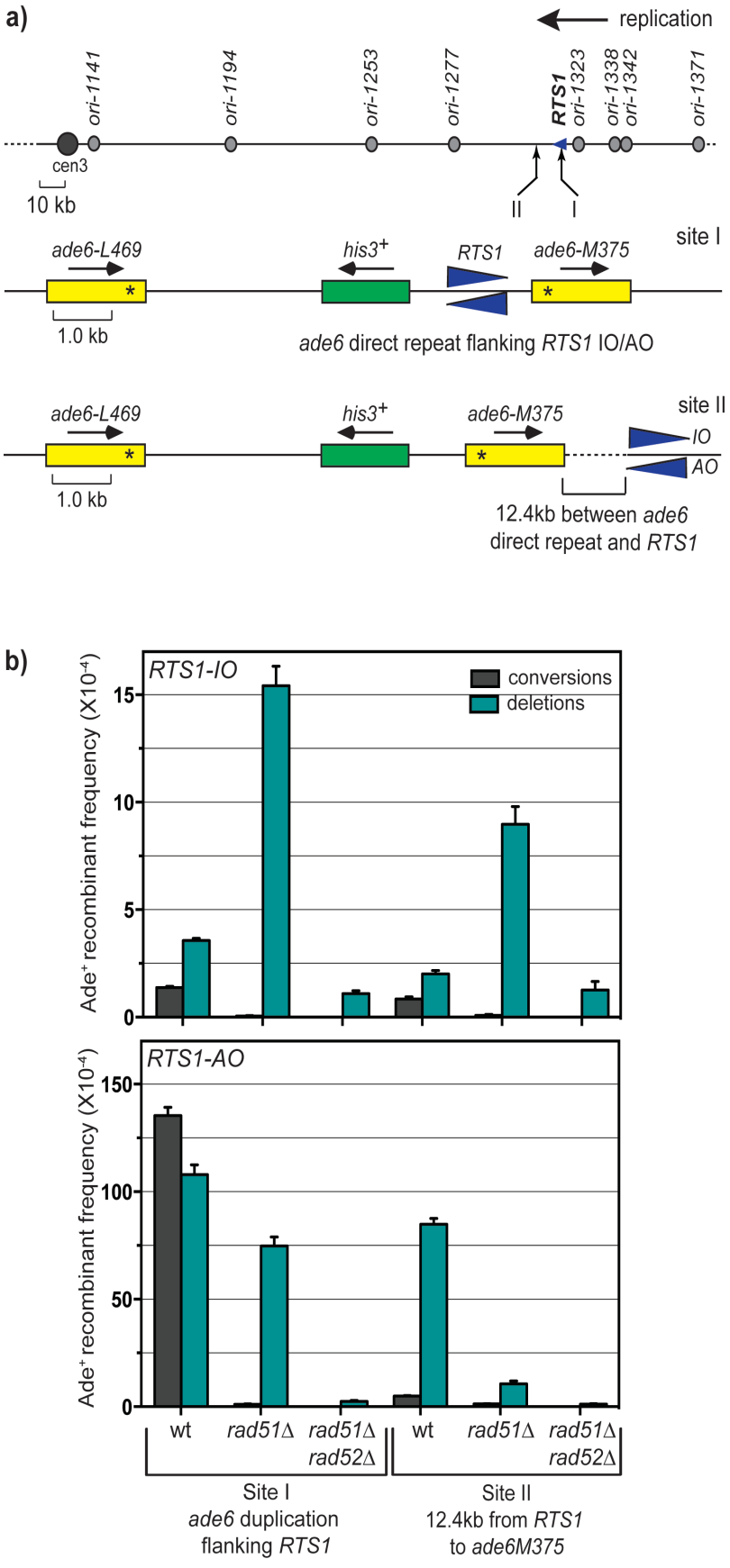


Fig. 3.v Rad51 and Rad52 are essential for direct repeat recombination downstream of *RTS1*.

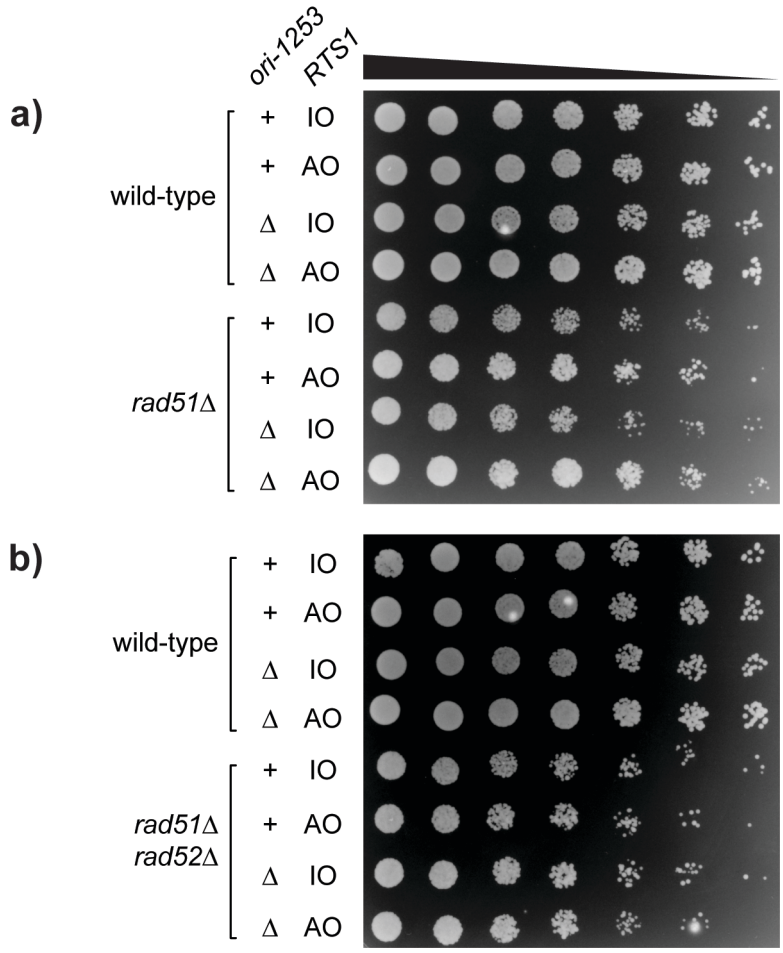


Fig. 3.vi Effect of *rad51*Δ and *rad52*Δ mutations on growth and viability of cells with *RTS1.*

a) Spot assays comparing the growth of MCW7224, MCW7223, MCW7277, MCW7279, MCW7360, MCW7362, MCW7364 and MCW7366. b) Spot assays comparing the growth of MCW7224, MCW7223, MCW7277, MCW7279, MCW7368, MCW7370, MCW7372 and MCW7374. 10µl of 5-fold dilutions were spotted on EMMG and the plates were photographed after 4 days of growth at 30°C.Note that even though there appears to be a difference in growth rates between the *RTS1-IO* and *RTS1-AO* strains in the mutant backgrounds, these are not significant as verified by a colony formation assay published in Nguyen et al. (2015).

the mutants showed any reduction in growth/viability when the *RTS1-AO* strains were compared to the *RTS1-IO* strains. To test whether timely fork convergence at the barrier was responsible for efficient completion of DNA replication and, therefore, maintenance of cell viability*, oriIII-1253* was deleted to delay fork convergence and maximize the amount of RDR initiated. However, deletion of *oriIII-1253* made no difference to the growth/viability of either wild-type or mutant strains carrying *RTS1-AO* or *RTS1-IO* [Fig. 3.vi]. These data show that RDR, despite being induced within approximately 10 minutes following encounter with the barrier, is not essential for cell viability (Nguyen et al., 2015).

3.2.4 Effect of *rad54* deletion on direct repeat recombination downstream of *RTS1*

Rad54 is a member of the Snf2 family of DNA-dependent ATPases, which can translocate on DNA but do not display strand displacement activity. Multiple roles in recombination have been ascribed to it, and as such it has been described as "the jack of all trades" (Heyer et al., 2006; Mazin et al., 2010; Raoul Tan et al., 2003; Thomä et al., 2005). Its roles include: stimulation of Rad51's DNA strand exchange activity (Van Komen et al., 2000; Mazin et al., 2003, 2000; Petukhova et al., 1999; Sung et al., 1998); chromatin remodeling (Alexeev et al., 2003); branch migration of Holliday junctions (Bugreev et al., 2006); and dissociation of Rad51 from the DNA following strand exchange to allow nascent DNA synthesis (Li and Heyer, 2009; Solinger et al., 2002).

Previous work in the lab by Michael Nguyen and Fikret Osman had shown that deletion of *rad54* eliminates gene conversions when *RTS1-AO* is positioned within the *ade6*$^{-}$ reporter at site I [Fig. 3.vii.b & Table 8-1]. In contrast, an increase in the frequency of deletions was observed (~1.8 fold) compared to wild-type. These

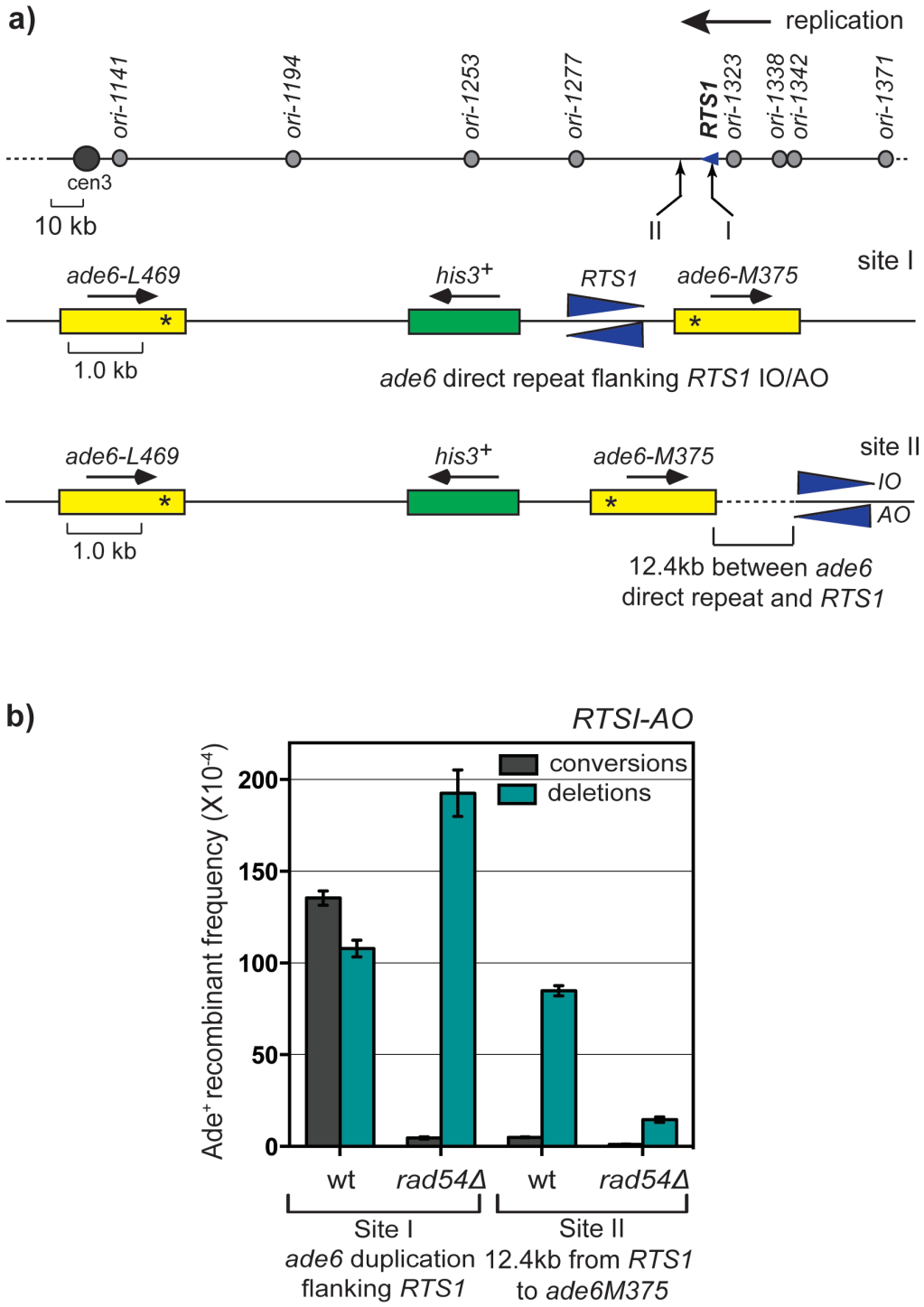


Fig. 3.vii The effect of *rad54Δ* on direct repeat recombination downstream of *RTS1.*

a) Schematic showing the relative positions on ChrIII where the *ade6*$^{-}$ reporter (shown in the bottom panel) is inserted downstream of *RTS1* which replaces the *ade6* gene at its endogenous locus. b) Bar chart showing the frequency of Ade^{+} recombinants in MCW4713*, MCW2656*, MCW7259 and MCW8222. Error bars represent ± standard error of the mean.

data are consistent with Rad54 being needed to promote Rad51 dependent gene conversions. However, they also indicate a potential role for Rad54 in suppressing deletions that is independent of Rad51. To determine whether *rad54*Δ similarly effects direct repeat recombination that is triggered by RDR, I measured the recombinant frequency at site II with *RTS1-AO* present at the upstream site [Fig. 3.vii.b & Table 8-1]. As expected, loss of *rad54* resulted in a ~4 fold reduction in gene conversions similar to a *rad51*Δ mutant [See Fig. 3.v.b]. It also resulted in a ~6 fold reduction in deletions, which is also equivalent to what is observed in a *rad51*Δ mutant. These data show that Rad54 is similarly required for direct repeat recombination downstream of *RTS1*-AO as Rad51, which is consistent with its roles in supporting Rad51 activity.

3.2.5 Pfh1 promotes recombination downstream of *RTS1.*

The two most extensively studied members of the Pif1 DNA helicase family are Rrm3 and Pif1 from *S. cerevisiae.* In *S. cerevisiae*, Rrm3 is needed for getting past barriers and Pif1 is needed for efficient progression of restarted replication (at least in the context of BIR) (Ivessa et al., 2000; Saini et al., 2013; Wilson et al., 2013). In *S.pombe*, like in humans, there is only one Pif1 family helicase, which is called Pfh1. Pfh1, like Rrm3, is needed for replication past barriers (Sabouri et al., 2012; Steinacher et al., 2012). However, it is unclear whether it performs a Pif1-like role and promotes efficient progression of restarted forks. To investigate this the effect of Pfh1 depletion on direct repeat recombination at and downstream of the *RTS1* barrier was analysed.

Our lab has previously investigated what impact loss of Pfh1 has on direct repeat recombination when *RTS1* is positioned between the repeats at site I [Fig. 3.viii.a]. As Pfh1 has an essential mitochondrial function, two nuclear depletion mutant alleles were used for these experiments: *pfh1-m21*, which encodes protein

with reduced localisation to the nucleus but normal mitochondrial localisation, and *pfh1-mt**, which encodes protein that is completely excluded from the nucleus but localises normally to the mitochondria (Pinter et al., 2008). With *pfh1-m21* the level of spontaneous recombination (i.e. when *RTS1-IO* is present) is similar to wild-type, whereas, with *pfh1-mt** there is a ~3 fold overall increase [Fig. 3.viii.b & Table 8-1]. Strikingly, the increase is much more dramatic in cells with *RTS1-AO*, with ~8 fold increase in the *pfh1-m21* mutant and ~7.3 fold increase in the *pfh1-mt** mutant [Fig. 3.viii.b & Table 8-1]. Notably, all the additional recombinants in the *pfh1* mutants are deletions [Fig. 3.viii.b & Table 8-1] (Steinacher et al., 2012).

Recent work has implicated the role of the Pif1 helicase in promoting BIR (Saini et al., 2013; Wilson et al., 2013). It has been demonstrated that Pif1 aids the recruitment of Pol δ and PCNA at the break sites (Wilson et al., 2013) and promotes long-range synthesis during BIR, Pif1 being the driving force behind the 'migrating bubble' (Saini et al., 2013). Owing to this property of Pif1, I wanted to test whether Pfh1 promoted the RDR that is initiated following replication fork blockage at *RTS1*. In order to gauge replication restart in the *pfh1* mutant backgrounds, I measured the recombination frequency of the *ade6*$^{-}$ reporter both at site I, with *RTS1* positioned 0.2 kb upstream, and site II, with *RTS1* positioned at the endogenous *ade6* site [Fig. 3.viii.a]. At site I, when *RTS1-AO* is present, there is no change in total recombinants in a *pfh1-m21* mutant, whereas, in a *pfh1-mt** mutant there is a ~3 fold reduction compared to wild-type. Upon deletion of *oriIII-1253*, there is a doubling of the recombinants at this site in both mutants. Further downstream of the barrier, at site II, there is a ~7 fold reduction in recombinants in a *pfh1-m21* mutant and a ~14 fold reduction in a *pfh1-mt** mutant when compared to the wild-type. As with site I, deletion of *oriIII-1253,* leads to an

Fig. 3.viii Pfh1 promotes recombination downstream of *RTS1.*
a) Schematic showing the relative positions on ChrIII where the *ade6*$^{-}$ reporter (shown in the bottom panel) is inserted downstream of the *ade*6 gene at its endogenous locus. The endogenous *ade6* gene is deleted and *RTS1* is inserted either flanked by the reporter at site I, before the reporter at site I or in place of the *ade6* gene at its endogenous locus and upstream of the reporter at site II. b) Bar chart showing the frequency of Ade^{+} recombinants in MCW4712*, MCW4940*, MCW4954*, MCW7131, MCW7599*, MCW7598*, MCW7603*, MCW7602*, MCW7257, MCW7421, MCW7423, MCW7425, MCW7427, MCW4713*, MCW4942*, MCW4956*, MCW7133, MCW7601*, MCW7600*, MCW7605*, MCW7604*, MCW7259, MCW7422, MCW7424, MCW7426 and MCW7428. Error bars represent ± standard error of the mean.

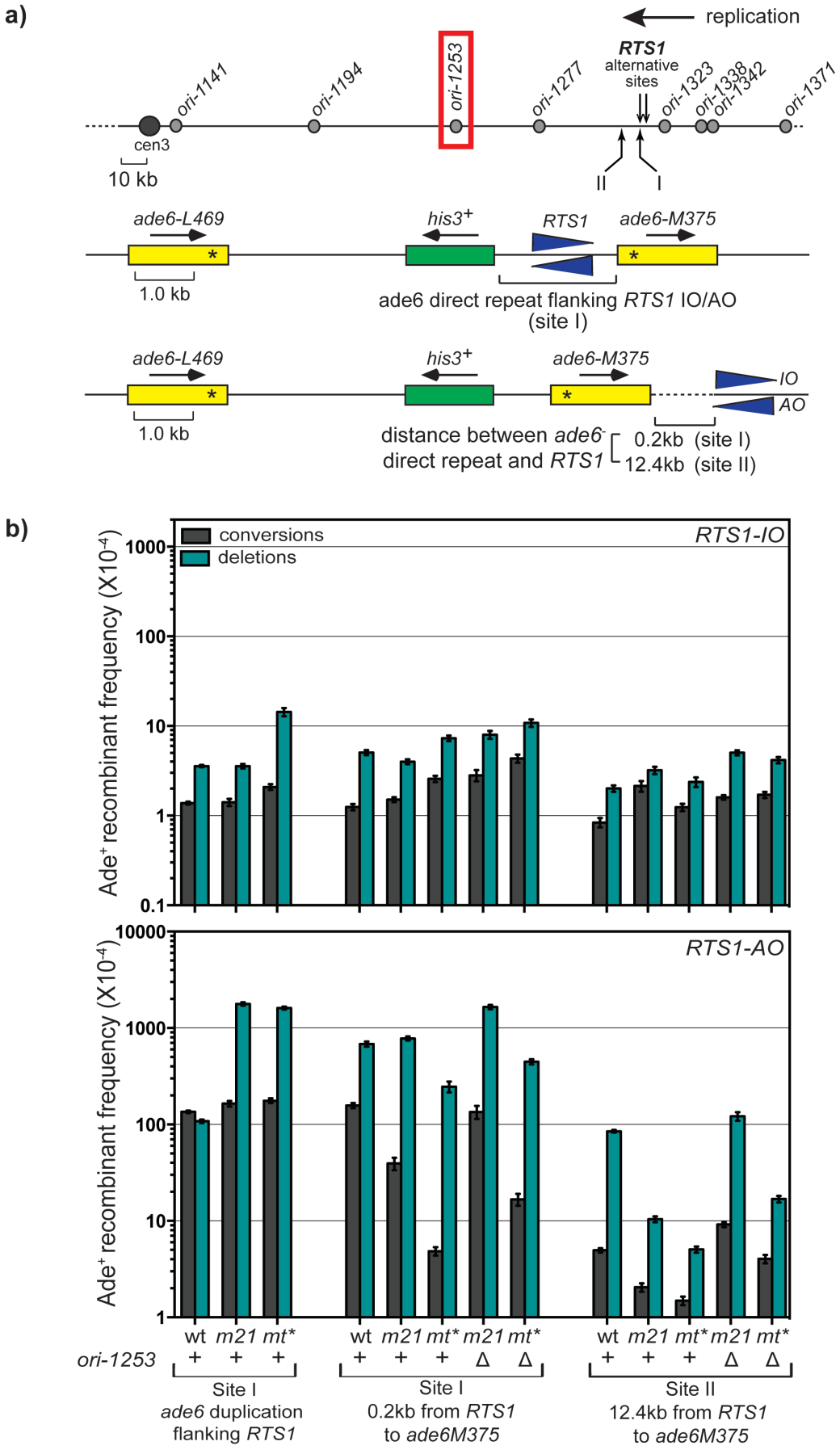


Fig. 3.viii Pfh1 promotes recombination downstream of *RTS1*.

increase in recombinants, but the effect is more striking here with a ~10 fold increase in recombinant frequency in a *pfh1-m21* mutant and a ~3 fold increase in a *pfh1-mt** mutant [Fig. 3.viii.b & Table 8-1]. Altogether these data show that Pfh1, whilst constraining direct recombination at the *RTS1* barrier, promotes that which is associated with restarted replication downstream of the barrier. Intriguingly, the reduced amount of Pfh1 in the nucleus, delivered by the *pfh1-m21* allele, whilst being sufficient to promote some recombination downstream of the barrier, appears to be totally inadequate for constraining recombination at the barrier. This highlights a potential difference in the mechanism by which Pfh1 affects recombination at these two sites. The significance of these findings will be discussed in Section 3.3.2.

3.2.6 Effect of the loss of Elg1 on direct repeat recombination downstream of *RTS1.*

Elg1 is an evolutionarily conserved gene essential for genome stability. Its main activities include prevention of gross chromosomal rearrangements, DNA damage tolerance and repair, maintenance of telomere length and the homeostasis between sister chromatid cohesion and DNA replication (Gazy et al., 2015; Johnson et al., 2016; Kubota et al., 2015; Lee et al., 2013, 2010; Shiomi and Nishitani, 2013). Elg1 is part of an RFC-like complex (RLC) along with four small RFC proteins, RFC2-5 (Majka and Burgers, 2004), which acts as a PCNA-clamp unloader, possibly during DNA replication, but more likely in response to fork stalling or collapse (Kubota et al., 2013). Retention of PCNA in an Elg1 mutant causes moderate genome instability in S-phase, which is aggravated through G2/M phase (Johnson et al., 2016).

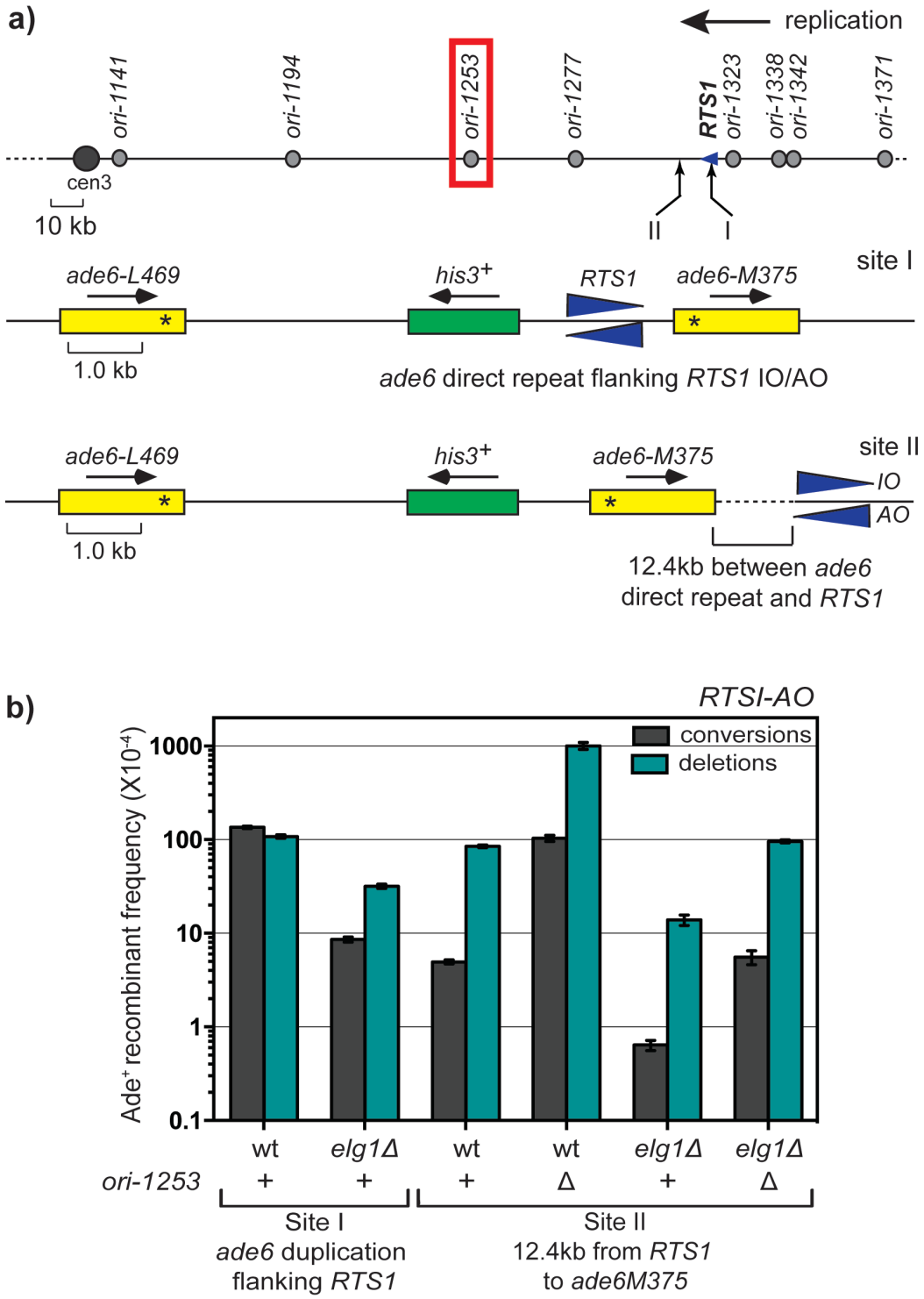


Fig. 3.ix The effect of *elg1Δ* on direct repeat recombination downstream of *RTS1.*
a) Schematic showing the relative positions on ChrIII where the *ade6*$^-$ reporter (shown in the bottom panel) is inserted either at the endogenous *ade6* locus flanking *RTS1* or downstream of *RTS1*, which itself is positioned in place of the endogenous *ade6* gene. b) Bar chart showing the frequency of Ade$^+$ recombinants in MCW4713*, MCW7708*, MCW7259, MCW7295, MCW8191 and MCW8290. Error bars represent ± standard error of the mean.

Recent work done in our lab by Sanjeeta Tamang and Fikret Osman suggests that loss of Elg1 results in reduced direct repeat recombination at site I when *RTS1-AO* is flanked by the two *ade6*$^{-}$ alleles (~16 fold reduction in gene conversions and ~3 fold reduction in deletions) [Fig. 3.ix.b & Table 8-1]. Importantly, *elg1*Δ has little effect on spontaneous direct repeat recombination, indicating that it is not required for required for recombination per se (data not shown). The specific reduction in *RTS1-AO*-induced recombination can be attributed to the fact that, in the absence of Elg1, PCNA remains associated with the blocked replication fork and thereby delays the recruitment of recombination proteins. This has been confirmed by time-lapse microscopy, where in an *elg1Δ* strain, there is prolonged persistence of PCNA and a delay in recruitment of Rad52 to the barrier when compared to wild-type (unpublished data).

To see if the delay in recombination protein recruitment to the blocked fork correlates with a reduction in RDR-associated recombination, I introduced the *elg1Δ* mutation into a strain containing *RTS1-AO* and the direct repeat positioned downstream at site II [Fig. 3.ix.a]. Compared to wild-type, the *elg1*Δ mutant strain exhibited ~8 fold reduction in gene conversions and ~6 fold reduction in deletions at this site [Fig. 3.ix.b & Table 8-1]. Providing more time for restart to occur, by deleting *oriIII-1253*, resulted in ~9 fold increase in gene conversions and ~7 fold increase in deletions in the *elg1*Δ mutant [Fig. 3.ix.b & Table 8-1]. However, this is less than the ~12-fold increase in the equivalent wild-type strain and suggests that simply providing more time for restart to occur is not enough to redress the difference between *elg1*Δ and wild-type strains. Together these data show that Elg1 promotes recombination both at and downstream of the *RTS1* barrier, most likely because it is needed for efficient removal of PCNA from the blocked replication fork so that recombination proteins can be recruited.

3.2.7 Helicases that limit genetic instability associated with replication restart.

Previous studies have identified several DNA helicases, including Rqh1, Fbh1 and Srs2, that constrain direct repeat recombination at the *RTS1* barrier (Ahn et al., 2005; Lorenz et al., 2009). Here, I determine whether these helicases also limit template switching during restarted replication by examining the effect of their deletion on direct repeat recombination downstream of *RTS1-AO*.

As discussed in Chapter 1, Srs2 plays a prominent role in controlling HR through its ability to disrupt Rad51 nucleofilaments and unwind D-loops. It has also been shown to promote efficient replication restart from *RTS1* and to constrain direct repeat recombination at the barrier site [Fig. 3.x.a & Table 8-1] (Lambert et al., 2010; Lorenz et al., 2009). To determine whether it affects recombination that is associated with restarted replication downstream of the barrier, I measured direct repeat recombination at site II downstream of *RTS1-AO* in a *srs2*Δ mutant [Fig. 3.x.b & Table 8-1]. Compared to wild-type, the *srs2*Δ mutant exhibits a ~6 fold increase in total recombinants, with ~21 fold increase in gene conversions. Importantly, the levels of recombination are much higher than would be expected for spontaneous recombination (Lorenz et al 2009) and, therefore, it is clear that at least some restarted replication progresses as far as 12.4 kb downstream of the barrier and that the restarted replication is more prone to template switching when Srs2 is absent.

Similar to Srs2, Rqh1 plays a major role in limiting direct repeat recombination that is associated with replication fork blockage at *RTS1* [Fig. 3.x.a & Table 8-1] (Ahn et al., 2005). Analysis of recombination downstream of *RTS1-AO* at site II in a *rqh1*Δ mutant shows that it also plays an important role in limiting direct repeat

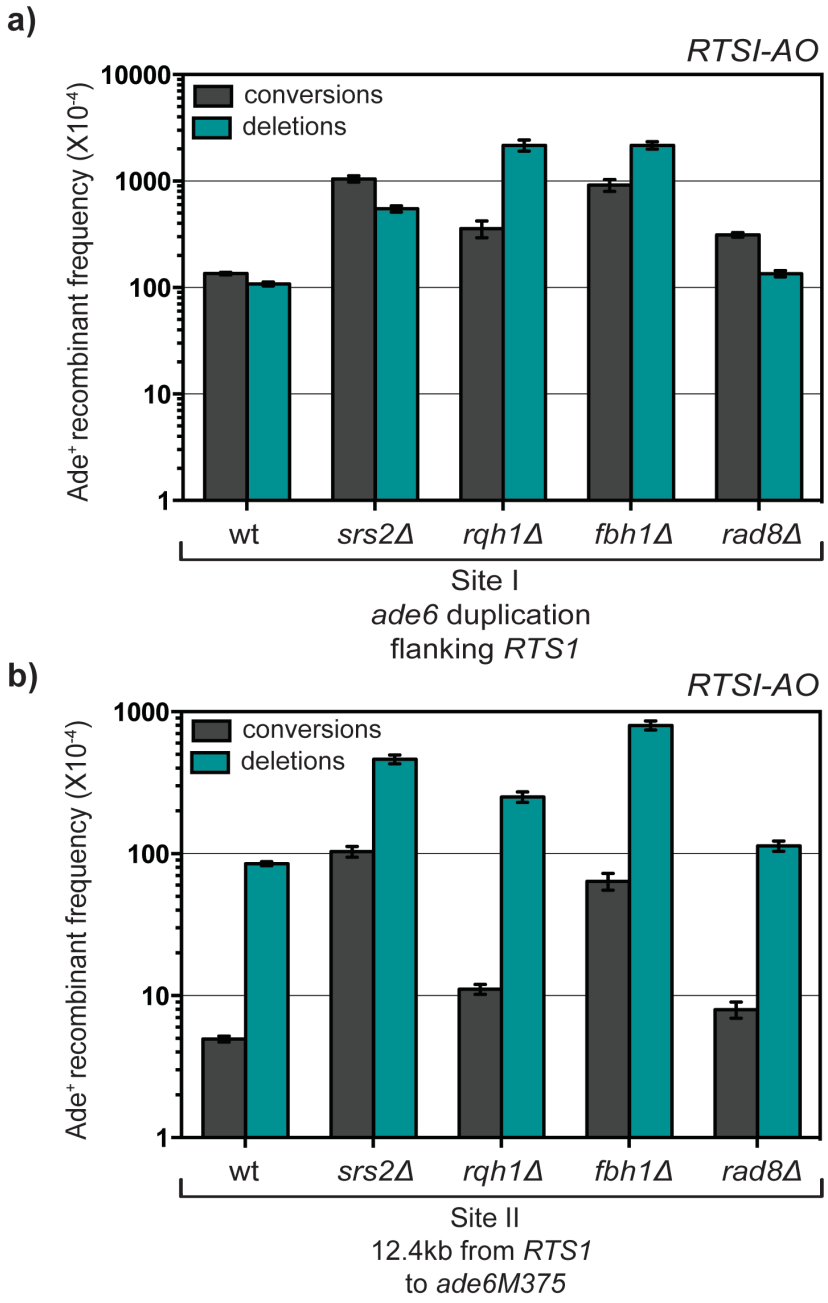


Fig. 3.x Hyper-levels of direct repeat recombination downstream of *RTS1* in *srs2*Δ, *rqh1*Δ and *fbh1*Δ mutants but not *rad8*Δ

a) Bar chart showing the frequency of Ade$^+$ recombinants in MCW4713*, FO1750*, MCW1447*, FO1836* and MCW3864*. Error bars represent ± standard error of the mean. b) Bar chart showing the frequency of Ade$^+$ recombinants in MCW7259, MCW8200, MCW8201, MCW8227 and MCW8197. Error bars represent ± standard error of the mean.

recombination that is associated with restarted replication [Fig. 3.x.b & Table 8-1]. Specifically, there is ~2 fold increase in gene conversions and ~3 fold increase in deletions in a *rqh1*∆ mutant. As Rqh1 neither promotes nor constrains replication restart (Lambert et al 2010), these data indicate that it either promotes more rapid progression of the restarted replication fork and/or constrains the amount of template switching.

The F-box DNA helicase Fbh1 has been shown to have a diametrically opposite role to that of Rad52 in that it limits the loading of Rad51 onto ssDNA, by acting as a Rad51 disruptase (Lorenz et al., 2009; Simandlova et al., 2013). It is especially important in preventing recombination when replication forks are blocked (Lorenz et al., 2009). Data from our lab has shown that the recombination frequency at site I, when *RTS1-AO* is positioned within the repeats, increases significantly in a *fbh1*Δ mutant [Fig. 3.x.a & Table 8-1]. Specifically, the gene conversions increase by ~7 fold and the deletions by ~20 fold, however, Fbh1 is not required to constrain spontaneous recombination (Lorenz et al 2009). To see if Fbh1 affects the frequency of recombination associated with restarted replication, I measured recombination values at site II, downstream of *RTS1-AO,* in a *fbh1Δ* mutant [Fig. 3.x.b & Table 8-1]. Compared to wild-type, the *fbh1*∆ mutant exhibited a ~13 fold increase in gene conversions and ~10 fold increase in deletions [Fig. 3.x.b & Table 8-1]. These data show that Fbh1 is equally important for constraining template switching during progression of the restarted replication fork as it is for limiting ectopic recombination during the process of restarting the replication fork.

Rad8, which is an orthologue of *S. cerevisiae* Rad5 and human HLTF, has been shown to promote the error-free branch of PRR. It is part of the Rad5-Rad18-Mms2 complex that accounts for the “template-switch” mode of lesion bypass (Branzei et al., 2004). It also has helicase-dependent fork reversal and restart

activity, which probably act in an alternate pathway to Rad51 (Blastyák et al., 2007; Ding and Forsburg, 2014). To test whether Rad8 affects the frequency of direct repeat recombination associated with restarting and/or restarted replication forks, recombinants were scored at site I (with *RTS1-AO* flanked by repeats) and site II (with *RTS1-AO* 12.4 kb upstream of the repeats) in a *rad8Δ* mutant [Fig. 3.vii.a & b]. Compared to wild-type, *rad8*Δ mutants exhibited ~2.5 fold increase in gene conversions, with little change in deletions, at site I, [Fig. 3.x.a & Table 8-1]. Similarly at site II, there was only a modest increase in recombinants (~1.6 fold increase in gene conversions and ~1.3 fold increase in deletions) [Fig. 3.x.b & Table 8-1]. These data suggest that Rad8 plays a relatively minor role in constraining direct repeat recombination associated with both restarting and restarted replication. Certainly, there is no evidence from these data that it is needed for either restarting replication or for efficient progression of the restarted fork.

3.2.8 Exo1 limits direct repeat recombination associated with restarted replication.

Exo1, a member of the Rad2 gene family, is a DNA repair nuclease with a 5'-3' exonuclease activity. It has a role in mitotic and meiotic recombination, Okazaki fragment processing and telomere maintenance (Keijzers et al., 2016). Exo1 has been shown to be recruited to stalled replication forks, promoting formation of ssDNA intermediates, thus counteracting fork reversal (Cotta-Ramusino et al., 2005). At *RTS1*, Exo1 is responsible for the resection behind the collapsed replication fork and aids in the recruitment of Rad52, thus promoting RDR (Tsang et al., 2014). At site I, when *RTS1-AO* is positioned such that it is flanked by the direct repeats [Fig. 3.vii.a], there is ~2 fold reduction in both gene conversions and

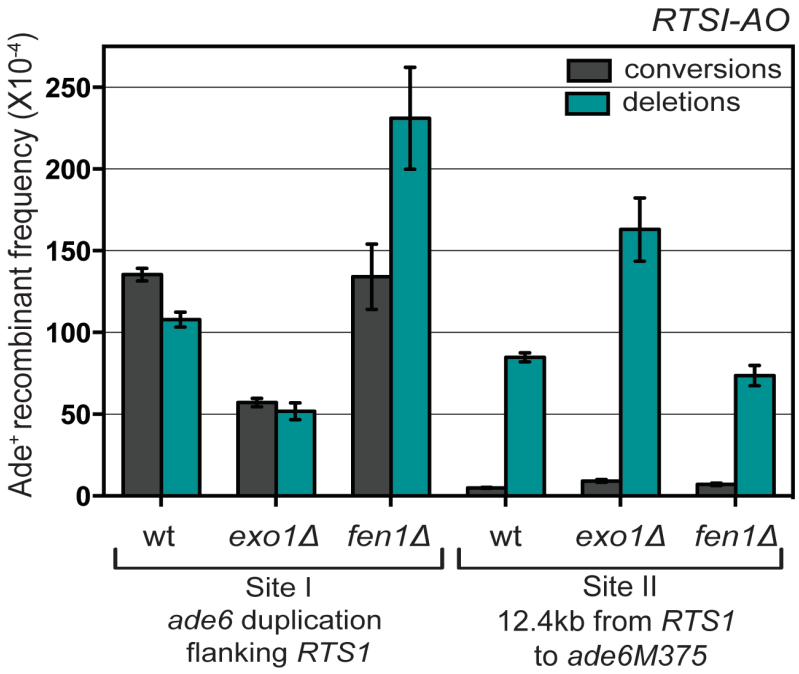


Fig. 3.xi Hyper-levels of direct repeat recombination downstream of *RTS1* in an *exo1Δ mutant but not fen1Δ*

Bar chart showing the frequency of Ade$^+$ recombinants in MCW4713*, MCW1742*, MCW2226*, MCW7259*, MCW8218 and MCW8220. Error bars represent ± standard error of the mean.

deletions in an *exo1Δ* mutant compared to the wild-type [Fig. 3.xi & Table 8-1] (Osman et al., 2016). In contrast, when the recombination is measured at site II, with *RTS1-AO* upstream, there is ~2 fold increase in gene conversions and deletions in an *exo1*△ mutant [Fig. 3.xi & Table 8-1]. These data show that Exo1 can both promote and constrain direct repeat recombination that is associated with RDR. A possible explanation for how it could have such contrasting roles is discussed in Section 3.3.7.

3.2.9 Fen1 does not affect direct repeat recombination associated with restarted replication.

S. pombe Fen1/Rad2, which is an orthologue of *S. cerevisiae* Rad27 and human FEN1, is a structure specific 5' flap endonuclease that has a major role in Okazaki fragment maturation during DNA replication as well as base excision repair (BER) (Stith et al., 2008; Stodola and Burgers, 2016; Zheng and Shen, 2011). In mice, FEN1's Okazaki fragment processing role is essential (Kucherlapati et al., 2002; Larsen et al., 2003; Zheng et al., 2007). In contrast, *rad27Δ* mutants in *S. cerevisiae* are viable, and this has been attributed to a redundancy in the nuclease that removes the RNA primer during Okazaki fragment maturation (Jin et al., 2001; Lee and Wilson, 1999). Intriguingly, Exo1 exhibits a 5' flap endonuclease activity and, therefore, could substitute for Rad27 in removing the RNA primers (Lee and Wilson, 1999). Consistent with this notion, deletion of both *rad27* and *exo1* causes synthetic lethality in yeast (Tishkoff et al., 1997). Given that there appears to be some overlap in activity between Rad27 and Exo1, I wanted to see if deletion of *fen1* in *S. pombe* had a similar effect on *RTS1*-induced direct repeat recombination as that of *exo1Δ.* Using the previously described recombination reporters, I determined that loss of *fen1* results in ~2-fold increase in deletions at site I when *RTS1-AO* is flanked by the reporter, but no significant difference at site

II when *RTS1-AO* is positioned 12.4 kb upstream (the gene conversions remain unchanged in both cases) [Fig. 3.xi & Table 8-1]. This suggests that Fen1 may play a role in limiting ectopic recombination that is associated with the replication restart process, but provides no evidence that it is needed for restart, progression of the restarted fork, or the template switching that is associated with restarted replication.

3.2.10 Mus81, Fml1 and Tid1 play little or no role in promoting or constraining direct repeat recombination associated with restarted replication.

Mus81, a member of the ERCC4/XPF family of structure-selective endonucleases, works as part of the Mus81-Mms4/Eme1 complex and is involved in the resolution of mitotic and meiotic recombination intermediates, including D-loops and Holliday junctions (Boddy et al., 2000; Osman and Whitby, 2007; West et al., 2016; Wyatt and West, 2014). It also plays an important role in processing collapsed and stalled replication forks (Doe et al., 2002; Forment et al., 2011; Froget et al., 2008; Hanada et al., 2007; Pepe et al., 2014; Regairaz et al., 2011). In recent work, Mayle et al showed that template switching associated with BIR, induced from a broken replication fork in *S. cerevisiae*, is limited by Mus81 (Mayle et al., 2015). In contrast, Pardo and Aguilera showed that Mus81 actually promotes template switching during BIR in *S. cerevisiae* (Pardo and Aguilera, 2012). Previous work in *S. pombe* has shown that Mus81 is not required for replication restart from *RTS1* (Lambert et al., 2010; Mizuno et al., 2009). To determine whether Mus81 is needed to promote or constrain template switching at or downstream of *RTS1*, I measured the frequency of direct repeat recombination at site I (with *RTS1-AO* flanked by the repeats) and site II (with *RTS1-AO* 12.4 kb upstream of the repeats)

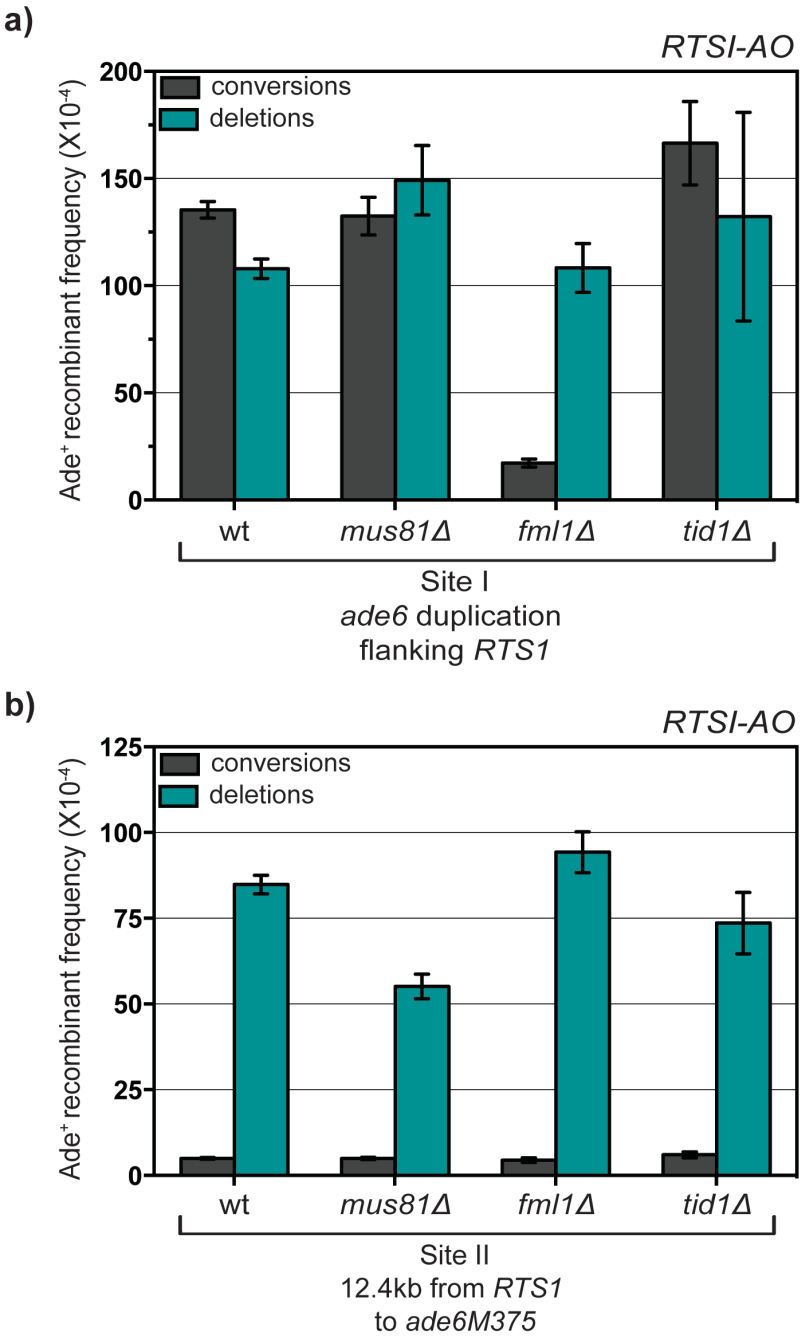


Fig. 3.xii The effect of *mus81*Δ, *fml1*Δ and *tid1*Δ on direct repeat recombination downstream of RTS1.

a) Bar chart showing the frequency of Ade$^+$ recombinants MCW4713*, MCW1452*, MCW3061* and MCW7740*. Error bars represent ± standard error of the mean. b) Bar chart showing the frequency of Ade$^+$ recombinants in MCW7259, MCW8195, MCW8193 and MCW8216. Error bars represent ± standard error of the mean.

in a *mus81*Δ mutant [Fig. 3.xii & Table 8-1]. At both sites the frequency of gene conversions remained unaltered in a *mus81*Δ mutant. However, at both sites modest changes in the frequency of deletions were observed, with a ~1.5-fold increase at site I and a ~1.5-fold decrease at site II [Fig. 3.xii & Table 8-1]. These data suggest that Mus81 may play a role in influencing the outcome of ectopic recombination events at the barrier, and may also promote template switching during restarted replication. The latter finding is consistent with data from Pardo and Aguilera for Mus81's involvement in BIR in budding yeast (Pardo and Aguilera, 2012)..

Fml1, a member of the FANCM family of DNA helicases, has been shown to catalyze fork remodeling, HJ branch migration and D-loop dissociation *in vitro* (Nandi and Whitby, 2012; Sun et al., 2008). At collapsed forks, Fml1 is thought to drive replication fork reversal to generate a substrate suitable for the loading of recombinases to promote RDR (Atkinson and McGlynn, 2009; Whitby, 2010). Consistent with this idea, our lab has shown that there is a significant reduction in Rad51-dependent gene conversions (~8 fold) in a *fml1Δ* mutant when recombinants are measured at site I with the direct repeat reporter flanking *RTS1-AO* [Fig. 3.xii.a & Table 8-1] (Sun et al., 2008). In *S. cerevisiae* the orthologue of Fml1, Mph1, has been shown to promote BIR-associated template switching (Stafa et al., 2014). To determine whether Fml1 is needed to promote template switching associated with replication that has restarted from *RTS1*, I measured the effect of *fml1* deletion on direct repeat recombination at site II, with *RTS1-AO* positioned 12.4 kb upstream [Fig. 3.xii.b & Table 8-1]. Surprisingly, there was no significant difference in recombinant frequency in the *fml1Δ* mutant compared to the wild-type. At face value, these data indicate that Fml1 is not needed for either efficient replication restart or template switching. Alternatively, if Fml1 has a role

in promoting replication restart, as previously proposed, then presumably Fml1 would have to function in limiting template switching. In this scenario any reduction in template switching caused by reduced numbers of restarted forks would be offset by increased levels of template switching associated with those forks that managed to restart. The net effect of this would be that the frequency of recombinants remains unchanged.

In budding yeast, the Rad54 homologue Tid1 (also known as Rdh54) plays a prominent and specific role in promoting template switching during BIR (Ira and Haber, 2002). To see if the same is true in *S. pombe* for RDR initiated following replication fork collapse at *RTS1*, I measured the frequency of direct repeat recombination at both site I (with *RTS1-AO* flanked by the repeats) and site II (with *RTS1-AO* 12.4 kb upstream of the repeats) in a *tid1*Δ mutant [Fig. 3.xii & Table 8-1]. No significant change in the frequency of deletions was observed at either site, but there were very modest increases (~1.2 fold at site I and site II) in gene conversion. These data suggest that Tid1 is not required for template switching during RDR in fission yeast.

3.2.11 Are restarted forks more susceptible to collapse at weak barriers than replication origin-derived forks?

Given that restarted replication forks are clearly different from canonical forks initiated from replication origins, I next wanted to determine whether their propensity for template switching is exacerbated by collision with RFBs. The two RFBs chosen for this study were a tRNA gene, which is representative of a constitutively active transcriptional site, and *ter2*, which is an example of an rDNA fork barrier.

It has been observed that tRNA genes act as weak RFBs, where tRNA-transcribing RNA polymerase III causes replication fork blockage by head-on

collision with the replisome (Deshpande and Newlon, 1996). However, at least in fission yeast, there does not seem to be a dramatic increase in genome instability induced by a single tRNA gene, which suggests that collisions between the replisome and RNA polymerase III are normally handled well (Pryce et al., 2009; Steinacher et al., 2012). In order to study the effect of the collision of the restarted fork with an actively transcribing tRNA gene, *tRNA*^{GLU08} was inserted between the direct repeats positioned at site II [Fig. 3.xiii.a]. Two constructs were made, differing in the orientation of *tRNA*^{GLU08}, such that the effect of the direction of transcription, relative to that of restarted replication from *RTS1-AO*, could be tested. To confirm that positioning the tRNA gene at site II did not lead to the formation of a recombination hot spot, recombination frequencies were compared with and without *tRNA*^{GLU08} in strains with no *RTS1* upstream or with *RTS1-IO* (no replication restart) upstream [Fig. 3.xiii.b & Table 8-1]. Neither orientation of *tRNA*^{GLU08} made a dramatic difference to the frequency of recombination, suggesting that canonical replication forks are not unduly affected by collision with actively transcribing RNA polymerase III. Next the effect of *RTS1-AO*, positioned 12.4 kb upstream, was tested [Fig. 3.xiii.b & Table 8-1]. With *tRNA*^{GLU08} orientated so that restarted replication and transcription were co-directional, no significant difference in recombination frequency was observed compared to a strain without the tRNA gene [Fig. 3.xiii.b & Table 8-1]. In contrast, positioning *tRNA*^{GLU08} in the opposite orientation, such that there was a head on collision between the transcription machinery and the restarted replication fork lead to ~2.3 fold increase in recombinants [Fig. 3.xiii.b & Table 8-1]. This indicates that a head-on collision between the restarted fork and transcription machinery increases template switching.

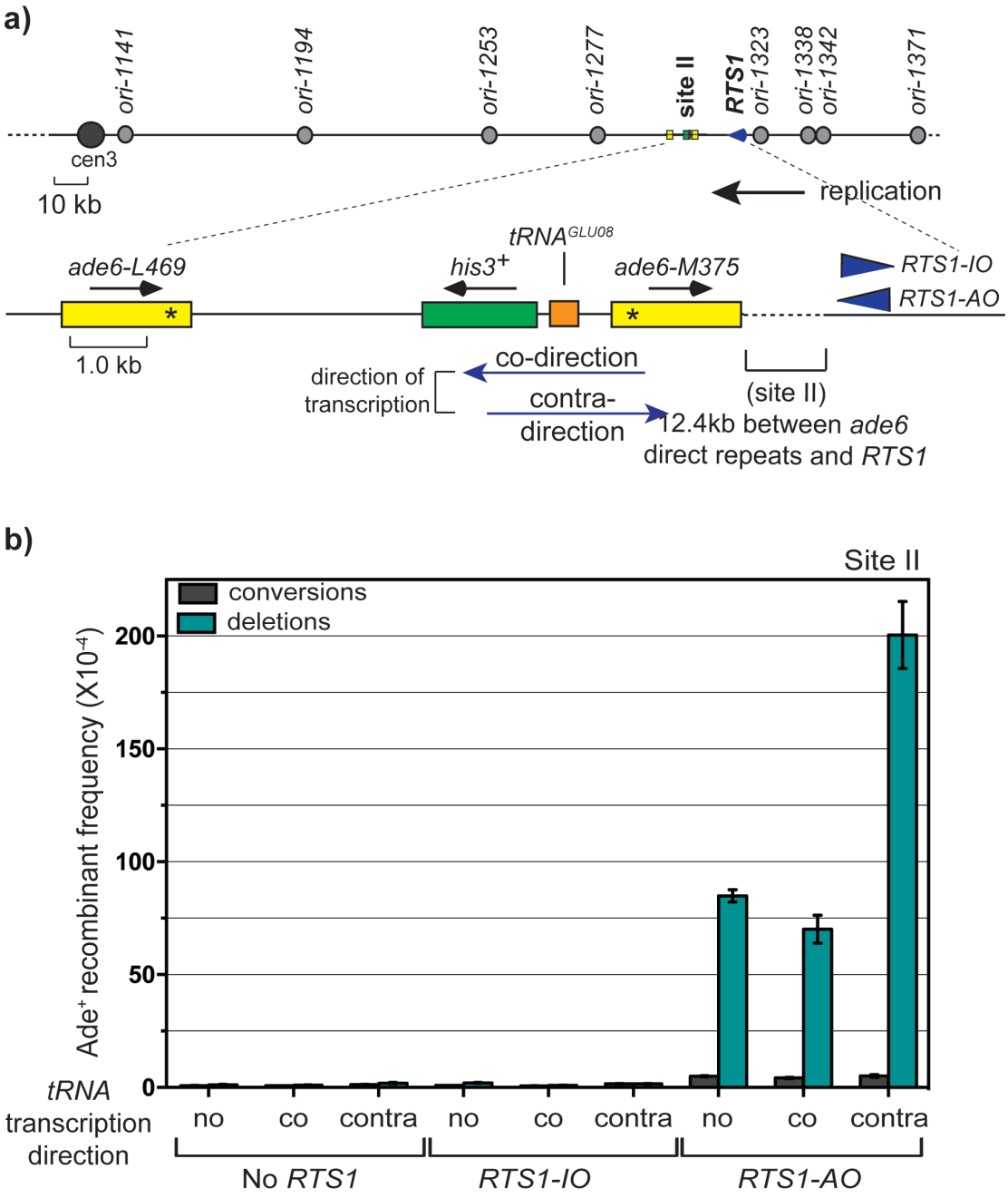


Fig. 3.xiii Head-on collision between restarted replication and t*RNA* transcription increases direct repeat recombination

a) Schematic showing the relative position of *RTS1* on ChrIII replacing the *ade6* gene along with the direct repeat recombination reporter with the $tRNA^{GLU08}$ gene positioned 12.4 kb downstream (site II). The direction of transcription across the *tRNA* gene is described as 'co-directional' or 'contra-directional' with respect to the incoming restarted replication from *RTS1-AO*. b) Bar chart showing the frequency of Ade^+ recombinants in MCW7229, MCW7434, MCW7433, MCW7257, MCW7519, MCW7515, MCW7259, MCW7521 and MCW7517. Error bars represent ± standard error of the mean.

Fig. 3.xiv 2D gel analysis of replication intermediates at a transcriptionally active site downstream of *RTS1-AO*.

a) Schematic showing the relative position of *RTS1* on ChrIII replacing the *ade6* gene along with the direct repeat recombination reporter with the $tRNA^{GLU08}$ gene positioned 12.4 kb downstream (site II). Probe A used for 2D gel analysis is also indicated. b) 2D gel analysis of replication intermediates within the *Pst*I fragment shown in (a) with *tRNA* gene being transcribed in both the 'co' and 'contra' direction in respect to the direction of restarted replication across the region from *RTS1-AO*. The top-left panel is a guide for interpreting the 2D gels. c) Quantification of the 2D gels displayed as bar charts. The DNA was extracted from asynchronously growing cultures of the strains MCW7433, MCW7434, MCW7517 and MCW7521.

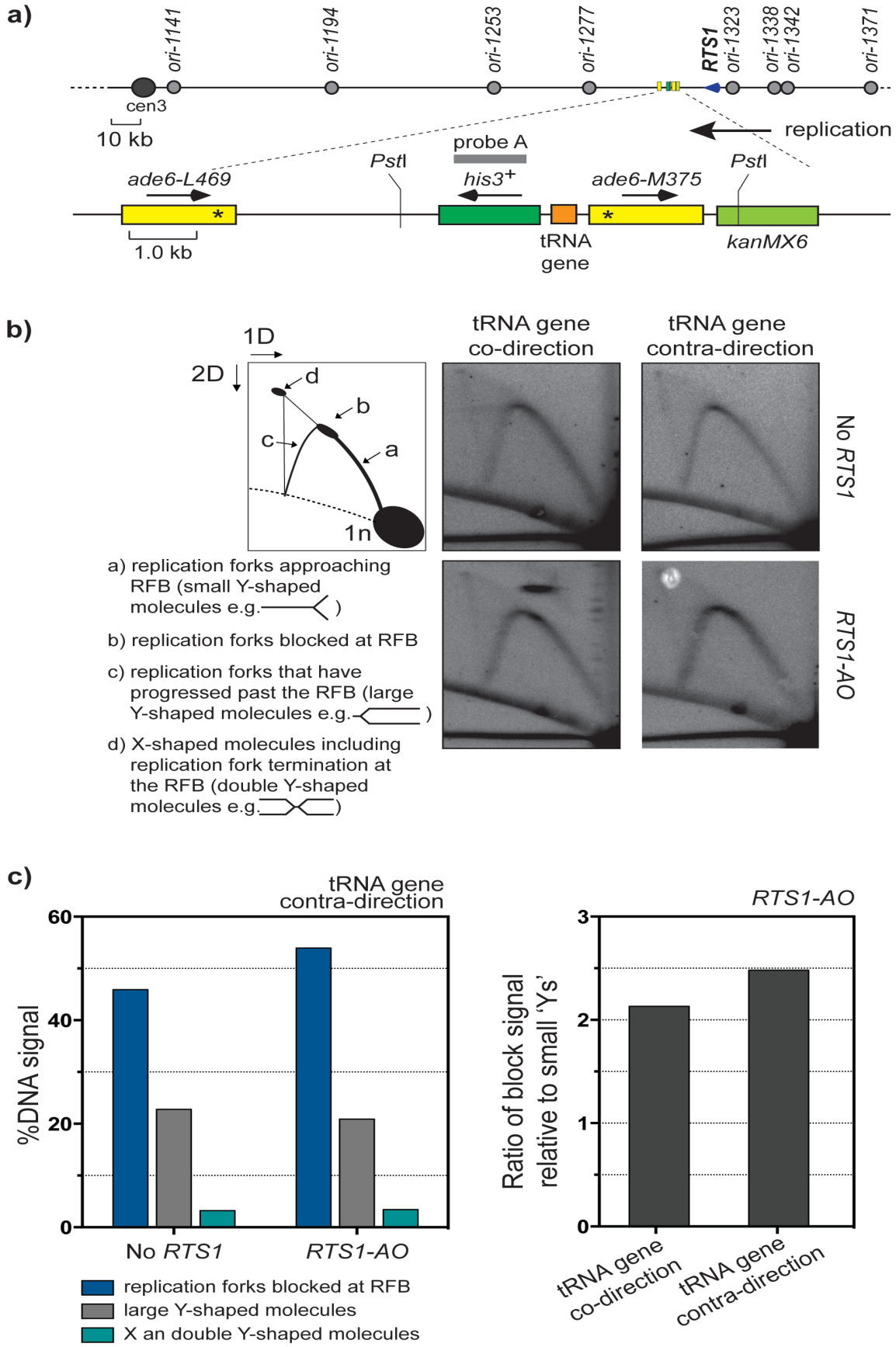


Fig. 3.xiv 2D gel analysis of replication intermediates at a transcriptionally active site downstream of *RTS1-AO*.

To determine if the collision of the restarted fork with the transcription machinery leads to increased pausing at the tRNA gene, I analysed the replication intermediates in and around the tRNA gene at site II, both in the presence and absence of *RTS1-AO* upstream [Fig. 3.xiv.a]. 2D gel analysis of this region exhibited a Y-arc of replication intermediates and a modest pause site at $tRNA^{GLU08}$ [Fig. 3.xiv.b]. However, only a slight increase in the extent of fork pausing was seen at the tRNA gene when comparing DNA from a strain with no *RTS1* (46%) to one with *RTS1-AO* (54%) [Fig. 3.xiv.c]. As this experiment was not repeated, the significance of this very slight difference is uncertain.

Ter2 is a polar replication fork barrier that promotes unidirectional replication within the rDNA array. However, unlike *RTS1*, it does not cause fork collapse, recruitment of recombination proteins or replication restart (Krings and Bastia, 2004; Mizuno et al., 2013; Sánchez-Gorostiaga et al., 2004). Our lab has previously shown that a tandem repeat of three *ter2s (ter2x3)*, inserted between the *ade6*$^{-}$ repeats at site I, does not trigger increased recombination (unpublished data). To study the consequence of the restarted fork encountering *ter2*x3, I inserted three copies of *ter2* in between the *ade6*$^{-}$ repeats at site II [Fig. 3.xv.a]. The *ter2*X3 was positioned in both orientations, the permissive (ORI1) and the obstructive (ORI2) orientation, with respect to the direction of restarted replication from *RTS1-AO*. In the absence of *RTS1*, or with *RTS1-IO* upstream, *ter2*X3 made little or no difference to the frequency of recombination regardless of its orientation [Fig. 3.xv.b & Table 8-1]. Surprisingly, when *RTS1-AO* is positioned upstream, there is ~2 fold reduction in recombinants when *ter2*X3 ORI1 (permissive) is present and ~37 fold reduction when *ter2*X3 ORI2 (obstructive) is present, which is almost back to spontaneous levels [Fig. 3.xv.b & Table 8-1]. Pairs of *ter* sites have been

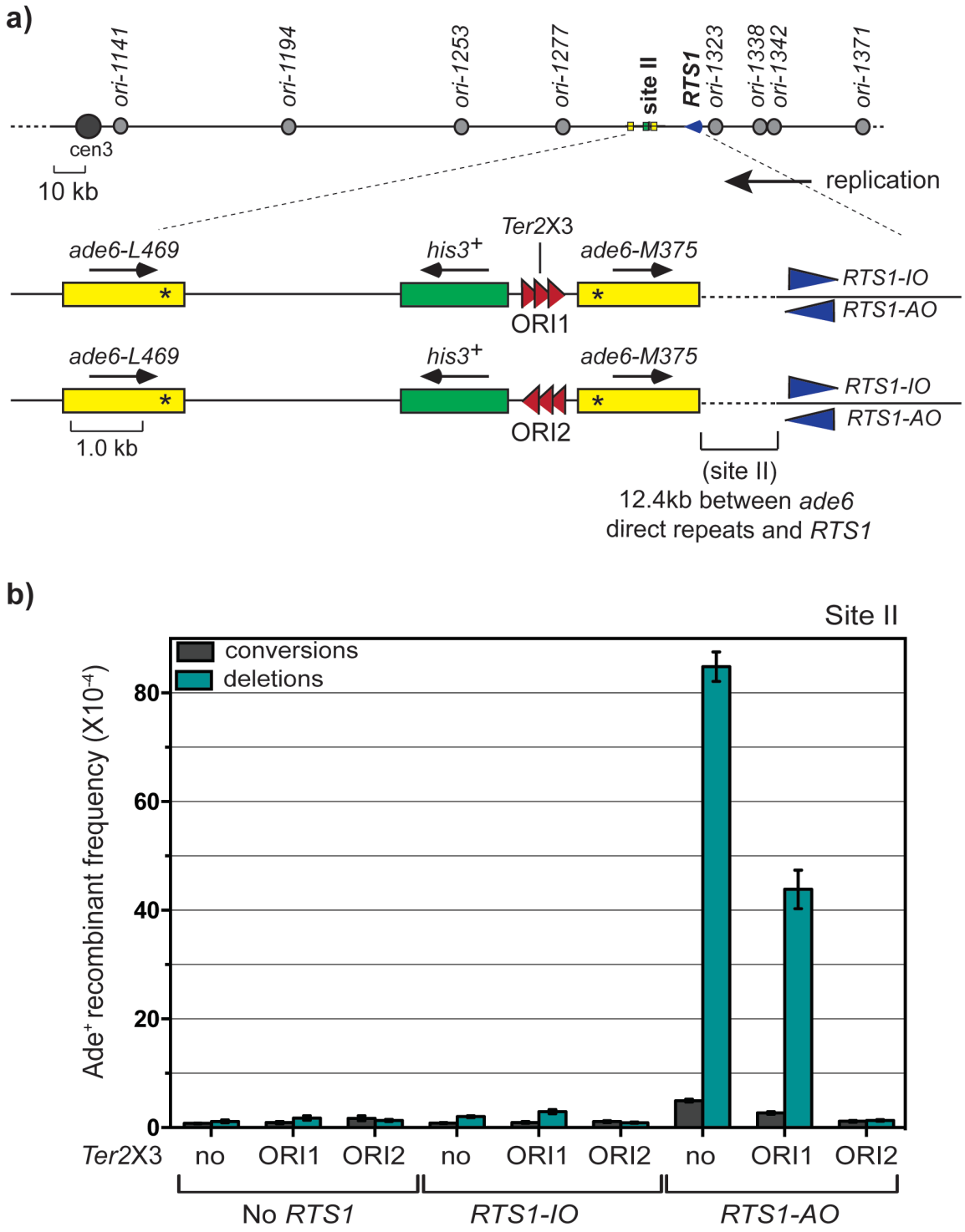


Fig. 3.xv Effect of the collision between restarted replication and a weak termination site on direct repeat recombination.

a) Schematic showing the relative position of *RTS1* on ChrIII replacing the *ade6* gene along with the direct repeat recombination reporter with the *ter2*X3 positioned 12.4 kb downstream (site II) in both the permissive (ORI1) and the blocking (ORI2) orientations. b) Bar chart showing the frequency of Ade$^+$ recombinants in MCW7229, MCW7431, MCW7432, MCW7257, MCW7507, MCW7511, MCW7259, MCW7509 and MCW7513. Error bars represent ± standard error of the mean.

shown to interact with each other, either on the same or different chromosomes, by a mechanism of “chromosome kissing”, which is mediated by the barrier protein Reb1 and causes looping of the intervening DNA (Singh et al., 2010). It is conceivable that *ter2*X3 at site II interacts with other *ter* sites elsewhere in the genome and thereby causes a change in chromosome architecture. In theory this could impact on replication restart from *RTS1*, perhaps by altering the timing and frequency of nearby replication origin firing or by somehow slowing the progression of the restarted fork. Alternatively, the restarted fork may be stably blocked at the *Ter2x3* barrier, and thereby prevented from undergoing template switch events.

3.3 Discussion

3.3.1 RDR induced by *RTS1* leads to genomic rearrangements as it progresses away from the site of its initiation.

Previous work has shown that break-independent RDR at *RTS1* is a default response to the collapsed fork and that recruitment of recombination proteins occurs as early as 10 minutes after fork stalling at the barrier (Ahn et al., 2005; Lambert et al., 2005; Nguyen et al., 2015). This contrasts starkly with BIR, which has a lag time of ~2 to 4 hours before replication is initiated (Jain et al., 2009; Malkova et al., 2005). Although, on one hand, RDR promotes genome stability by ensuring that replication is completed in a timely manner, its “error-prone” nature means that it can also cause non-allelic HR leading to chromosome rearrangements (Iraqui et al., 2012; Mizuno et al., 2013). In this chapter, I have shown that the infidelity of the restarted fork extends for at least 75 kb downstream from its point of initiation, with fork convergence curbing movement of the restarted fork [Fig. 3.iv]. The restarted fork does not seem to mature as it moves along, which contrasts with BIR where the migrating D-loop is susceptible to frequent

dissociation and template switching only up to a distance of 10 kb from the DSB (Smith et al., 2007; Stafa et al., 2014). Unlike the conservative replication in BIR that is primed by Pol δ (Saini et al., 2013; Wilson et al., 2013), recent work has shown that *RTS1*-induced RDR is semi-conservative, with Pol δ replicating both the leading and the lagging strands (Miyabe et al., 2015). However, both BIR and RDR proceed with normal replication speeds once initiated (Malkova et al., 2005; Miyabe et al., 2015).

Having established a system to study genomic rearrangements associated with the restart process, I went about systematically screening through selected genetic factors that could affect RDR and the progression of the restarted fork. A summary of my observations is provided in Table 3-1 and the key findings are discussed below.

3.3.2 Pfh1 promotes RDR and/or is needed for the progression of the restarted fork.

The reduction in direct repeat recombination, observed in both *pfh1* mutants investigated in my study, indicates that Pfh1 is needed for efficient replication restart from *RTS1* and/or for progression of the restarted fork. The observation that the fold reductions in recombination increase as the direct repeat is moved further from *RTS1* suggests that Pfh1 is needed for progression of the restarted fork. Moreover, the fact that the frequencies of recombination downstream of *RTS1* remain higher than the spontaneous levels, and are increased by deletion of *ori-1253*, indicates that replication restart and progression of the restarted fork can occur without Pfh1, albeit at a much reduced efficiency. Based on my data, I can also conclude that the efficiency of restart and/or progression of the restarted fork can be influenced by the amount of nuclear Pfh1 that is available. Overall, my data

Table 3-1: Role of genetic factors in preventing and promoting recombination at and downstream of *RTS1*.

Mutant	Fold change in recombination at the barrier*		Fold change in recombination 12.4 kb downstream of the barrier*	
	Gene conversions	Deletions	Gene conversions	Deletions
rad51Δ	2700 fold ↓	7 fold ↓	4 fold ↓	8 fold ↓
rad51Δ rad52Δ	4835 fold ↓	43 fold ↓	4950 fold ↓	70 fold ↓
rad54Δ	29 fold ↓	1.8 fold ↑	4 fold ↓	6 fold ↓
pfh1-m21	1.2 fold ↑	17 fold ↑	2 fold ↓	8 fold ↓
pfh1-mt*	1.3 fold ↑	15 fold ↑	4 fold ↓	36 fold ↓
elg1Δ	16 fold ↓	3 fold ↓	8 fold ↓	6 fold ↓
srs2Δ	8 fold ↑	5 fold ↑	21 fold ↑	5 fold ↑
rqh1Δ	3 fold ↑	20 fold ↑	2 fold ↑	3 fold ↑
fbh1Δ	7 fold ↑	20 fold ↑	13 fold ↑	10 fold ↑
rad8Δ	2.5 fold ↑	↔	1.6 fold ↑	↔
exo1Δ	2 fold ↓	2 fold ↓	2 fold ↑	2 fold ↑
fen1Δ	↔	2 fold ↓	↔	↔
mus81Δ	↔	1.5 fold ↑	↔	1.5 fold ↓
fml1Δ	8 fold ↓	↔	↔	↔
tid1Δ	↔	↔	↔	↔

↑-increase
↓-decrease
↔-no change
*-relative to wild-type

are consistent with the notion that Pfh1 performs a similar function as Pif1 in *S. cerevisiae*, which has been shown to promote BIR through aiding the progression of the migrating D-loop (Saini et al., 2013; Wilson et al., 2013). However, unlike Pif1, Pfh1 also has an Rrm3-like role in promoting replication termination and progression of forks past protein-DNA barriers (Steinacher et al., 2012). How these different roles are controlled within the context of a single protein is a fascinating question that should be addressed in future studies.

3.3.3 Loss of Elg1 delays replication restart from *RTS1*.

From the data in Section 3.2.6, it is observed that there is a reduction in direct repeat recombination downstream of the barrier in an *elg1*Δ mutant, which suggests that Elg1 might be needed for replication restart [Fig. 3.ix]. Indeed, this would be consistent with the hypothesis that Elg1 is the primary PCNA clamp unloader at stalled replication forks, and that removal of PCNA is one of the essential steps enabling fork remodeling and recombination protein recruitment (Kubota et al., 2013). Thus, in the absence of Elg1, there would be a delay in RDR at collapsed replication forks. The residual level of recombination, observed at the downstream reporter in an *elg1*Δ mutant, presumably indicates that some restart does occur either in the presence of unloaded PCNA or because PCNA unloading can occur by other, less efficient, mechanisms. In this regard, it is important to note that PCNA unloading by RFC, and other RFC-like complexes, has been demonstrated *in vitro* (Majka and Burgers, 2004)

3.3.4 Srs2 constrains template switching of the restarted fork.

Previous work has shown that Srs2 plays an important role in promoting RDR at *RTS1* (Lambert et al., 2010). However, as seen in Section 3.2.7, loss of Srs2 leads to a similar increase (~5 fold) in deletion-type recombinants, both at and

downstream of the barrier [Fig. 3.x & Table 3-1]. This contrasts with the *pfh1* mutants, which exhibit an increase in recombination at the barrier but a marked decrease downstream [Fig. 3.viii & Table 3-1]. Thus, if indeed Srs2 is needed for restart, the residual levels of restart in a *srs2*Δ mutant must be far more prone to template switching than would be the case in the wild-type cells. How Srs2 acts at and downstream of the barrier to limit recombination is an interesting question that warrants further investigation. Possibly, it can be attributed to the two distinct roles of Srs2, Rad51-nucleofilament disruption and D-loop dissociation (Dupaigne et al., 2008; Krejci et al., 2003; Veaute et al., 2003).

3.3.5 Loss of Rqh1 leads to increased genome instability by the restarted replication fork.

The *rqh1*Δ mutant exhibits hyper-recombination downstream of *RTS1* as described in Section 3.2.7. This could be explained either by increased RDR at the barrier, faster progression of the restarted fork or increased template switching in the absence of Rqh1. Previous work has shown that Rqh1 does not affect the efficiency of replication restart at the barrier (Lambert et al., 2010) and, therefore, it is more likely that the increase in recombination downstream of *RTS1* reflects faster movement of the restarted fork and/or an increased frequency of template switching. RecQ helicases have been shown to have anti-recombinogenic activities such as Rad51-ssDNA filament disruption and D-loop unwinding (Bugreev et al., 2007; Chu and Hickson, 2009; Hu et al., 2007). It is easy to imagine how a reduction in D-loop unwinding could result in an increase in template switching. Interestingly, deletion of *rqh1* results in a bigger fold increase in recombination at the barrier than downstream of it [Table 3-1], suggesting that Rqh1's role in limiting template switching may be less critical during progression of the restarted fork than it is during the initial phase of restarting replication.

3.3.6 Fbh1 is essential for limiting template switching during RDR

Our lab has previously shown that loss of Fbh1, even though not affecting spontaneous recombination, leads to a dramatic increase in ectopic recombination at *RTS1* [Table 3-1](Lorenz et al., 2009). Interestingly, in the *fbh1*Δ mutant, there is a surge of recombinants downstream of *RTS1*, even more so than that seen in either a *srs2*Δ or *rqh1*Δ mutant [Table 3-1]. These data indicate that Fbh1 is as important for constraining template switching during progression of the restarted replication fork as it is for limiting ectopic recombination during the process of restarting the replication fork. Potentially, it is the Rad51-disruptase activity of Fbh1 that limits template switching (Lorenz et al., 2009; Simandlova et al., 2013), either by aborting or preventing strand invasion events, especially at ectopic sites. However, if this is true, then it is puzzling why Srs2, which has a similar Rad51 nucleofilament disruptase activity, cannot substitute for Fbh1. Presumably, there are mechanisms at play that determine the precise deployment of these helicases. For example, one might work before strand invasion and the other might function during or after strand invasion. Whatever the explanation, it is clear that Fbh1, Srs2 and Rqh1, despite exhibiting similar activities *in vitro*, must all have distinct and non-redundant functions in limiting template switching during both the initiation of replication restart and the progression of the restarted fork.

3.3.7 Exo1 maintains the stability of the restarted fork.

From the results in Section 3.2.8, it would seem that Exo1 has contrasting roles in direct repeat recombination associated with the initial steps of RDR to that which is linked to progression of the restarted fork [Fig. 3.xi]. At *RTS1,* an *exo1Δ* mutant exhibits limited DNA resection behind the barrier leading to less extensive regions of ssDNA for loading of recombination proteins, such as Rad52 and Rad51, and, therefore, lower rates of recombination (Osman et al., 2016; Tsang et al., 2014;

Zhu et al., 2008). However, the increased frequency of direct repeat recombination observed downstream of the barrier suggests that restart still occurs, even though the extent of recombination protein loading at the barrier may be more limited. In fact the less extensive loading of recombination proteins behind the barrier could result in more efficient restart and, therefore, explain the increase in recombination downstream. Alternatively, the reduced level of DNA resection in a *exo1*Δ mutant might result in D-loops being formed with shorter ssDNA tails. Such D-loops may be "smaller" than regular D-loops and, therefore, be more susceptible to being unwound. If restarted replication proceeds in the form of a migrating D-loop, then anything that would decrease the stability of the D-loop might increase the frequency of template switching. However, one might also argue that a reduction in D-loop stability could also result in an overall slower progression of restarted replication, which would tend to reduce the frequency of direct repeat recombination downstream of the barrier. In order to distinguish between these possibilities it will be important to directly measure the efficiency of restart and rate of progression of the restarted fork in an *exo1*Δ mutant.

3.3.8 A hypothetical model for replication restart from the barrier.

Based on current data, a hypothetical model for RFB-induced RDR can be envisaged [Fig. 3.xvi] (Nguyen et al., 2015). It has been previously proposed that upon encountering an RFB, such as *RTS1*, the replication fork collapses [Fig. 3.xvi.a] (Ahn et al., 2005; Lambert et al., 2005). Fork reversal (carried out by Fml1) and resection (carried out by Exo1) of the collapsed fork then gives rise to a ssDNA tail onto which RPA, Rad52 and Rad51 would sequentially load (Sun et al., 2008). This is followed by strand invasion into homologous sequences, creating a D-loop onto which replication proteins assemble and commence DNA synthesis.

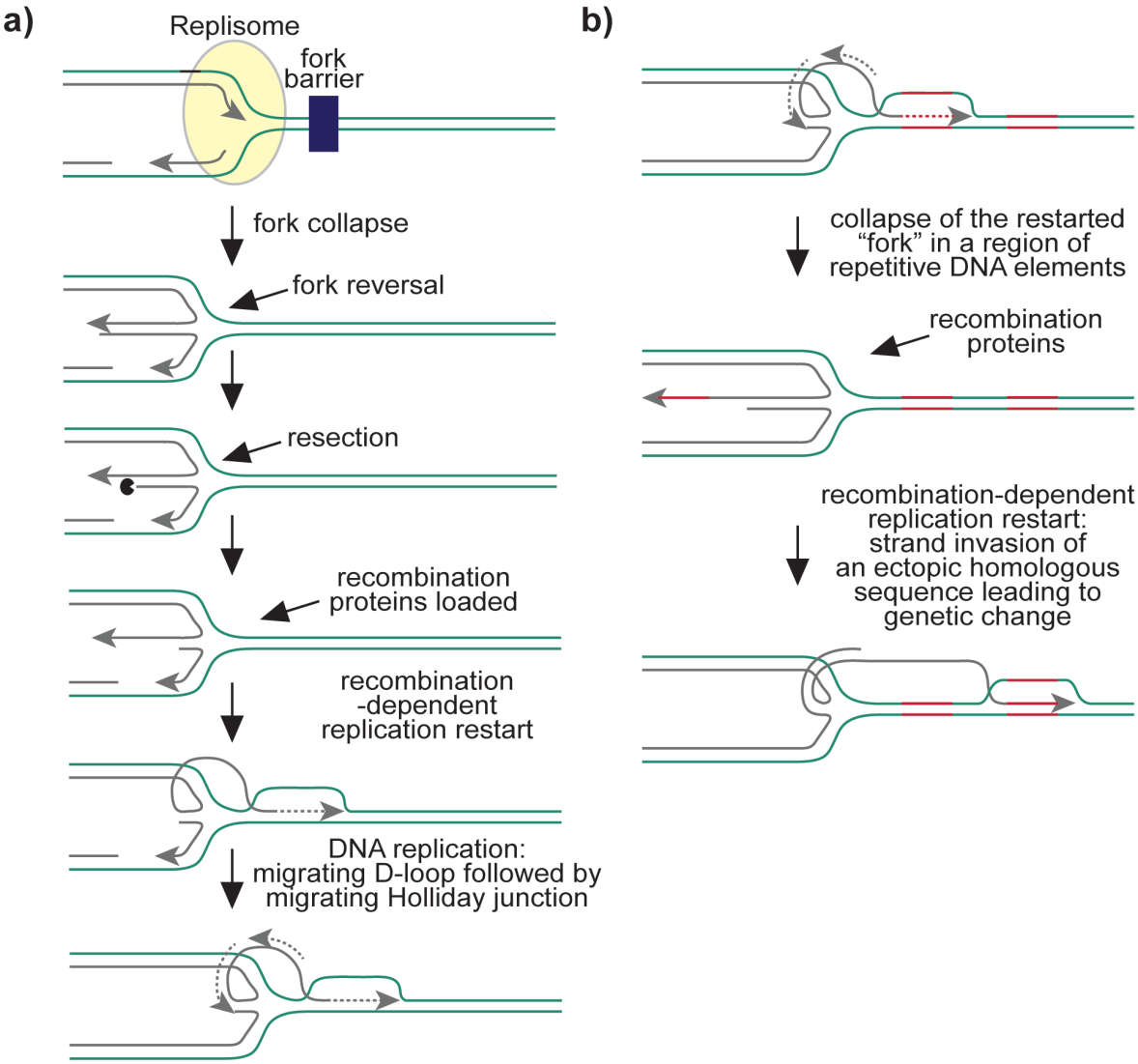


Fig. 3.xvi Hypothetical model for RFB-induced RDR.
a) Schematic model of the steps involved in RDR. Parental DNA strands are shown in green and the nascent strands in grey with arrows indicating the direction of DNA synthesis. b) Model for how RDR might give rise to inter-repeat recombination. The two patches of DNA highlighted in red represent a direct repeat of homologous sequences. Adapted from Nguyen et al., 2015.

Migration of restarted replication appears to be driven by the replisome's accessory DNA helicase, Pfh1 [Fig. 3.viii]. The error-prone nature of the restarted fork can be attributed to frequent template switching, which results in recurrent recruitment of HR proteins such as Rad51 that can catalyse ectopic recombination (Iraqui et al., 2012; Mizuno et al., 2013). This potentially arises because mechanistically RFB-induced RDR is similar to BIR involving a migrating bubble or D-loop at which replication occurs (Miyabe et al., 2015; Nguyen et al., 2015; Saini et al., 2013; Wilson et al., 2013). The major difference lies in the fact that the invading DNA strand might remain connected to the reversed fork structure from where it originated. Thus, the reversed fork is converted into a four-way DNA junction resembling a HJ by lagging strand synthesis that can then branch migrate behind the D-loop. This potentially aids in providing a substrate for efficient fork convergence aided by Pfh1 (Nguyen et al., 2015). Srs2, Rqh1 and Fbh1 seem to play an important role in limiting the template switching due to their anti-recombinase properties [Fig. 3.x]. However, some factors that influence template switching during BIR in *S. cerevisiae*, namely Mus81, Rdh54 and Fml1^{Mph1}, do not seem to do the same for restarted replication from *RTS1* [Fig. 3.xii].

If indeed the restarted "fork" traverses with a HJ moving behind a migrating D-loop, then any dis-coordination of the rate of transit of the two junctions could trigger template switching. For example, if the D-loop migration is impeded, the HJ behind might 'catch-up' with it leading to its dissociation and reformation of a reversed fork. HR proteins could then load onto the reversed fork and potentially catalyse ectopic recombination (i.e. template switching) [Fig. 3.xvi.b] (Nguyen et al., 2015). The high frequencies of ectopic recombination downstream of *RTS1* suggest that the putative D-loop migrating through *ade6-M375* dissociates frequently giving rise to strand invasions within the *ade6-L469* sequence [Fig. 3.iii].

The high proportion of deletions indicate that the re-established D-loop tends to move beyond the *ade6-L469* sequence rather than collapsing a second time within it, diminishing the chances of triggering a second re-invasion into *ade6-M375* to form an Ade^+ gene conversion.

3.3.9 Restarted forks are more susceptible to collapse at transcriptionally active sites.

As seen from the data in Section 3.2.11, there is increased recombinant formation when the restarted fork collides head-on with the transcription machinery at the tRNA gene [Fig. 3.xiii]. This increased template switching may also be attributed to the unstable nature of the D-loop and associated migrating HJ as proposed in the model [Fig. 3.xvi.a]. Increased genome instability due to the presence of weak RFBs has previously been observed in BIR where collisions between Ty elements and restarted replication has been shown to induce chromosomal rearrangements via increased template switching (Anand et al., 2014).

3.3.10 Measuring replication restart quantitatively

One of the limitations of my study is that changes in direct repeat recombination downstream of *RTS1* can be caused either by a change in replication restart or by a change in template switching. Therefore, if we knew what the efficiency of replication restart was in all cases, we could more accurately determine whether changes in direct repeat recombination reflected actual changes in template switching. One approach that could be used to accurately measure restart, as well as progression of the restarted fork, is polymerase usage sequencing (Pu-Seq) (Keszthelyi et al., 2015). This is a next generation sequencing technique that enables one to quantify what proportion of the Crick and Watson strands are replicated by Pol ε and Pol δ at any genomic site. Using Pu-Seq, Miyabe et. al. showed that restart from *RTS1* is semi-conservative and that Pol δ replicates both

the leading and lagging strands (Miyabe et al., 2015). In order to use Pu-seq to analyse replication restart, I had to introduce genes encoding mutant versions of Pol ε and Pol δ catalytic subunits, which mis-incorporate ribonucleotides at high rates, into the genetic background of my assay system. In addition, the cells were deleted for *rnh201*, the gene encoding the catalytic subunit of RNase H2, which is the proof-reading enzyme responsible for removing mis-incorporated ribonucleotides (Keszthelyi et al., 2015). *RTS1* is placed at the endogenous *ade6* locus so that I could study the effect of the various mutants on the rate of replication restart [Fig. 3.xvii.a].

Before proceeding with construction of the various mutant strains, I thought it prudent to determine whether replication past *RTS1* in the polymerase mutants (i.e. *cdc20*^{M603F} and *cdc6*^{L591G}) is similar to that in wild type. The replication intermediates in the vicinity of *RTS1* from both polymerase mutants look comparable to those from wild-type as judged by 2D gel analysis, with similar levels of replication fork blockage, termination and restart [Fig. 3.xvii.b & c]. Having confirmed that replication fork blockage and restart appear similar in both wild-type and polymerase mutants, the next step is to introduce mutants, such as *pfh1-m21* and *exo1*Δ, into the 'Pu-seq strain' background so that the Pu-Seq analysis can be performed to assess restart efficiency. Unfortunately, due to time constraints, this has yet to be done.

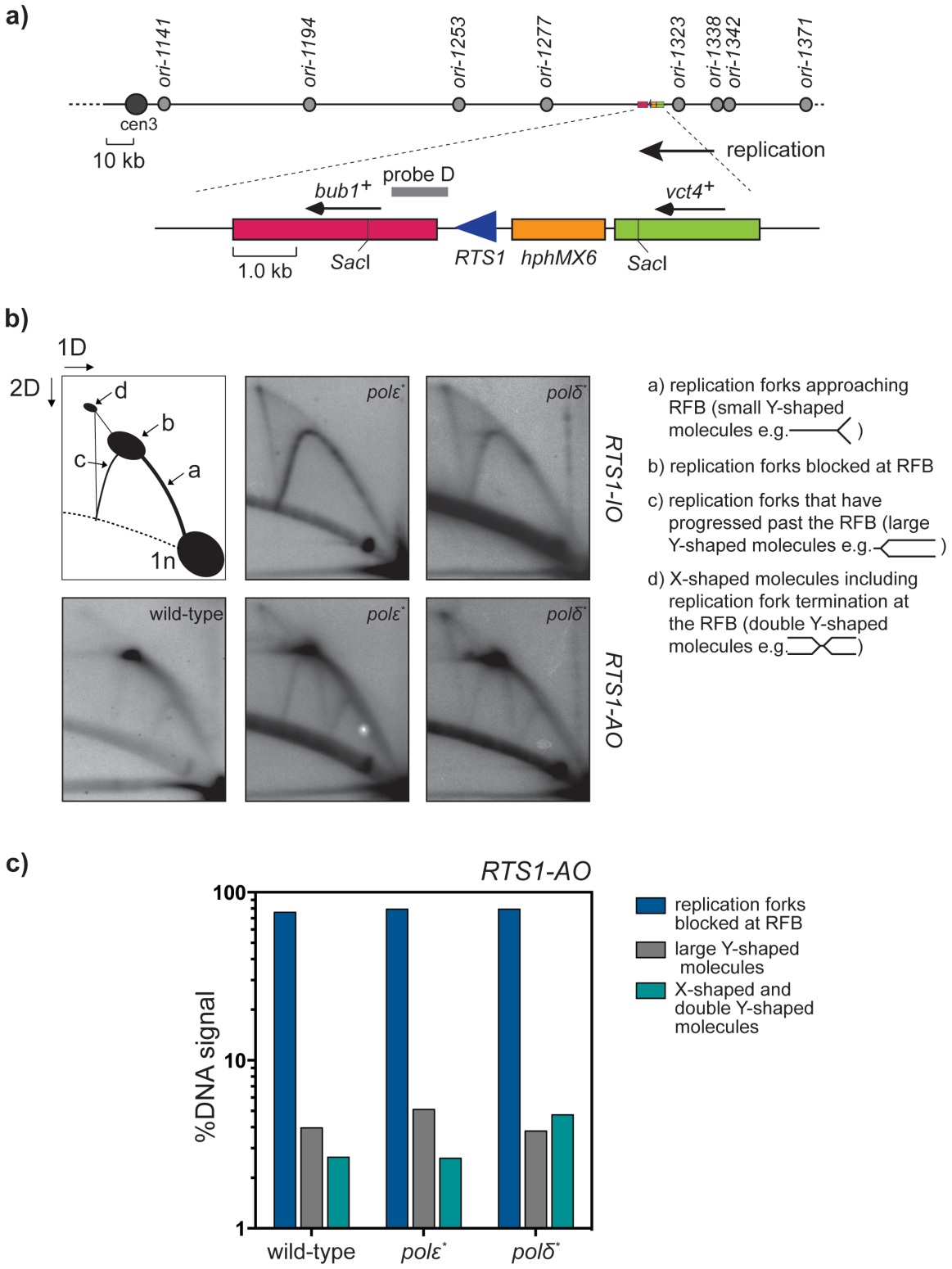


Fig. 3.xvii 2D gel analysis of replication intermediates at *RTS1* in wild-type and polymerase mutants.

a) Schematic showing the relative position of *RTS1* on ChrIII replacing the *ade6* gene and Probe D used for 2D gel analysis. b) 2D gel analysis of replication intermediates within the *Sac*I fragment shown in (a). The top-left panel is a guide for interpreting the 2D gels. c) Quantification of the 2D gels displayed as bar charts. The DNA was extracted from asynchronously growing cultures of the strains MCW7223, MCW8030, MCW8031, MCW8032 and MCW8033. The *Pol ε** mutant is *cdc2O*^{M603F} and the *Pol δ** mutant is *cdc6*^{L591G}

Chapter 4

Developing a novel accidental protein-DNA barrier for studying the cellular response to replication fork blockage

4.1 Introduction

Much of our current understanding of how protein-DNA RFBs induce HR in eukaryotes comes from the study of the site-specific RFB, *RTS1*, which is native to fission yeast (Ahn et al., 2005; Lambert et al., 2005, 2010; Pryce et al., 2009). However, this programmed RFB has evolved to work closely with the replisome and components of the fork protection complex to create a very strong polar block to replication (Pryce et al., 2009). *RTS1* predominantly causes replication fork collapse and elicits DSB-independent RDR and, in doing so, occasionally causes genome rearrangements. If RDR is inhibited, replication is completed by convergence of the opposite fork. In order to study what happens when a replication fork encounters an "accidental" protein-DNA barrier, *lacO* arrays bound by LacI have been used. In contrast to *RTS1*, *lacO*-LacI forms a weak bi-directional RFB in fission yeast that can cause DNA breaks that are repaired by single-strand annealing (SSA) (Sofueva et al., 2011). However, in order to create a functional barrier that induced high rates of replication stress, multiple copies (115) of the *lacO* sequence had to be introduced into the fission yeast genome. This has led to questions about the physiological relevance of such large arrays and whether they truly represent what happens at naturally occurring accidental protein-DNA barriers. In order to gain further insight into the universality of the recombinational response to RFBs, I engineered a novel site-specific protein-DNA barrier system (called Mariner Block or MarBl), modeled on the human *Tc1-mariner* transposon, *Hsmar1*.

Hsmar1 (*Homo sapiens mariner 1*) was the first *Tc1-mariner* transposon to be identified in the human genome (Cordaux et al., 2006). It is proposed to have been active in the primate genome about 50 million years ago and is classified as a Class II or DNA-mediated transposable element. It generally consists of a single

gene encoding a transposase flanked by short terminal inverted-repeats (TIR) that are usually <30bp in length (Cordaux et al., 2006; Miskey et al., 2007; Robertson and Zumpano, 1997). Its mobilization is catalyzed by the transposase, a member of the recombinase family of proteins, which acts by a 'cut-and-paste' mechanism [Fig. 4.i] using a single-active site to cleave both strands via a DNA-hairpin intermediate (Claeys Bouuaert and Chalmers, 2009; Claeys Bouuaert et al., 2013; Plasterk et al., 1999). *In vitro* Hsmar1 cleaves both strands of the DNA at either end of the transposon, however if it is provided with only one transposon end, it cleaves only one strand (Claeys Bouuaert and Chalmers, 2009). Importantly, the Hsmar1 transposase binds very tightly to a single TIR, with a half-life of more than 30 minutes (R. Chalmers, personal communication).

Exploiting these properties of *Hsmar1*, a non-native protein-DNA barrier was engineered in fission yeast, consisting of a modified version of the *Hsmar1* transposase tightly binding to the TIR sequence of its transposon, potentially impeding the progression of the replication fork past the barrier. By characterising what happens when a replication fork encounters Hsmar1 bound to a single TIR, I aimed to elucidate the cellular response that is triggered when there is a collision between the replisome and a naturally occurring strong accidental protein-DNA barrier. Moreover, by studying it in the same chromosomal context as *RTS1*, my aim was to draw a direct comparison between accidental and programmed site-specific RFBs.

4.2 Results

4.2.1 Constructing an accidental RFB using a reconstituted human *Tc1-mariner* transposase

Tc1-mariner transposons mobilise DNA via a cut-and-paste mechanism as shown in Fig. 4.i (Claeys Bouuaert and Chalmers, 2009; Skipper et al., 2013). The

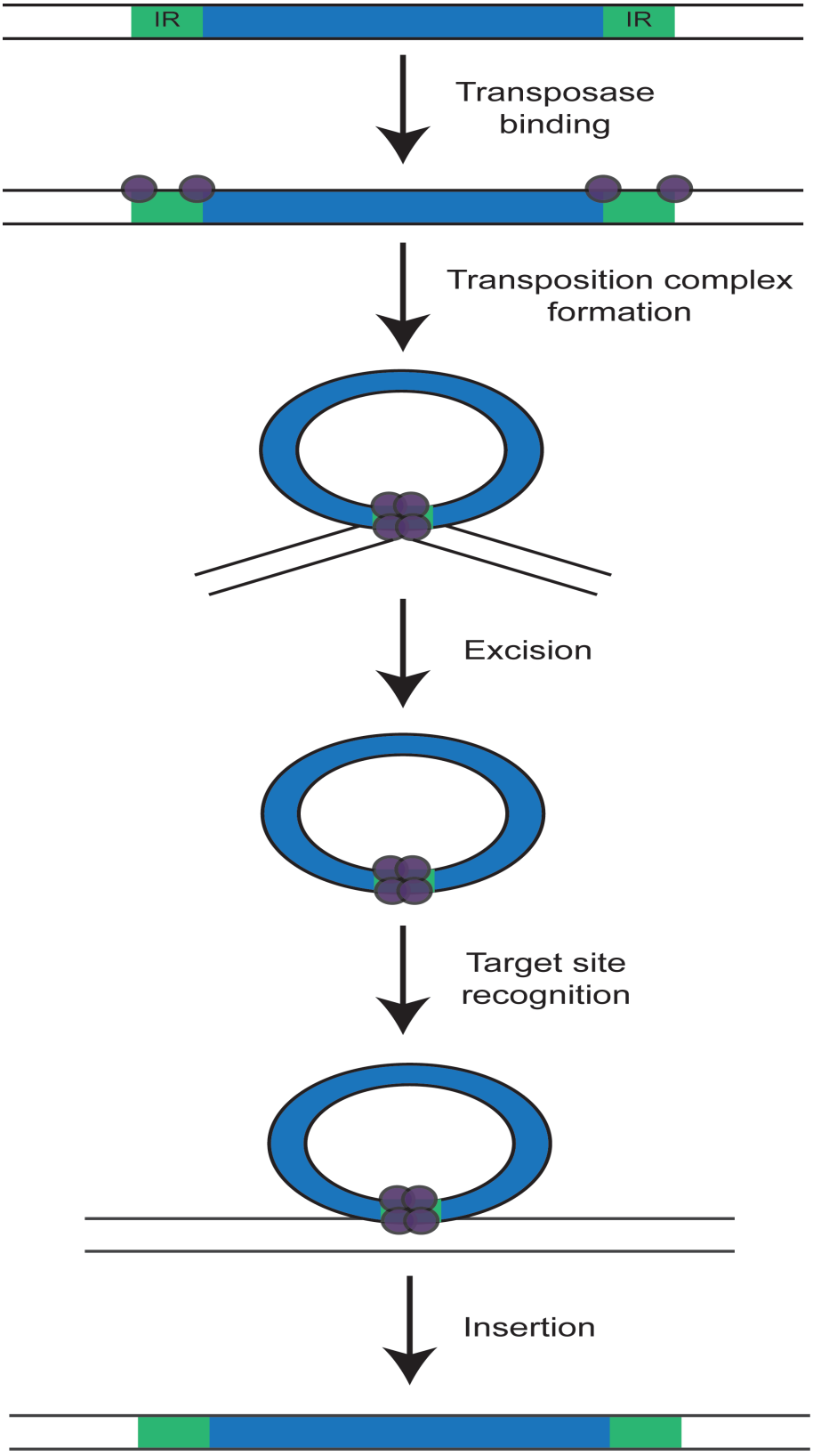


Fig. 4.i Model for the transposition action performed by the Tc1/mariner element. A schematic representation of the steps involved in the 'cut-and-paste' reaction performed by the mariner transposase. Green boxes marked with IR represent the TIRs at the ends of the transposon (blue box). The purple spheres represent the transposase (Modified from Skipper et al., 2013).

transposase proteins recognise the TIRs and form a circular pre-excision synaptic complex from which the transposon is excised by a transposase-mediated DSB, leaving behind 2 or 3 bp 3' overhangs at the transposon ends. Formation of the complex allows close association of the two transposon ends, held together by a tertramer of transposase. Subsequently, the transposition complex recognises a TA-dinucleotide target site and the transposase proteins mediate integration of the transposon.

A resurrected copy of the *Hsmar1* transposase, which was deduced by computational analysis of "fossil" *Hsmar1* elements, has been shown to be highly active *in vitro* (Claeys Bouuaert and Chalmers, 2009; Miskey et al., 2007). *Hsmar1* differs from other cut-and-paste transposase in that it makes the first nick at the transposon end and joins it to the target site, the second strand is cut by a related type II restriction endonuclease (Claeys Bouuaert and Chalmers, 2009). Work done to characterise the resurrected *Hsmar1* by the Chalmers lab has shown that a dimer of the *Hsmar1* transposase binds very tightly to a single transposon end sequence *in vitro* (Claeys Bouuaert and Chalmers, 2009).

In order to establish the MarBI system, the 30 bp *Hsmar1* transposon end sequence (including the flanking TA dinucleotide) was inserted between the direct repeat of *ade6*$^{-}$ heteroalleles at site I on ChrIII at an equivalent position to where *RTS1* had been inserted previously [Fig. 4.ii.a]. Thus the effect of MarBI on recombinant formation can be scored in a similar way as with the *RTS1* system [See Chapter 3, Fig. 3.i.a]. Two strains were constructed, one for each orientation of the transposon end so that any effect of its polarity, with respect to the direction of replication, could be assessed. For the sake of brevity, the two orientations of the transposon end sequence will be referred to as TO1 and TO2 (for transposon

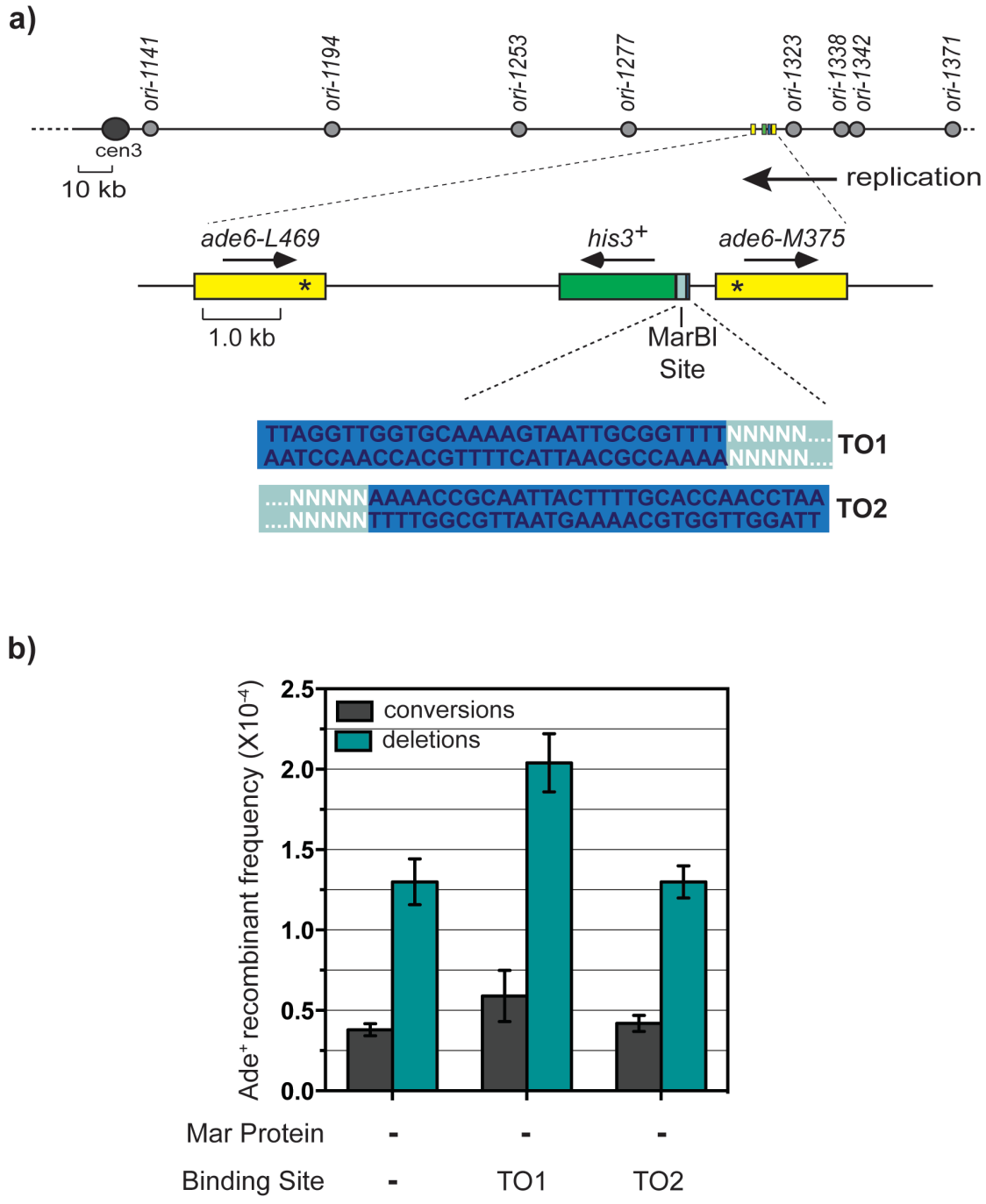


Fig. 4.ii The MarBI system: MarBI site.
a) Schematic showing the relative position of the *ade6*$^{-}$ intra-chromosomal recombination substrate flanking the *his3*$^{+}$ gene and the MarBI site in relation to nearby replication origins (grey circles) on ChrIII. The two orientations of the MarBI site are represented in the schematic below. b) Bar chart showing the frequency of Ade^{+} recombinants in strains with no MarBI site, TO1 and TO2 in the absence of expression of Mar. Error bars represent ± standard error of the mean. The strains are MCW39*, MCW3118 and MCW3258.

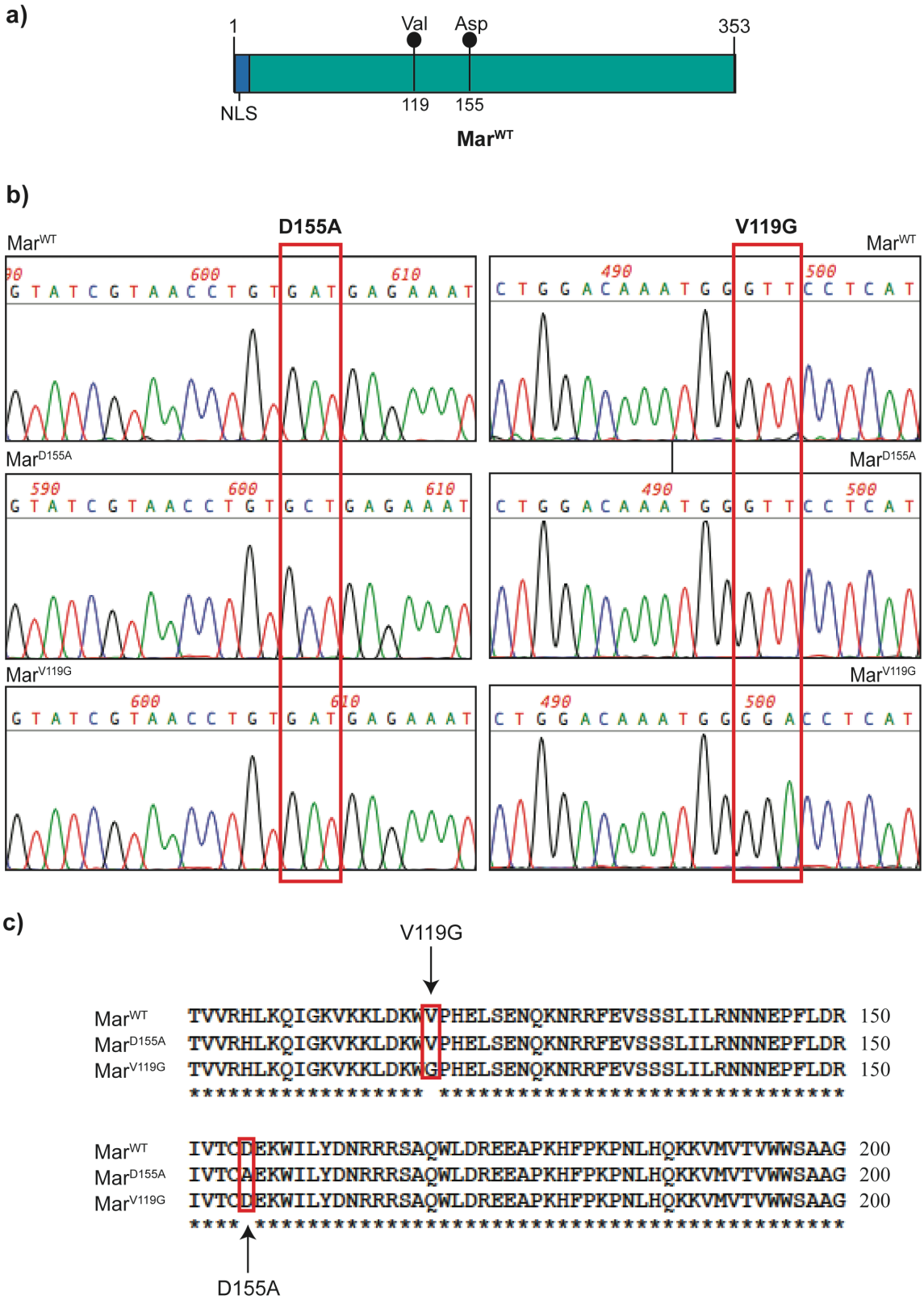


Fig. 4.iii The MarBI system: Mar Protein.
a) Schematic showing the wild-type Mar protein that has an NLS sequence at the N-terminal. The residues that are altered in the mutants are marked. b) Sequencing results of the plasmids to confirm the**.** **T**he plasmids are pMJ5 (NLS-MAR^{WT}), pMJ13 (NLS-MAR^{D155A}) and pMJ14 (NLS-MAR^{V119G}) sequenced using the primer oMW1172. c) ClustalW2 alignment of the mutants.

end orientation 1 and 2, respectively). In the case of TO1, the sequence that is bound by *Hsmar1* is positioned in the leading template strand (assuming DNA replication across the region is in the telomere to centromere direction), whereas, for TO2 it is in the lagging template strand [Fig. 4.ii.a]. To confirm that the inclusion of either TO1 or TO2 had no effect on the background level of spontaneous recombination, I compared the frequency of direct repeat recombination in strains with and without TO1/2 [Fig. 4.ii.b &Table 8-2]. The presence of either TO1 or TO2 made little or no difference to the frequency of spontaneous recombination.

Having established strains containing the *Hsmar1* binding site, I next made constructs for the expression of *Hsmar1* transposase in *S. pombe*. For the sake of brevity I will refer to the *Hsmar1* protein as Mar henceforth. For my preliminary experiments, a nuclear localization signal (NLS) was fused to the N-terminus of Mar and the resulting NLS-Mar protein was expressed from the thiamine-repressible *nmt41* promoter in the plasmid pREP41. However, for the majority of experiments described below, NLS-Mar was expressed from the *nmt1* promoter integrated either at the *lys1* locus on ChrI or the *ura4* locus on ChrIII.

Expression of NLS-Mar^{WT}, from the pREP41 plasmid in a strain with TO1, caused a ~340 fold increase in gene conversions and ~87 fold increase in deletions [Fig. 4.iv.b &Table 8-2]. In contrast, the control strain containing TO1, transformed with an empty pREP41 plasmid, showed recombination frequencies similar to that of a wild-type strain [Fig. 4.iv.b &Table 8-2]. Intriguingly, Mar-induced recombination is biased towards gene conversions (52%), which is similar to what is seen with *RTS1*, and quite different from *lacO*-LacI, which induces mainly Rad51-independent recombinants (Ahn et al., 2005; Sofueva et al., 2011).

The Hsmar1 transposase has two basic activities, DNA binding and DNA cleavage. As both protein-DNA binding and nicked DNA can potentially impede

replication fork progression (Ahn et al., 2005; Osman et al., 2016), it was essential to determine which of these two functions was causing the induction of recombination. To do this I compared the activity of the "wild-type" Mar protein and two of its mutant forms, which had previously been characterised *in vitro* by the Chalmers lab [Fig. 4.iii.a & c]. The mutants in question are Mar^{D155A}, which is totally devoid of nucleolytic activity, and Mar^{V119G}, which exhibits impaired nucleolytic activity (R. Chalmers, personal communication). Importantly, both mutant proteins bind just as well as the wild-type protein to the transposon TIR sequence (R. Chalmers, personal communication). The genes encoding the mutant versions of Mar were cloned into pREP41, and verified by DNA sequencing [Fig. 4.iii.b].

In order to ascribe the recombination-inducing activity of MarBl to either its DNA binding or nucleolytic activity, recombination frequencies at the *ade6*$^{-}$ reporter were compared for Mar^{WT}, Mar^{D155A} and Mar^{V119G}. For this experiment the different versions of Mar were expressed with a C-terminal GFP fusion from the *nmt41* promoter in pREP41 so that their expression levels could be monitored. On assaying for Ade^{+} recombinants, it was observed that the number of Ade^{+} recombinants with Mar^{D155A} was comparable to the spontaneous Ade^{+} recombination levels with the empty pREP41 plasmid, with no significant difference in both the gene conversions and deletions [Fig. 4.iv.c &Table 8-2]. In contrast, expression of Mar^{V119G} yielded a noticeable induction of both gene conversions and deletions, however, this was still significantly less than the level obtained with the wild-type Mar protein [Fig. 4.iv.c &Table 8-2]. These data suggest that the nucleolytic activity of Mar is essential for inducing direct-repeat recombination and that the binding of Mar to TO1 alone does not induce recombination. Hence, it was concluded that the MarBl system was a novel

Fig. 4.iv The effect of MarBl on direct repeat recombination at the endogenous *ade6* locus on ChrIII.

a) Schematic showing the relative position of the direct repeat recombination reporter with the MarBl site in orientation TO1. b) Bar chart showing the frequency of Ade^{+} recombinants in strains expressing Mar^{WT} from the *nmt41* promoter of the pREP41 plasmid. Strains with no plasmid and expressing the empty vector are analysed as controls. Error bars represent ± standard error of the mean. c) Bar chart showing the frequency of Ade^{+} recombinants in strains expressing the C-terminal eGFP tagged Mar^{WT}, Mar^{D155A} or Mar^{V119G} from the *nmt41* promoter of the pREP41 plasmid. The strain expressing the empty vector is analysed as control. d) Western-blot analysis of the expression levels of Mar-eGFP in the strains. Tubulin is used as a loading control. Error bars represent ± standard error of the mean. The strains are MCW3118, MCW3119, MCW3120, MCW3121, MCW6630 and MCW6631. e) Expression analysis of strains expressing wild-type and mutant Mar protein in the presence (repressed) and absence (de-repressed) thiamine to check if there is an adverse effect on growth. The strains are FO656 (-), MCW6371 (+), MCW6626 (D155A) and MCW6627 (V119G).

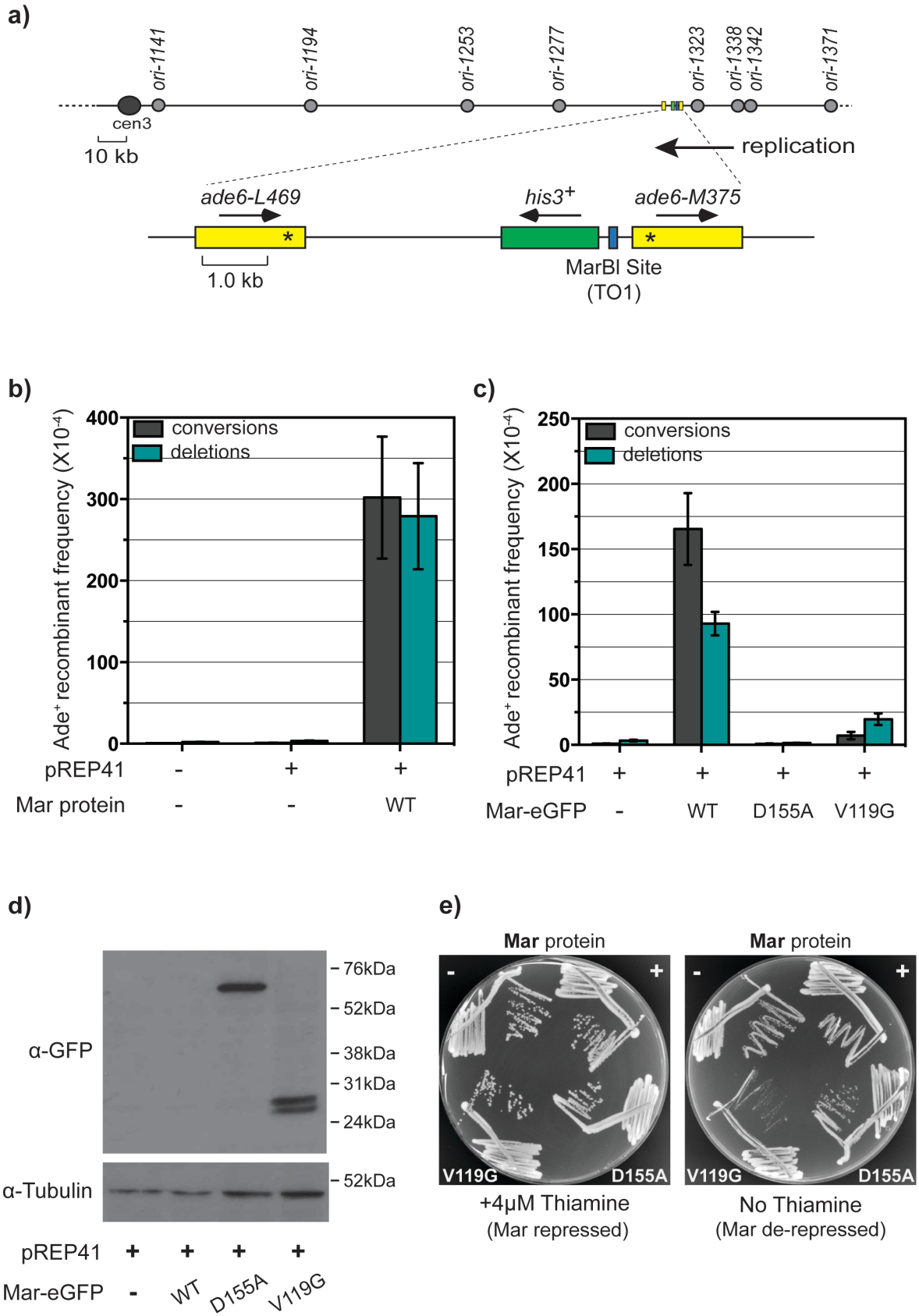


Fig. 4.iv The effect of MarBI on direct repeat recombination at the endogenous *ade6* locus on ChrIII.

site-specific nick inducing system that could be used to study the effect of ssDNA breaks on perturbing the progress of the replication fork. Both Mar^{D155A} and Mar^{V119G} would act as perfect controls for this system.

To confirm that these differences in recombination frequency were not due to a lack of mutant Mar protein expression, I performed a western blot analysis of the level of Mar-GFP in the colonies taken from the same plates that were used for the recombination assay [Fig. 4.iv.d]. Despite strongly inducing the formation of Ade^+ recombinants, I failed to detect "wild-type" Mar-GFP, whereas Mar^{D155A}-GFP was readily detected. Intriguingly, no full-length Mar^{V119G}-GFP was detectable, only two shorter fragments [Fig. 4.iv.d]. This is presumably the product of proteolysis and suggested that there might be differential turnover rates of the three proteins in the cell.

4.2.2 Binding of Mar to a single transposon end induces direct repeat recombination

In order to limit cell-to-cell variation in Mar protein levels owing to unequal copy number of the Mar protein expressing plasmid, a single copy of the *Mar* gene was integrated into the yeast genome. It was fused to a NLS and the *nmt1* promoter controlled its expression. Unlike with the expression plasmids described in the previous section, the chromosomally integrated copy of *mar* did not encode a C-terminal GFP fusion. To verify that expression of Mar did not cause any general toxicity to the cell, the growth rate of cells expressing the three different Mar alleles were compared under both repressed (+ thiamine) and de-repressed (no thiamine) conditions [Fig. 4.iv.e]. Interestingly, expression of Mar^{V119G} resulted in poor growth, whereas, cells expressing either Mar^{WT} or Mar^{D155A} did not. Therefore, it was decided to focus on Mar^{WT} and use Mar^{D155A} as the sole control.

In order to confirm that protein expressed from the integrated copy of the Mar gene was sufficient to elicit a recombinational response, in a similar manner to when it was expressed from the plasmid, a direct repeat recombination assay was performed [Fig. 4.v.b & Table 8-2]. On this occasion, the assay was conducted both in the presence and absence of thiamine (1μM) to determine whether induced levels of recombination would only occur when the Mar protein was fully expressed. In the presence of thiamine, or in the absence of TO1/2, Mar^{WT} caused no induction of recombination over spontaneous levels [Fig. 4.v.b & Table 8-2]. However, as seen before, upon full expression of the Mar^{WT} protein in the absence of thiamine, and presence of either TO1 or TO2, strong induction of recombination was observed [Fig. 4.v.b & Table 8-2]. In the case of TO1, the gene conversions increased by ~786 fold and the deletions by ~565 fold. For TO2, the gene conversions increased by ~1000 fold and the deletions by ~620 fold. These data confirm that MarBI is an inducible site-specific system that activates recombination. Moreover, both orientations of the Mar binding site result in similar high levels of recombination.

I next wanted to test whether there was no recombination induced due to the protein-DNA block created when Mar binds to its transposon end, as observed in the plasmid based assay. A side-by-side comparison of recombination induced by Mar^{WT} and Mar^{D155A} was therefore performed, with both being expressed in the absence of thiamine from equivalent integrated gene constructs [Fig. 4.vi.a & Table 8-2]. To my surprise, I observed that Mar^{D155A} induced recombinant formation to at least the same extent as Mar^{WT}. When TO1 was present, there was ~2300 fold increase in gene conversion and ~1300 fold in deletions compared to the no transposon end control [Fig. 4.vi.a & Table 8-2]. Similarly, with TO2 there was a ~2760 fold increase in gene conversions and ~1800 fold increase in

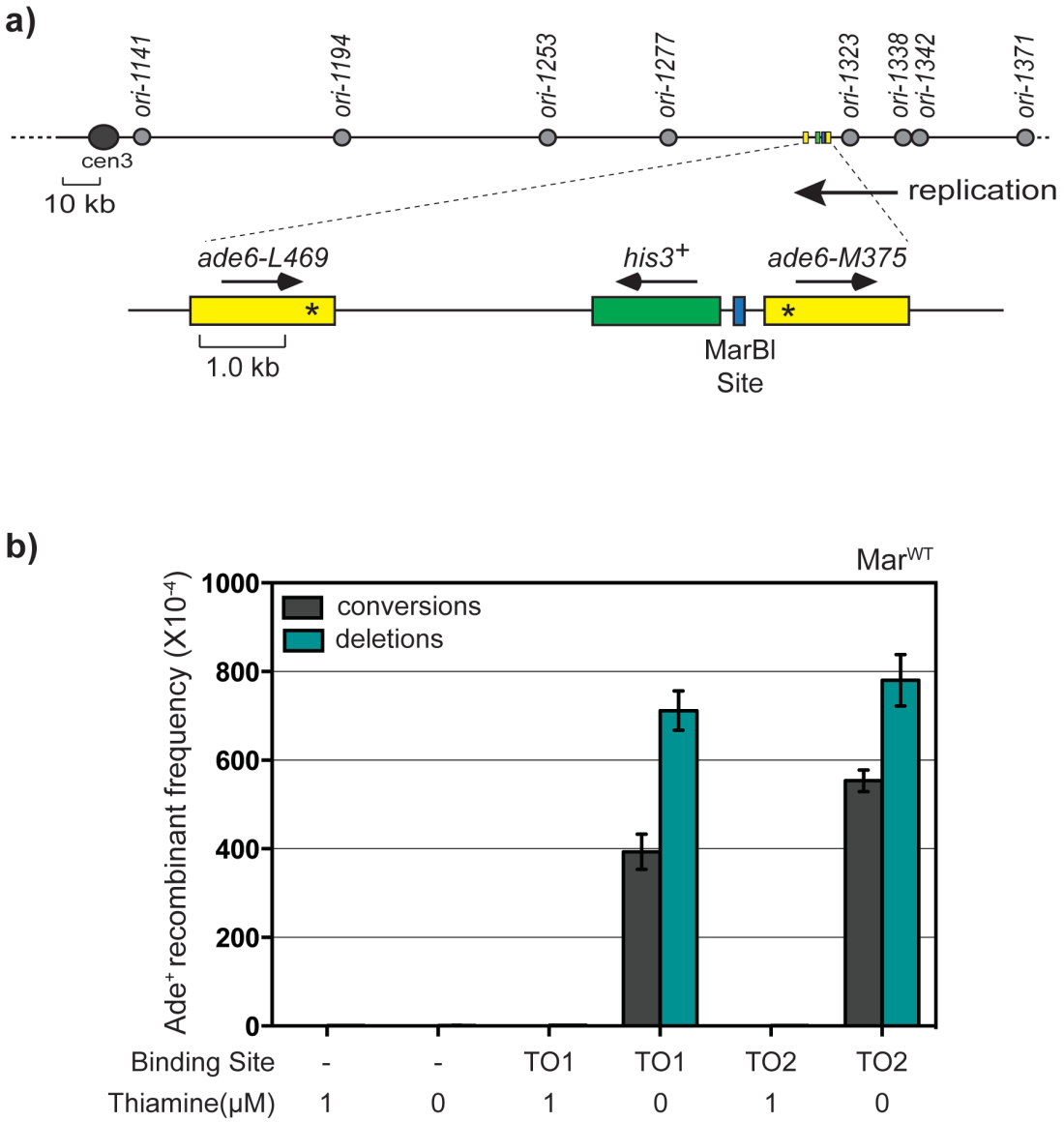


Fig. 4.v The MarBI system induces direct repeat recombination.
a) Schematic showing the relative position of the direct repeat recombination reporter with the MarBI site. b) Bar chart showing the frequency of Ade^+ recombinants in strains expressing Mar^{WT} from the *nmt1* promoter integrated in the yeast genome. The MarBI site is present either in TO1 or TO2. The no binding site strain is analysed as the control. The inducibility of the system is tested by performing the assay either in the presence (repressed) or absence (de-repressed) of 1μM thiamine. Error bars represent ± standard error of the mean. The strains are MCW7096, MCW7098 and MCW7099.

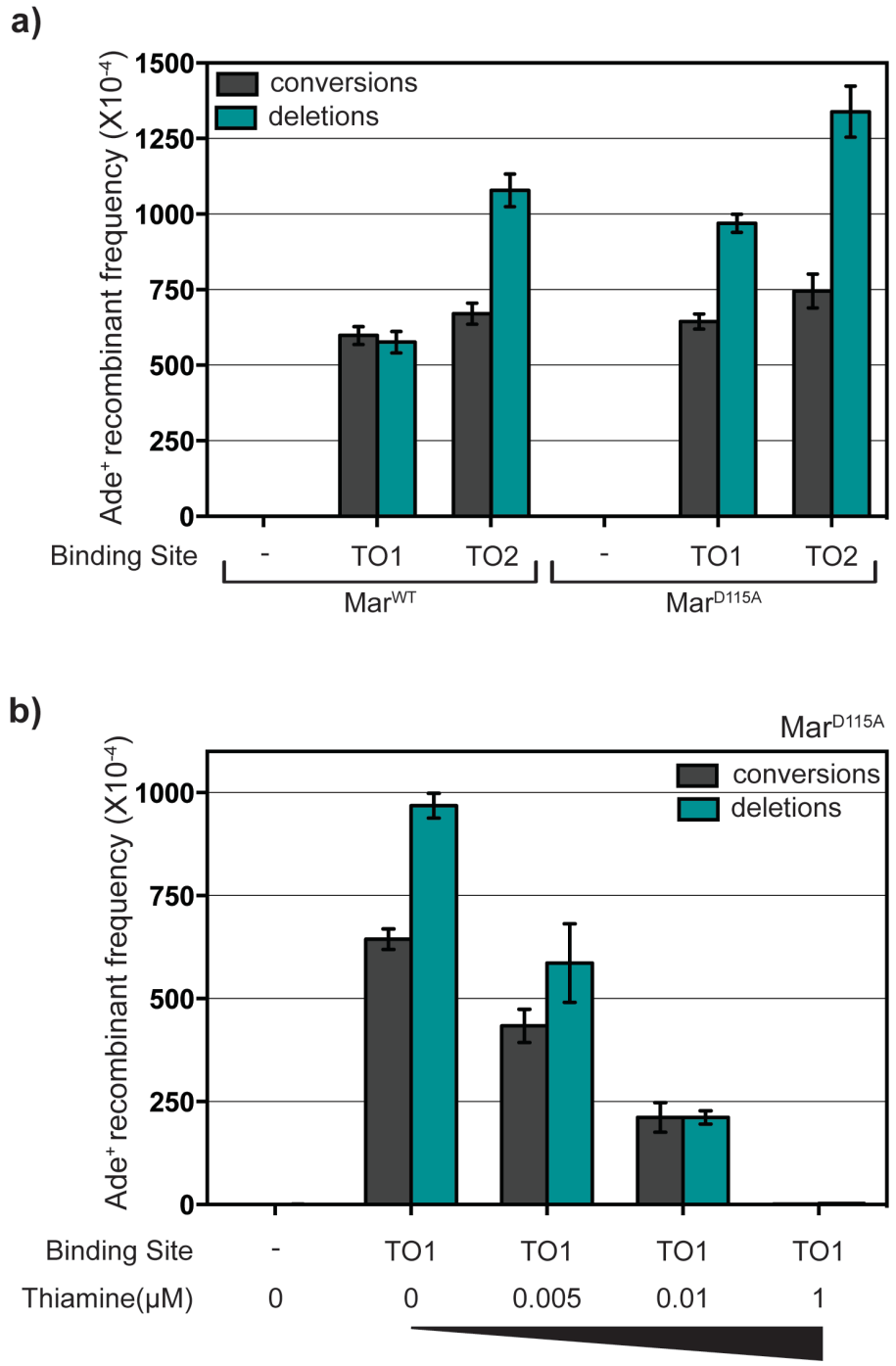


Fig. 4.vi The catalytically-dead version of MarBl (MAR^{D155A}) induces direct repeat recombination.

a) Bar chart showing the frequency of Ade^{+} recombinants in MCW6481, MCW6487, MCW6489, MCW8239, MCW7076 and MCW7098. (The Mar protein expression driven from the integrated *nmt1* promoter and the binding site is present either in TO1 or TO2.) Error bars represent ± standard error of the mean. b) Bar chart showing the increasing frequency of Ade^{+} recombinants in a dose-dependent manner in response to de-repression of the *nmt1* promoter. Error bars represent ± standard error of the mean. The strains are MCW8239 and MCW7076.

deletions. Importantly, Mar^{D155A} expression in the absence of the transposon end did not induce recombination over and above the spontaneous level [Fig. 4.vi.a &Table 8-2], indicating that the interaction of the Mar protein to its binding site is essential for inducing recombination. Altogether, these data suggest that it is the DNA binding property of MarBI that is the primary factor in inducing recombination, and that its putative nucleolytic activity may make little or no contribution. The discrepancy between the experiments performed with plasmid-based expression of Mar and chromosomal-based expression may relate to the presence and absence of the GFP tag. I suspect that the GFP tag impairs DNA binding by the Mar protein. For reasons that are still unclear, it seems that Mar^{WT} is affected less by the GFP tag than Mar^{D155A}, perhaps because the tag is more readily clipped off it *in vivo*, leaving fully functional untagged protein to bind DNA.

To further characterize the MarBI system, I performed a recombination assay with increasing concentrations of thiamine (0μM, 0.005μM, 0.01μM and 1μM) to study the dose-dependent effect of the Mar^{D155A} protein on recombinant formation [Fig. 4.vi.b &Table 8-2]. As expected, there is a significant drop in both gene conversions and deletions with increasing thiamine concentration. These data suggest that increasing the level of Mar protein increases the probability that it will block replication and elicit a recombinational response.

4.2.3 MarBI is a bi-directional RFB.

For ease of representation in this study, I have defined two states of the MarBI system: MarBI ON and MarBI OFF. Based on the nature of the Mar protein and presence and absence of the TO site, the various “isoforms” of the MarBI OFF and ON are described in Table 4-1. However, it is important to note that there is no significant difference in the cellular response to the different forms of the inactive barrier (MarBI OFF), and a recombinational response is only elicited with MarBI

ON (i.e. when either TO1 or TO2 is present and when either Mar^{WT} or Mar^{D155A} is expressed). MarBI ON^1 and MarBI ON^2 represent an active barrier differing only with respect to the orientation of the transposon end (TO1 and TO2).

To determine whether MarBI perturbs replication fork progression 2D gel electrophoresis was performed to analyse replication intermediates within the *ade6*$^-$ duplication region as described in Section 2.4.4. [Fig. 4.vii.a]. Replication intermediates in the EcoNI fragment containing MarBI run as a Y-arc from a 1C (unreplicated DNA) spot to the 2C (replicated DNA) intersection on the linear arc. If replication forks are blocked at a defined position, accumulation of intermediates should form a “spot” somewhere on the Y-arc. If the forks are blocked long enough at the barrier for replication to be completed by the opposing fork, it results in fork merging indicated by the accumulation of double Y-shaped DNA molecules [Fig. 4.vii.b-left panel]. With MarBI OFF (expression of either Mar^{WT} or Mar^{D155A} in the absence of TO1), a simple Y-arc was observed representing replication forks progressing through the EcoNI fragment [Fig. 4.vii.b]. In contrast, with all of the different variants of MarBI ON, a point of increased signal intensity was observed at or close to the apex of the Y-arc, which is indicative of replication fork pausing. Moreover, unlike with MarBI OFF, a prominent signal in the expected position for X-shaped or double Y-shaped molecules is present in each of the MarBI ON samples [Fig. 4.vii.b]. Quantification of the signal intensities within small well-defined sections of the Y-arc in two independent experiments confirmed these observations. The replication fork pause signal with MarBI ON^{+2} or MarBI ON^2 appears to be spread over a larger area along the apex of the Y-arc when compared to the signal with the MarBI ON^1 variants. This likely reflects the slightly different positions in which Mar will be binding to the DNA relative to the incoming

Table 4-1: Different 'isoforms' of the MarBI ON-OFF system.

MarBI System	Mar Protein	Transposon End
MarBI OFF$^{+\zeta}$	Mar^{WT}	-
MarBI ON^{+1}	Mar^{WT}	TO1
MarBI ON^{+2}	Mar^{WT}	TO2
MarBI OFF$^{\pi}$	-	-
MarBI OFF§	-	TO1
MarBI OFF$^{\zeta}$	Mar^{D155A}	-
MarBI ON^{1}	Mar^{D155A}	TO1
MarBI ON^{2}	Mar^{D155A}	TO2

A table defining the two stated of the MarBI system, MarBI ON and MarBI OFF based on the nature of the Mar protein and the presence or absence of the TO site.

Fig. 4.vii 2D gel analysis of replication intermediates at MarBI.
a) Schematic showing the relative position of the direct repeat recombination reporter with the MarBI site and Probe A used for 2D gel analysis. b) 2D gel analysis of replication intermediates within the *Eco*NI fragment shown in (a). The far left panel is a guide for interpreting the 2D gels. Arrows on the right hand panel indicate the pause sites. c) Quantification of the 2D gels displayed as bar charts showing the mean values from two independent experiments. Error bar represents the standard error error of the mean. The DNA was extracted from asynchronously growing cultures of the strains MCW6481, MCW6487, MCW6489, MCW7075, MCW7076 and MCW7078. MarBI $OFF^{+\xi}$ represents the system where the Mar^{WT} protein is expressed but the transposon end is absent, MarBI ON^{+1} where Mar^{WT} is expressed and TO1 is present and MarBI ON^{+2} where Mar^{WT} is expressed and TO2 is present. MarBI OFF^{ζ} represents the system where the Mar^{D155A} protein is expressed but the transposon end is absent, MarBI ON^{1} where Mar^{D155A} is expressed and TO1 is present and MarBI ON^{2} where Mar^{D155A} is expressed and TO2 is present.

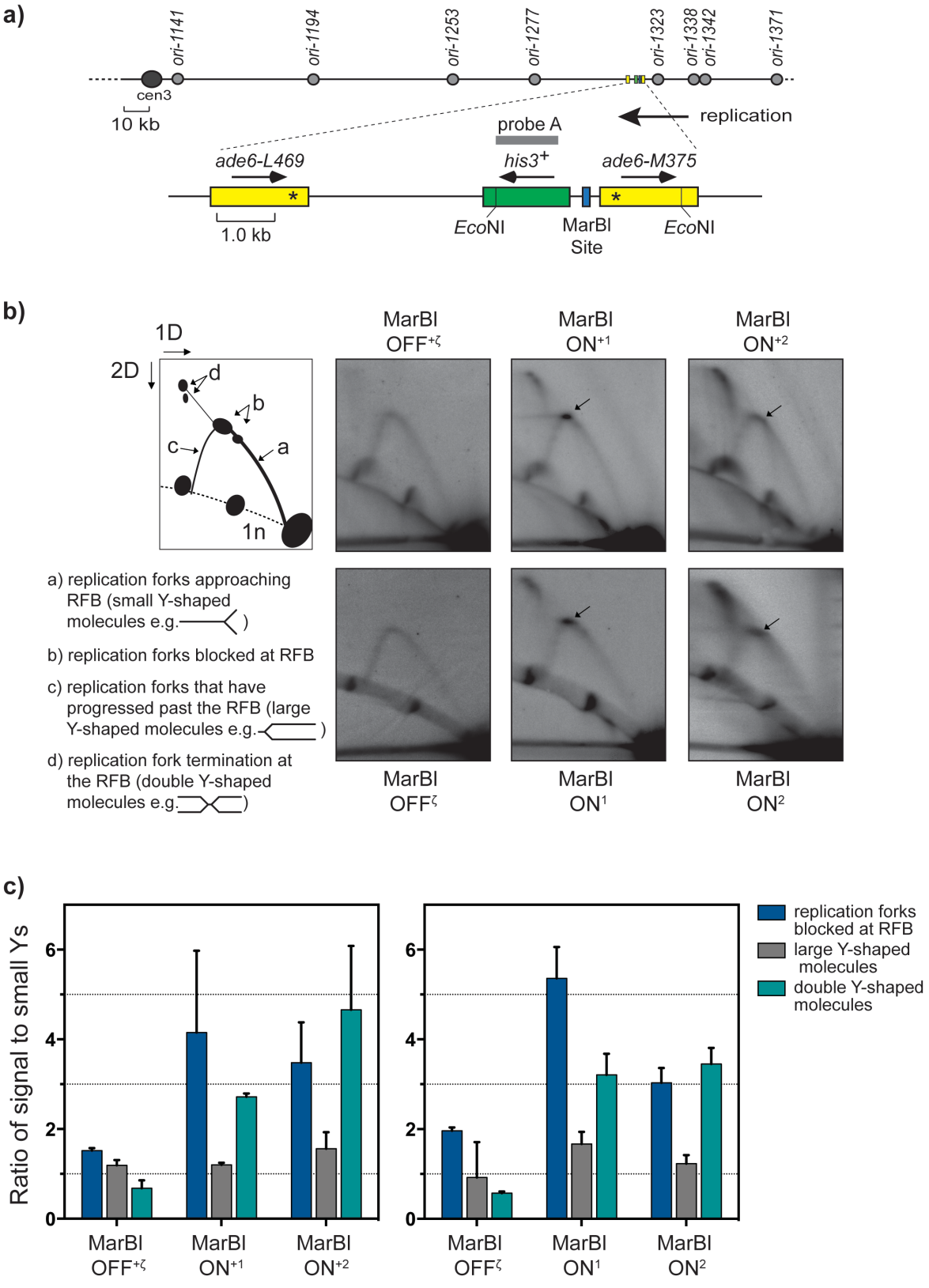


Fig. 4.vii 2D gel analysis of replication intermediates at MarBI.

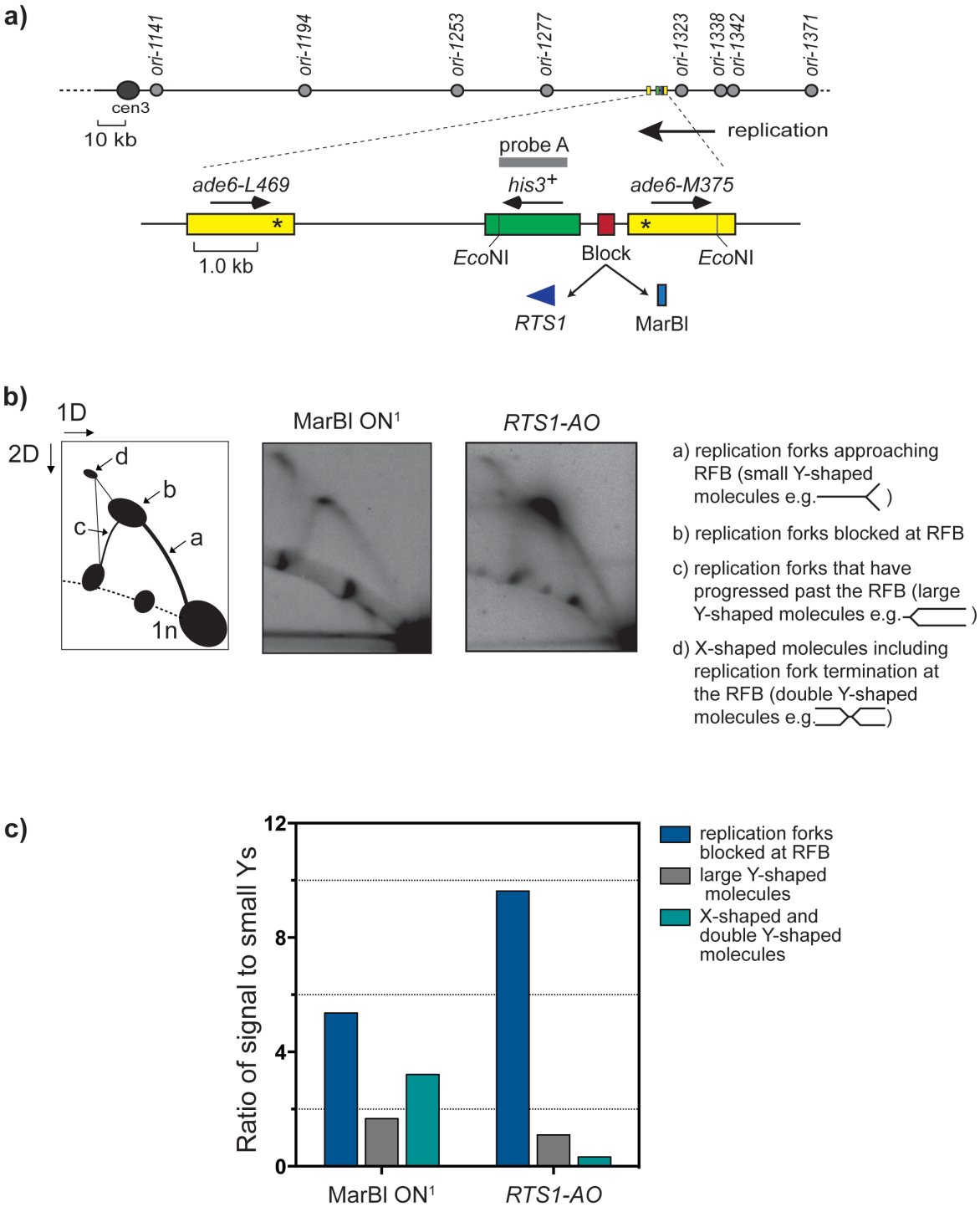


Fig. 4.viii 2D gel analysis comparing replication intermediates at MarBI and *RTS1*
a) Schematic showing the relative position of the direct repeat recombination reporter with the block site and Probe A used for 2D gel analysis. b) 2D gel analysis of replication intermediates within the *Eco*NI fragment shown in (a). The far left panel is a guide for interpreting the 2D gels. Arrows on the right hand panel indicate the pause sites. c) Quantification of the 2D gels displayed as bar charts. The DNA was extracted from asynchronously growing cultures of the strains MCW7076 and MCW4713. MarBI ON[1] represents the system where MarD155A is expressed and TO1 is present.

replication fork. Altogether, these data confirm that MarBI is a protein-DNA RFB, which causes replication fork stalling. Moreover, the absence of any major difference in the amount of replication fork stalling observed with Mar^{WT} and Mar^{D155A}, is consistent with them both inducing recombination by acting as RFBs. Intriguingly, all variants of MarBI ON resulted in a very strong accumulation of X-shaped and/or double Y-shaped molecules. I suspect that the majority of these molecules are in fact double Y-shaped, which accumulate because MarBI is a bi-directional barrier that impedes replication termination.

To compare replication fork stalling and termination at MarBI and *RTS1*, I performed a side-by-side 2D gel analysis [Fig. 4.viii]. Based on this analysis it is clear that *RTS1* is the stronger RFB, whereas, MarBI causes a greater accumulation of X-shaped and/or double Y-shaped molecules [Fig. 4.viii.b & c]. This latter difference probably reflects the fact that MarBI is a bi-directional barrier, whereas *RTS1* is a unidirectional barrier.

4.2.4 MarBI induced direct repeat recombination is partially dependent on Rad51, Rad52 and Rad54.

Nearly all spontaneous direct repeat recombination in fission yeast is dependent on Rad52, which operates both to promote Rad51-dependent HR and Rad51-independent SSA (Doe et al., 2004). Similarly, at *RTS1*, RDR has been shown to be partially dependent upon Rad51 and completely dependent on Rad52 (Ahn et al., 2005; Lambert et al., 2005). In the case of Rad54, it appears to have a dual role in promoting Rad51-dependent gene conversions whilst at the same time suppressing Rad51-independent deletions that can be induced by replication fork blockage at *RTS1* (unpublished data).

To determine whether MarBI-induced recombination is dependent on Rad51 and/or Rad52, the Ade^+ frequencies of wild-type, *rad51*Δ and *rad51*Δ*rad52*Δ

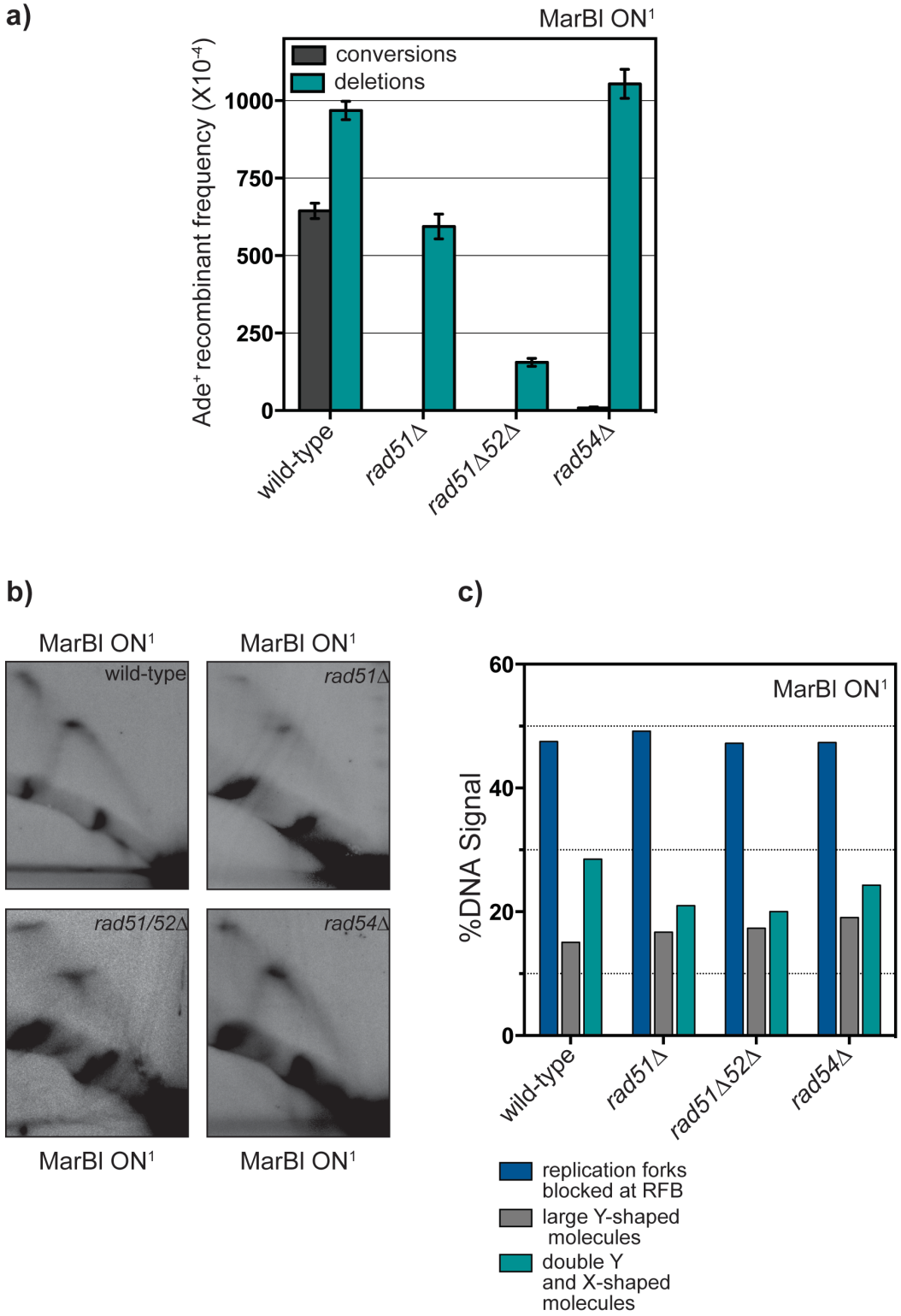


Fig. 4.ix MarBI induced direct repeat recombination is partially dependent on Rad51, Rad52 and Rad54.

a) Bar chart showing the frequency of Ade$^+$ recombinants in strains MCW7076, MCW8156, MCW8160 and MCW8165. Error bars represent ± standard error of the mean. b) 2D gel analysis of replication intermediates within the *Eco*NI fragment shown in Fig. 4.vii from wild-type, *rad51*Δ, *rad51*Δ rad*52*Δ and *rad54*Δ cells. c) Quantification of the 2D gels displayed as bar charts. The DNA was extracted from asynchronously growing cultures of the strains MCW7076, MCW8156, MCW8160 and MCW8165. MarBI ON^1 represents the system where Mar^{D155A} is expressed and TO1 is present.

strains were compared [Fig. 4.ix.a & Table 8-2]. With MarBI ON[1], there was a complete loss of gene conversions in both the *rad51*Δ and the *rad51*Δ*rad52*Δ backgrounds as expected. In the *rad51*Δ mutant, there was ~1.6 fold reduction in deletions, whereas, in the *rad51*Δ*rad52*Δ mutant the reduction was ~6 fold. This indicates that while all the gene conversion events at MarBI are Rad51-dependent, deletions arise by both Rad51-dependent and Rad51-independent mechanisms. The significant reduction in deletions in the *rad51*Δ*rad52*Δ double mutant indicates that the Rad51-independent deletions depend on Rad52.

Analysis of the recombinant frequency in the *rad54*Δ strain revealed that there was almost a complete loss of the gene conversions but no significant difference in the frequency of deletions [Fig. 4.ix.a & Table 8-2]. This suggests that Rad54 both promotes gene conversions and suppresses Rad51-independent deletions at MarBI, similar to its role at *RTS1*.

Native 2D gel analysis of DNA from the recombination mutants was performed to confirm that the observed changes in recombination frequency were not a consequence of an alteration in the MarBI barrier strength. Whilst the quality of the 2D gels is not optimal, it is reasonably clear from the data in Fig. 4.ix.b and c, that there is little or no alteration of the replication fork pause signal in the *rad51*Δ, *rad51*Δ*rad52*Δ and *rad54*Δ mutants compared to the wild-type. However, there does appear to be a small reduction in the accumulation of X-shaped and/or double Y-shaped molecules, which suggests that some of these molecules may be Rad51-dependent recombination intermediates (e.g. Holliday junctions) [Fig. 4.ix. b & c].

4.2.5 MarBI causes DNA breakage.

One way in which recombination may be induced by MarBI is if the stalled fork is cleaved by a nuclease resulting in the formation of a DSB. In order to investigate

this possibility, genomic DNA was extracted from exponentially growing asynchronous cultures of wild-type cells containing either MarBI ON^1 or MarBI ON^2. Cultures were grown both in the presence and absence of 4μM thiamine so that the effect of Mar^{D155A} expression could be determined, and DNA was prepared in agarose plugs to prevent shearing (Section 2.4.2). Following extraction, the DNA was digested with NdeI, separated on an agarose gel and analysed by Southern blotting using radiolabeled probes A and E [Fig. 4.x]. Probes A and E are specific to regions that flank MarBI [Fig. 4.x.a] and, reassuringly, both detected the full length NdeI fragment (~3.2 kb) from wild-type cells with either MarBI ON^1 or MarBI ON^2 (± 4μM thiamine) [Fig. 4.x.b]. When Mar^{D115} was expressed, an additional band was detected with probe A, which had the expected size of the putative DSB product [Fig. 4.x.b lanes b and d]. In the case of MarBI ON^1 this size is ~2.1 kb, whereas, with MarBI ON^2 it is ~2.3 kb, and this difference is likely due to the slightly different positions that Mar blocks the replication fork. Although DNA fragments indicative of a DSB are detected for both orientations of the transposon end sequence, the intensity of the break signal with MarBI ON^2 is noticeably weaker than with MarBI ON^1, which correlates with the difference in the amount of fork blockage seen on the 2D gels shown earlier [Fig. 4.vii.b, bottom panel]. In contrast to probe A, no break signal was initially detected with probe E, regardless of MarBI orientation [Fig. 4.x.b]. Indeed, it seems that the DNA fragment that constitutes the other side of the DSB is far less stable than the side detected by probe A and, therefore is much harder to detect. Nevertheless, as shown in Fig. 4.xi b, in some cases I have been able to detect a break signal of the correct size with probe E. Altogether, these data show that MarBI induces DNA breakage as well as replication fork stalling.

One possible explanation for why the probe A side of the DSB is easier to

Fig. 4.x 1D gel analysis for the detection of replication fork breakage at MarBI.

a) Schematic showing the relative position of the direct repeat recombination reporter with the MarBI site, the position of the *Nde*I restriction sites, the predicted fragment sizes when the binding site is positioned in either orientations and the probes used for the analysis of the 1D gels. b) Neutral 1D gel analysis of genomic DNA from asynchronous cultures of wild-type cells grown either in the presence or absence of 4μM thiamine. DNA was digested with *Nde*I and detected using Probe A or Probe E. c) Same as (b) except genomic DNA was extracted from *rad50*Δ cells and analyzed. d) Model for how replication forks potentially break at the barrier. The blots were first probed with Probe A before being stripped and re-probed by Probe E. Each of the strains were analyzed twice independently. The image shown is the representative data. The strains are MCW7076 (lane a & b), MCW7078 (lane c & d) and MCW8275 (lane e & f). MarBI ON^1 represents a system where Mar^{D155A} is expressed and TO1 is present and MarBI ON^2 where Mar^{D155A} is expressed and TO2 is present.

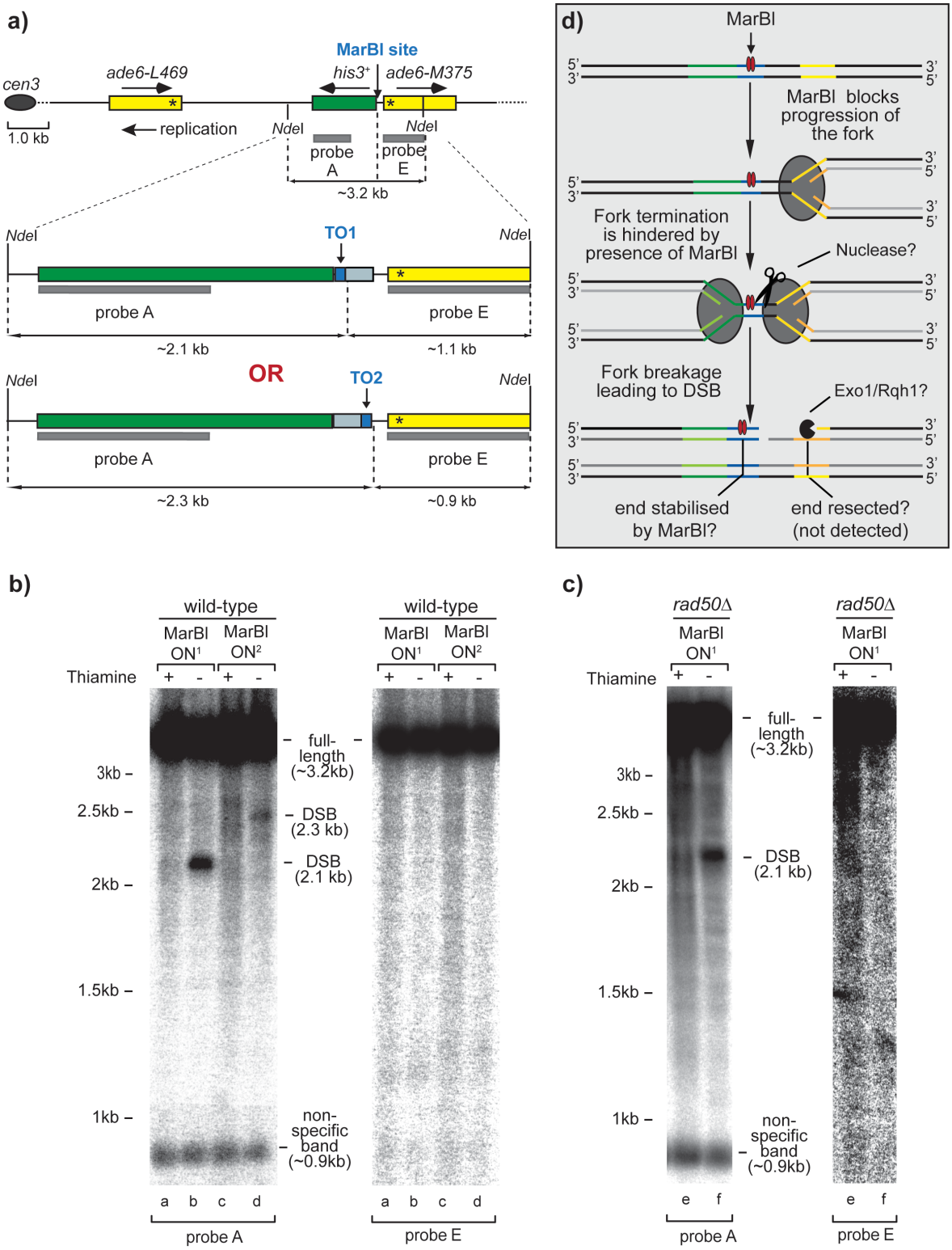


Fig. 4.x 1D gel analysis for the detection of replication fork breakage at MarBI.

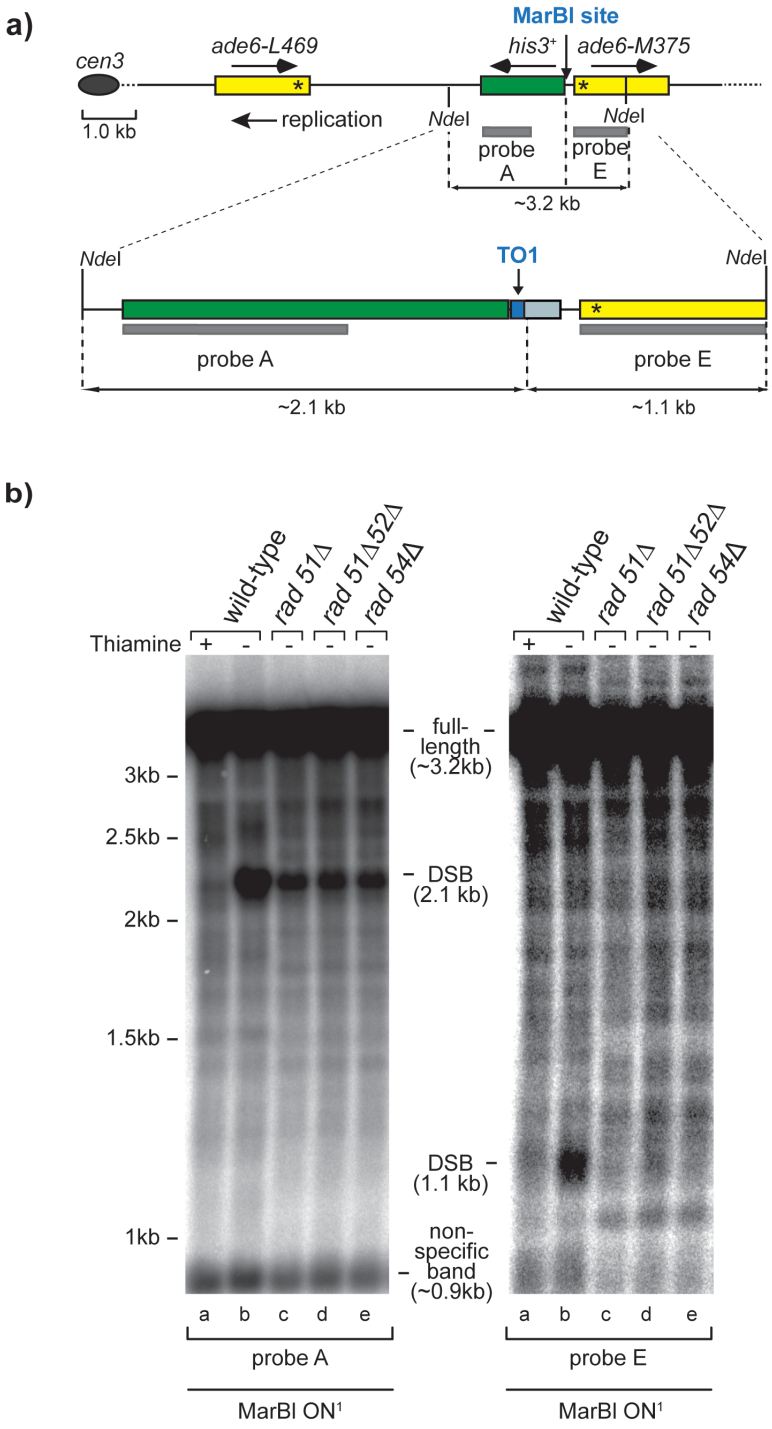


Fig. 4.xi 1D gel analysis for the detection of replication fork breakage at MarBI in recombination mutant backgrounds.

a) Schematic showing the relative position of the direct repeat recombination reporter with the MarBI site, the position of the *Nde*I restriction sites, the predicted fragment sizes when the binding site is positioned in either orientations and the probes used for the analysis of the 1D gels. b) Neutral 1D gel analysis of genomic DNA from asynchronous cultures of wild-type, *rad51*Δ, *rad51*Δ52Δ and *rad54*Δ cells grown either in the presence or absence of 4μM thiamine. DNA was digested with *Nde*I and detected using Probe A or Probe E. c) Same as (b) except Probe E is used instead of Probe A. The blot was first probed with Probe A before being stripped and re-probed by Probe E. Each of the strains were analyzed twice independently. The image shown is the representative data. The strains are MCW7076 (lane a & b), MCW8156 (lane c), MCW8160 (lane d) and MCW8165 (lane e). MarBI ON[1] represents a system where Mar^{D155A} is expressed and TO1 is present.

detect than the probe E side is that the Mar protein may remain bound to the DNA following breakage and thereby protect one end of the DSB from extensive resection [Fig. 4.x.c]. In order to try and stabilize the probe E side of the DSB from its putative degradation, I repeated the experiment with a *rad50*Δ MarBI ON^{1} strain (± 4μM thiamine) [Fig. 4.x.d], which should be defective in MRN-dependent short-range DNA resection (Limbo et al., 2007). However, even in the *rad50*Δ MarBI ON^{1} strain, a DSB signal was detected only with probe A and not with probe E.

I next wanted to determine whether DSB formation was dependent on homologous recombination. To do this I compared the amount of breakage in wild-type and *rad51*Δ, *rad51*Δ*rad52*Δ and *rad54*Δ mutant backgrounds [Fig. 4.xi.b]. As mentioned above, on this occasion both sides of the DSB were detected in DNA prepared from wild-type cells. In contrast, only the probe A side of the break was detected in the DNA samples from the mutant cells. Nevertheless, these data show that the formation of the DSB is independent of the central recombination proteins Rad51, Rad52 and Rad54.

4.2.6 MarBI does not affect cell viability even in the absence of Rad51 and Rad52.

If replication fork stalling at MarBI results in the formation of DSBs that are repaired by HR, then there might be a detectable change in the growth/viability of *rad51*Δ and/or *rad52*Δ mutants harbouring it. To test this, the growth of wild-type, *rad51*Δ and *rad51*Δ*rad52*Δ cells containing MarBI ON^{1} was compared in the presence and absence of thiamine [Fig. 4.xii]. With Mar^{D115A} expression repressed in the presence of thiamine, there was little difference in the growth of strains with and without TO1. Upon induction of Mar^{D115A} expression, in the absence of thiamine, the wild-type strain appeared to grow more poorly when TO1 was absent. Moreover, both *rad51*Δ and *rad51*Δ *rad52*Δ mutant strains grew more

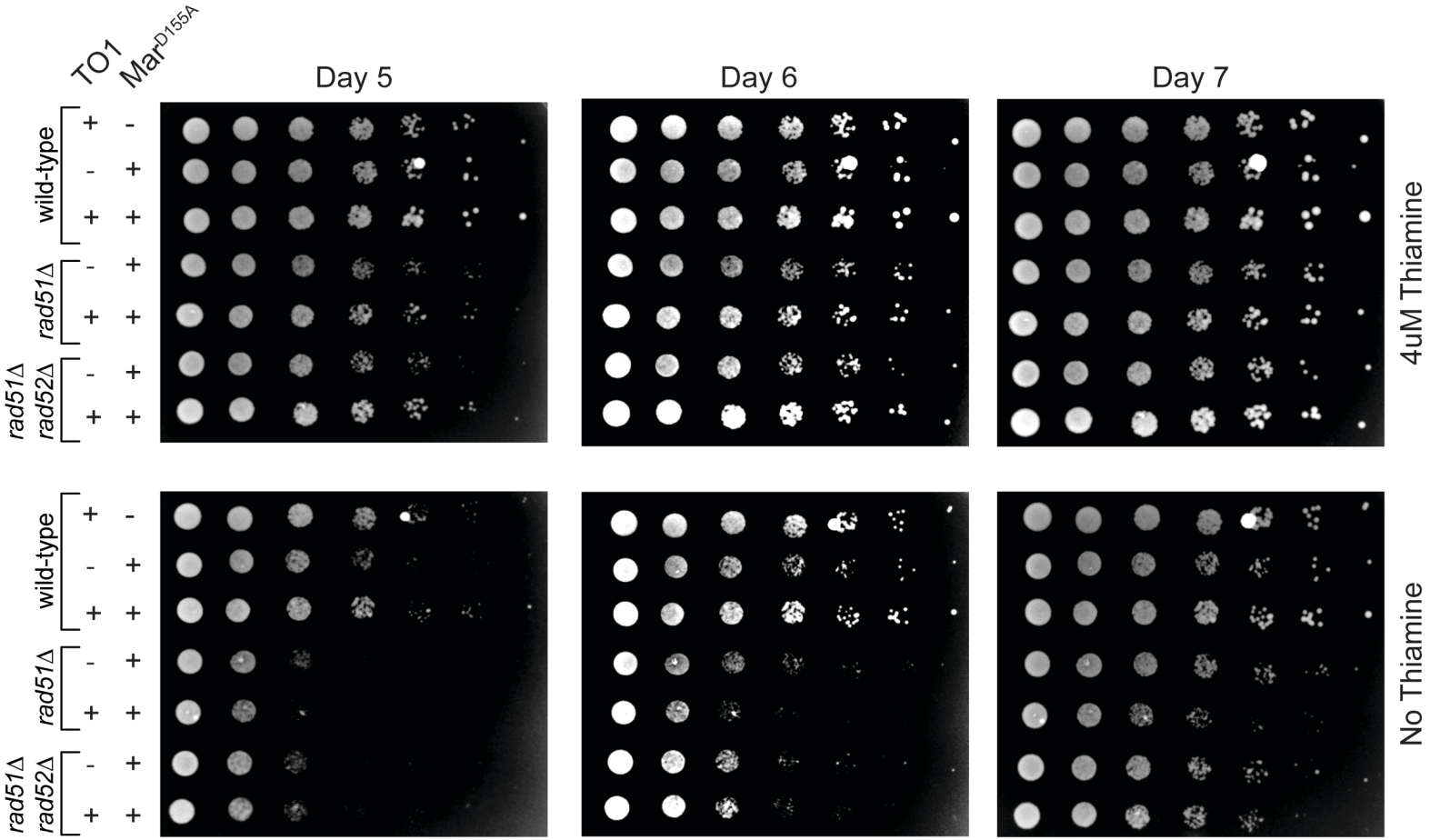


Fig. 4.xii Effect of rad51Δ and rad52Δ on growth and viability of cells with MarBl.
Spot assays comparing the growth of MCW7440, MCW7524, MCW7540, MCW8229, MCW8106, MCW8232 and MCW8152. 10µl of 5-fold dilutions were spotted on EMMG (± thiamine) and the plates were photographed after 5,6 and 7 days of growth at 30°C.

slowly than wild-type, regardless of the presence or absence of TO1. It should be noted, however, that *rad51*Δ and *rad52*Δ mutant strains generally grow slower than wild-type, especially in the absence of thiamine and, therefore, it is unclear from these data whether expression of Mar^{D115A} is causing a general toxicity in these mutants. Nevertheless, the absence of a major difference in growth between mutant cells with and without TO1 suggests that HR is not critical for survival in the presence of MarBI.

4.2.7 Studying the spatio-temporal dynamics of recruitment of recombination proteins at MarBI by live-cell imaging

4.2.7.1 Establishing the system to study Rad52 recruitment to MarBI

From the previous data it is clear that MarBI can cause replication fork pausing, DNA breakage and induce a recombinational response (Section 4.2.2, 4.2.3 and 4.2.5). However, it is unclear if this response is triggered in all cells or only a subset of the population. It is also unclear what stage of the cell cycle the recombinational response is induced. To address these questions, I decided to use live cell imaging to determine the frequency and temporal dynamics of recombination protein recruitment to MarBI. In order to do this I first had to make and test a series of strains in which the imaging could be done. To begin with, a 115 X *lacO* array was placed downstream of the MarBI binding site so that its location could be tracked in cells expressing the LacI repressor fused to the far-red fluorescent protein tdKatushka2 using time-lapse microscopy [Fig. 4.xiii.a]. Mindful of the fact that the *lacO*-LacI interaction has previously been shown to act as an RFB (Sofueva et al., 2011), it was necessary to establish imaging parameters in which the level of LacI expression was just sufficient to visualise the location of the *lacO* array without itself inducing recombination (Nguyen et al., 2015; Sofueva et al., 2011). As both LacI and Mar^{D115A} are expressed from *nmt* promoters, the

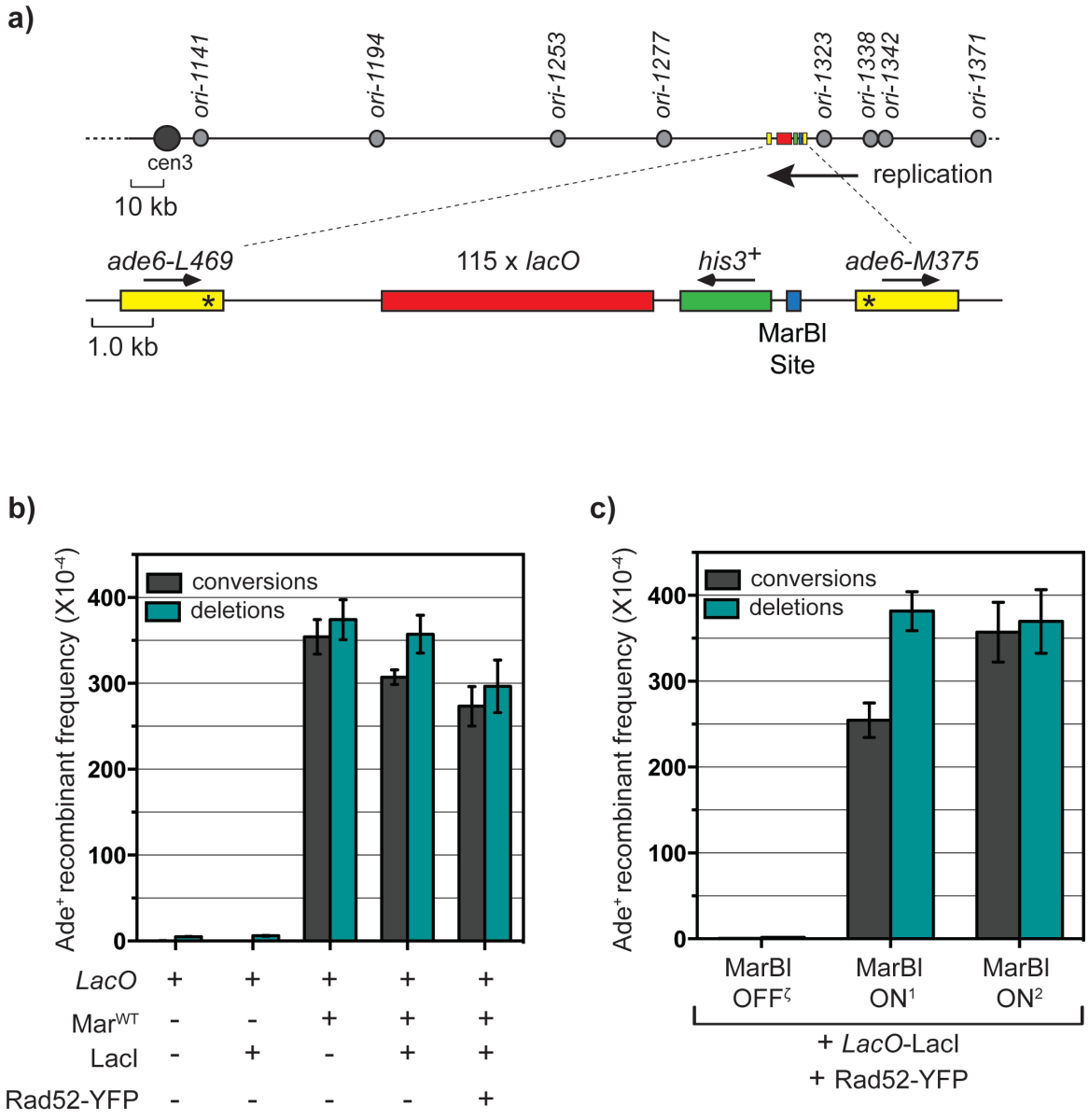


Fig. 4.xiii Effect of LacI expression on direct-repeat recombination at MarBI in the strains used for time-lapse microscopy containing the *lacO* array in between the repeats.

a) Schematic showing the modification of the direct repeat recombination reporter for time-lapse microscopy. b) Bar chart showing the frequency of Ade+ recombinants in strains MCW7226, MCW7470, MCW7476, MCW7482 and MCW7488. The MarBI site is present in TO1. c) Bar chart showing the frequency of Ade+ recombinants in strains MCW7577, MCW7573 and MCW7581. The strains contain the *lacO* array, P_{nmt81}LacI and Rad52-YFP. Error bars represent ± standard error of the mean.

addition of thiamine to partially repress expression of LacI was not an option. Instead I used a mutated version of the *nmt* promoter to obtain just the right level of LacI expression in the absence of thiamine. To confirm that this level of LacI did not induce recombination, the frequency of direct repeat recombination was compared in a strain containing the *lacO* array with and without LacI [Fig. 4.xiii.b & Table 8-3]. Reassuringly, the expression of LacI made no difference to the frequency of recombination. Moreover, it also made little difference to the frequency of recombination induced by MarBI [Fig. 4.xiii.b & Table 8-3].

Having constructed strains containing MarBI, *lacO* and LacI, I next made derivatives in which Rad52 was tagged at its C-terminus with yellow fluorescent protein (YFP). These strains were also assayed for direct repeat recombination to confirm that the tag on Rad52 did not influence MarBI-induced recombination [Fig. 4.xiii.b and c & Table 8-3]. With either MarBI ON^{1} or MarBI ON^{2} there was a strong induction of recombination, albeit not quite as strong as observed in previous assays. Possibly, the increase in distance between the *ade6*$^{-}$ repeats, caused by the introduction of the *lacO* array, reduces the frequency of recombination between them. Nevertheless, these data confirm that the introduction of both the *lacO*-LacI array and Rad52-YFP does not unduly affect MarBI-induced recombination.

4.2.7.2 Does MarBI ON induce more Rad52 foci spontaneously?

Having established the appropriate yeast strains and conditions, live cells were imaged by fluorescence time-lapse microscopy (Nguyen et al. 2015). Rad52-YFP has previously been shown to form foci in response to damaged DNA, similar to its homologue in *S. cerevisiae* (Lisby et al., 2001; Meister et al., 2003). The time-lapse movies of the cells, with images taken every 5 minutes, were staged relative

to anaphase, and the presence or absence of Rad52 foci and their co-localisation with *lacO*-LacI recorded over a time period of 160 minutes [Fig. 4.xiv].

The majority of cells (≥70%), with either MarBI OFF or MarBI ON, exhibit a Rad52 focus at some point during the 160 minutes following anaphase, and in most cases these foci do not appear until at least 20 minutes after anaphase [Fig. 4.xiv.b & Fig. 4.xv.b]. The presence of these Rad52 foci in MarBI OFF cells, as well as MarBI ON cells, indicates that HR is routinely needed to process perturbed replication forks and damaged DNA that occurs during the cell cycle. Unlike with *RTS1*, where a higher percentage of *RTS1-AO* (89%) cells exhibit a Rad52 focus as compared to *RTS1-IO* (79%) (Nguyen et al., 2015), both MarBI OFF and ON cells show no significant difference in either the proportion of cells with a Rad52 focus nor the frequency of their distribution across the 160 minute post anaphase period [Fig. 4.xv.a & c].

4.2.7.3 Is Rad52 recruited to MarBI ON?

In addition to the spontaneous Rad52 foci, I also marked the time points when the Rad52-YFP focus co-localised (red) and was adjacent (blue) to the *lacO*-LacI focus marking the MarBI site [Fig. 4.xiv.b & Fig. 4.xvi]. Perfect co-localisation was manually assessed and scored as foci in separate channels overlapping in x, y and z by a minimum of 2 pixels. As MarBI causes DNA breakage, it is possible that the two sides of the DSB may become separated and this could result in the distance between the *lacO* array and the MarBI site increasing. To accommodate this possibility, I decided to also score 'adjacent' foci, with a maximum of one pixel distance between them. Overall, 34% of the cells containing MarBI ON[1], and 42% of the cells with MarBI ON[2], exhibited a co-localising Rad52 focus in the first 160 minutes post anaphase compared to less than 10% with MarBI OFF [Fig. 4.xvii.a, left panel]. If adjacent Rad52 foci are also considered, the percentage increases to

53% in MarBI ON^1 and 58% in MarBI ON^2, with a doubling of foci observed in MarBI OFF [Fig. 4.xvii.a, right panel]. Whilst adjacent foci may be representative of events at MarBI, for the sake of stringency, I have generally excluded them from the analysis described in the following sections.

As seen from the time-lapse microscopy, Rad52 foci that co-localise with *lacO*-LacI appear to persist longer with MarBI ON than with MarBI OFF [Fig. 4.xvii.b & c]. The total number of time points in which co-localisation is observed ranges from 1 to 6 with MarBI ON^1 (excluding one outlier) and 1 to 8 with MarBI ON^2 compared to 1 to 4 time points with MarBI OFF [Fig. 4.xvii.b]. On average, MarBI ON^1 cells exhibit ~1.2 and MarBI ON^2 cells ~1.3 time points in which a Rad52 focus co-localises with a *lacO*-LacI focus in the first 160 minutes post anaphase, compared to ~0.2 time points in MarBI OFF cells (considering all cells including the ones that have 0 time points of co-localisation) [Fig. 4.xvii.c]. If only the longest track of consecutive time points with co-localising foci in each cell is considered, then the duration of any single event ranges from 1 to 4 time points for MarBI ON^1 (average = 0.8) and 1 to 5 for MarBI ON^2 (average = 1.2), which equates to >0 to <25 minutes [See Appendix Fig. 8.iv]. Thus, when Rad52 is recruited to MarBI, on average it remains there for between >0 to 6 minutes. However, as the images are captured at 5-minute intervals, it is impossible to be certain whether Rad52 remains associated with the site for the entire duration of image acquisition. Nevertheless, these data indicate that Rad52 is recruited specifically to MarBI ON.

4.2.7.4 When is Rad52 recruited to MarBI post anaphase?

The proportion of cells with a co-localising focus was plotted as a function of time for both MarBI ON and OFF to gain a better understanding of the Rad52 recruitment dynamics in relationship to cell cycle progression [Fig. 4.xviii.a]. The earliest recruitment of Rad52 to MarBI in cells that show a co-localising focus is

Fig. 4.xiv Tracking Rad52-YFP focus localisation at MarBI by time-lapse microscopy.

a) Schematic showing the modification of the direct repeat recombination reporter for time-lapse microscopy. b) Analysis of time-lapse movies. The presence of a Rad52 focus and whether it co-localises with the *lacO*-LacI-tdKatushka2 focus is recorded every 5 minutes for a period of 160 minutes post anaphase in each cell. The top panel is a schematic of *S. pombe* cells at various stages post anaphase with nuclear *lacO*-LacI foci in grey, Rad52 foci in green, co-localising foci in red and a Rad52 focus adjacent to the *lacO*-LacI focus in blue. The estimated time of fork arrival and fork merging is indicated below as established earlier in Nguyen et al. (2015**)**. The strains are MCW7578 (n=40), MCW7574 (n=38) and MCW7582 (n=26). MarBI OFF^{ζ} represents the system where the Mar^{D155A} protein is expressed but the transposon end is absent, MarBI ON^{1} where Mar^{D155A} is expressed and TO1 is present and MarBI ON^{2} where Mar^{D155A} is expressed and TO2 is present

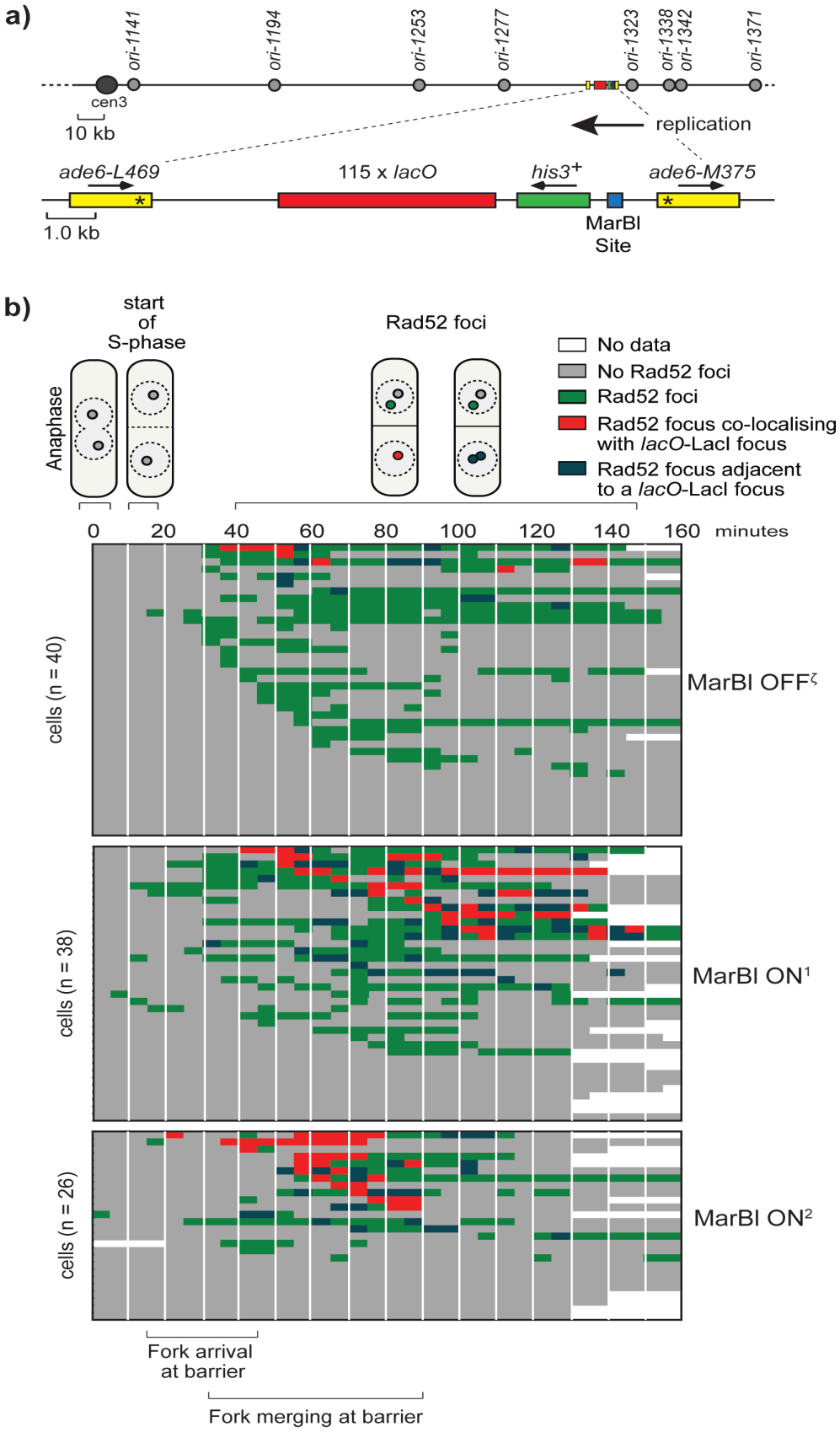


Fig. 4.xiv Tracking Rad52-YFP focus localisation at MarBI by time-lapse microscopy.

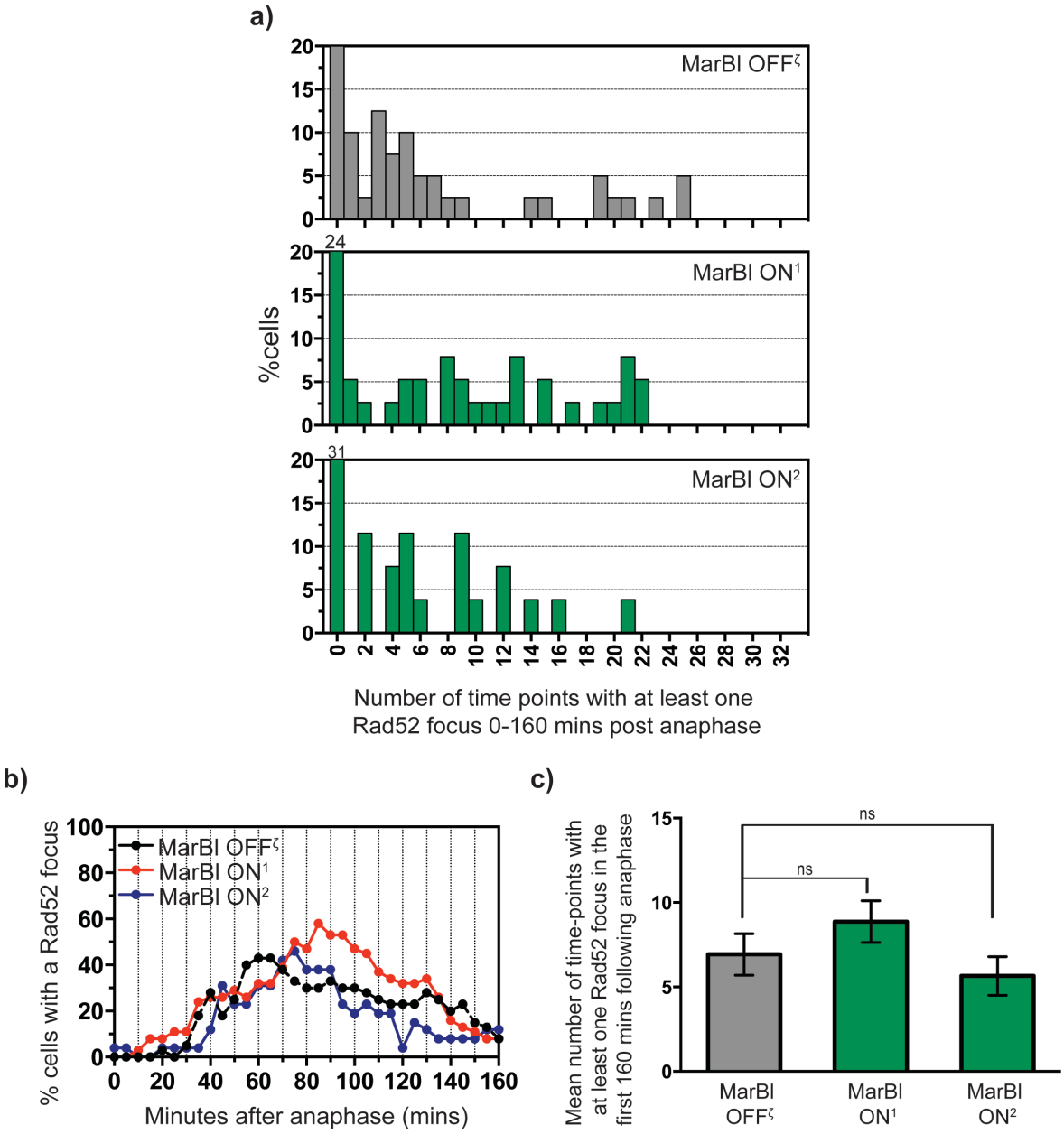


Fig. 4.xv Comparison of the total Rad52 foci observed in cells with MarBI ON and MarBI OFF.

a) Histograms showing the percentage of cells with a given number of time points with at least one Rad52-YFP focus within the first 160 minutes following anaphase. b) Line graphs of the percentage of cells with at least one Rad52-YFP focus during the first 160 minutes following anaphase (excluding multiple foci at a given time point). c) Bar charts showing the mean number of time points that cells have at least one Rad52-YFP focus during the first 160 minutes following anaphase. The strains are MCW7578 (n=40), MCW7574 (n=38) and MCW7582 (n=26. MarBI OFF$^{\zeta}$ represents the system where the Mar^{D155A} protein is expressed but the transposon end is absent, MarBI ON^{1} where Mar^{D155A} is expressed and TO1 is present and MarBI ON^{2} where Mar^{D155A} is expressed and TO2 is present. Error bars represent ± standard error of the mean. P-values calculated using the Shapiro-Wilk normality test (ns $p>0.05$, *$p<0.05$, **$p<0.01$, ***$p<0.001$, ***$p<0.0001$). When the bar on the histogram extends beyond the scale of the Y-axis, the value is indicated by the number in the bar.

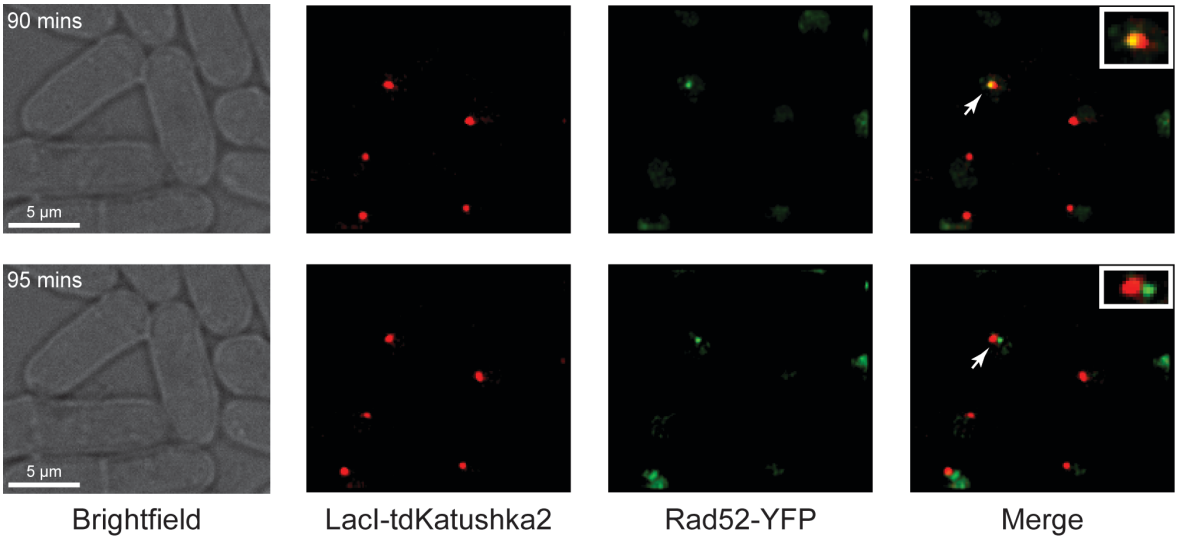


Fig. 4.xvi Representative still images showing Rad52-YFP co-localizing with MarBl. Example snapshots taken from a time-lapse movie of cells with MarBl ON[1]. At the 90-minute time point a Rad52-YFP focus is seen co-localising with a *lacO*-LacI-tdKatushka2 focus (indicated by the arrow). However, 5 minutes later the two foci have shifted apart and are no longer co-localising but adjacent (indicated by the arrow). The scale bar represents 5µm. The time represents the minutes after anaphase when the snapshot was captured. The strain shown is MCW7574. MarBl ON[1] represents a system where Mar^{D155A} is expressed and TO1 is present.

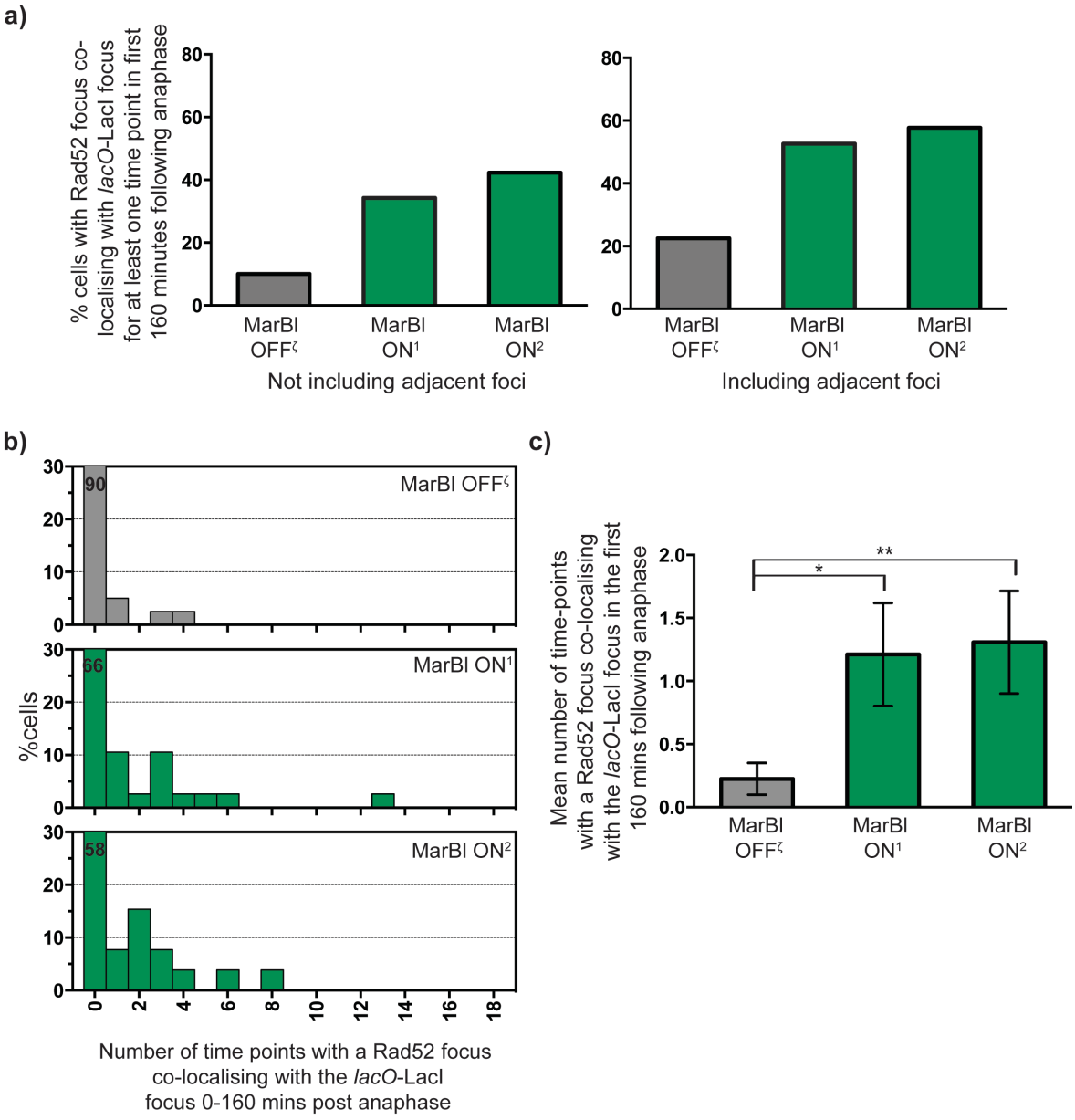


Fig. 4.xvii. Cells with MarBI ON exhibit increased co-localisation of the Rad52-YFP foci at the barrier.

a) Bar charts of the percentage of cells that exhibit a Rad52-YFP focus co-localising with the *lacO*-LacI focus for at least one time in the first 160 minutes following anaphase. b) Histograms showing the percentage of cells with a given number of time points in which a Rad52-YFP focus co-localises with the *lacO*-LacI focus within the first 160 minutes following anaphase. c) Bar chart showing the mean number of time points that cells have a Rad52-YFP focus that co-localises with the *lacO*-LacI focus during the first 160 minutes following anaphase. The strains are MCW7578 (n=40), MCW7574 (n=38) and MCW7582 (n=26). MarBI OFF$^{\zeta}$ represents the system where the Mar^{D155A} protein is expressed but the transposon end is absent, MarBI ON^{1} where Mar^{D155A} is expressed and TO1 is present and MarBI ON^{2} where Mar^{D155A} is expressed and TO2 is present. Error bars represent ± standard error of the mean. P-values calculated using the Shapiro-Wilk normality test (ns $p>0.05$, *$p<0.05$, **$p<0.01$, ***$p<0.001$, ***$p<0.0001$). When the bar on the histogram extends beyond the scale of the Y-axis, the number in the bar indicates the value.

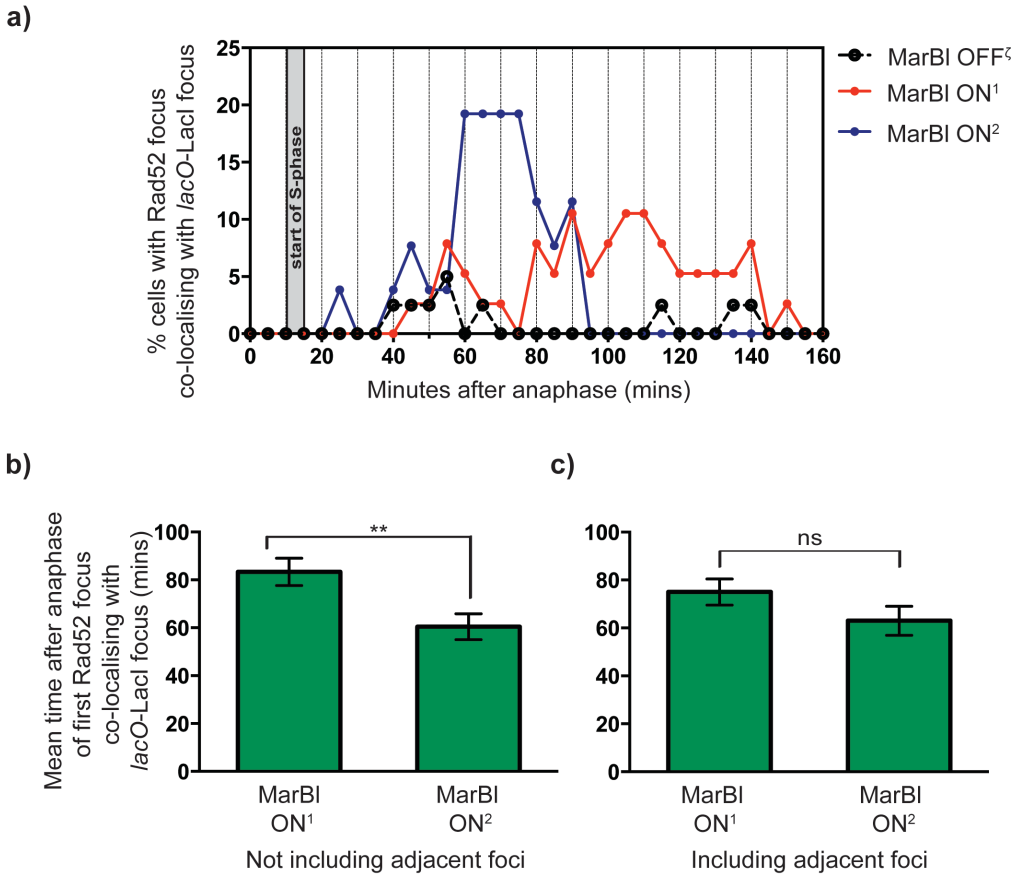


Fig. 4.xviii Temporal kinetics of the Rad52-YFP foci co-localising with MarBI.
a) Line graphs of the percentage of cells with a Rad52-YFP focus that co-localises with the *lacO*-LacI focus during the first 160 minutes following anaphase. . b) Bar chart showing the mean time after anaphase when the first Rad52-YFP co-localises with the *lacO*-LacI focus. The strains are MCW7578 (n=40), MCW7574 (n=38), MCW7582 (n=26) and MCW6556 (n=78). The strains are MCW7578 (n=40), MCW7574 (n=38) and MCW7582 (n=26). MarBI OFF$^{\zeta}$ represents the system where the Mar^{D155A} protein is expressed but the transposon end is absent, MarBI ON^{1} where Mar^{D155A} is expressed and TO1 is present and MarBI ON^{2} where Mar^{D155A} is expressed and TO2 is present. Error bars represent ± standard error of the mean. P-values calculated using the Shapiro-Wilk normality test (ns $p>0.05$, *$p<0.05$, **$p<0.01$, ***$p<0.001$, ***$p<0.0001$).

40-55 minutes post anaphase for MarBI ON^1 (~15% of total cells scored) and 35-40 minutes in MarBI ON^2 (~13% of total cells scored), if we exclude the one cell with a co-localising focus at 20 minutes as a chance event [Fig. 4.xiv.b & Fig. 4.xviii.a]. To gauge precisely when in the cell cycle Rad52 is recruited to replication forks blocked at MarBI, it is important to know when S-phase starts as well as its duration. Using the pattern of PCNA foci formation, our lab previously has shown that S-phase normally starts between 10 and 15 minutes post anaphase under our imaging conditions and is completed approximately 35-50 later (Nguyen et al., 2015). On average, Rad52 foci co-localise with *lacO*-LacI foci 83 minutes post anaphase in MarBI ON^1 cells and 60 minutes post anaphase in MarBI ON^2 cells [Fig. 4.xviii.b]. However, this difference changes to 75 minutes in MarBI ON^1 cells and 63 minutes in MarBI ON^2 cells if adjacent foci are factored in, and becomes non significant [Fig. 4.xviii. c]. If we factor in the timings of S-phase, the average time of first co-localisation of Rad52 with the array is 68 to 73 minutes past the start of S-phase for MarBI ON^1 and 55 to 60 minutes for MarBI ON^2. Altogether these data suggest that Rad52 foci co-localise with MarBI in late S- and G2-phase of the cell cycle.

4.2.7.5 Rad54 dynamics at MarBI

Having established the spatiotemporal dynamics of Rad52 foci in cells with MarBI ON and MarBI OFF, I next wanted to determine whether Rad54 foci would show similar dynamics. For this analysis a strain expressing Rad54 fused to GFP was used. Importantly, Rad54-GFP has previously been characterised and shown to be fully functional (Maki et al., 2011).

Using time-lapse microscopy I monitored Rad54-GFP foci in an asynchronous population of live cells with either MarBI OFF§ or MarBI ON^1 [Fig. 4.xix]. Almost all of the cells exhibited a spontaneous Rad54 focus in the first 160 minutes following

Fig. 4.xix Tracking Rad54-GFP focus localisation at MarBI by time-lapse microscopy.

a) Schematic showing the modification of the direct repeat recombination reporter for time-lapse microscopy. b) Analysis of time-lapse movies. The presence of a Rad54 focus and whether it co-localises with the *lacO*-LacI-tdKatushka2 focus is recorded every 5 minutes for a period of 160 minutes post anaphase in each cell. The top panel is a schematic of *S. pombe* cells at various stages post anaphase with nuclear *lacO*-LacI foci in grey, Rad54 foci in green, co-localising foci in red and a Rad54 focus adjacent to the *lacO*-LacI focus in blue. The estimated time of fork arrival and fork merging is indicated below as established earlier in Nguyen et al. (2015). The strains are MCW7924 (n=47) and MCW8167 (n=45). MarBI OFF§ represents a system where Mar^{D155A} is not expressed but TO1 is present and MarBI ON^{1} where Mar^{D155A} is expressed and TO1 is present.

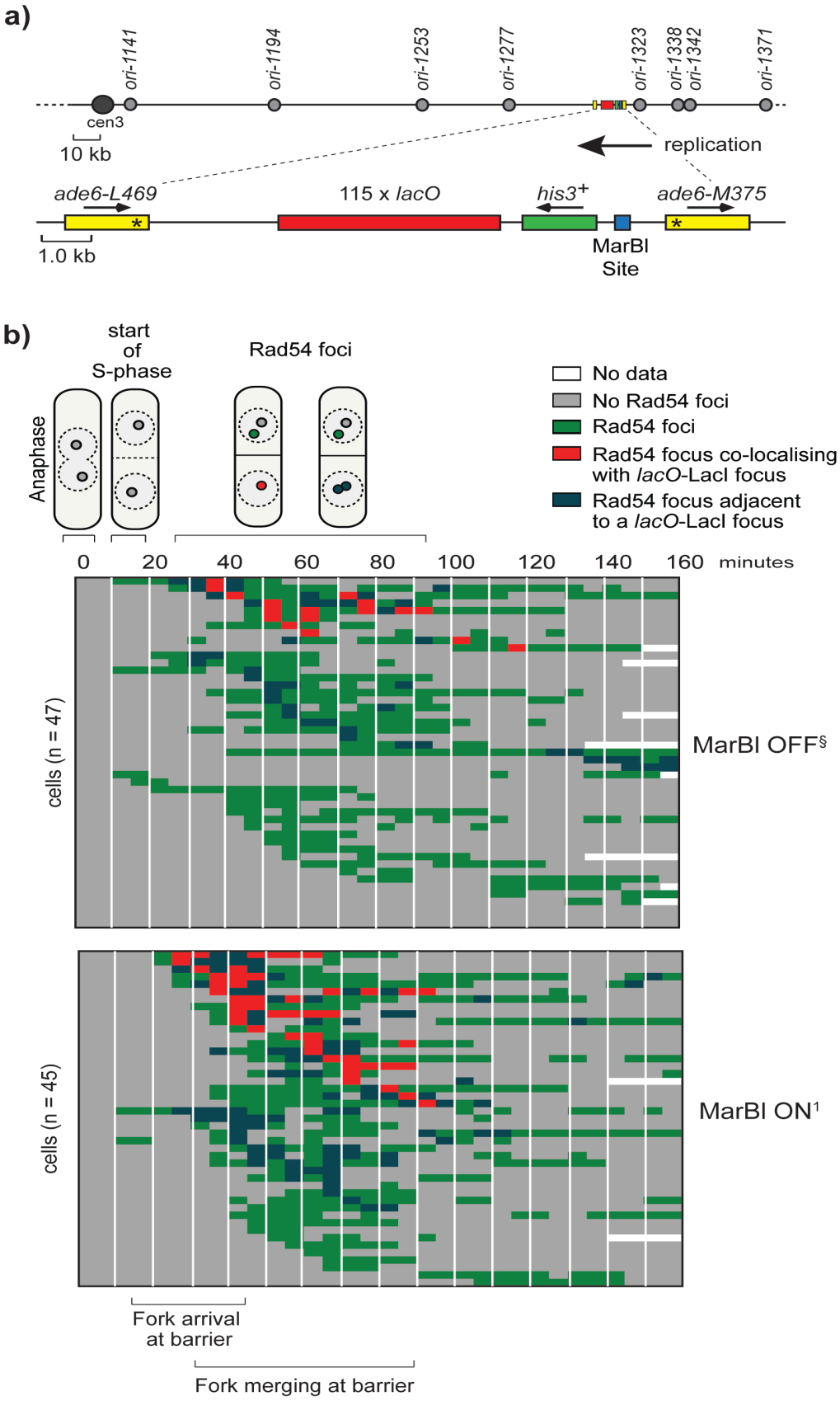


Fig. 4.xix Tracking Rad54-GFP focus localisation at MarBI by time-lapse microscopy.

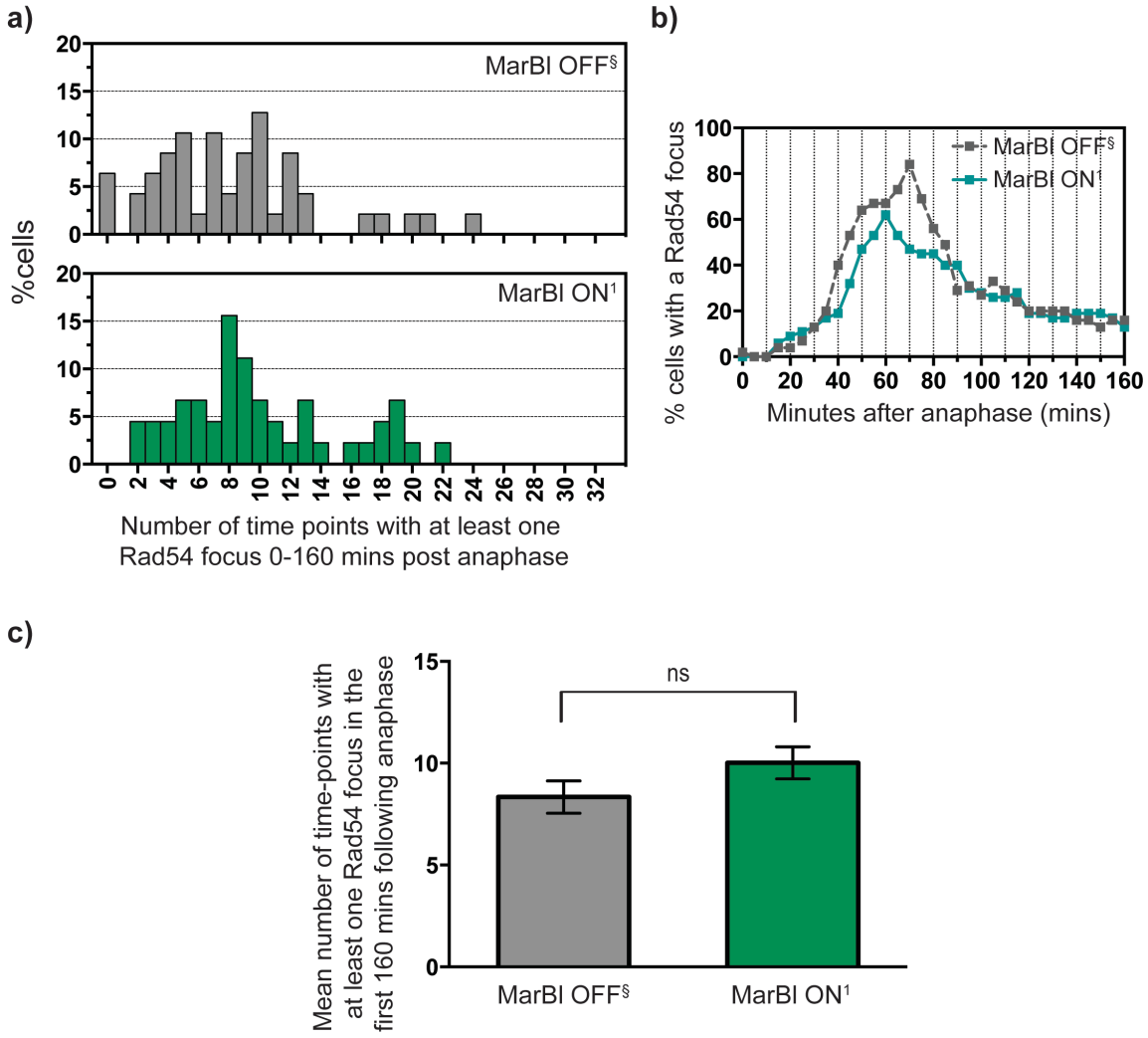


Fig. 4.xx Comparison of the total Rad54 foci observed in cells with MarBI ON and MarBI OFF.

a) Histograms showing the percentage of cells with a given number of time points with at least one Rad54-GFP focus within the first 160 minutes following anaphase. b) Line graph of the percentage of cells with a Rad54-GFP focus during the first 160 minutes following anaphase (excluding multiple foci at a given time point). c) Bar chart showing the mean number of time points that cells have at least one Rad54-GFP focus during the first 160 minutes following anaphase. The strains are MCW7924 (n=47) and MCW8167 (n=45). MarBI OFF§ represents a system where Mar^{D155A} is not expressed but TO1 is present and MarBI ON^{1} where Mar^{D155A} is expressed and TO1 is present. Error bars represent ± standard error of the mean. P-values calculated using the Shapiro-Wilk normality test (ns p>0.05, *p<0.05, **p<0.01, ***p<0.001, ***p<0.0001). When the bar on the histogram extends beyond the scale of the Y-axis, the value is indicated by the number in the bar.

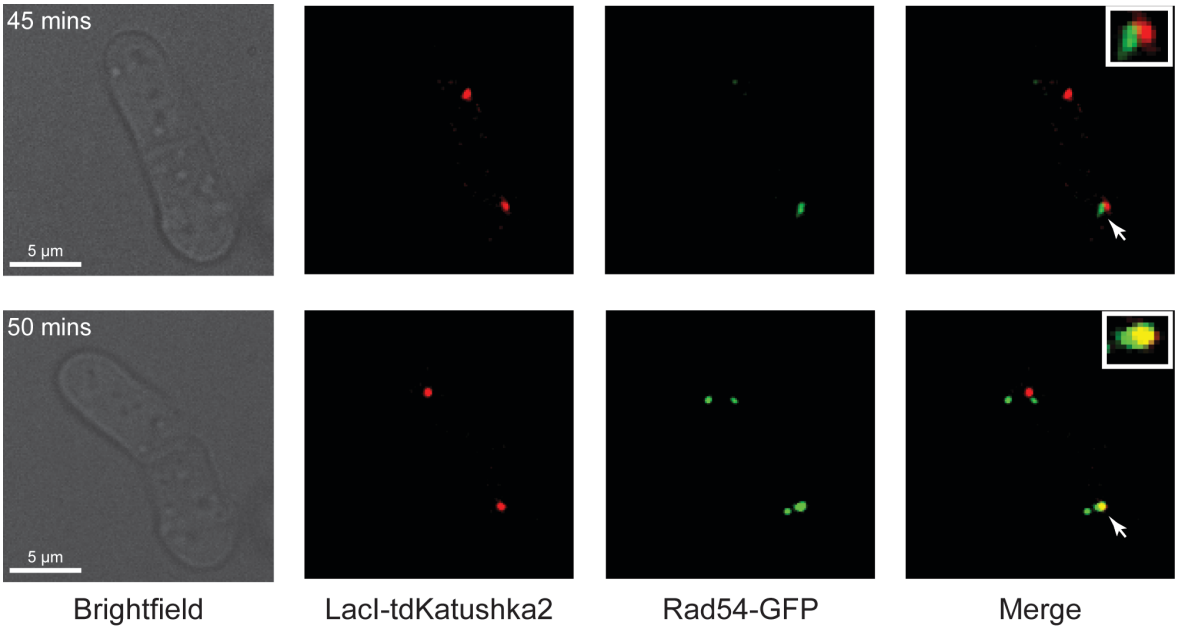


Fig. 4.xxi Representative still images showing Rad54-GFP co-localizing with MarBI.

Example snapshots taken from a time-lapse movie of cells with MarBI ON[1]. At the 50-minute time point a Rad54-GFP focus is seen to be 'next to' (adjacent) with a *lacO*-LacI-tdKatushka2 focus (indicated by the arrow). However, 5 minutes later the two foci are co-localising (indicated by the arrow). The scale bar represents 5µm. The time represents the minutes after anaphase when the snapshot was captured. The strain shown is MCW8167. MarBI ON[1] represents a system where Mar^{D155A} is expressed and TO1 is present.

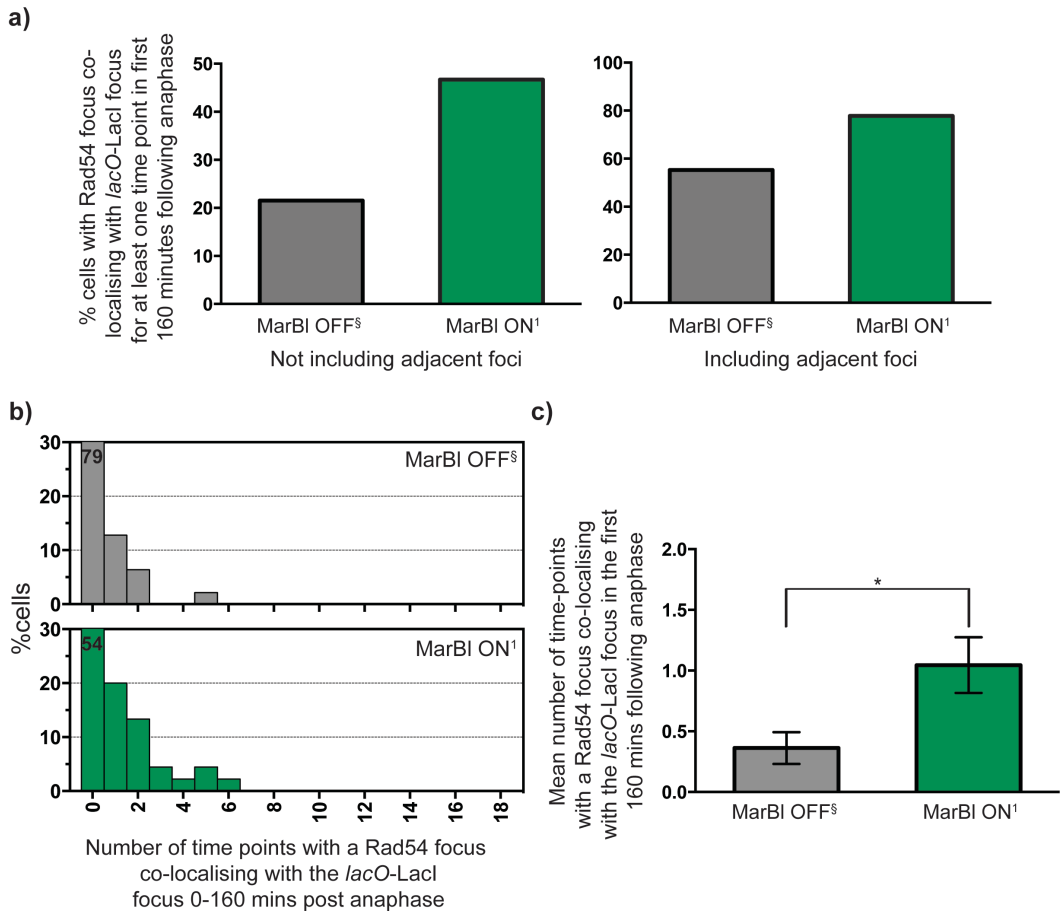


Fig. 4.xxii Cells with MarBI ON exhibit increased co-localisation of the Rad54-GFP foci at the barrier.

a) Bar chart of the percentage of cells that exhibit a Rad54-GFP focus co-localising with the *lacO*-LacI focus for at least one time point in the first 160 minutes following anaphase. b) Histograms showing the percentage of cells with a given number of time points in which a Rad54-GFP focus co-localises with the *lacO*-LacI focus within the first 160 minutes following anaphase. c) Bar chart showing the mean number of time points that cells have a Rad54-GFP focus that co-localises with the *lacO*-LacI focus during the first 160 minutes following anaphase. The strains are MCW7924 (n=47) and MCW8167 (n=45). MarBI OFF§ represents a system where Mar^{D155A} is not expressed but TO1 is present and MarBI ON^{1} where Mar^{D155A} is expressed and TO1 is present. Error bars represent ± standard error of the mean. P-values calculated using the Shapiro-Wilk normality test (ns $p>0.05$, *$p<0.05$, **$p<0.01$, ***$p<0.001$, ***$p<0.0001$). When the bar on the histogram extends beyond the scale of the Y-axis, the number in the bar indicates the value.

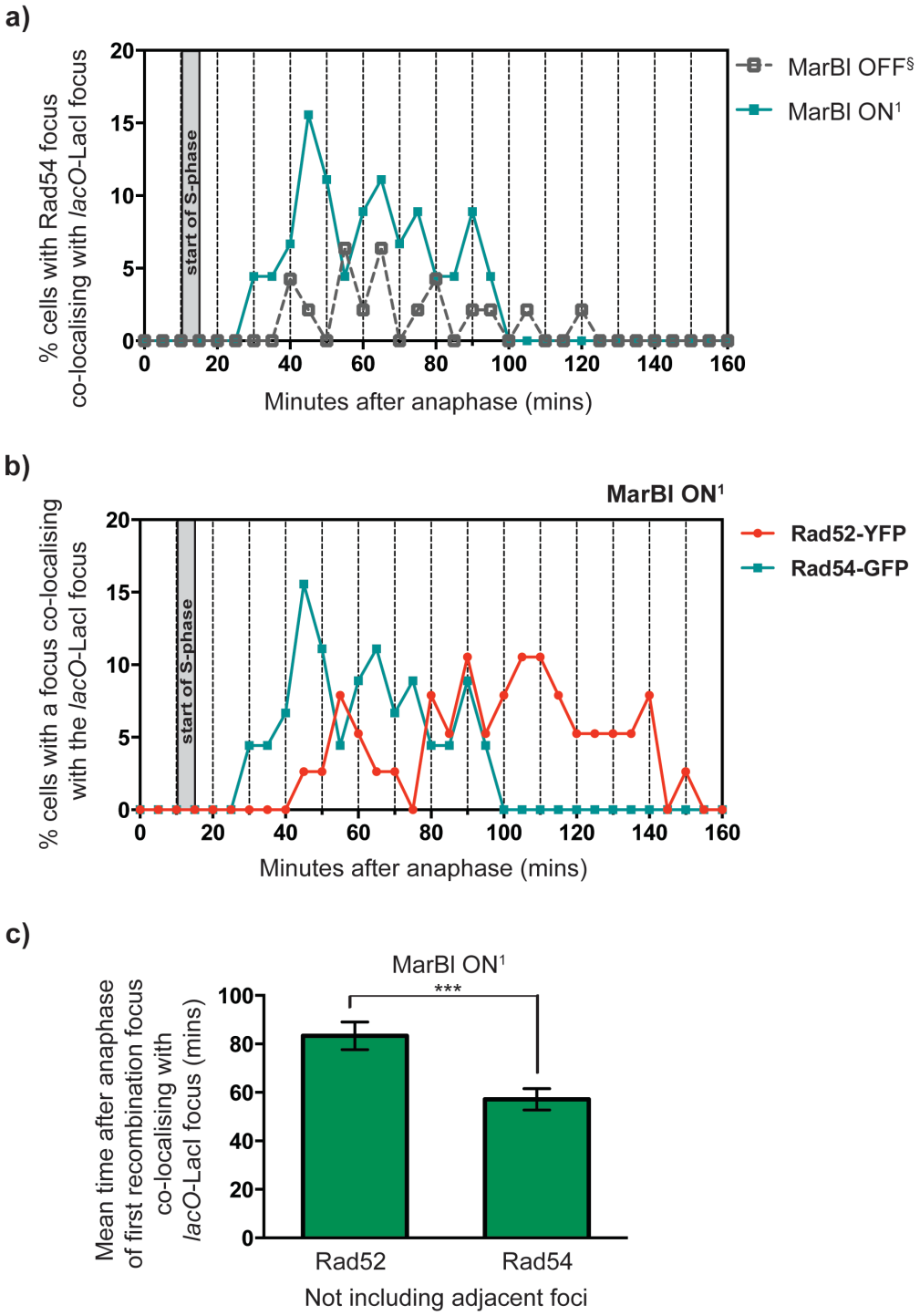


Fig. 4.xxiii Temporal kinetics of Rad54-GFP foci co-localising with MarBI compared to Rad52-YFP.

a) Line graphs of the percentage of cells with a Rad54-GFP focus that co-localises with the *lacO*-LacI focus during the first 160 minutes following anaphase. b) Line graph showing a comparison of the co-localisation of Rad52-YFP and Rad54-GFP foci with the *lacO*-LacI focus during the first 160 minutes following anaphase. c) Bar charts showing the mean time after anaphase comparing when the first Rad52-YFP and Rad54-GFP co-localise with the *lacO*-LacI focus. The strains are MCW7574 (n=38), MCW7924 (n=47) and MCW8167 (n=45). MarBI OFF§ represents a system where Mar^{D155A} is not expressed but TO1 is present and MarBI ON^{1} where Mar^{D155A} is expressed and TO1 is present. Error bars represent ± standard error of the mean. P-values calculated using the Shapiro-Wilk normality test (ns p>0.05, *p<0.05, **p<0.01, ***p<0.001, ***p<0.0001).

anaphase, regardless of whether the cells contained MarBI OFF or MarBI ON [Fig. 4.xix.b & Fig. 4.xx.a]. Both MarBI OFF and ON[1] cells show no significant difference in either the proportion of cells with a Rad54 focus nor the frequency of their distribution across the 160 minute post anaphase period [Fig. 4.xx a, b & c].

As with the Rad52 foci, I also marked the time points when a Rad54-GFP focus co-localised (red) or was adjacent (blue) to the *lacO*-LacI focus marking the MarBI site [Fig. 4.xix.b & Fig. 4.xxi]. Of the total Rad54 foci observed, approximately 47% of the cells with MarBI ON[1] have a co-localising focus in at least one time point compared to 20% when MarBI OFF is present [Fig. 4.xxii.a]. Generally, Rad54 co-localises with *lacO*-LacI in more time points in cells with MarBI ON[1] than with MarBI OFF, the total number of time points ranging from 1 to 6 in MarBI ON (average = 1.44 including cells with 0 time points of co-localisation) compared to 1 to 2 in the majority of cells with MarBI OFF (average = 0.4 including cells with 0 time points of co-localisation) [Fig. 4.xxii.b & c]. These data indicate that Rad54, like Rad52, is specifically recruited to MarBI ON.

Analysis of the timing of Rad54 focus co-localisation with *lacO*-LacI indicates that the earliest Rad54 is recruited to MarBI is 30 minutes post anaphase or 15 to 20 minutes following the start of S-phase [Fig. 4.xxiii]. On average the recruitment time is ~57 minutes post anaphase (or 42 to 47 minutes following the start of S-phase) [Fig. 4.xxiii.c]. This is earlier than observed for the recruitment of Rad52 to MarBI ON, for example the average recruitment time for Rad52 to MarBI ON[1] is ~ 83 minutes post anaphase [Fig. 4.xxiii.b & c]. Why Rad54 should be recruited earlier to MarBI ON than Rad52 is unclear.

4.3 Discussion

MarBI:a novel site-specific RFB that induces recombination in *S. pombe*

There have been a number of studies in yeast and mammalian cells that have investigated the cellular response to replication fork stalling by protein-DNA barriers (Ahn et al., 2005; Lambert et al., 2005; Larsen et al., 2014; Rothstein et al., 2000; Sofueva et al., 2011; Willis et al., 2014). In the majority of these studies programmed RFBs, such as the Fob1-dependent barrier from the rDNA array in *S. cerevisiae* and *RTS1* barrier in *S. pombe*, have been used. These barriers are typically unidirectional and variously induce a recombinational response. For example, the Fob1-dependent barrier does not induce recombination, whereas, *RTS1* does. Indeed, *RTS1* appears to be unique amongst those programmed RFBs that have been studied in its ability to induce recombination (Ahn et al., 2005; Branzei and Foiani, 2010; Lambert et al., 2010). This has led some to question whether it represents a “typical” barrier. To try and answer this question it is important to compare the cellular response to *RTS1* with that elicited by other site-specific RFBs, ideally in the same organism and at the same genetic locus. A previous attempt to do this in *S. pombe*, using a *lacO* array bound by LacI, revealed some marked differences with the response induced by *RTS1* (Sofueva et al., 2011). Cells with the *lacO*-LacI array exhibited an increased frequency of anaphase bridges and DSBs. There was also a strong induction of direct repeat recombination but unlike with *RTS1*, the recombinants appeared to derive almost entirely from Rad52/Swi10-dependent SSA rather than Rad51-dependent strand invasion. To explain these data it was proposed that the *lacO*-LacI array prevented forks from converging in some cells, resulting in a region of unreplicated DNA that manifested as an anaphase bridge during mitosis. Resolution of the bridge was proposed to involve DNA breakage followed by repair by SSA (Sofueva et al.,

2011). However, the large size of the *lacO* array used to elicit this response was deemed by some to be non-physiological. In this chapter, I have described the development of a novel site-specific RFB (MarBI) that is formed by the non-covalent binding of a single dimer of Mar protein to a single 30 bp DNA site. Like *RTS1* and *lacO*-LacI, MarBI induces a recombinational response, but as discussed below, this response is again different from that elicited by the other RFBs.

Like *RTS1* and *lacO*-LacI, MarBI induces direct repeat recombination when it is flanked by the repeated DNAs. However, unlike *lacO*-LacI, which induces mostly deletions, MarBI induces an approximately equal mix of gene conversions and deletions. This is more similar to the response elicited by *RTS1*, and indicates that much of the recombination derives from Rad51-dependent strand invasion events. Indeed, in the absence of Rad51, gene conversions are lost and there is a significant reduction in deletions similar to what is seen at *RTS1*. However, the frequency of recombination induced by MarBI is far higher than that induced by *RTS1*, even though the amount of fork stalling, judged by 2D gel analysis, is much less. Moreover, both the frequency and duration of Rad52 focus co-localisation with the MarBI site is far less than observed previously at *RTS1* [Fig. 4.xxiv.a & b] (Nguyen et al., 2015). This apparent discrepancy, between the genetic assay and physical assays, can be explained if events elicited by MarBI are far more likely to result in direct repeat recombination than those at *RTS1*.

Unlike *RTS1*, MarBI is a bi-directional barrier, and based on the accumulation of putative double Y-shaped DNA molecules observed on 2D gels, seems to cause problems with the two forks merging at the final stages of replication termination. Two other differences with *RTS1* are the appearance of DSBs at MarBI and the much later recruitment of Rad52 to the barrier site, which occurs in late S-phase and G2 phase of the cell cycle [Fig. 4.x & Fig. 4.xxiv.c].

Based on these observations, a plausible model for what happens at MarBI can be proposed. Upon encounter of MarBI a replication fork stalls, however, unlike at *RTS1*, it tends not to collapse. Instead, it either overcomes the barrier, and replicates past it, or persists at the barrier long enough for the opposing replication fork to arrive and attempt to merge with it. Based on the appearance of DSBs and timing of Rad52 recruitment to the barrier site, I suspect that it is at the point of fork merging that problems arise. Unlike at the *lacO*-LacI array, the two forks manage to almost fully converge at MarBI and, therefore, may form a structure that is targeted by DNA structure-specific nucleases during G2. Endonucleolytic cleavage would effectively cause a DSB in one of the two sister chromatids, which could be repaired by Rad51-dependent homologous recombination [Fig. 4.xxv]. I suspect that this repair is far more likely to give rise to a direct repeat recombinant than the type of RDR that is induced at *RTS1*. To investigate the validity of this model, it will be important to verify the timing of DSB formation and to identify the nuclease(s) involved in making the break.

The seemingly different ways in which *RTS1*, *lacO*-LacI and MarBI induce recombination, highlights the diversity of mechanisms that are employed to tackle protein-DNA RFBs. How common each type of barrier is remains an open question. However, the fact that none of the barriers cause any significant loss of viability, suggests that they represent problems that the cell has evolved to deal with. In the case of MarBI, the response that it elicits seems to be quite different from any that has been described before. Indeed, recent work in mammalian cells has suggested that incomplete DNA replication leads to problems that are only recognized and dealt with during mitosis (Ghamrasni et al., 2016; Moreno et al., 2016; Naim et al., 2013; Ying et al., 2013). I suspect that the main difference between MarBI and problems like the *lacO*-LacI array and common fragile sites in

human cells, is the proximity of the two converging replication forks to each other. With *lacO*-LacI, or at common fragile sites, converging forks may not come close enough to form a structure that can be sensed by the cell during G2 and, therefore, the failure to complete replication may only become apparent during mitosis when the chromosomes condense or attempt to segregate (Minocherhomji et al., 2015). Exactly how the closely converged forks at MarBI would be sensed remains a mystery. However, the observation that Rad54 seems to be recruited to the MarBI site before Rad52 may indicate its involvement. Indeed this earlier recruitment is quite different from what is observed at DSBs and at *RTS1* (Lisby et al., 2004 and unpublished data).

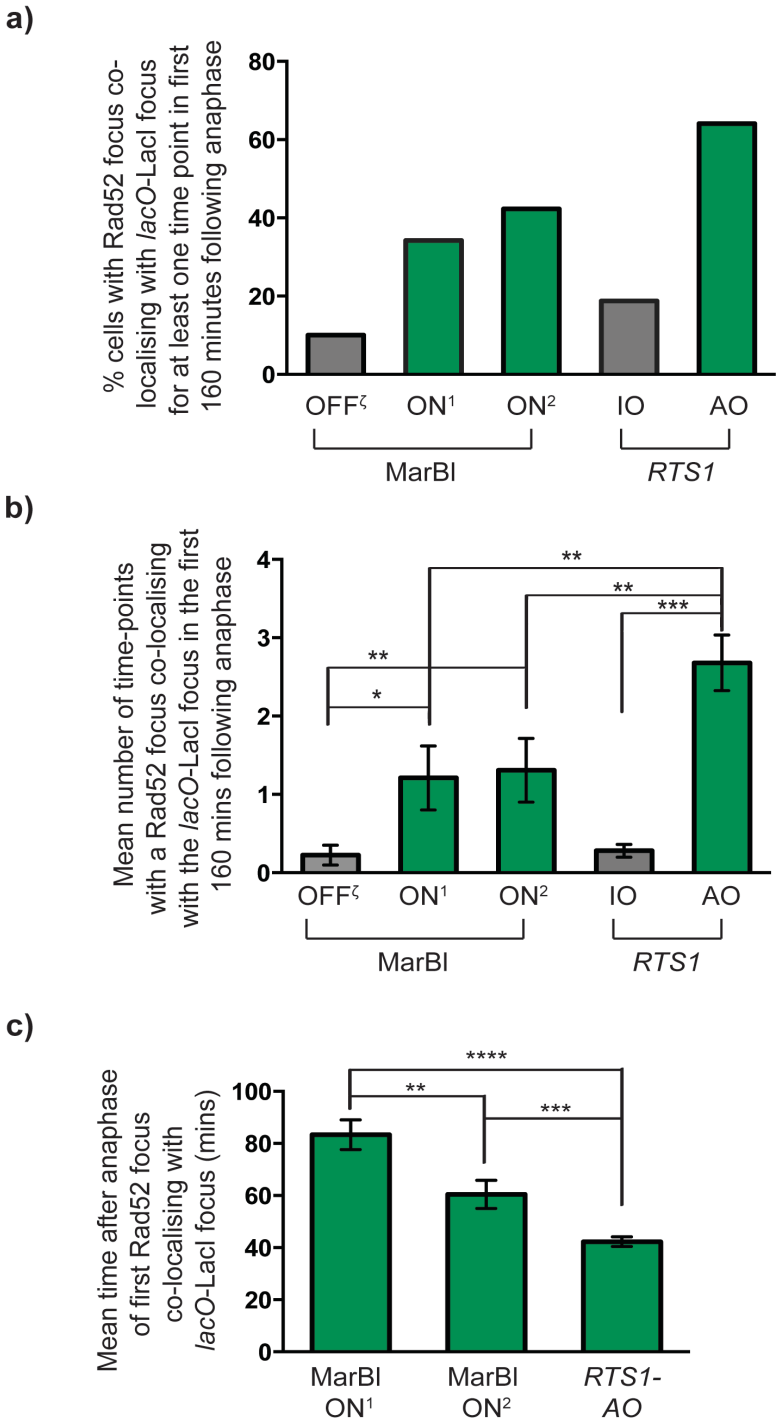


Fig. 4.xxiv Comparison of the Rad52 foci dynamics co-localising with MarBI versus *RTS1*.

a) Bar charts of the percentage of cells that exhibit a Rad52-YFP focus co-localising with the *lacO*-LacI focus for at least one time point in the first 160 minutes following anaphase. b) Bar chart showing the mean number of time points that cells have a Rad52-YFP focus that co-localises with the *lacO*-LacI focus during the first 160 minutes following anaphase. c) Bar chart showing the mean time after anaphase when the first Rad52-YFP co-localises with the *lacO*-LacI focus. The strains are MCW7578 (n=40), MCW7574 (n=38), MCW7582 (n=26) and MCW6556 (n=78). MarBI OFF$^{\zeta}$ represents the system where the Mar^{D155A} protein is expressed but the transposon end is absent, MarBI ON^{1} where Mar^{D155A} is expressed and TO1 is present and MarBI ON^{2} where Mar^{D155A} is expressed and TO2 is present. Error bars represent ± standard error of the mean. P-values calculated using the Shapiro-Wilk normality test (ns $p>0.05$, *$p<0.05$, **$p<0.01$, ***$p<0.001$, ***$p<0.0001$).

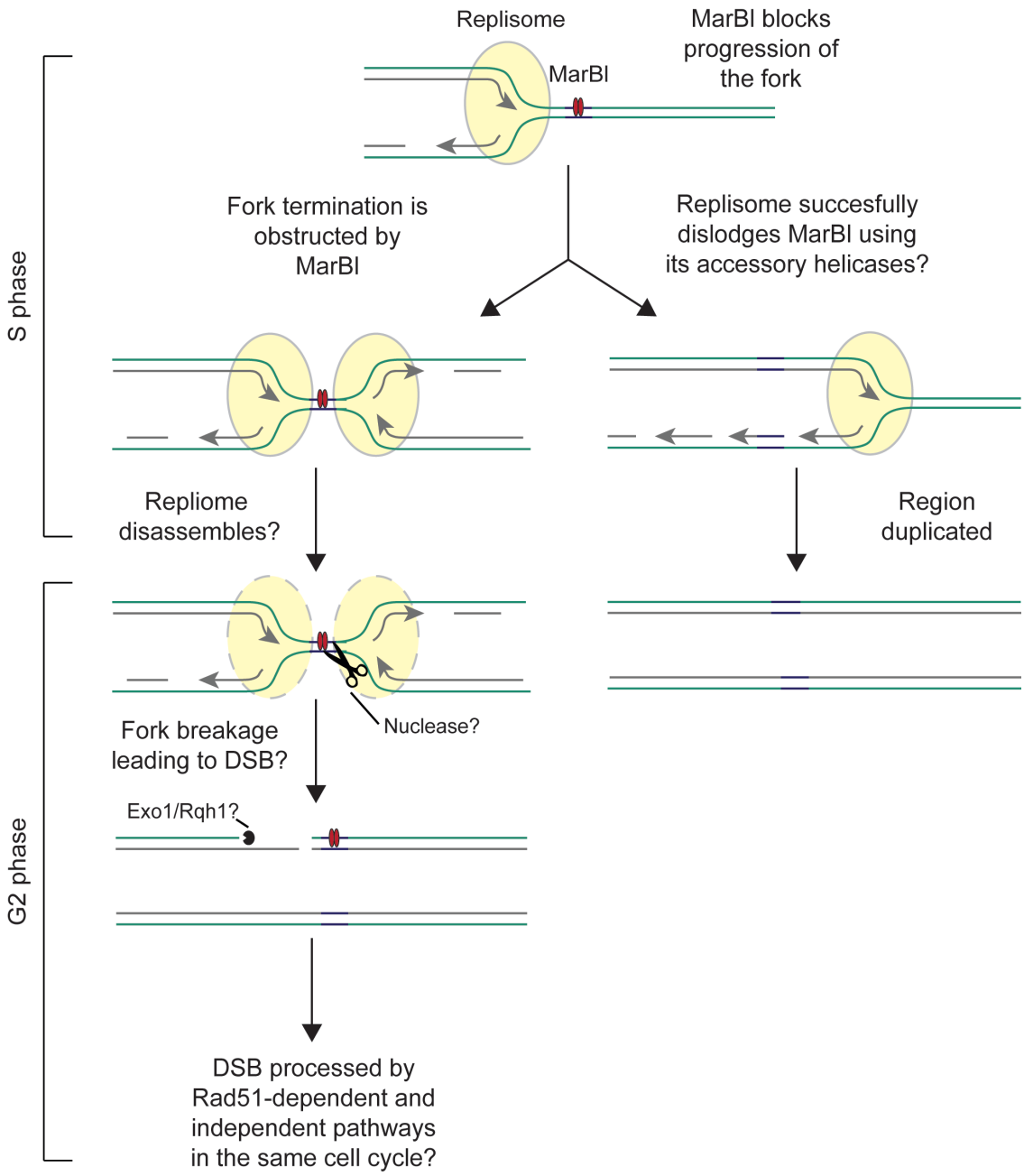


Fig. 4.xxv Hypothetical model for the cellular response to MarBI.
Schematic model of the proposed steps involved when the replisome encounters MarBI. Parental DNA strands are shown in green and the nascent strands in grey with arrows indicating the direction of DNA synthesis.

Chapter 5

Further analysis of MarBl-induced recombination and comparison to other RFBs

5.1 Introduction

As established in the previous chapter, MarBI is an accidental protein-DNA barrier that stochastically causes replication fork stalling and strongly induces illegitimate recombination. However, the cellular response invoked when the replisome encounters MarBI seems to differ significantly from the native RFB, *RTS1.* In contrast to the DSB-independent RDR initiated at *RTS1*, replication fork stalling at MarBI correlates with DNA breakage. Moreover, the bi-directional nature of replication fork stalling at MarBI results in a strong accumulation of converged replication forks, which is not seen at *RTS1*. Finally, Rad52 recruitment to MarBI occurs much later in the cell cycle than it does at *RTS1*. Owing to these differences, I wanted to further characterise the cellular response to replication fork stalling at MarBI by: a) determining which genetic factors influence MarBI-induced recombination, and b) assessing whether MarBI causes replication fork collapse and RDR, as seen at *RTS1* (Nguyen et al., 2015). In addition, I wanted to see whether other accidental protein-DNA barriers would elicit the same responses as MarBI.

5.2 Results

5.2.1 Does MarBI induce direct repeat recombination at sites downstream of it similar to *RTS1*?

Replication restart at *RTS1* has been shown to be error-prone, giving rise to genome rearrangements as it travels away from its point of initiation. If template switching is considered to be an intrinsic property of the restarted fork (Iraqui et al., 2012; Lambert et al., 2010; Mizuno et al., 2013; Nguyen et al., 2015; Smith et al., 2007), then determining the frequency of direct repeat recombination downstream of MarBI should provide a measure of whether it induces RDR or not.

To determine if there is any measurable RDR from MarBI, the barrier site was re-positioned 0.2 kb upstream of the *ade6*$^{-}$ direct repeats such that the replication fork would be blocked by MarBI before it enters either *ade6*$^{-}$ heteroallele [Fig. 5.i.a : site I]. In this experimental set-up, the frequency of direct repeat recombination was at background spontaneous levels with MarBI OFF§ [Fig. 5.i.b]. However, with MarBI ON^{1} and MarBI ON^{2} the total recombinants increase by ~18 fold and ~22 fold, respectively [Fig. 5.i.b & Table 8-2]. These data suggest that MarBI may induce RDR, however, it is also possible that this increase in direct repeat recombination could result from the spread of recombination proteins away from the DSB that is formed at MarBI.

To gain a further measure of MarBI-induced RDR, I placed the *ade6*$^{-}$ direct repeat reporter 12.4 kb downstream of the endogenous *ade6* locus where MarBI was positioned [Fig. 5.i.a : 12.4kb (site II)]. Again, both MarBI ON^{1} and ON^{2} caused a marked induction of recombination at this downstream site when compared to MarBI OFF$^{\pi}$ [Fig. 5.i.b & Table 8-2]. As shown in Chapter 3, deletion of *oriIII-1253* results in more time for RDR to occur following replication fork stalling at *RTS1* and, therefore, much higher levels of direct repeat recombination downstream of the barrier. To see if the same is true for MarBI, I deleted *oriIII-1253* in the strains with the *ade6*$^{-}$ direct repeat reporter 12.4 kb downstream of MarBI and measured the frequency of Ade^{+} recombinants [Fig. 5.i.b & Table 8-2]. To my surprise, the frequencies of recombinants were less than observed in the equivalent *oriIII-1253*$^{+}$ strains and, in fact, differed very little from the *oriIII-1253*$^{+}$ MarBI OFF$^{\pi}$ level. Altogether these data do not provide convincing evidence for there being high rates of RDR from MarBI. Certainly, the rates of recombination downstream of MarBI are far less than observed with *RTS1*, and this is despite them being far higher at the barrier.

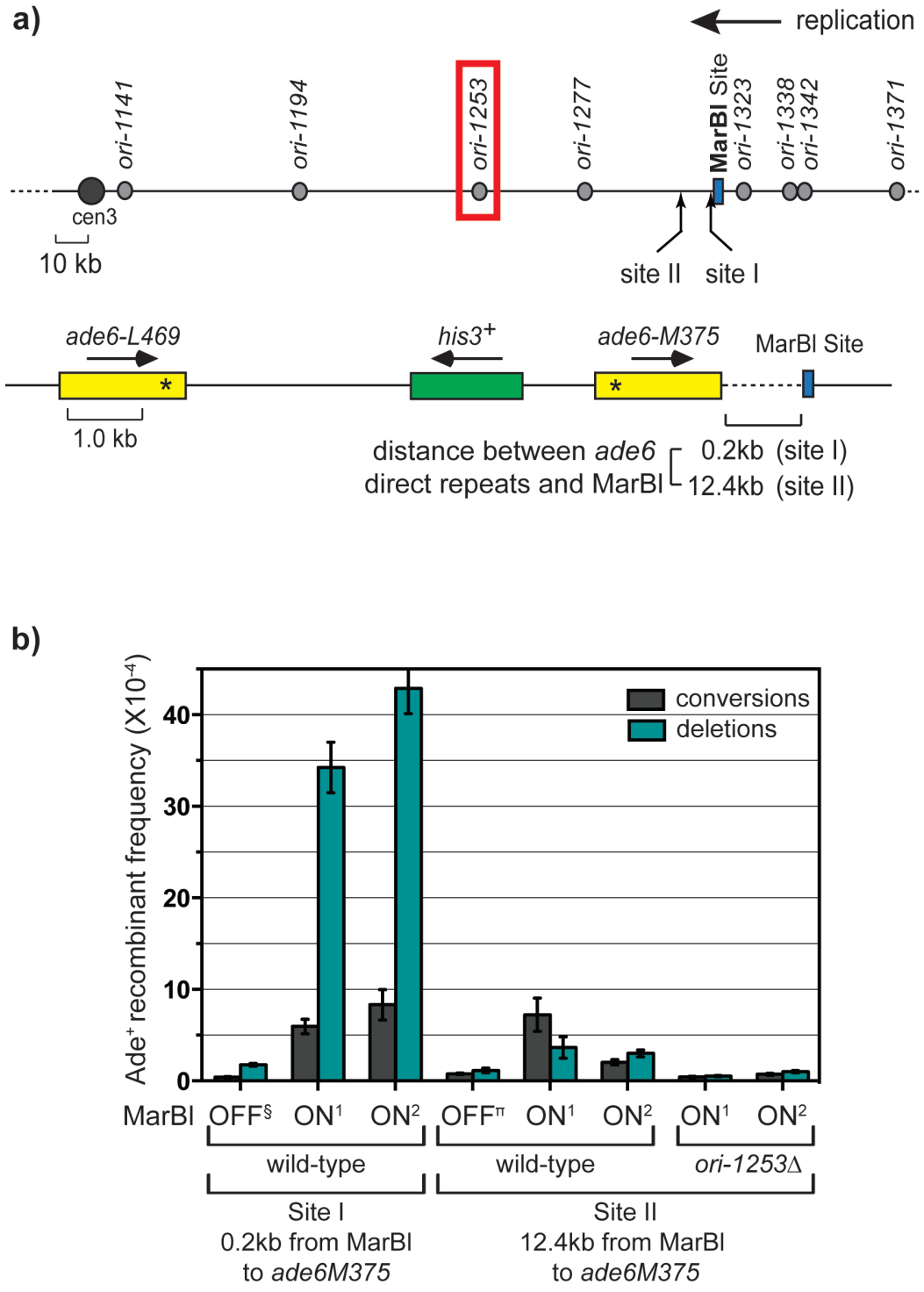


Fig. 5.i Direct repeat recombination downstream of MarBI.
a) Schematic showing the relative positions on ChrIII where the *ade6*$^{-}$ reporter (shown in the bottom panel) is inserted downstream of or at the endogenous *ade6* locus. The MarBI site is positioned before the reporter (site I) or replacing the endogenous *ade6* gene (site II). b) Bar chart showing the frequency of Ade^{+} recombinants in strains MCW7444, MCW7624, MCW7622, MCW7229, MCW7733, MCW7731, MCW7737 and MCW7735. Error bars represent ± standard error of the mean. MarBI OFF§ represents a system where Mar^{D155A} is not expressed but TO1 is present, MarBI OFF^{π} where Mar^{D155A} is not expressed and TO1 is absent, MarBI ON^{1} where Mar^{D155A} is expressed and TO1 is present and MarBI ON^{2} where Mar^{D155A} is expressed and TO2 is present.

5.2.2 Is the absence of replication restart due to the stabilisation of the replication fork by the fork protection complex?

The FPC, consisting of Swi1 and Swi3, is intimately associated with the replisome and is thought to prevent replication fork collapse at difficult to replicate regions (Noguchi et al., 2003). Consequently *swi1*Δ and *swi3*Δ mutants exhibit a spontaneous hyper-recombination phenotype and increased levels of genome instability at weak RFBs, such as tRNA genes (Pryce et al., 2009). In contrast, the FPC is required for the activity of many programmed RFBs and, therefore, its loss results in the abolition of *RTS1*-induced recombination. To see whether the FPC is needed for replication fork stalling at MarBI, I compared replication intermediates in the vicinity of MarBI OFF and MarBI ON[1] in both wild-type and *swi1*Δ mutant strains [Fig. 5.ii.a]. Compared to wild-type, the *swi1*Δ mutant exhibited slightly reduced levels of stalled fork and double Y-shaped molecule signals [Fig. 5.ii.a & b]. There also appears to be a slight increase in large Y-shaped molecules [Fig. 5.ii.a & b]. These data suggest that there may be slightly less fork stalling at MarBI when the FPC is missing, however, it is important to note that the 2D gel analysis was not repeated, so the differences observed could be explained by experimental variation.

Having established that MarBI still blocks replication forks in a *swi1*Δ mutant background, I next determined what effect, if any, *swi1*Δ has on MarBI-induced recombination [Fig. 5.ii.c]. With MarBI ON[1] there is a modest reduction in deletions (~1.5 fold) but no significant change in gene conversions when comparing *swi1*Δ with wild-type cells [Fig. 5.ii.c and Table 8-2]. Similarly, with MarBI ON[2] there is a reduction in deletions in the *swi1*Δ mutant, but in this case the gene conversions are also reduced [Fig. 5.ii.c and Table 8-2]. As expected, with MarBI OFF, *swi1*Δ exhibits a large increase in spontaneous recombination (~22 fold increase in gene

conversions and ~21 fold increase in deletions) [Fig. 5.ii.c and Table 8-2]. Together, these data indicate that the FPC has some role in promoting recombination at MarBI. To see if this is also true for the recombination downstream of MarBI, I next measured the frequency of Ade^+ recombinants in a *swi1*Δ mutant where MarBI was positioned 0.2 kb upstream of the *ade6*$^-$ direct repeat [Fig. 5.iii.a]. Intriguingly, in this case there was ~3 fold increase in gene conversions and ~5 fold increase in deletions in the *swi1*Δ mutant with MarBI ON^1, and overall the frequency of recombinants is ~7 fold higher than with MarBI OFF [Fig. 5.iii.b & Table 3-1]. Altogether, these data suggest that there may be increased levels of RDR at MarBI when the FPC is missing (see Section 5.3.2).

As discussed in Chapter 4, Rad52 appears to be recruited to MarBI much later during the cell cycle than it is to *RTS1*. I speculated that this difference could be due to the fact that very little fork collapse and RDR occur at MarBI. However, without the FPC there may be an increase in fork collapse, which might result in Rad52 being recruited earlier. To test this possibility, I performed time-lapse imaging of Rad52-YFP foci in *swi1*Δ cells with MarBI ON^1 and MarBI OFF, and scored both the overall frequency of Rad52-YFP foci and their specific co-localisation with the *lacO*-LacI array immediately downstream of MarBI [Fig. 5.iv]. Compared to wild-type, a greater percentage of *swi1*Δ mutant cells with MarBI ON^1 exhibited Rad52-YFP foci that co-localised with *lacO*-LacI in the 40 minute period following the start of S-phase [Fig. 5.v.b]. Indeed, amongst all cells with at least one co-localising Rad52 focus, the mean time of first co-localisation is 61 minutes for *swi1*Δ with MarBI ON^1 versus 83 minutes for wild-type with MarBI ON^1 [Fig. 5.v.c]. However, *swi1*Δ mutant cells exhibit far higher levels of spontaneous Rad52-YFP foci than wild-type cells both in terms of the frequency of foci [Fig. 5.vi.a & d] and in terms of the number of foci per cell [Fig. 5.vi.b & c]. Therefore,

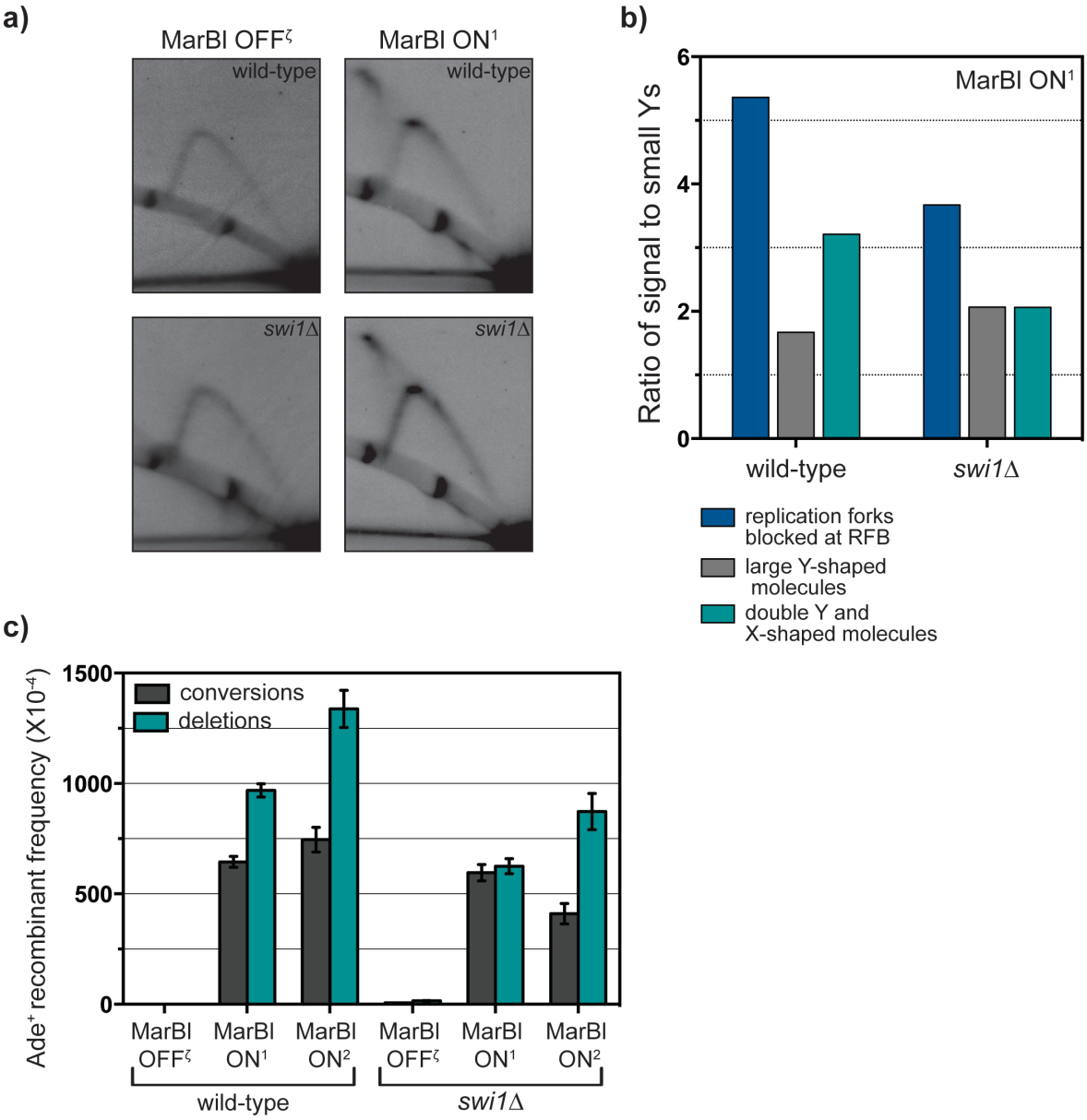


Fig. 5.ii Effect of *swi1*Δ mutation on replication fork progression and recombination at MarBI.

a) 2D gel analysis of replication intermediates within the *Eco*NI fragment shown in Fig. 4.vii from wild-type and *swi1*Δ cells. b) Quantification of the 2D gels displayed as bar charts. The DNA was extracted from asynchronously growing cultures of the strains MCW7075, MCW7076, MCW7753 and MCW7755. c) Bar chart showing the frequency of Ade^+ recombinants in strains MCW8239, MCW7076, MCW7078, MCW7753, MCW7755 and MCW7757. Error bars represent ± standard error of the mean. MarBI OFF^{ζ} represents the system where the Mar^{D155A} protein is expressed but the transposon end is absent, MarBI ON^1 where Mar^{D155A} is expressed and TO1 is present and MarBI ON^2 where Mar^{D155A} is expressed and TO2 is present.

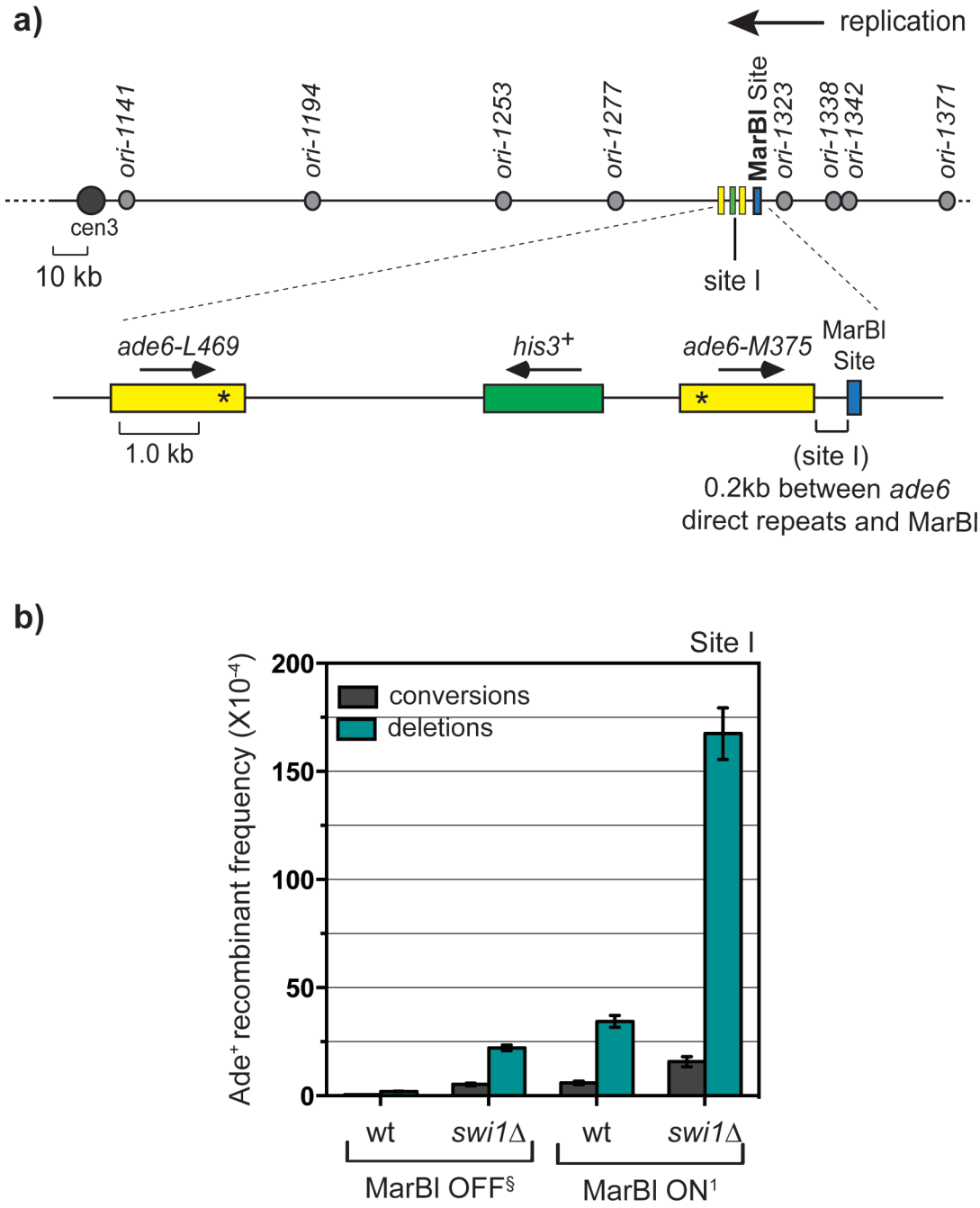


Fig. 5.iii The effect of *swi1*Δ on direct repeat recombination downstream of MarBI. a) Schematic showing the relative positions on ChrIII where the *ade6*$^{-}$ reporter (shown in the bottom panel) is inserted at the endogenous *ade6* locus. The MarBI site is positioned before the reporter (site I). b) Bar chart showing the frequency of Ade^{+} recombinants in strains MCW7500, MCW8282, MCW7624 and MCW8284. Error bars represent ± standard error of the mean. MarBI OFF§ represents a system where Mar^{D155A} is not expressed but TO1 is present and MarBI ON^{1} where Mar^{D155A} is expressed and TO1 is present.

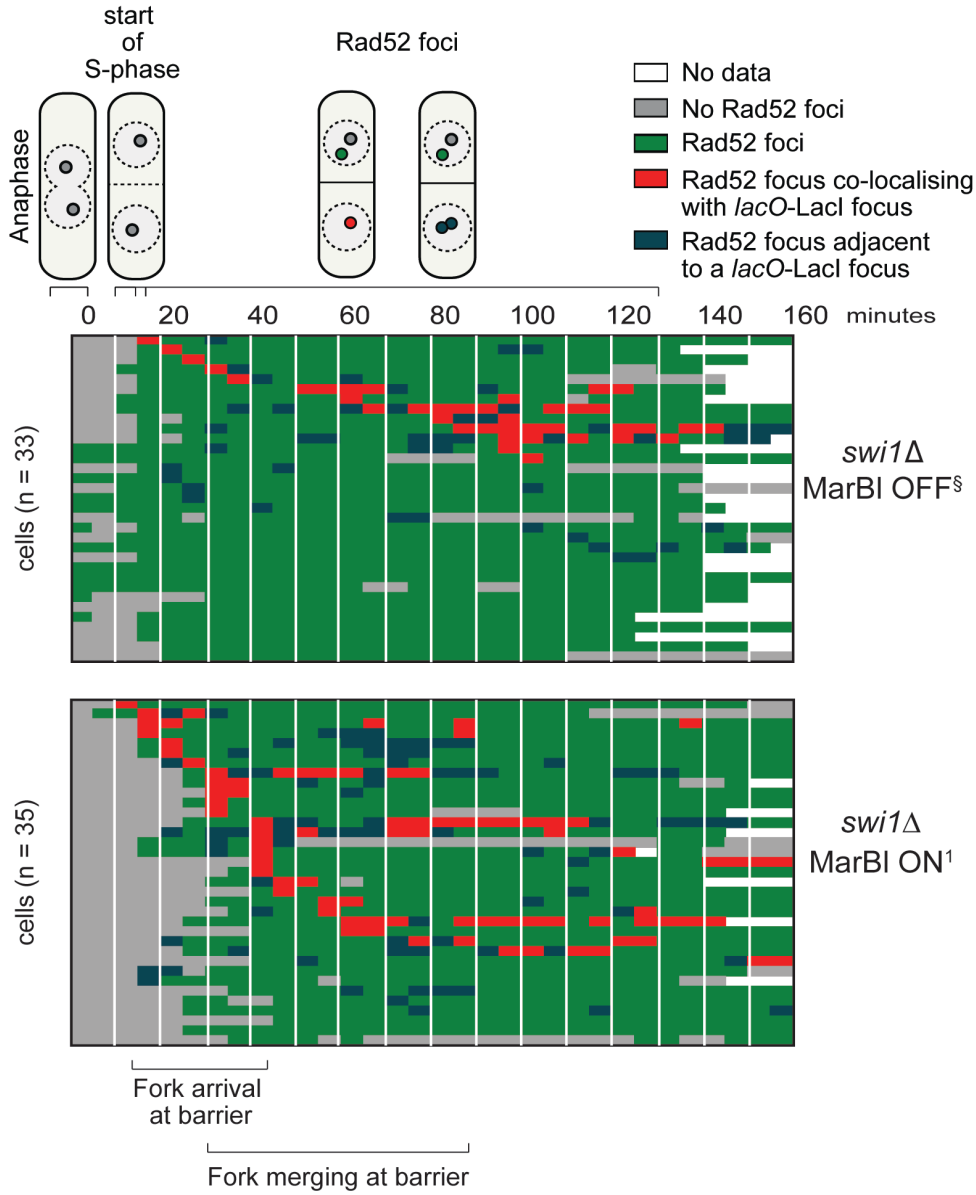


Fig. 5.iv Tracking Rad52-YFP focus localisation at MarBI in a *swi1*Δ mutant cell by time-lapse microscopy.

Analysis of the time-lapse movies. The presence of a Rad52 focus and whether it co-localises with the *lacO*-LacI-tdKatushka2 focus is recorded every 5 minutes for a period of 160 minutes post anaphase in each cell in *swi1*Δ cells. The top panel is a schematic of *S. pombe* cells at various stages post anaphase with nuclear *lacO*-LacI foci in grey, Rad52 foci in green, co-localising foci in red and a Rad52 focus adjacent to the *lacO*-LacI focus in blue. The estimated time of fork arrival and fork merging is indicated below as established earlier in Nguyen et al. (2015). The strains are MCW8312 (n=33) and MCW8233 (n=35). MarBI OFF§ represents a system where Mar^{D155A} is not expressed but TO1 is present and MarBI ON^{1} where Mar^{D155A} is expressed and TO1 is present.

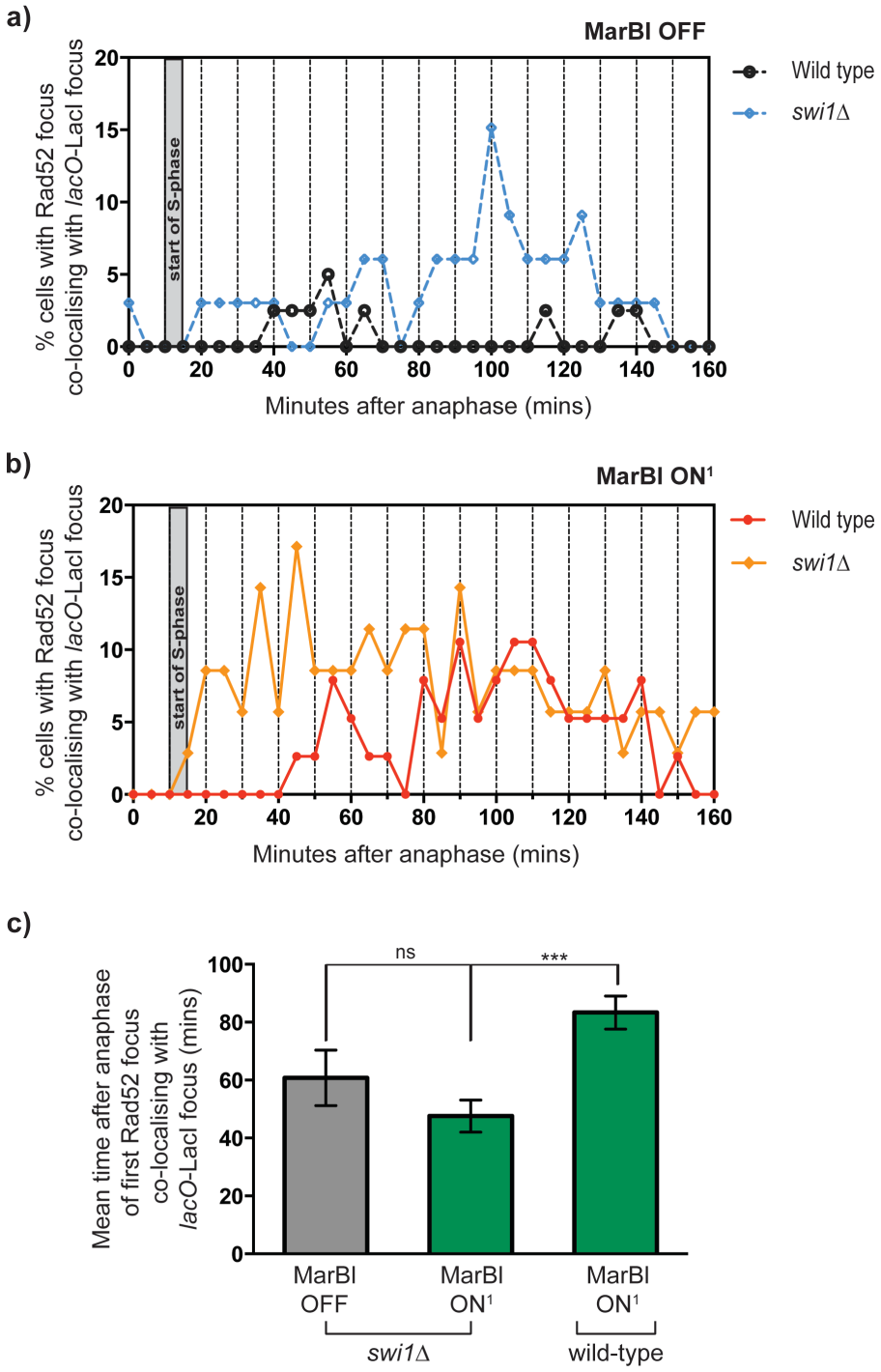


Fig. 5.v Earlier recruitment of Rad52-YFP to MarBI is observed in the absence of Swi1.

a) Line graph showing a comparison of the co-localisation of Rad52-YFP foci with the *lacO*-LacI focus in wild-type and *swi1*Δ cells in the presence of MarBI OFF during the first 160 minutes following anaphase. b) Line graph showing a comparison of the co-localisation of Rad52-YFP foci with the *lacO*-LacI focus in wild-type and *swi1*Δ cells when MarBI ON^{1} is present during the first 160 minutes following anaphase. c) Bar charts showing the mean time after anaphase comparing when the first Rad52-YFP co-localises with the *lacO*-LacI focus in wild-type and *swi1*Δ cells. The strains are MCW7578 (n=40), MCW7574 (n=38), MCW8312 (n=33) and MCW8233 (n=35). MarBI OFF represents a system where Mar^{D155A} is not expressed but TO1 is present and MarBI ON^{1} where Mar^{D155A} is expressed and TO1 is present. Error bars represent ± standard error of the mean. P-values calculated using the Shapiro-Wilk normality test (ns p>0.05, *p<0.05, **p<0.01, ***p<0.001, ***p<0.0001).

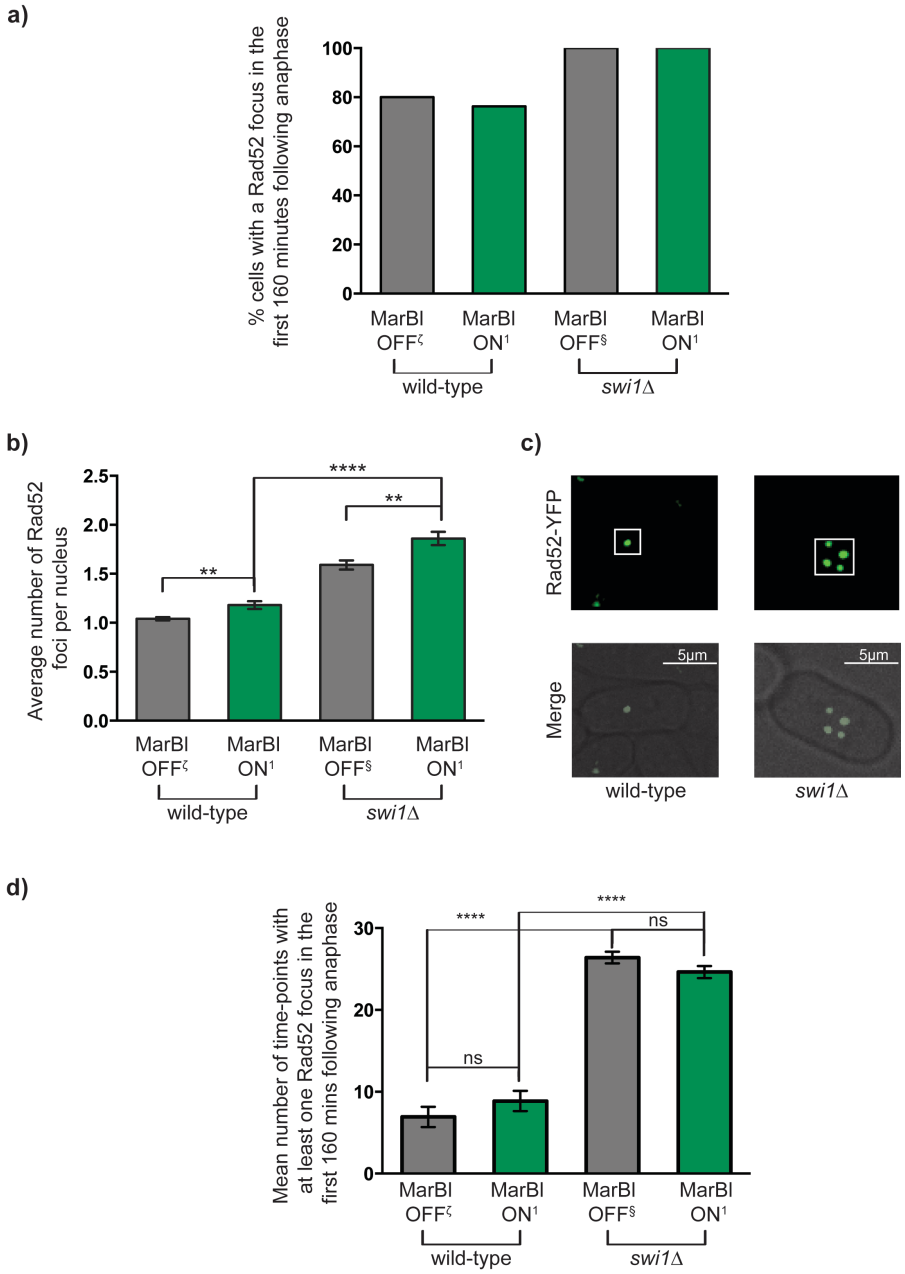


Fig. 5.vi In the absence of Swi1, there is a general increase in overall Rad52 when compared to wild-type cells.

a) Bar chart showing the percentage cells that exhibits at least one Rad52 focus in *swi1*Δ cells in the first 160 minutes following anaphase. b) Bar chart of the average number of Rad52 foci per nucleus observed in cells that exhibit a focus in the first 160 minutes following anaphase. c) Representative stills taken from a time-lapse movie showing a cell with one or four Rad52-YFP foci per nucleus respectively in a wild-type and *swi1*Δ cell. The bottom panel is a merge of the brightfield image and Rad52-YFP.The scale bar represents 5μm. The strain shown is MCW 7574 and MCW8233. d) Bar chart showing the mean number of time points that cells have at least one Rad52-YFP focus during the first 160 minutes following anaphase. The strains are MCW7578 (n=40; range from 1-3 foci per time-point), MCW7574 (n=38; range from 1-2 foci per time-point), MCW8312 (n=33; range from 1-4 foci per time-point) and MCW8233 (n=35; range from 1-4 foci per time-point). MarBI OFF$^{\zeta}$ represents the system where the Mar^{D155A} protein is expressed but the transposon end is absent, MarBI OFF§ where Mar^{D155A} is not expressed but TO1 is present and MarBI ON^{1} where Mar^{D155A} is expressed and TO1 is present. Error bars represent ± standard error of the mean. P-values calculated using the Shapiro-Wilk normality test (ns p>0.05, *p<0.05, **p<0.01, ***p<0.001, ***p<0.0001).

there is a much greater probability that a Rad52-YFP focus will co-localise with a *lacO*-LacI focus by chance. Indeed co-localisations are far more common in the *swi1*Δ mutant with MarBI OFF than in the equivalent wild-type strain [Fig. 5.v.a]. However, the mean time of first co-localisation of Rad52-YFP and *lacO*-LacI foci is 48 minutes for *swi1*Δ with MarBI OFF, is not significantly (p=0.213) different than with MarBI ON[1] [Fig. 5.v.c]. This can be attributed to the small sample size and the experiment will have to be repeated to increase robustness. Altogether, these data suggest that, in the absence of the FPC, Rad52 may be recruited earlier to MarBI ON during the cell cycle.

5.2.3 Does replication past MarBI depend on Pfh1?

It is clear from Section 4.2.3 that MarBI can stall forks long enough for replication fork convergence to occur at it. However, it is also evident that many forks are able to progress past MarBI, and seemingly this can occur without the need for recombination proteins such as Rad51 and Rad52. Pfh1 is proposed to act as an accessory DNA helicase for the replisome enabling it to progress past DNA-protein barriers (Sabouri et al., 2012; Steinacher et al., 2012). In addition, Pfh1 has been proposed to play a role in aiding replication termination by promoting fork convergence (Sabouri et al., 2012; Steinacher et al., 2012). To see if Pfh1 is needed for replication forks to traverse and/or merge at MarBI, I first compared the profiles of replication intermediates in the vicinity of the barrier from both wild-type and *pfh1-m21* strains by 2D gel analysis [Fig. 5.vii.b]. There is little or no difference between wild-type and *pfh1-m21* in terms of the amount of fork stalling or convergence at MarBI ON[1] [Fig. 5.vii.b & c]. Next, I measured the frequency of direct repeat recombination at the barrier [Fig. 5.vii.a &Table 8-2]. With MarBI OFF, there is little difference between wild-type and *pfh1-m21* in the frequency of recombinants, however, with both MarBI ON[1] and ON[2] there is ~2-fold increase in

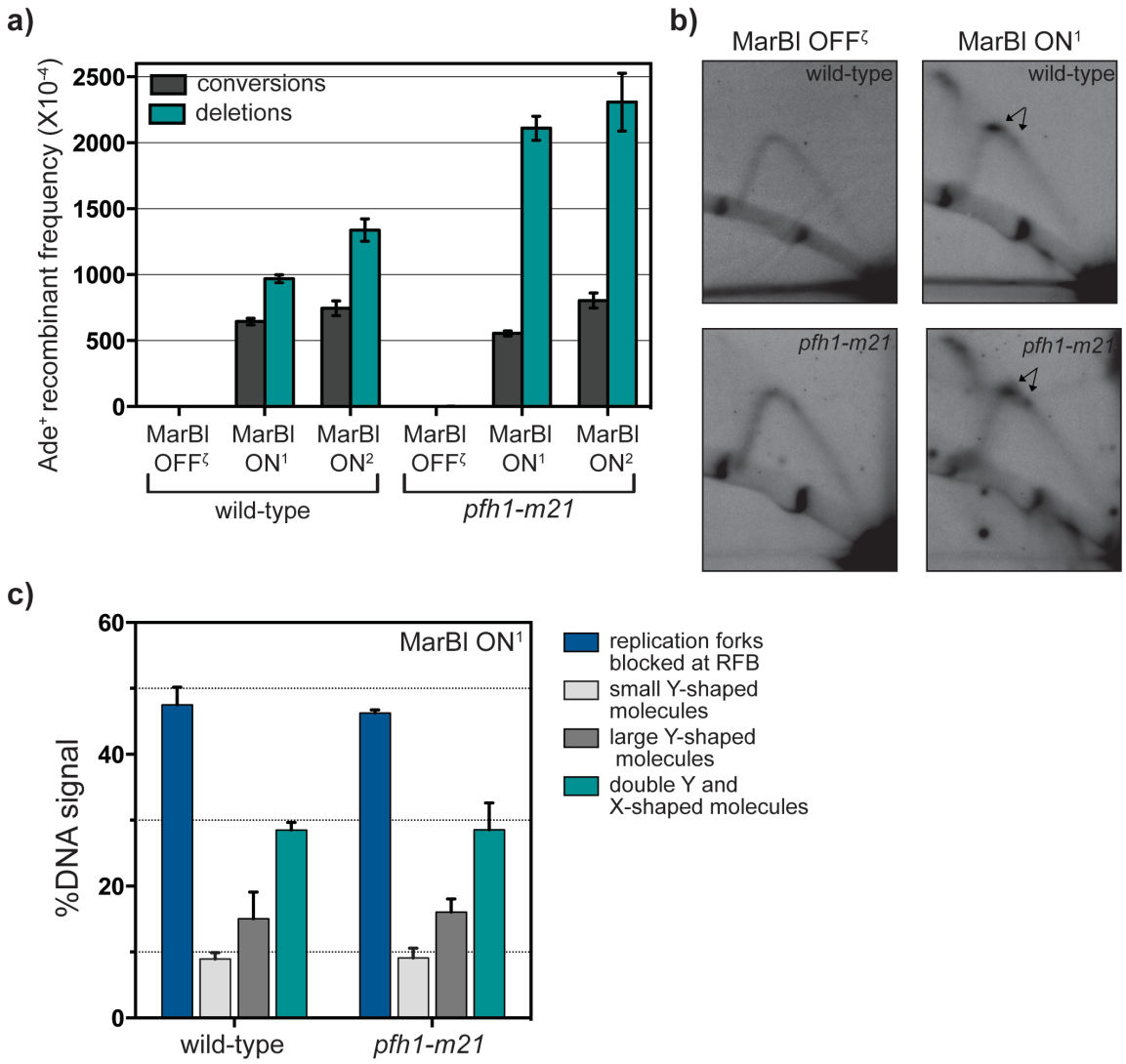


Fig. 5.vii Effect of *pfh1-m21* mutation on replication fork progression and recombination at MarBI.

a) Bar chart showing the frequency of Ade$^+$ recombinants in strains MCW8239, MCW7076, MCW7078, MCW7762, MCW7764 and MCW7766. Error bars represent ± standard error of the mean. b) 2D gel analysis of replication intermediates within the *Eco*NI fragment shown in Fig. 4.vii from wild-type and *pfh1-m21* cells. Arrows on the right hand panel indicate the pause sites. c) Quantification of the 2D gels displayed as bar charts showing the mean values from two independent experiments. Error bar represents the standard error error of the mean. The DNA was extracted from asynchronously growing cultures of the strains MCW7075, MCW7076, MCW7761 and MCW7763. Error bars represent ± standard error of the mean. MarBI OFF$^{\zeta}$ represents the system where the Mar^{D155A} protein is expressed but the transposon end is absent, MarBI ON^1 where Mar^{D155A} is expressed and TO1 is present and MarBI ON^2 where Mar^{D155A} is expressed and TO2 is present.

deletions in the *pfh1-m21* mutant [Fig. 5.vii.a]. Altogether, these data show that Pfh1 is needed to constrain MarBI-induced direct repeat recombination, however, whether this is achieved by promoting replication past the barrier or by aiding fork convergence is unclear.

5.2.4 Elg1 promotes MarBI induced recombination.

As discussed in Chapter 3, the PCNA clamp unloader Elg1 appears to promote RDR at the *RTS1* barrier. To see if Elg1 has any role in promoting or constraining MarBI-induced recombination, I measured the frequency of direct repeat recombination at MarBI OFF and MarBI ON[1] in a *elg1*Δ mutant [Fig. 5.viii.a & Table 8-2]. With MarBI OFF, there is a ~8 fold increase in gene conversions and a ~4 fold increase in deletions in a *elg1*Δ mutant compared to wild-type, which is consistent with the hyper-recombination phenotype that has previously been ascribed to *elg1*Δ mutants in budding yeast (Johnson et al., 2016). However, with MarBI ON[1], there is ~2 fold reduction in gene conversions and ~1.8 fold reduction in deletions compared to wild-type [Fig. 5.viii.a & Table 8-2]. 2D gel analysis reveals little or no difference in the profile of replication intermediates at and around MarBI from wild-type and *elg1*Δ strains [Fig. 5.viii.b & c]. Therefore, the reduction in recombinants cannot be attributed to a reduction in the number of replication forks blocked by MarBI. Together, these data show that Elg1 promotes MarBI-induced recombination, albeit not to the same extent as at *RTS1*.

5.2.5 Is Fml1 involved in processing replication forks perturbed by MarBI?

Fml1 has the ability to stimulate the regression of stalled replication forks through its branch migration activity, and this is maybe how it promotes Rad51-dependent gene conversions at *RTS1* (Sun et al., 2008). To see if it has a similar role in processing forks blocked at MarBI, I measured the frequency of direct repeat

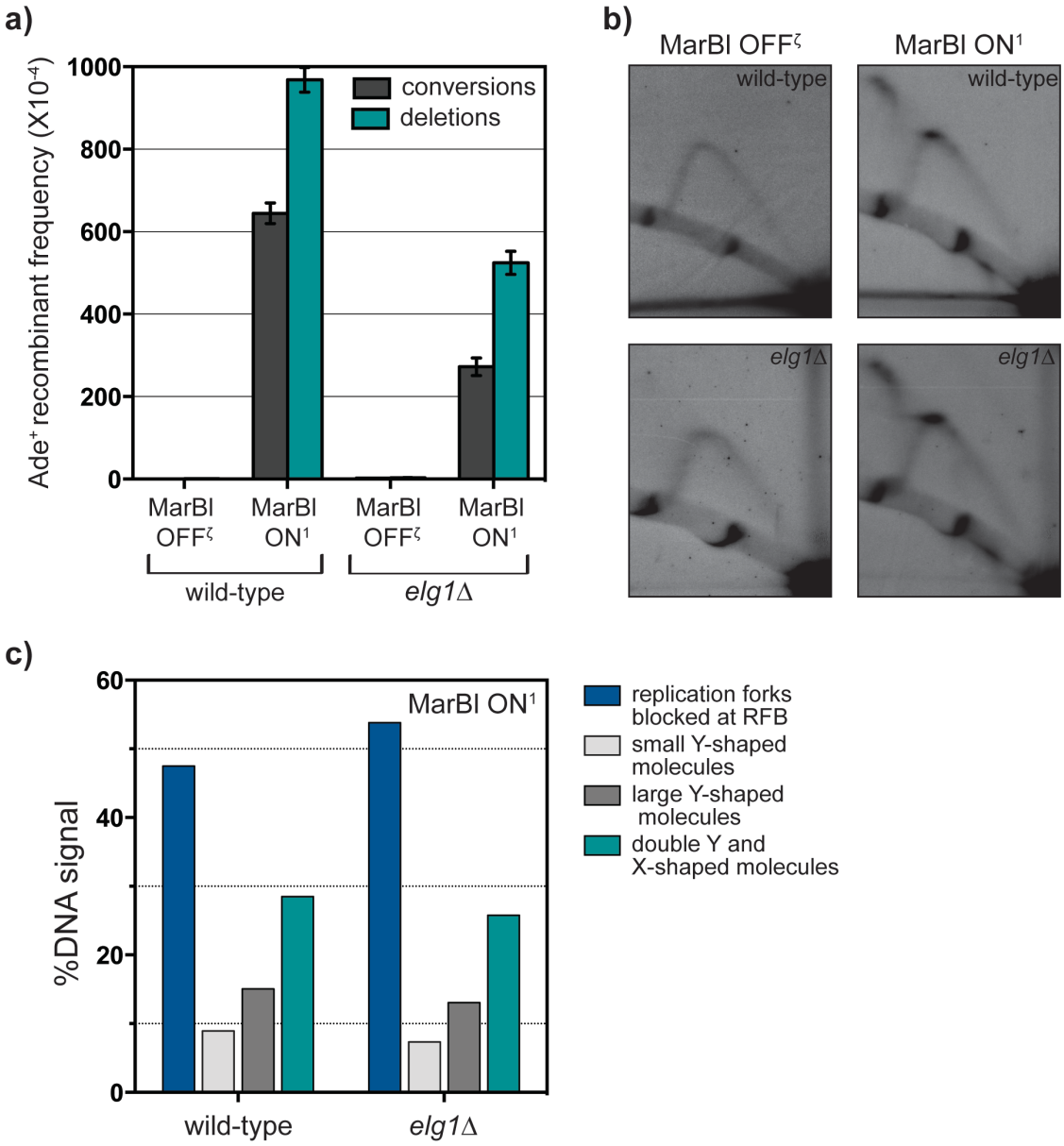


Fig. 5.viii Effect of *elg1*Δ mutation on replication fork progression and recombination at MarBI.

a) Bar chart showing the frequency of Ade$^+$ recombinants in strains MCW8239, MCW7076, MCW8038 and MCW8040. Error bars represent ± standard error of the mean. b) 2D gel analysis of replication intermediates within the *Eco*NI fragment shown in Fig. 4.vii from wild-type and *elg1*Δ cells. c) Quantification of the 2D gels displayed as bar charts. The DNA was extracted from asynchronously growing cultures of the strains MCW7075, MCW7076, MCW8038 and MCW8040. MarBI OFF$^{\zeta}$ represents the system where the Mar^{D155A} protein is expressed but the transposon end is absent and MarBI ON^1, where Mar^{D155A} is expressed and TO1 is present.

recombination in a *fml1*Δ mutant containing MarBI ON[1] flanked by *ade6*[-] heteroalleles [Fig. 5.ix.a & Table 8-2]. There is a significant reduction in both gene conversions (~7 fold) and deletions (~1.6 fold) in a *fml1*Δ mutant compared to wild type [Fig. 5.ix.a & Table 8-2]. In contrast, there does not appear to be any significant difference in the profile of replication intermediates in the vicinity of MarBI, from wild-type and *fml1*Δ cells, as judged by 2D gel analysis [Fig. 5.ix.b & c]. However, the relatively poor quality of the 2D gel, and lack of a biological replicate, means that further analysis is needed to confirm this. Together, these data show that Fml1 promotes MarBI-induced direct repeat recombination. In particular it promotes Rad51-dependent gene conversions, like it does at *RTS1*.

5.2.6 Dose Mus81 cleave replication forks stalled at MarBI?

Mus81 has been implicated in processing stalled and collapsed replication forks by converting them into DSBs, acting as a back up option in the absence of the RecQ helicases (Doe et al., 2002; Forment et al., 2011; Froget et al., 2008; Hanada et al., 2007; Pepe et al., 2014; Regairaz et al., 2011). As seen in Section 4.2.5, replication forks that are perturbed by MarBI eventually undergo cleavage to give rise to DSBs. Hence, I wanted to see whether Mus81 was the endonuclease responsible for the breaks observed at MarBI. First, I determined whether deletion of *mus81* affected the frequency of MarBI-induced direct repeat recombination [Fig. 5.ix.a & Table 8-2]. The overall frequency of Ade[+] recombinants is very similar in wild-type and *mus81*Δ strains, albeit there might be a slight reduction in gene conversions in the mutant. Next, I performed 2D gel analysis of replication intermediates at and around MarBI ON[1], which revealed little difference between wild-type and *mus81*Δ in terms of the amount of fork pausing and termination at the barrier [Fig. 5.ix.b & c]. Finally, I compared the amount of DNA breakage at MarBI ON[1] in wild-type and *mus81*Δ mutant backgrounds using the same assay as

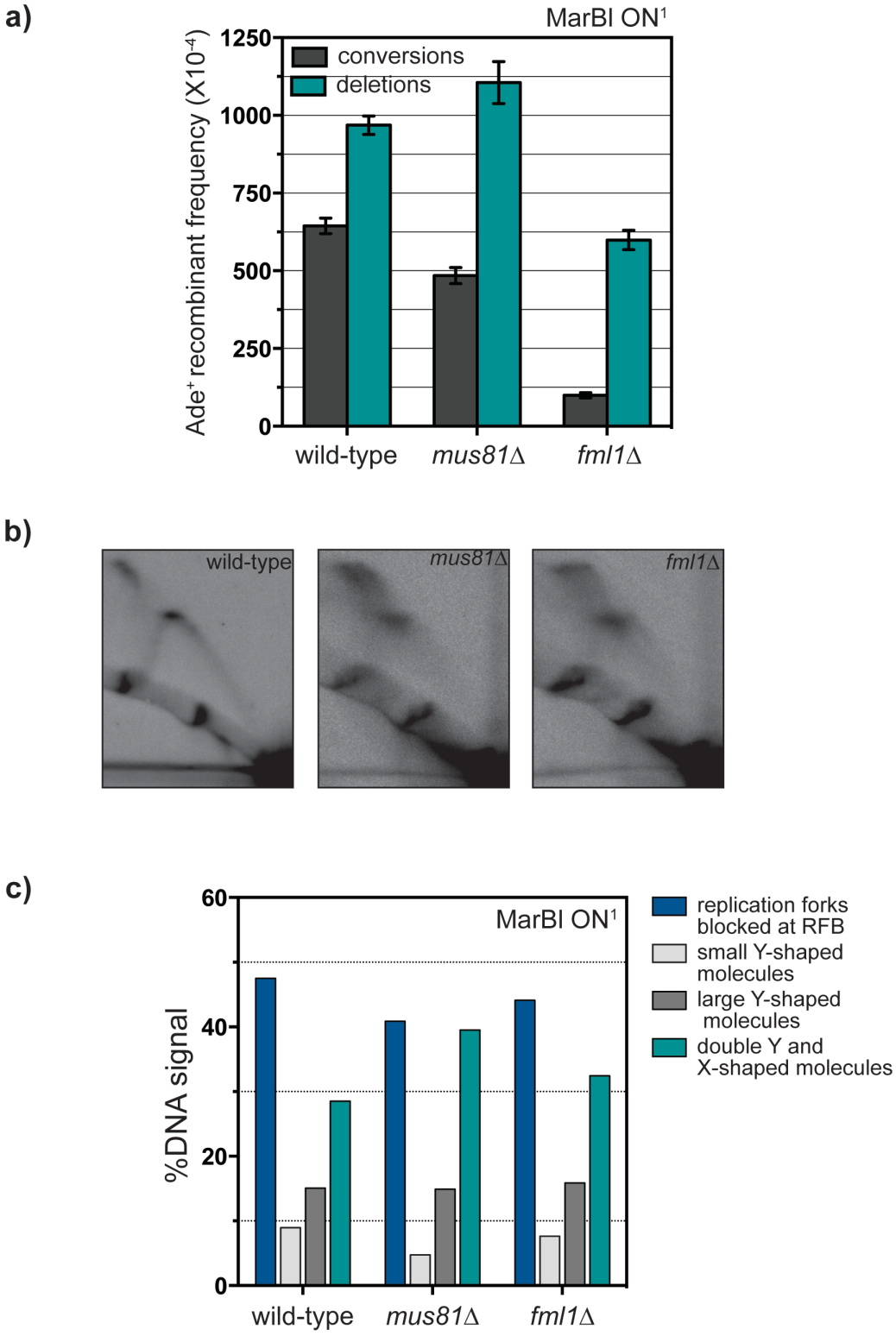


Fig. 5.ix Effect of *mus81*Δ and *fml1*Δ mutations on replication fork progression and recombination at MarBI.

a) Bar chart showing the frequency of Ade$^+$ recombinants in strains MCW7076, MCW8308 and MCW8304. Error bars represent ± standard error of the mean. b) 2D gel analysis of replication intermediates within the *Eco*NI fragment shown in Fig. 4.vii from wild-type, *mus81*Δ and *fml1*Δ cells. c) Quantification of the 2D gels displayed as bar charts. The DNA was extracted from asynchronously growing cultures of the strains MCW7076, MCW8308 and MCW8304. MarBI ON^1 represents the system where Mar^{D155A} is expressed and TO1 is present.

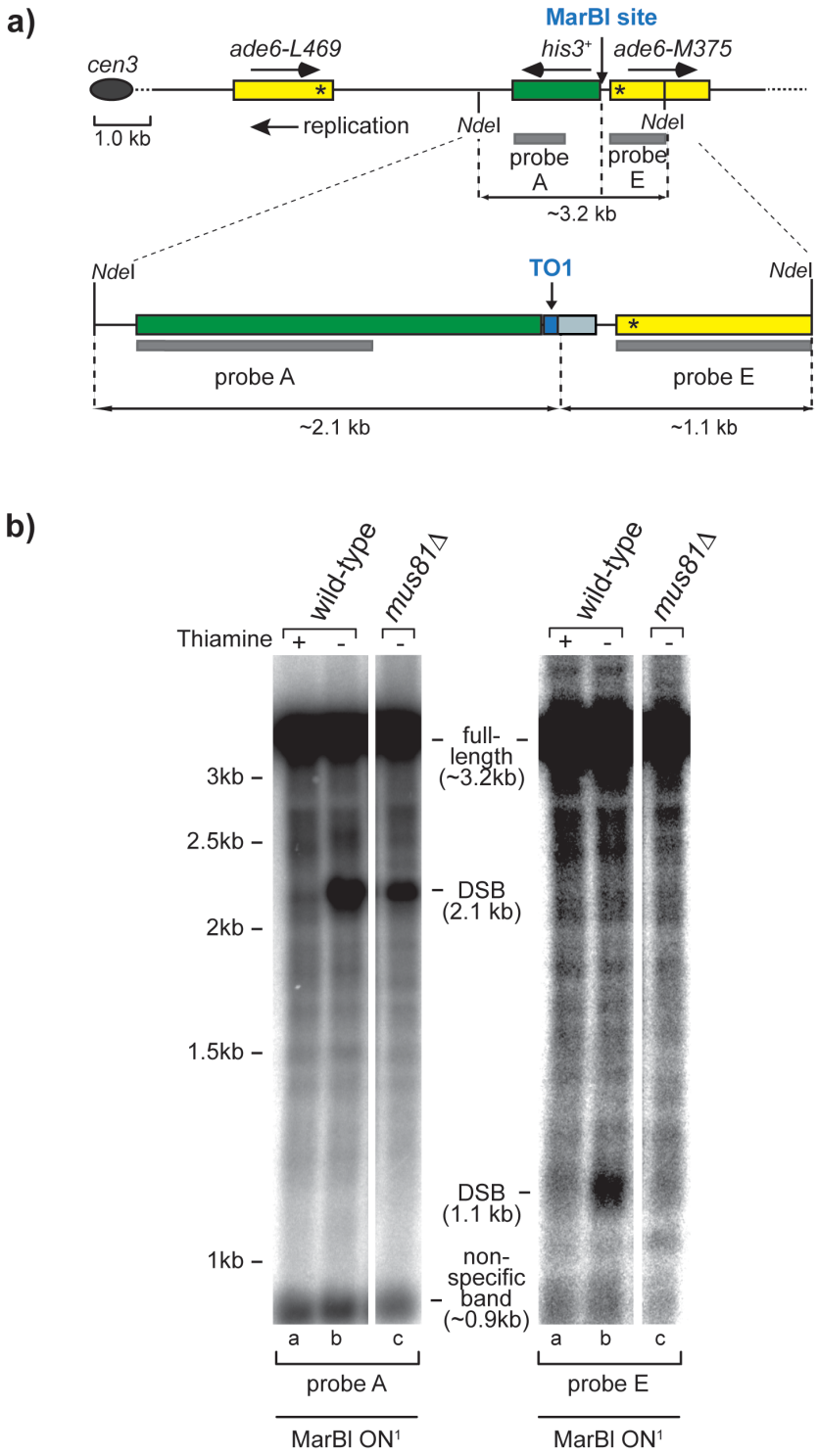


Fig. 5.x 1D gel analysis for the detection of replication fork breakage at MarBI in both wild-type and *mus81*Δ strains.

a) Schematic showing the relative position of the direct repeat recombination reporter with the MarBI site, the position of the *Nde*I restriction sites, the predicted fragment sizes and the probes used for the analysis of the 1D gels. b) Neutral 1D gel analysis of genomic DNA from asynchronous cultures of wild-type and *mus81*Δ cells grown either in the presence or absence of 4μM thiamine. DNA was digested with *Nde*I and detected using Probe A. c) Same as (b) except Probe E is used instead of Probe A. The blot was first probed with Probe A before being stripped and re-probed by Probe E. Each of the strains were analyzed twice independently. The image shown is the representative data. The strains are MCW7076 (lane a & b) and MCW8308 (lane c). MarBI ON[1] represents a system where Mar^{D155A} is expressed and TO1 is present.

described in Section 4.2.5. As shown in Chapter 4, the 3.2 kb NdeI restriction fragment that encompasses the MarBI site is split into 2.1 kb and 1.1 kb fragments, following DNA breakage at MarBI ON[1], and these are detected by probe A and probe E, respectively [Fig. 5.x.a]. Both these fragments are detected in genomic DNA prepared from wild-type cells [Fig. 5.x.b lane b]. In contrast, only the 2.1 kb fragment is detected in the sample from the *mus81*Δ mutant, and its amount appears to be slightly less than in the wild-type sample [Fig. 5.x.b lane c and data not shown]. At first inspection, these data seem to show that DNA breakage at MarBI ON[1] is reduced in the absence of Mus81. However, detection of the 1.1 kb fragment is variable even in samples from wild-type cells and, therefore, its absence does not necessarily imply a reduction in DNA breakage. Further biological replicates are needed to determine whether there is indeed a significant reduction in DNA breakage at MarBI ON[1] in a *mus81*Δ mutant. Whatever the outcome of these experiments, it is clear that at least some DNA breakage still occurs at MarBI even in the absence of Mus81.

5.2.7 Do other accidental RFBs induce recombination in the same manner as MarBI?

Recent work done by the Hickson and Scully labs has established a heterologous barrier system using the *E. coli* replication termination complex, TusB-*TerB*, both in *S. cerevisiae* and mammalian cells. In both cases, a short array of *TerB* repeats (3–6) bound by TusB was shown to function as an RFB that triggers a recombinational response. TusB-*TerB* is a polar RFB in *E. coli* and in *S. cerevisiae* respectively (Larsen et al., 2014; Willis et al., 2014). However, in mammalian cells it appears to behave as a bi-directional barrier (Amin and Hurwitz, 1992; Larsen et al., 2014; Willis et al., 2014)

In order to verify if TusB-*TerB* blocks replication fork progression in fission yeast, and to directly compare it to MarBI and *RTS1*, I introduced the TusB-*TerB* system into *S.pombe*. Six repeats of the 23 bp *TerB* sequence, interspersed with shorter spacer sequences, were inserted between the direct repeat of *ade6*$^{-}$ heteroalleles at site I on ChrIII at the equivalent position that MarBI and *RTS1* had been inserted previously [Fig. 5.xi.a]. Two strains were constructed differing in the orientation of *TerBx6*. Based on its known polarity in *E. coli* and *S. cerevisae*, Orientation 1 should be permissive to replication forks travelling in the telomere to centromere direction, whereas Orientation 2 should be restrictive [Fig. 5.xi.a] (Larsen et al., 2014). A construct for the expression of TusB with an N-terminal NLS was integrated at the *lys1* locus on ChrI. Expression of the *TusB* gene was driven from a *nmt1* promoter, which is thiamine-repressible. For ease of representation, I have defined three states of the system: TerB OFF, TerB ON^{1} and TerB ON^{2}. TerB OFF represents the system where the TusB protein is expressed but *TerB* is absent, TerB ON^{1} where TusB is expressed and *TerB* is in Orientation 1 and TerB ON^{2} where TusB is expressed and *TerB* is in Orientation 2.

Having established the Tus-*Ter* system in *S. pombe*, I first determined whether it acts as an effective RFB. To do this I performed 2D gel analysis of replication intermediates in the EcoNI restriction fragment that encompasses the *TerB*x6 site [Fig. 5.xi.a]. With TerB OFF a typical arc of replication forks is seen, with no obvious site of fork pausing. In contrast, with both TerB ON^{1} and ON^{2} there is an accumulation of forks at the barrier site, which is noticeably more pronounced with TerB ON^{2} [Fig. 5.xi.b]. However, quantification of these signals seems to show little difference in the amount of fork pausing between TerB ON^{1} and TerB ON^{2} [Fig. 5.xi.d]. The signals have been standardised relative to the ascending Y-arc signal, which is assumed not to be affected by the presence of the barrier.

However, the ascending Y-arc for TerB ON^2 appears to be much stronger than it is for TerB ON^1 and, therefore, it is possible that TerB ON^2 causes forks to slow down even before they reach it. If this is true, then the comparison of ratios in [Fig. 5.xi.b] would give a false impression of the relative amount of fork pausing at TerB ON^1 and TerB ON^2. A more telling comparison is perhaps the downward Y-arc signal (large Y-shaped molecules), which is much less with TerB ON^2 than TerB ON^1. Altogether, these data indicate that Tus-*Terx6* acts as a bi-directional RFB in *S. pombe*, albeit it more strongly blocks replication forks in the orientation that it is known to do so in *E. coli* and *S. cerevisiae*. Therefore, it does appear to retain some of its polarity in *S. pombe*. Compared to *RTS1*, both TerB ON^1 and TerB ON^2 appear to be weaker barriers, whereas, compared to MarBI ON^1 they appear to be similar or slightly stronger [Fig. 5.xi.c]. However, neither TerB ON^1 nor TerB ON^2 cause double Y-shaped or X-shaped molecules to accumulate to the same extent as they do with MarBI ON.

Having confirmed that Tus-*Terx6* acts as a RFB in *S. pombe*, I next determined what effect it has on direct repeat recombination [Fig. 5.xii.a]. Both TerB ON^1 and TerB ON^2 cause a significant increase in the frequency of Ade$^+$ recombinants, with TerB ON^1 inducing a ~573 fold increase in gene conversions and ~200 fold increase in deletions and TerB ON^2 inducing a ~1330 fold increase in gene conversions and ~572 fold increase in deletions. Reassuringly, TusB expression in the absence of *TerBx6* did not induce any recombinant formation over and above the spontaneous level [Fig. 5.xii.b & Table 8-4], indicating that the TusB-*TerB* interaction is essential for inducing recombination. Moreover, the higher level of recombination observed with TerB ON^2, compared to TerB ON^1, correlates with the relative amount of fork stalling at the two barriers. Intriguingly, even though *RTS1* is a stronger barrier than TerB ON$^{1/2}$, it induces much less direct repeat

Fig. 5.xi Analysis of replication intermediates at TerB as compared to *RTS1* and MarBI.

a) Schematic showing the relative position of the direct repeat recombination reporter with the block site and Probe A used for 2D gel analysis. b) 2D gel analysis of replication intermediates within the *Eco*NI fragment shown in (a) at 6X *TerB*. The top-left panel is a guide for interpreting the 2D gels. c) 2D gel analysis of replication intermediates at *RTS1-AO* and MarBI ON[1]. d) Quantification of the 2D gels displayed as bar charts. The DNA was extracted from asynchronously growing cultures of the strains MCW7528, MCW7530, MCW7532, MCW4713 and MCW7076.TerB ON[1] represents a system where TusB is expressed and 6X*TerB* is present in orientation 1 (permissive orientation; Larsen et al., 2014) and TerB ON[2] where TusB is expressed and 6X*TerB* is present in orientation 2 (blocking orientation; Larsen et al., 2014)**.** MarBI ON[1] represents the system where Mar^{D155A} is expressed and TO1 is present.

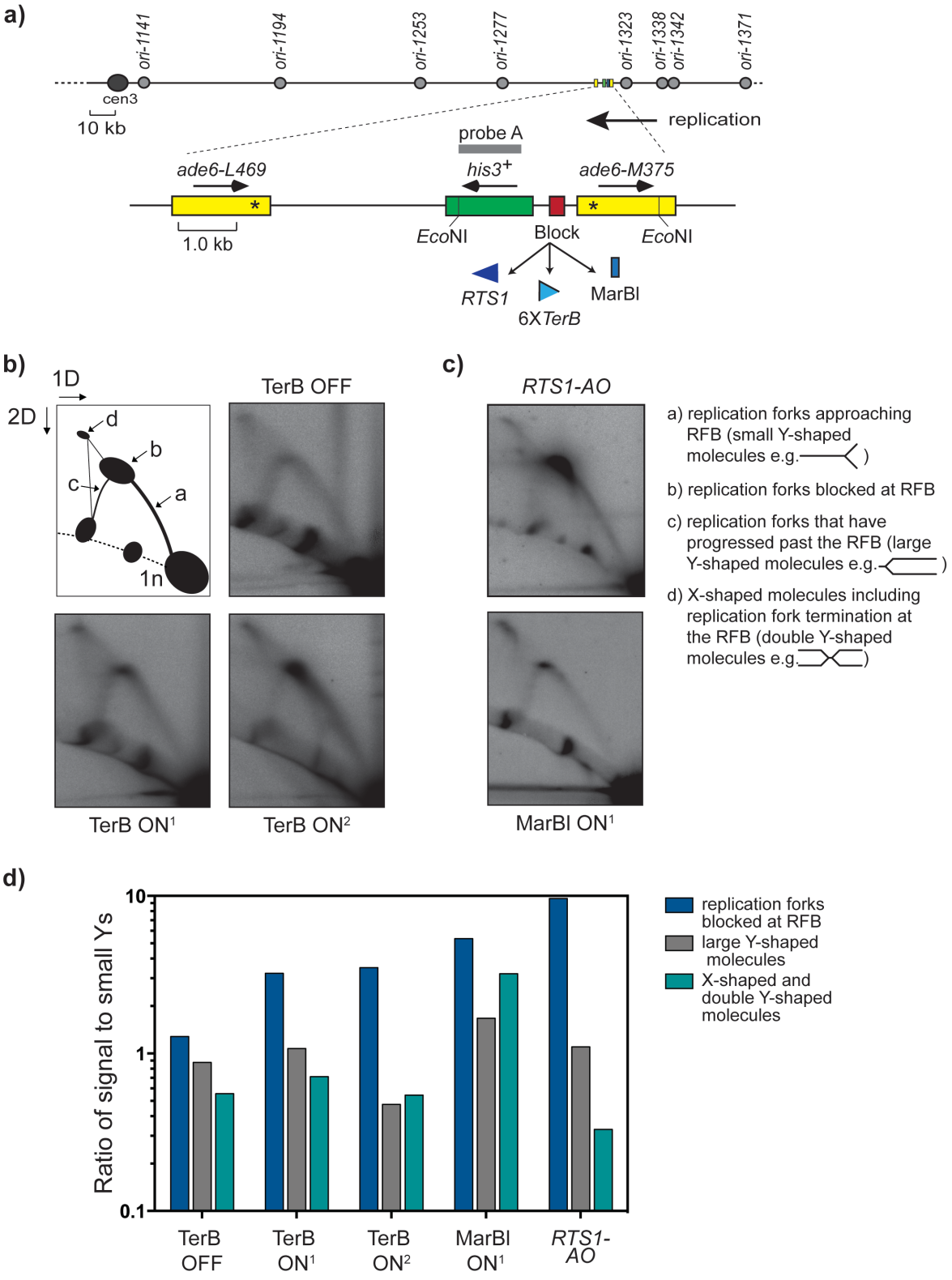


Fig. 5.xi Analysis of replication intermediates at TerB as compared to *RTS1* and MarBI.

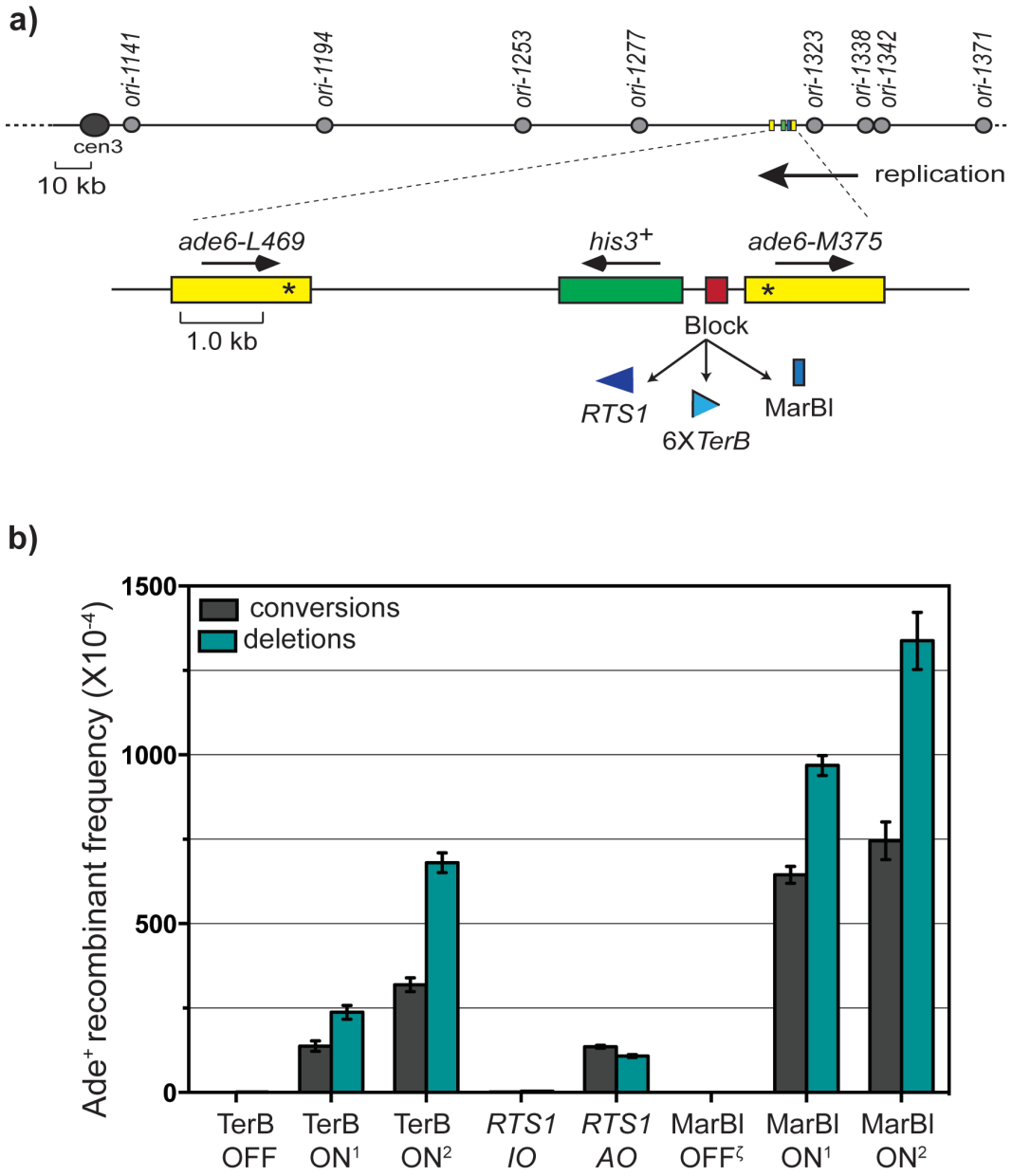


Fig. 5.xii Analysis of direct repeat recombination induced at TerB as compared to *RTS1* and MarBI.

a) Schematic showing the relative position of the direct repeat recombination reporter with the block site. b) Bar chart showing the frequency of Ade$^+$ recombinants in strains MCW7528, MCW7530, MCW7532, MCW4712, MCW4713, MCW8239, MCW7076 and MCW7078. Error bars represent ± standard error of the mean. TerB ON^1 represents a system where TusB is expressed and 6X*TerB* is present in orientation 1 (permissive orientation; Larsen et al., 2014) and TerB ON^2 where TusB is expressed and 6X*TerB* is present in orientation 2 (blocking orientation; Larsen et al., 2014). MarBI OFF$^\zeta$ represents the system where the Mar^{D155A} protein is expressed but the transposon end is absent, MarBI ON^1 where Mar^{D155A} is expressed and TO1 is present and MarBI ON^2 where Mar^{D155A} is expressed and TO2 is present.

recombination, whereas, MarBI, which is perhaps a weaker barrier than TerB ON[1] [or 2], induces much more [Fig. 5.xii.b].

5.3 Discussion

5.3.1 There is very little measurable RDR at MarBI

Despite inducing very high rates of direct repeat recombination when placed between the repeats, MarBI causes very little recombination downstream of it. This is in stark contrast to what happens with *RTS1*, which induces less direct repeat recombination when the repeats flank it, but far more when the repeats are positioned downstream. Several studies have shown that replication that is restarted by recombination gives rise to high rates of template switching downstream from its point of initiation (Iraqui et al., 2012; Lambert et al., 2010; Mizuno et al., 2013; Nguyen et al., 2015; Smith et al., 2007). Therefore, it is reasonable to assume that this is a hallmark of RDR. The fact that there is very little template switching downstream of MarBI, therefore suggests that replication fork stalling at MarBI does not tend to lead to RDR, or at least to productive RDR. This highlights a further difference between MarBI and *RTS1*, and is consistent with the model proposed in Chapter 4, which postulates that replication forks that stall at MarBI do so without collapsing, and only give rise to recombination following a failure of fork merging during replication termination.

5.3.2 The fork protection complex prevents RDR at MarBI

The fork protection complex has previously been shown to prevent replication fork collapse at difficult to replicate regions of the genome like the rDNA array (Noguchi et al., 2003). In Section 5.2.2, it is apparent that in the absence of Swi1, replication termination is reduced at MarBI and there is an increase in recombination at a site immediately downstream of the barrier [Fig. 5.ii & Fig. 5.iii]. Moreover, the timing of

recruitment of Rad52 to MarBI, in the absence of Swi1, is similar to what is seen with *RTS1* [Fig. 5.iv & Fig. 5.v] (Nguyen et al., 2015). Altogether, these data suggest that there may be an increased frequency of RDR at MarBI when the FPC is absent. This could occur if the FPC is needed to prevent fork collapse at MarBI. In such a scenario, there would be more RDR in a *swi1*Δ mutant and, therefore, more template switching downstream of the barrier. Moreover, more restart would result in less fork convergence at MarBI, which might result in less DNA breakage. I suspect that the very high rates of recombination observed when the *ade6*$^{-}$ heteroalleles flank MarBI, largely stem from DSB repair, which is likely to cause more direct repeat recombination than RDR. To investigate this further the level of DNA breakage at MarBI will need to be measured in a *swi1*Δ mutant. Additionally, it will be necessary to obtain a direct measurement of replication protein retention at MarBI in wild-type and *swi1*Δ strains using ChIP. It would also be prudent to confirm that a *swi3*Δ mutant exhibits the same phenotypes as a *swi1*Δ mutant with respect to fork pausing and recombination at MarBI.

5.3.3 Pfh1's "sweepase" activity appears to be ineffective at MarBI

Pfh1 can both promote replication fork progression past DNA-protein barriers and also promote fork merging at replication termination sites (Sabouri et al., 2012; Steinacher et al., 2012). It would seem from the data in Section 5.2.3 that there is little or no increased fork pausing or termination at MarBI in a *pfh1-m21* mutant. However, there is a significant increase in the frequency of MarBI-induced deletions in a *pfh1-m21* mutant compared to wild-type [Fig. 5.vii]. It is conceivable that the direct repeat recombination assay is a more sensitive measure of problems of fork progression and/or termination at MarBI than the 2D gel assay. Alternatively, the absence of a detectable change in fork progression or termination may indicate that Pfh1 has an additional role in limiting direct repeat

recombination. Even if this is the case, it is still surprising that Pfh1 does not appear to utilize its sweepase activity to dislodge the Mar protein and thereby aid fork progression and/or termination. However, it is important to note that I have only tested the *pfh1-m21* mutant, which still produces some Pfh1 protein that localises to the nucleus. Indeed, as shown in Chapter 3, this reduced amount of protein is sufficient to prevent hyper-recombination at *RTS1-IO* and to promote at least some progression of the restarted replication fork downstream of *RTS1-AO*. It is possible that the reduced levels of Pfh1 in the nucleus that are delivered by *pfh1-m21* are sufficient to cope with MarBI. It will be important to test this in future work.

5.3.4 Elg1 promotes MarBI induced recombination.

Like at *RTS1*, Elg1 promotes direct repeat recombination at MarBI, albeit not to the same extent. At *RTS1* Elg1 promotes recruitment of Rad52, presumably by helping to orchestrate replisome disassembly via unloading PCNA from DNA. However, fork collapse does not appear to be the predominant response at MarBI and, therefore, it is puzzling how loss of Elg1 causes a reduction in direct repeat recombination given that Elg1 is not required for recombination per se. It is possible that some of the direct repeat recombination that is induced by MarBI does stem from fork collapse and attempted RDR and, therefore, loss of Elg1 could restrict this. Alternatively, in the absence of Elg1 fork convergence at MarBI may somehow be less likely to cause direct repeat recombination. Perhaps slower removal of PCNA from DNA provides more time for replication to be completed without the intervention of a nuclease to cleave the converged fork structure.

5.3.5 Mus81 does not appear to cleave replication forks stalled at MarBI

As reported in Chapter 4 (Section 4.2.5) replication forks blocked at MarBI appear to undergo nucleolytic cleavage to create a DSB. Mus81 has been implicated in the processing of stalled and collapsed replication forks by converting them into DSBs (Doe et al., 2002; Forment et al., 2011; Froget et al., 2008; Hanada et al., 2007; Pepe et al., 2014; Regairaz et al., 2011). Hence, it was a prime candidate for promoting the formation of DSBs at MarBI. However, surprisingly, there was still a significant amount of breakage detectable at MarBI in the absence of Mus81 [Fig. 5.x], indicating that that there are other nucleases that must be able to cleave the replication fork at MarBI. A prime candidate is Slx1-Slx4, which can cleave a variety of branched DNA structures and has been proposed to resolve converged replication fork structures in the rDNA array (Coulon et al., 2004, 2006; Fricke and Brill, 2003; Wyatt and West, 2014).

5.3.6 TusB-*TerB* induces recombination similar to MarBI in fission yeast.

Like MarBI, TusB binding to *TerB*x6 strongly induces direct repeat recombination in fission yeast. The presence of both deletions and gene conversions in the recombinant population indicates that at least a proportion of TusB-*TerB*-induced recombination is dependent on Rad51. However, it has yet to be determined whether it gives rise to RDR like *RTS1* or DNA breakage like MarBI. However, the fact that it induces more recombinants than *RTS1*, even though it is a weaker barrier, suggests that the problem it causes is one that is more likely to promote direct repeat recombination. I suspect, therefore, that it is like MarBI and gives rise to DNA breaks by causing problems with fork convergence. Interestingly, in murine cells TusB-*TerB*x6 promotes recombination, which is partially dependent on Slx4

(Willis et al., 2014). Moreover, like in *S. pombe*, TusB-*TerB*x6 acts as a bi-directional barrier in mammalian cells (Willis et al., 2014). Therefore, it is possible that TusB-*TerB*x6 elicits DNA breakage in both fission yeast and mammals. In contrast, TusB-*TerB* acts as a polar RFB in *S. cerevisiae*, which does not induce DNA breaks, but instead provokes template switching behind the barrier (Larsen et al., 2014). What accounts for these differences is unclear, but it is possible that the mechanisms that deal with accidental protein-DNA RFBs in mammalian cells are more similar to those in *S. pombe* than those in *S. cerevisiae*.

Chapter 6

Loss of a strong replication origin in *S. pombe* can cause genomic instability

6.1 Introduction

DNA replication initiates at defined sites on the chromosome called origins that serve as binding sites for initiator proteins that recruit the replication machinery. In eukaryotes, the regularly spaced origins ensure complete genome duplication in the shortest time possible. In any given cell cycle, there is between 3- to 20- fold extra loading of the MCM2-7 complex onto DNA over the number of origins that are actually used, with the majority remaining 'dormant'. The DNA sequence, chromatin environment and nuclear architecture all contribute to the dynamic selection and activation of replication origins (Alver et al., 2014; Cayrou et al., 2015; Prioleau and MacAlpine, 2016). Because dormant origins can be activated in the absence of other active origins, they can act as backup sites for replication initiation when surrounding origins are inactivated or when replication forks stall (Kawabata et al., 2011; Vujcic et al., 1999).Thus, in theory, the loss of a single origin should not have any effect on the genome stability of the cell.

Surprisingly, while investigating the recombination associated with replication restart, I observed that deleting a single early-firing replication origin can lead to a localised region of genomic instability. In this chapter, I explore the generality of this observation by investigating whether deleting early-firing replication origins on other chromosomes similarly affects genome stability.

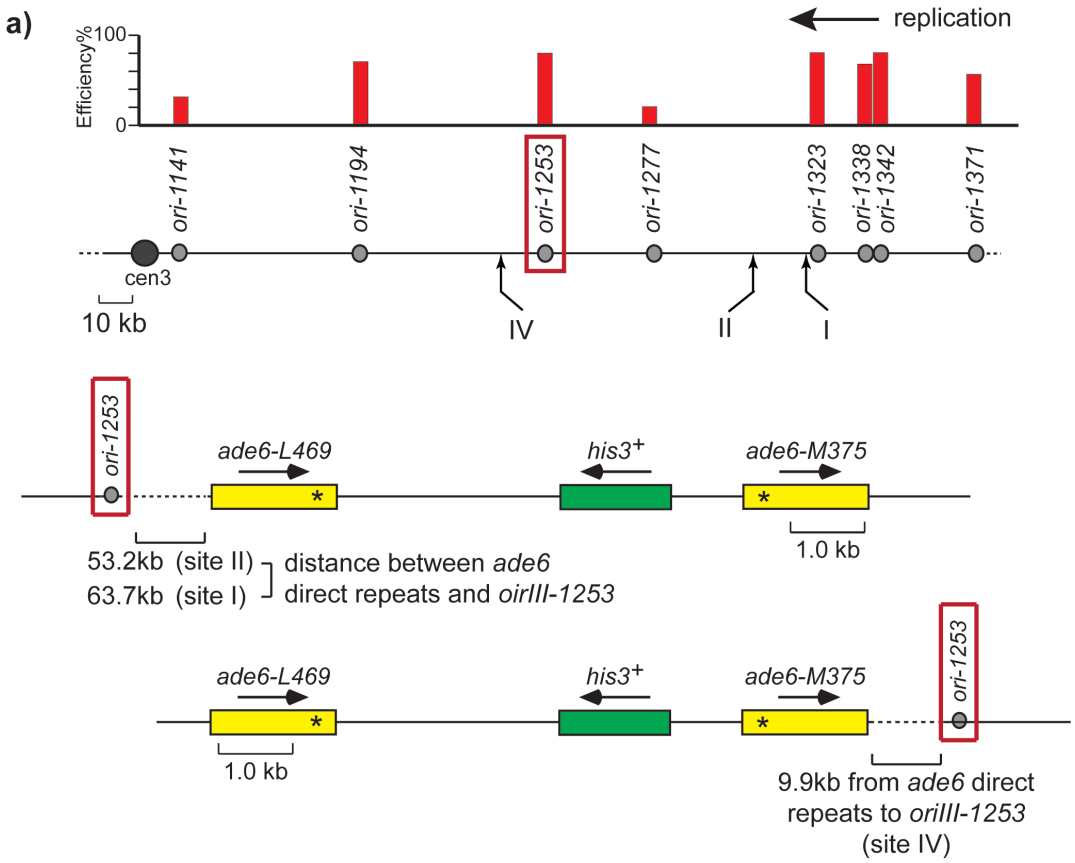
6.2 Results

6.2.1 Loss of *oriIII-1253* causes a localised zone of hyper-recombination on ChrIII

The first step was to confirm that the localised increase in recombinants observed when *oriIII-1253* was deleted on ChrIII was not a consequence of inserting *RTS1* at the endogenous *ade6* locus [See Chapter 3, Fig. 3.iii]. In order to do this, a

series of strains was constructed in which *oriIII-1253* was deleted and the *ade6*$^{-}$ direct repeat reporter was positioned at and downstream of the endogenous *ade6* locus in the absence of *RTS1* [Fig. 6.i.a]. The total recombinant frequency was then measured at each of these sites in the presence and absence of *oriIII-1253* [Fig. 6.i.b]. At site I (*ade6*$^{-}$ direct repeats at endogenous locus, 63.7 kb away from *oriIII-1253*), there was no significant difference in the frequency of recombination with and without *oriIII-1253* [Fig. 6.i.b & Table 8-5]. However, at site II (*ade6*$^{-}$ reporter 53.2 kb away from *oriIII-1253*), there was a modest but significant increase ($p<0.05$) in both gene conversions (~1.6 fold) and deletions (~2 fold) when *oriIII-1253* is deleted [Fig. 6.i.b & Table 8-5]. A small increase in deletions (~1.3 fold) was also observed at site IV (*ade6*$^{-}$ reporter 9.9 kb away from *oriIII-1253*) [Fig. 6.i.b & Table 8-5].

I next wanted to verify that deleting *oriIII-1253* only had a localised *cis*-effect and did not lead to an increase in ectopic recombination on other chromosomes as well. In order to do this, I re-positioned the *ade6*$^{-}$ direct repeat recombination reporter at an intergenic region on ChrII ensuring that no known gene was disrupted [Fig. 6.ii.a: site VI]. The correct integration of the reporter was confirmed by Southern blot analysis [See Appendix Fig. 8.ii] and its spontaneous level of recombination determined to see if it differed from that on ChrIII [Fig. 6.ii.b &Table 8-5]. The total recombinant frequency at site VI was comparable to that at site I (the endogenous *ade6* locus). There was also no increase in the frequency of recombinants when *oriIII-1253* was deleted. Altogether, these data suggest that deleting *oriIII-1253* may cause a very localised and modest increase in the frequency of recombination.



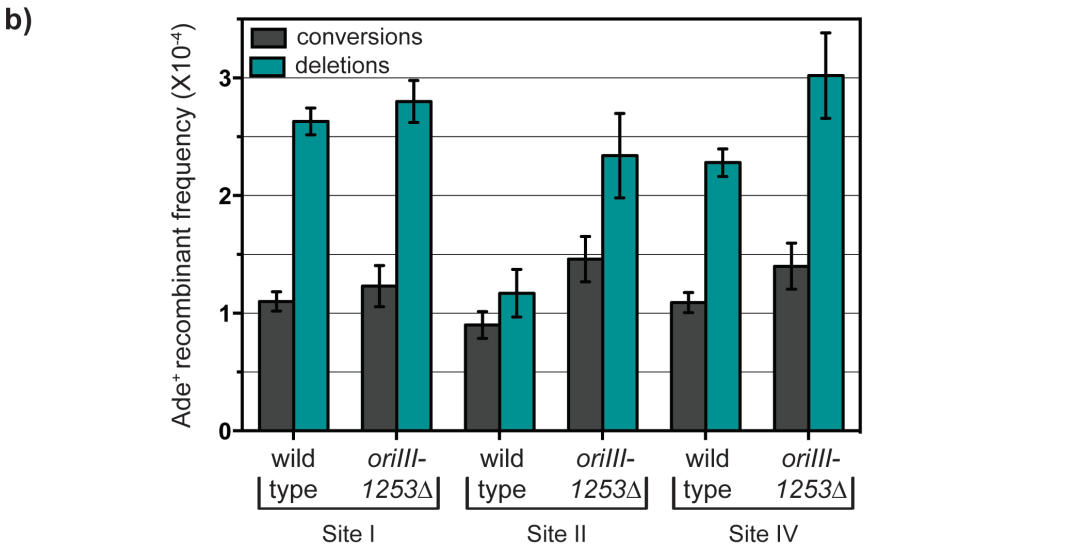


Fig. 6.i Deleting *oriIII-1253* creates a localised zone of spontaneous hyper-recombination.

a) Schematic showing the relative positions on ChrIII where the *ade6*$^{-}$ reporter (shown in the bottom panel) is inserted at and downstream of the *ade6* gene at its endogenous locus. The sites I, II and IV are marked on the chromosome arm and their relative distance from *oriIII-1253* is indicated. The genomic locations of the origins are according to OriDB, a DNA replication origin database (Nieduszynski et al., 2007). The top panel indicates the firing efficiencies of the near-by origins (Daigaku et al., 2015). b) Bar chart showing the spontaneous frequency of Ade^{+} recombinants in MCW429*, MCW7377*, MCW7229, MCW8241, MCW7430 and MCW7987. Error bars represent ± standard error of the mean.

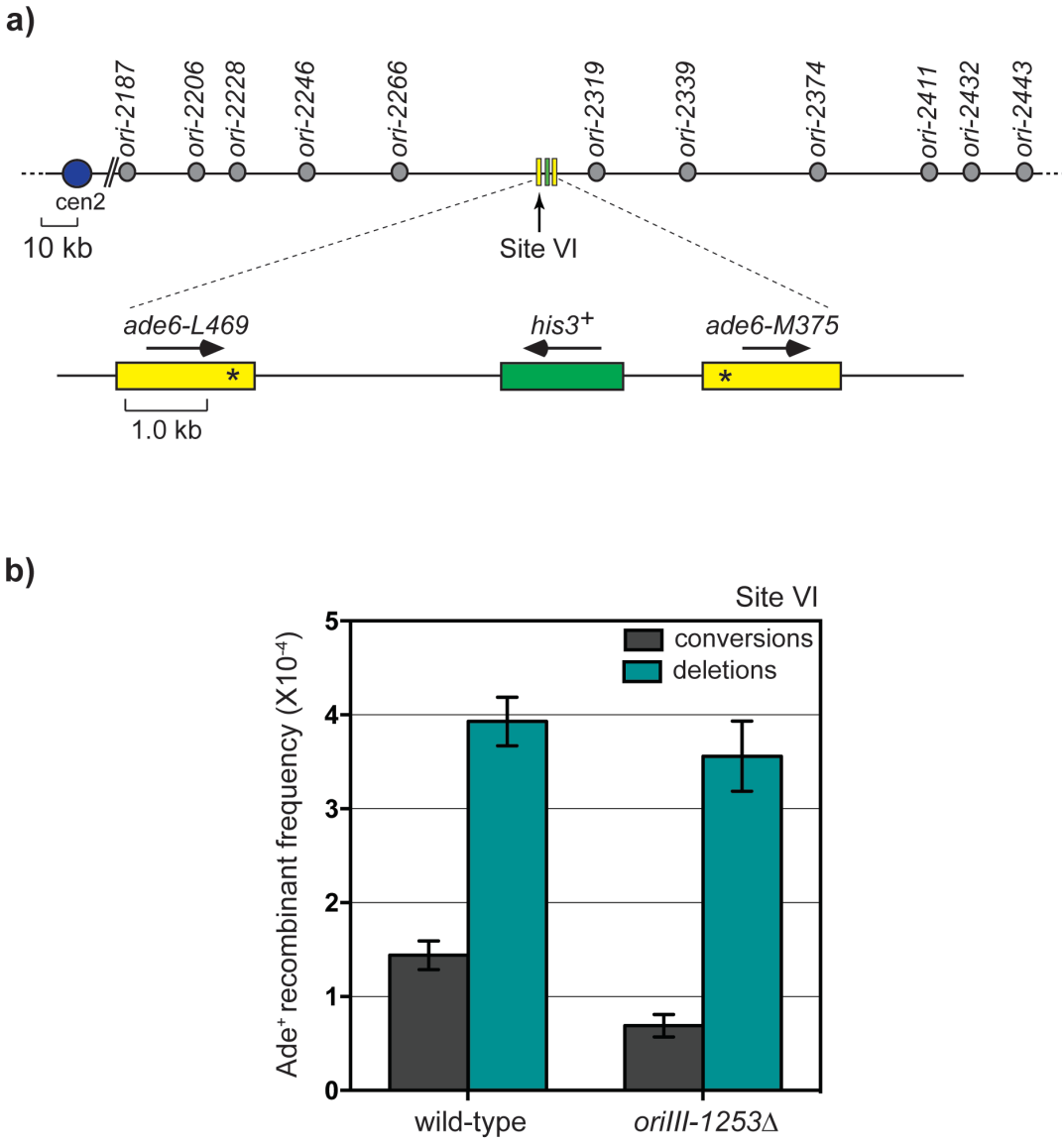


Fig. 6.ii Deleting *oriIII-1253* does not create global spontaneous hyper-recombination.

a) Schematic showing the relative position on ChrII where the *ade6*$^{-}$ reporter (shown in the bottom panel) is inserted at site VI as indicated. The genomic locations of the origins are according to OriDB, a DNA replication origin database (Nieduszynski et al., 2007). b) Bar chart showing the spontaneous frequency of Ade^{+} recombinants in MCW8045 and MCW8243. Error bars represent ± standard error of the mean.

6.2.2 *OriIII-1253* is not the only strong origin important for maintaining genome stability in *S. pombe.*

Having observed that deleting *oriIII-1253* may create a zone of localised genome instability, I wanted to see whether this is a common phenomenon. As I had already established a strain with the *ade6*$^{-}$ reporter on ChrII, I first deleted the strongest origin in this chromosomal region (*oriII-2319*), which happened to be 20 kb away from the direct repeat reporter, and re-measured recombination at site VI [Fig. 6.iii.a]. Interestingly, deletion of *oriII-2319* resulted in a ~4 fold increase in gene conversions and ~7 fold increase in deletions [Fig. 6.iii.a & Table 8-5].

I next placed the *ade6*$^{-}$ reporter at an intergenic region on ChrI [Fig. 6.iv.a: site VII], once again confirming correct integration by Southern blot analysis [See Appendix Fig. 8.iii]. Intriguingly, spontaneous recombination at site VII on ChrI is ~4-6 fold higher than sites I – VI on ChrII and III [Fig. 6.iv.b &Table 8-5]. This might be due to the local chromatin architecture, which could influence the frequency of spontaneous recombination (Méchali et al., 2013; Smith and Aladjem, 2014). Having established the spontaneous level of recombination, I next deleted the strongest replication origin (*oriI*-4739) within the vicinity of site VII, and determined whether this had any affect on the frequency of recombination. Unlike at site VI on ChrII, the deletion of the origin made no significant difference to the frequency of recombination [Fig. 6.iv.b &Table 8-5]. Thus, the removal of a strong replication origin does not always lead to an increase in direct repeat recombination nearby.

6.3 Discussion

In this chapter, I have shown that deleting a replication origin can sometimes result in an increase in direct repeat recombination at a nearby site. This is true both for

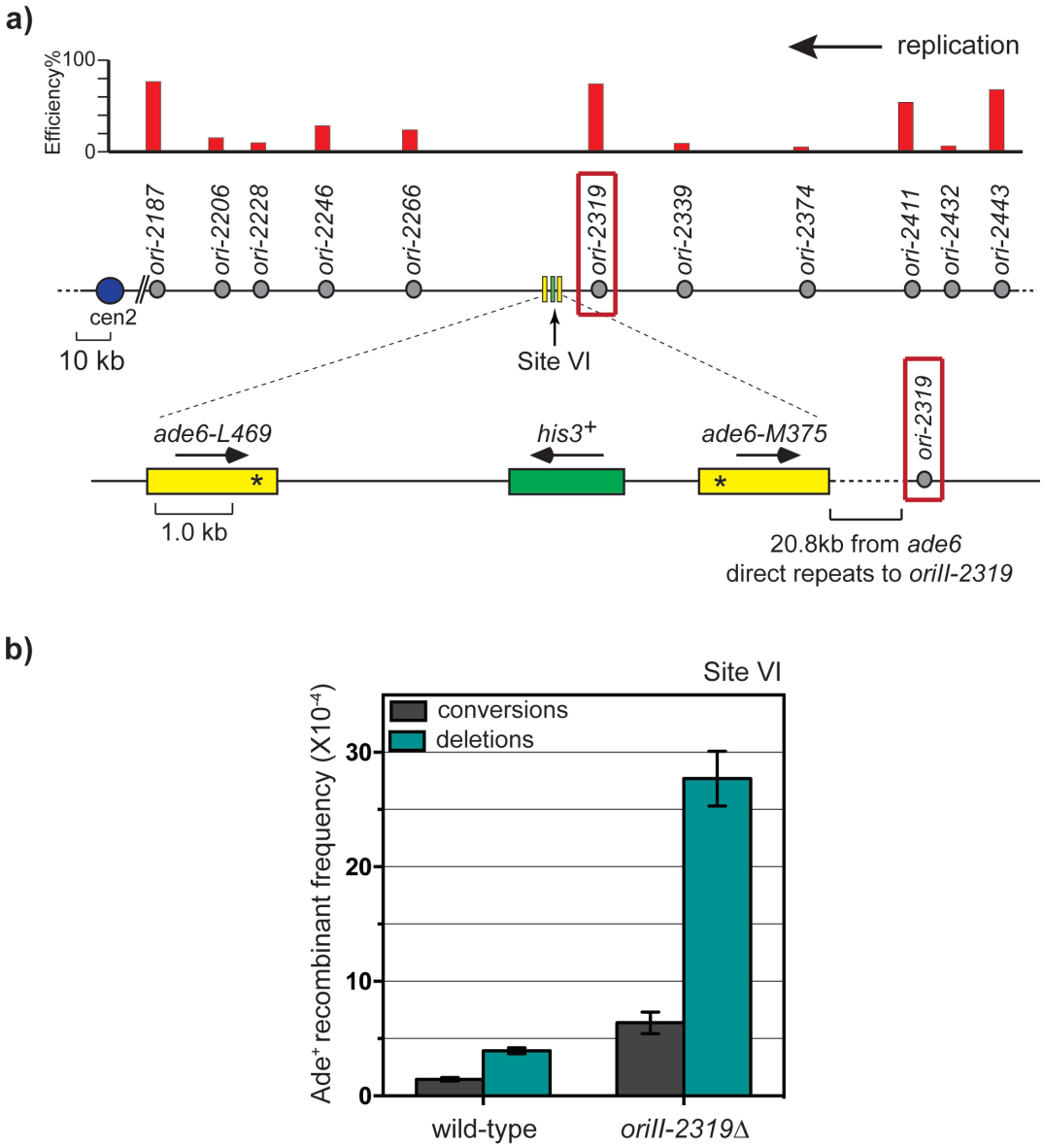


Fig. 6.iii Deleting *oriII-2319* creates a localised zone of spontaneous hyper-recombination.

a) Schematic showing the relative position on ChrII where the *ade6*$^{-}$ reporter (shown in the bottom panel) is inserted at site VI 20.8 kb from *oriII-2319* is indicated. The genomic locations of the origins are according to OriDB, a DNA replication origin database (Nieduszynski et al., 2007). The top panel indicates the firing efficiencies of the near-by origins (Daigaku et al., 2015). b) Bar chart showing the spontaneous frequency of Ade^{+} recombinants in MCW8045 and MCW8057. Error bars represent ± standard error of the mean.

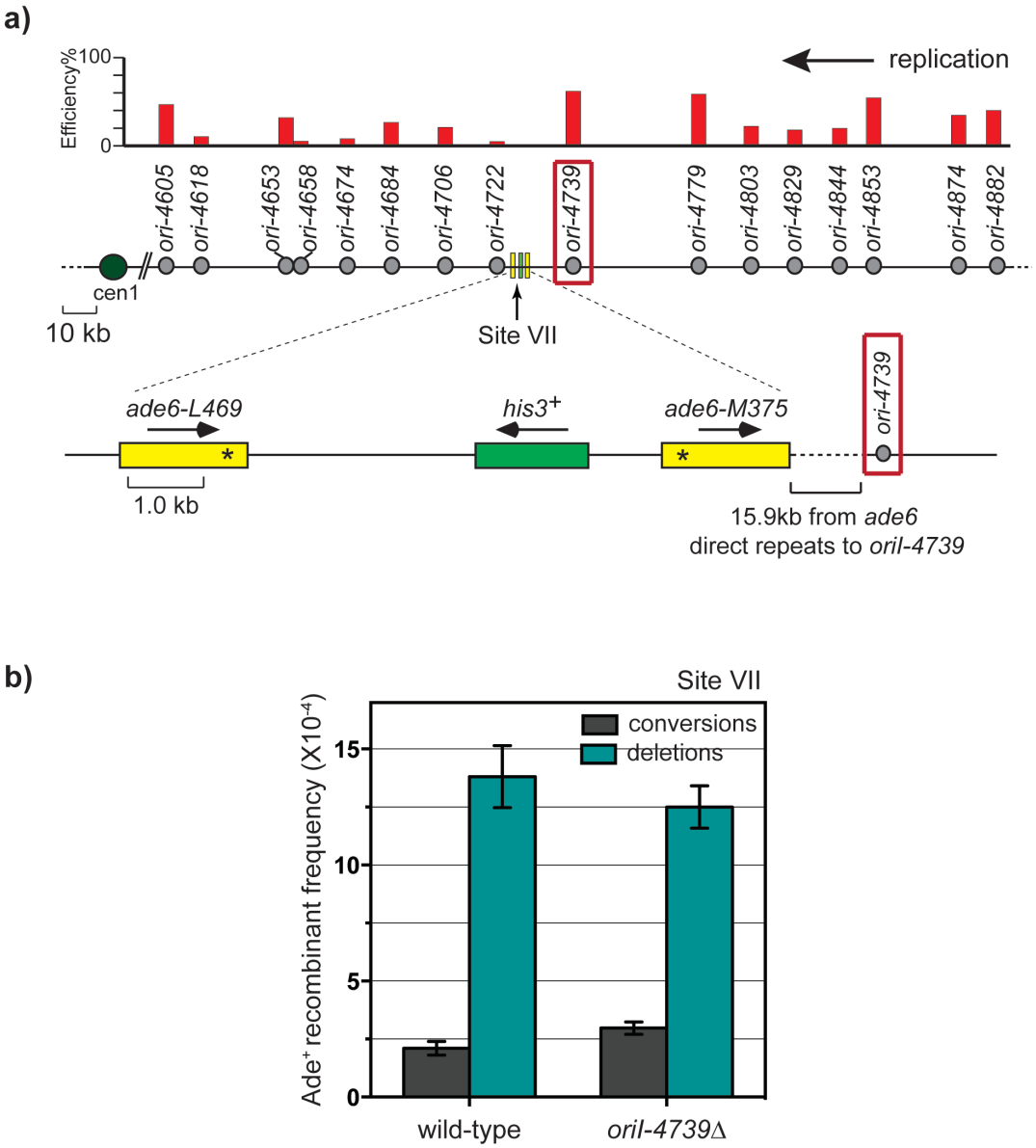


Fig. 6.iv Deleting *oril-4739* does not increase the localised spontaneous hyper-recombination.

a) Schematic showing the relative position on ChrI where the *ade6*$^{-}$ reporter (shown in the bottom panel) is inserted at site VII 15.9 kb from *oril-4739* is indicated. The genomic locations of the origins are according to OriDB, a DNA replication origin database (Nieduszynski et al., 2007). The top panel indicates the firing efficiencies of the near-by origins (Daigaku et al., 2015). b) Bar chart showing the spontaneous frequency of Ade^{+} recombinants in MCW8044 and MCW8238. Error bars represent ± standard error of the mean.

oriIII-1253 on ChrIII and for *oriII-2319* on ChrII, but not for *oriI-4739* on ChrI. Deletion of *oriII-2319* caused the greatest increase in recombination, whereas, the effect of deleting *oriIII-1253* was far more subtle. Exactly what the cause of this heightened recombination is remains unclear, but some ideas are discussed below.

There have been several previous reports describing the effects of deleting replication origins in budding yeast. In particular, one study found that deleting an early replicating origin on ChrVI of *S. cerevisiae* resulted in an increased mutation rate nearby (Lang and Murray, 2011). Moreover, it was found that the mutation rate can vary quite dramatically (6-fold) across a single chromosome and this is correlated with replication timing. Regions adjacent to early replicating regions appear to have a lower mutation rate, whereas, regions that replicate later exhibit a higher mutation rate (Lang and Murray, 2011). The favored explanation for this phenomenon is that error-prone DNA repair pathways are used more extensively in late S-phase than in early S-phase (Donley and Thayer, 2013; Lang and Murray, 2011; Stamatoyannopoulos et al., 2009).

Late replicating regions can also be prone to genetic instability due to an increased chance of them not being replicated prior to mitosis (Liu et al., 2014). It is thought that a failure to complete DNA replication leads to the formation of an anaphase bridge, which can result in catastrophic chromosome missegregation (Crasta et al., 2012; Gelot et al., 2015; Liu et al., 2014). Indeed, it was observed that deleting highly active origins from a ring-derivative of ChrIII led to an increase in the rate of loss of the circular chromosome in *S. cerevisiae* (Dershowitz and Newlon, 1993). In human cells, genomic regions that appear to be especially prone to these problems are known as common fragile sites, and are typified by a low density of replication origins and an increased frequency of DNA breakage

(Minocherhomji S et al 2015; Letessier A et al 2011). To avoid catastrophic chromosome missegregation, the cell deploys various recombination/repair proteins, even as late as anaphase, to complete replication (Gelot et al., 2015; Minocherhomji and Hickson, 2014; Minocherhomji et al., 2015). However, as discussed extensively in this thesis, such strategies result in elevated levels of recombination.

It is conceivable that the increases in direct repeat recombination that are caused by deleting *oriIII-1253* and *oriII-2319* might result from a localized delay in the timing of replication. Similar to the examples listed above, a delay in replication timing could lead to heightened recombination either because of some kind of differential use of recombination proteins during S-phase, or because the region is less likely to be replicated prior to mitosis. Indeed, the relatively high level of spontaneous recombination at site VII on ChrI might result from this region being replicated in late S-phase (Daigaku et al., 2015). However, the correlation, between replication timing and frequency of direct repeat recombination, is far from perfect. For example, it is unclear why site II on ChrIII exhibits an increase in direct repeat recombination following the deletion of *oriIII-1253*, as it should still be efficiently replicated by forks emanating from the cluster of nearby early firing origins on its telomere proximal side [Fig. 6.i.a].

It is known that the local chromatin architecture has a profound influence on the co-ordination of origin firing. In general, euchromatic regions are more enriched with origins that fire early in S-phase, and heterochromatic regions are enriched with origins that fire late. Studies of the temporal organization of origin firing in fission yeast have shown that origins near the centromeres and mating type region fire early in S-phase, whereas origins in sub-telomeric regions fire late in S-phase (Alver et al., 2014; Hayano et al., 2012; Kim and Huberman, 2001;

Smith and Aladjem, 2014). It is conceivable that deleting a replication origin might alter local chromatin architecture and/or the position of the chromosomal region in the nucleus, which, in turn, could influence the replication timings of nearby origins. It is therefore possible that deleting *oriIII-1253* and *oriII-2319* could have a negative effect on the firing of nearby replication origins, which would further delay the replication of Sites II, IV and VI. If true, then the correlation between replication timing and frequency of direct repeat recombination might be better than it appears.

Delaying the time at which a particular chromosomal region is replicated can also potentially reduce the number of transcripts produced from the genes in that region (Cayrou et al., 2011; Fraser, 2013). This is because only the parental DNA is available as a template for transcription as opposed to two copies of the daughter strands. Intriguingly, it has been observed that genes that are most highly transcribed during S-phase replicate early, whereas those repressed in S-phase replicate late (Fraser, 2013). As seen in Table 6-1, *oriII-2319* is flanked by a number of genes that have a potential role in maintaining genome integrity. For example, Rev7 has been implicated in suppressing DSB resection in addition to its role in TLS (Boersma et al., 2015; Sale, 2015; Xu et al., 2015). Potentially a delay in replicating the *rev7* gene could result in a reduced level of Rev7 protein at a critical point during S-phase, which in turn could result in a decrease in TLS and an increase in HR. If true, a *rev7*Δ mutant should exhibit increased direct repeat recombination, and the effect of deleting *oriII-2319* on recombination should be genome-wide.

As alluded to above, in order to gain a better understanding of how deleting *oriIII-1253* and *oriII-2319* induces direct repeat recombination, replication profiling across each of the chromosomal regions should be done using the Pu-Seq

technique described in Section 3.3.10 (Keszthelyi et al., 2015). Using this advanced sequencing technique, one would be able to determine if deleting either *oriIII-1253* or *oriII-2319* significantly delays the replication of adjacent regions. One would also discover what effect, if any, it had on the firing of neighboring replication origins.

Table 6-1: List of genes flanking *orill-2319*

Systematic ID	Gene Name	Chromosomal co-ordinates (bp)	Coding Sequence (CDS) co-ordinates (bp)	Distance of the CDS from *orill-2319* (bp)	Gene Product
SPBC12D12.01	*sad1*	2303681-2306661	2304182-2305726	-13224	spindle pole body protein Sad1
SPBC12D12.02c	*cdm1*	2306339-2305691	2306240-2305758	-13192	DNA polymerase delta subunit Cdm1
SPBC12D12.03	*cct1*	2307309-2309574	2307436-2309436	-9514	chaperonin-containing T-complex alpha subunit Cct1
SPBC12D12.04c	*pck2*	2313301-2309126	2312837-2309787	-9163	protein kinase C (PKC)-like Pck2
SPBC12D12.09	*rev7*	2313096-2314605	2313544-2314476	-4474	DNA polymerase zeta Rev7 (predicted)
SPBC12D12.05c	Unassigned	2316047-2314207	2315986-2314669	-4281	mitochondrial carrier, calcium binding subfamily (predicted)
SPBC12D12.06	*srb11*	2316099-2317654	2316168-2317408	-1542	cyclin CycC, Srb mediator subunit Srb11
SPBC12D12.07c	*trx2*	2318581-2317361	2318467-2317984	-966	mitochondrial thioredoxin Trx2
orill-2319					
SPBC12D12.08c	*ned8*	2320292-2319758	2320256-2319851	1306	ubiquitin-like protein modifier Ned8
SPBC24C6.02	*spb4*	2320336-2322561	2320383-2322332	1433	ATP-dependent RNA helicase Spb4 (predicted)
SPBC24C6.03	Unassigned	2322711-2324873	2323024-2324301	4074	mitochondrial proline-tRNA ligase (predicted)
SPBC24C6.04	Unassigned	2325032-2327098	2325256-2326902	6306	delta-1-pyrroline-5-carboxylate dehydrogenase (predicted)
SPBC24C6.05	*sec28*	2327364-2328501	2327506-2328416	8556	coatomer epsilon subunit (predicted)
SPBC24C6.06	*gpa1*	2329672-2331890	2330338-2331561	11388	G-protein alpha subunit
SPBC24C6.07	*cdc14*	2332020-2335029	2332270-2332992	13320	SIN component Cdc14

Chapter 7

Concluding Remarks

It has been well established that the cell can use its recombination machinery to restart replication at perturbed replication forks (Lambert and Carr, 2013). In an effort to learn more about barrier-induced recombination, our lab and others have exploited a site-specific RFB, *RTS1*, in *S. pombe* to investigate the consequences of perturbing a single replication fork (Ahn et al., 2005; Lambert et al., 2005). It has been demonstrated that replication fork blockage by this polar protein-DNA barrier leads to 'fork collapse' and the cell induces DSB-independent RDR to rescue the replication fork. However, recent work has demonstrated that the restarted replication fork is less stable, similar to BIR, and can cause gross genomic rearrangements at least within the first 2.4kb downstream of the barrier (Iraqui et al., 2012; Mizuno et al., 2013).

In Chapter 3, I extended these findings by showing that the genomic instability induced by the restarted fork can extend up to a distance of at least 75 kb downstream of the point of initiation. Unlike BIR, the restarted replication fork initiated by RDR does not seem to mature as it moves along, and the template switching events are only curtailed by fork convergence. Having established the extent of template switching caused by RDR, I went on to characterise some of the key genetic factors that promote or prevent it. Like BIR, RDR is completely dependent on Rad52 and requires Rad51 and Rad54 (Mehta and Haber, 2014). Also similar to BIR, the Pif1 orthologue in fission yeast, Pfh1, promotes template switching downstream of *RTS1*, most likely because it is needed for efficient progression of the restarted replication (Saini et al., 2013; Wilson et al., 2013). However, the *S. pombe* orthologues of certain other key factors that influence BIR, such as Mph1, Tid1 and Mus81, had at best only a modest effect on template switching downstream of the barrier (Ira and Haber, 2002; Mayle et al., 2015; Pardo and Aguilera, 2012; Stafa et al., 2014). These differences between *RTS1*-

induced RDR and BIR might be attributed to species specificity, with the genetic requirements for replication restart in fission yeast differing from those in budding yeast. Alternatively, the differences that I have discovered may reflect fundamental mechanistic distinctions between replication restart initiated from a DSB versus that initiated from a collapsed, yet unbroken, fork. In order to distinguish between these possibilities it will be essential to study both processes in the same model organism, and ideally at the same genetic locus. This could be achieved in *S. pombe* by introducing a site-specific single-strand break at the same chromosomal site that has been used to study *RTS1*-induced RDR. In principle, one could use a minimal cleavage site for the HO endonuclease or even CRISPR/Cas9 technology to generate a site-specific single-strand break (Jinek et al., 2012; Sandell et al., 1993).

To fully understand how RDR differs from canonical DNA replication, the precise protein composition and structure of the restarted replication fork needs to be defined. We already know that budding yeast BIR uses all of the core replisome components, and seemingly only differs in its requirement for the non-essential Pol δ subunit, Pol32 (Costantino et al., 2014; Lydeard et al., 2010). A more radical difference is its D-loop or bubble structure, but even this might mature into a fully-fledged replication fork after a few kbs (Deem et al., 2011; Mayle et al., 2015; Saini et al., 2013; Smith et al., 2007; Wilson et al., 2013). There is also evidence that *RTS1*-induced RDR in fission yeast uses Pol δ to synthesise both the leading and lagging strand (Miyabe et al., 2015). Whether these are the only differences between RDR and canonical DNA replication, or there are still further proteins and structural peculiarities to be defined, is yet to be determined. Both novel genetic screens with *RTS1* and proteomic analysis of the restarted replication fork (Dungrawala and Cortez, 2015; Sirbu et al., 2012; Yu et al., 2015) might prove

fruitful in dissecting “replisome” composition. Another approach that might be useful is time-lapse microscopy. The system that we have developed to visualize the recruitment of recombination and replication proteins to a site-specific RFB in real time could be used to systematically track changes in protein composition during RDR (Nguyen et al., 2015). Moreover, it may be possible to follow the progression of the restarted fork away from the barrier, and determine whether template switching involves recombination proteins “coming and going” or their retention at the fork throughout its passage. In order to be able to track the movement of the restarted fork in real time, I decided to modify the existing system. Currently, the RFB is marked by a *lacO* array that is positioned just downstream of it so that its location can be tracked in cells expressing fluorescently labeled LacI-tdKatushka2. To be able to see whether recombination protein foci, such as formed by Rad52-YFP, shift from co-localising with the *lacO*-LacI array-marked RFB to a nearby adjacent site, I inserted a *tetO* array 35 kb downstream of the barrier [Fig. 7.i.a]. In cells expressing fluorescent TetR-eCFP, movement of recombinase and replication proteins can be tracked as they traverse from the *lacO* array, marking *RTS1*, to the *tetO* array. Fig. 7.i.b shows some representative snap-shots demonstrating that *lacO*-LacI and *tetO*-TetR foci can be resolved, and that Rad52 foci can be visualized at the same time. This system will enable us to study the spatio-temporal dynamics of the proteins in terms of their recruitment at the barrier and their role in progression of the restarted fork.

Much of our understanding of how cells respond to replication fork collision with barriers comes from studies using *RTS1*, a programmed RFB. However, it has been unclear whether the cell’s response to *RTS1* is representative of what happens at accidental protein-DNA barriers. In Chapters 4 and 5, I tried to address

this question by establishing a novel site-specific barrier system, MarBI, formed by the modified *Hsmar1* transposase binding to a single transposon end. As discussed in Chapter 4, MarBI is a bi-directional barrier that perturbs replication fork movement and induces a strong recombinational response that is mostly driven by Rad51-dependent strand invasions. 2D gel analysis reveals that MarBI seems to cause problems with fork convergence at the final stages of replication termination. Additionally, unlike *RTS1*, DSBs are detected at MarBI and there appears to be much later recruitment of Rad52 to the barrier site as compared to *RTS1*. To explain these observations, I formulated a model for what happens when the replication fork encounters MarBI. Upon collision with the barrier, the replication fork stalls but does not collapse. Instead, it either displaces the barrier, replicating past the region, or persists at the barrier waiting for the opposing fork to arrive and attempt fork convergence. It appears that it is the point of fork merging where the problem arises. As the two forks manage to almost fully converge, it is conceivable that they form a structure that is recognized as a threat to the successful completion of replication. This could be the target for a structure-specific nuclease, which cleaves the nearly converged forks resulting in the formation of a DSB in G2. The DSB could then be repaired by Rad51-dependent HR using the intact sister-chromatid DNA. Unlike *RTS1*, there is very little measurable RDR observed at MarBI. Thus MarBI can be used as a novel system to study the cellular response to fork convergence perturbations. The novelty of the system lies in the fact that, unlike previously established systems, MarBI does not require the intervention of the replisome to establish the barrier. Additionally, a proteomics based approach could be developed to compare the composition of the replication fork at MarBI versus *RTS1*, providing a better insight into the properties of a collapsed versus stalled replication fork in the same organism.

A highly relevant question in a wider context is: are the pathological phenotypes observed here specific for MarBI or do other accidental RFBs evoke similar responses? In order to address this, I introduced the TusB-*TerB*X6 RFB in *S. pombe* at the same locus at which *RTS1* and MarBI had been inserted. Similar to MarBI, TusB-*TerB*X6 acts as a bi-directional RFB and induces a recombinational response that is at least in part dependent upon Rad51. However, it has yet to be determined whether it gives rise to RDR like *RTS1* or DNA breakage like MarBI. Interestingly, when the TusB-*TerB*X6 RFB is introduced in mouse cells, it perturbed replication forks bi-directionally and induced a recombinational response (Willis et al., 2014). In contrast, TusB-*TerB* acts as a polar RFB in *S. cerevisiae*, which does not require the intervention of recombinases (Larsen et al., 2014). Thus, it appears that the cellular response to accidental protein-DNA RFBs in mammalian cells is more similar to that in *S. pombe* than it is to the response in *S. cerevisiae.* To confirm this it would be prudent to introduce MarBI into mamalian cells and examine the cellular response.

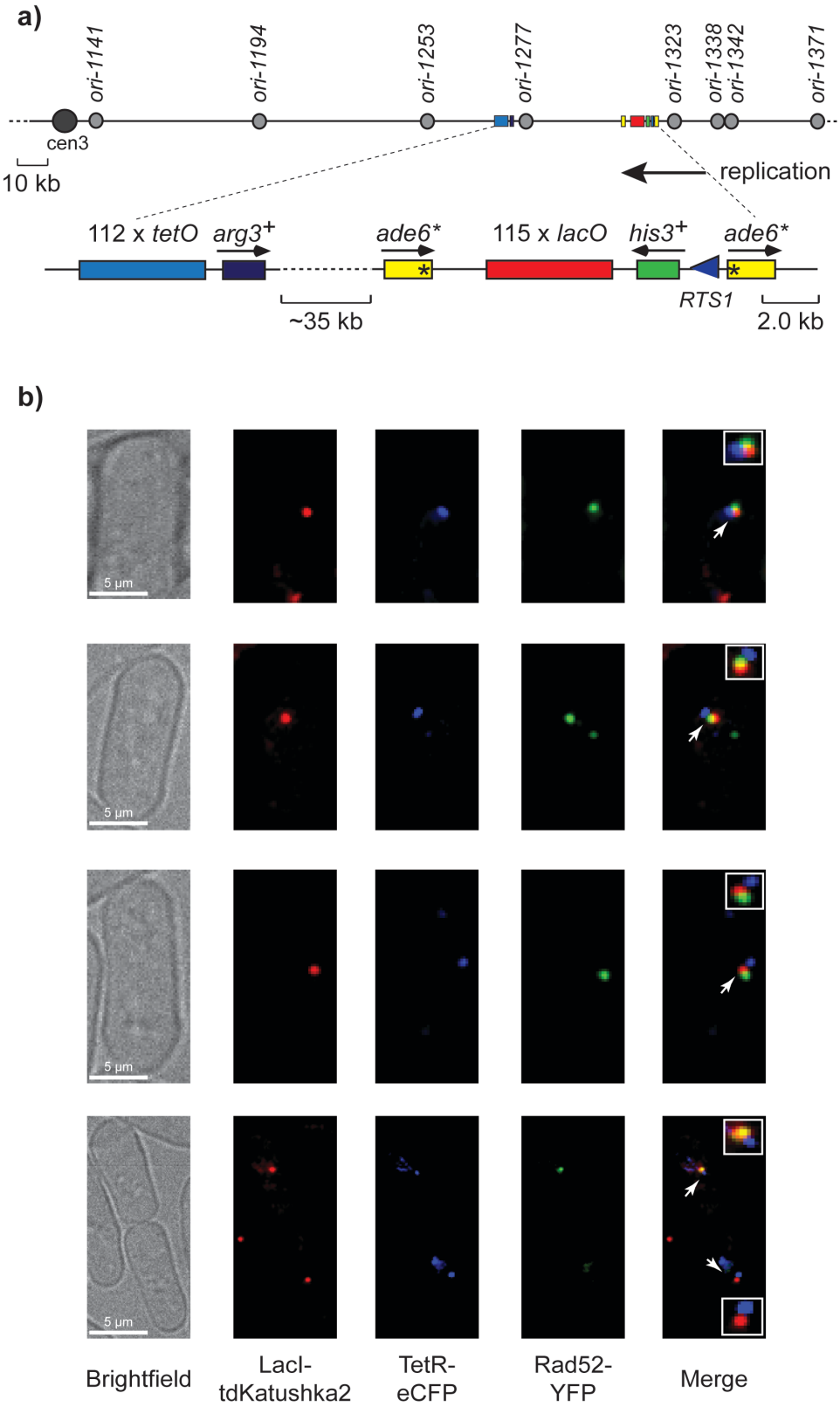


Fig. 7.i Establishing a system to study the spatio-temporal dynamics of the components of the restarted replication fork through live cell microscopy.
a) Schematic showing the modification of the direct repeat recombination reporter for time-lapse microscopy. The *tetO* array is placed at a position that is 35 kb downstream of *RTS1*. b) Representative stills from cells showing the *lacO*-LacI-tdKatushka2 focus and the *tetO*-TetR-eCFP focus and the Rad52-YFP focus co-localising with either, both or none (indicated by the arrow) when *RTS1-AO* is present. The strain is MCW8202*.

Chapter 8

Appendix

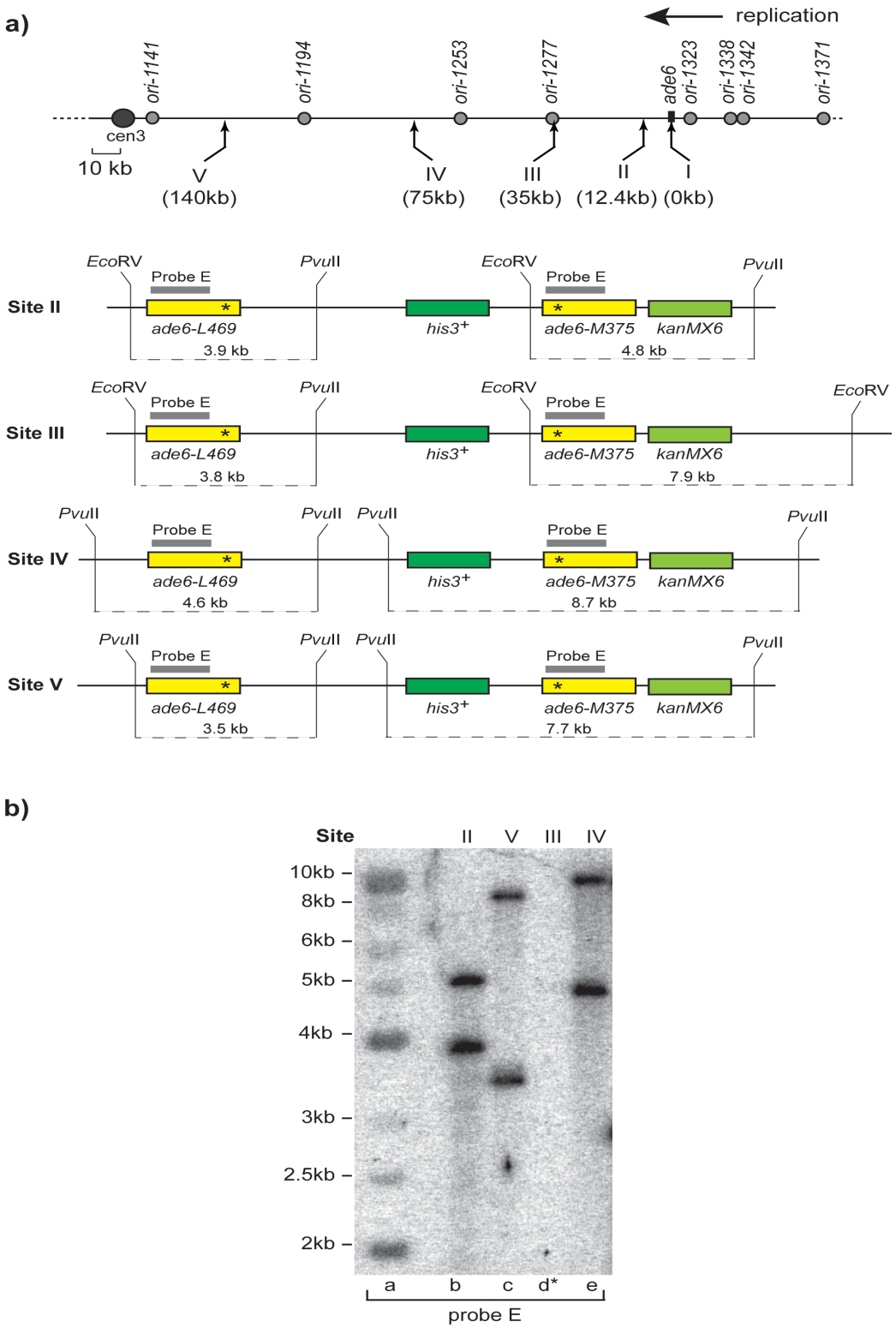


Fig. 8.i Southern blot analysis of the genomic locus to confirm the correct integration of the *ade6*⁻ reporter at sites II-V on ChrIII.

a) Schematic showing the relative positions on ChrIII where the *ade6*⁻ reporter (shown in the bottom panel) is inserted downstream of the *ade6* gene at its endogenous locus. The sites II-V are marked on the chromosome arm. The digests used to confirm the integration and the expected fragment size is indicated in the bottom panel. b) Neutral 1D gel analysis of the restriction digests of genomic DNA from asynchronous cultures. DNA was detected using probe E. The strains are MCW7229 (lane b), MCW7297 (lane c), MCW7429 (lane d) and MCW7430 (lane e). The DNA ladder was run in lane a. The * indicates the degraded sample.

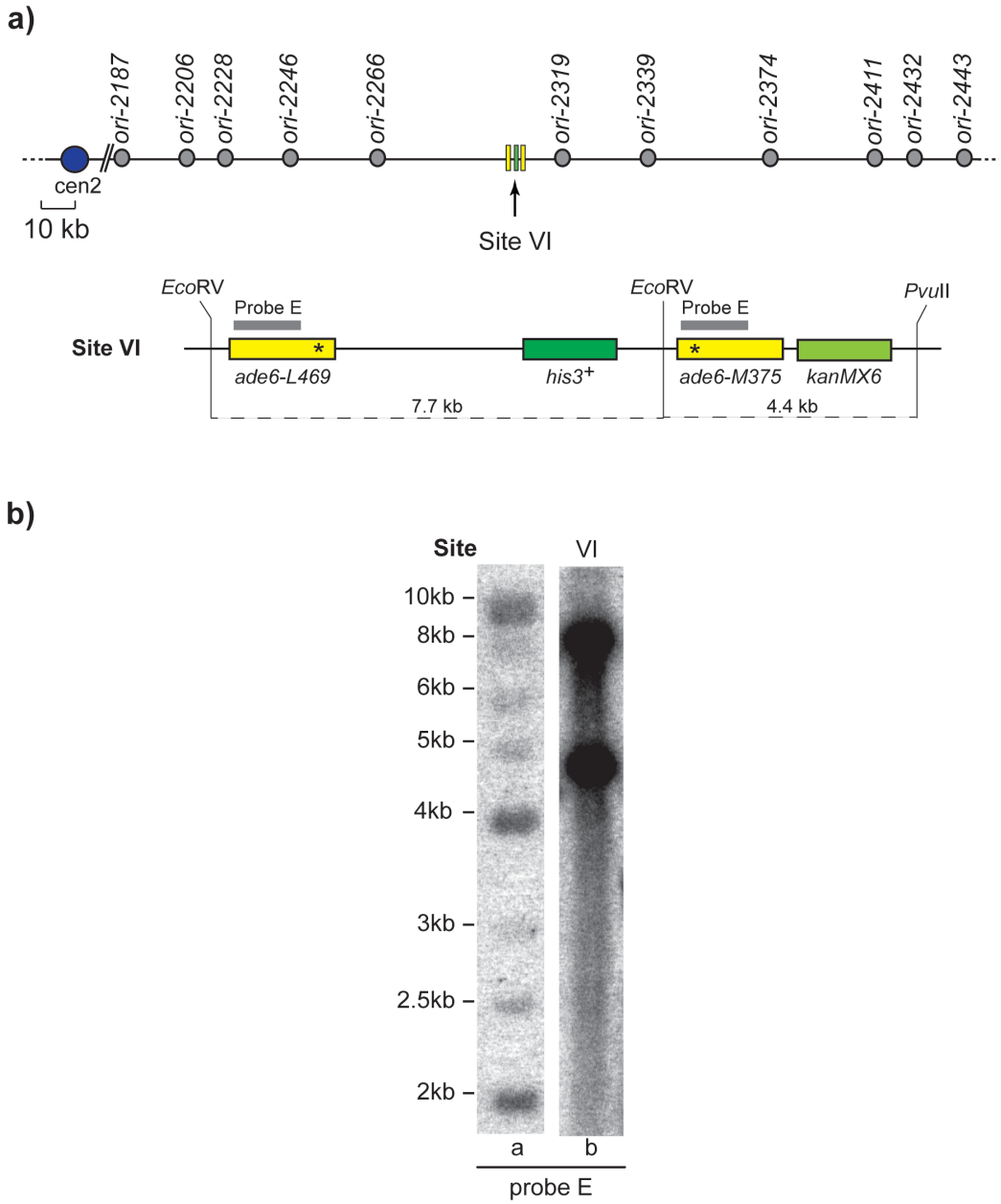


Fig. 8.ii Southern blot analysis of the genomic locus to confirm the correct integration of the *ade6*$^{-}$ reporter at sites VI on ChrII.

a) Schematic showing the relative position on ChrII where the *ade6*$^{-}$ reporter (shown in the bottom panel) is inserted at position VI. The digests used to confirm the integration and the expected fragment size is indicated in the bottom panel. b) Neutral 1D gel analysis of the restriction digests of genomic DNA from asynchronous cultures. DNA was detected using probe E. The strain is MCW8045 (lane b). The DNA ladder was run in lane a.

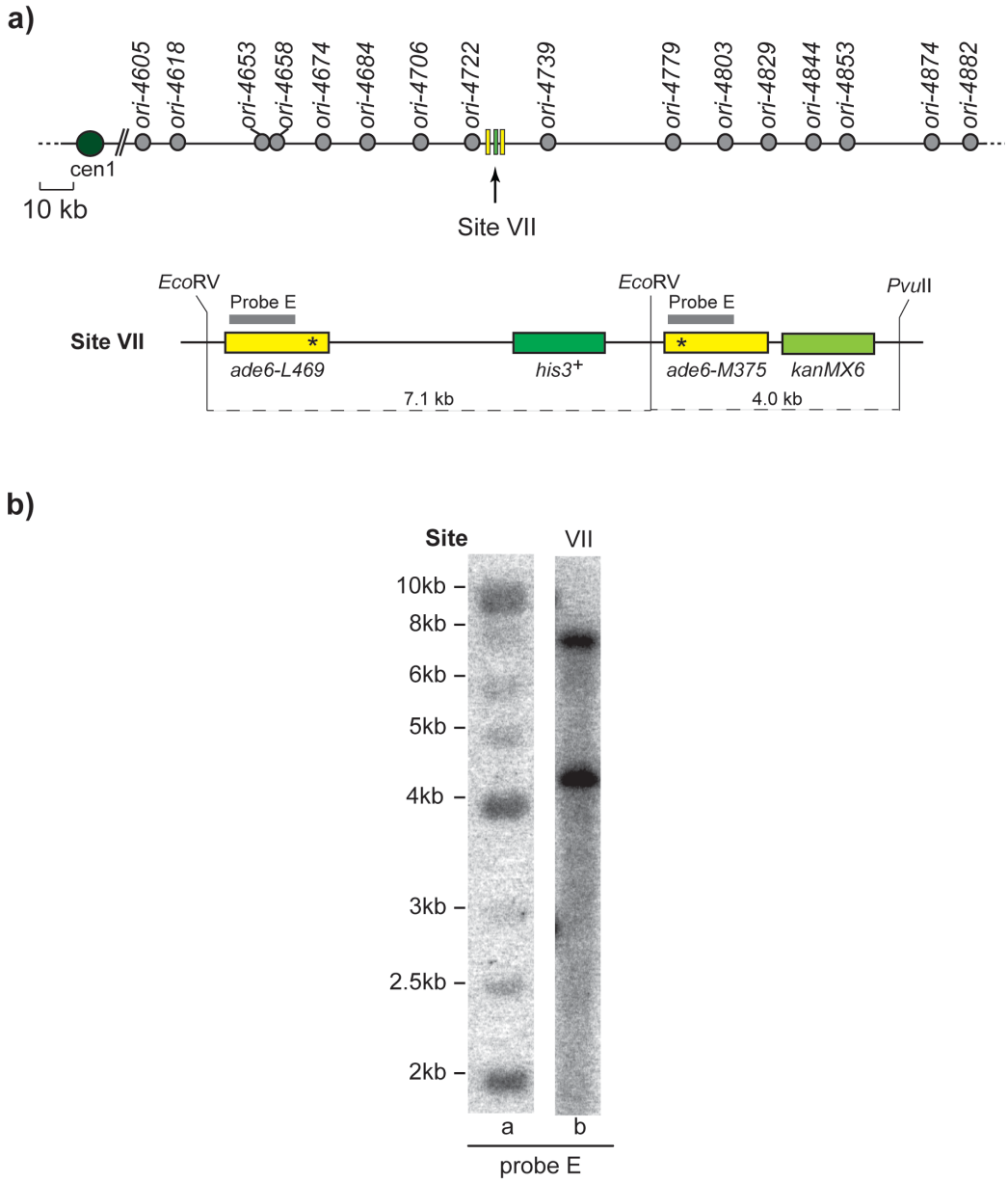


Fig. 8.iii Southern blot analysis of the genomic locus to confirm the correct integration of the *ade6*$^{-}$ reporter at sites VII on ChrI.

a) Schematic showing the relative position on ChrI where the *ade6*$^{-}$ reporter (shown in the bottom panel) is inserted at position VII. The digests used to confirm the integration and the expected fragment size is indicated in the bottom panel. b) Neutral 1D gel analysis of the restriction digests of genomic DNA from asynchronous cultures. DNA was detected using probe E. The strain is MCW8044 (lane b). The DNA ladder was run in lane a.

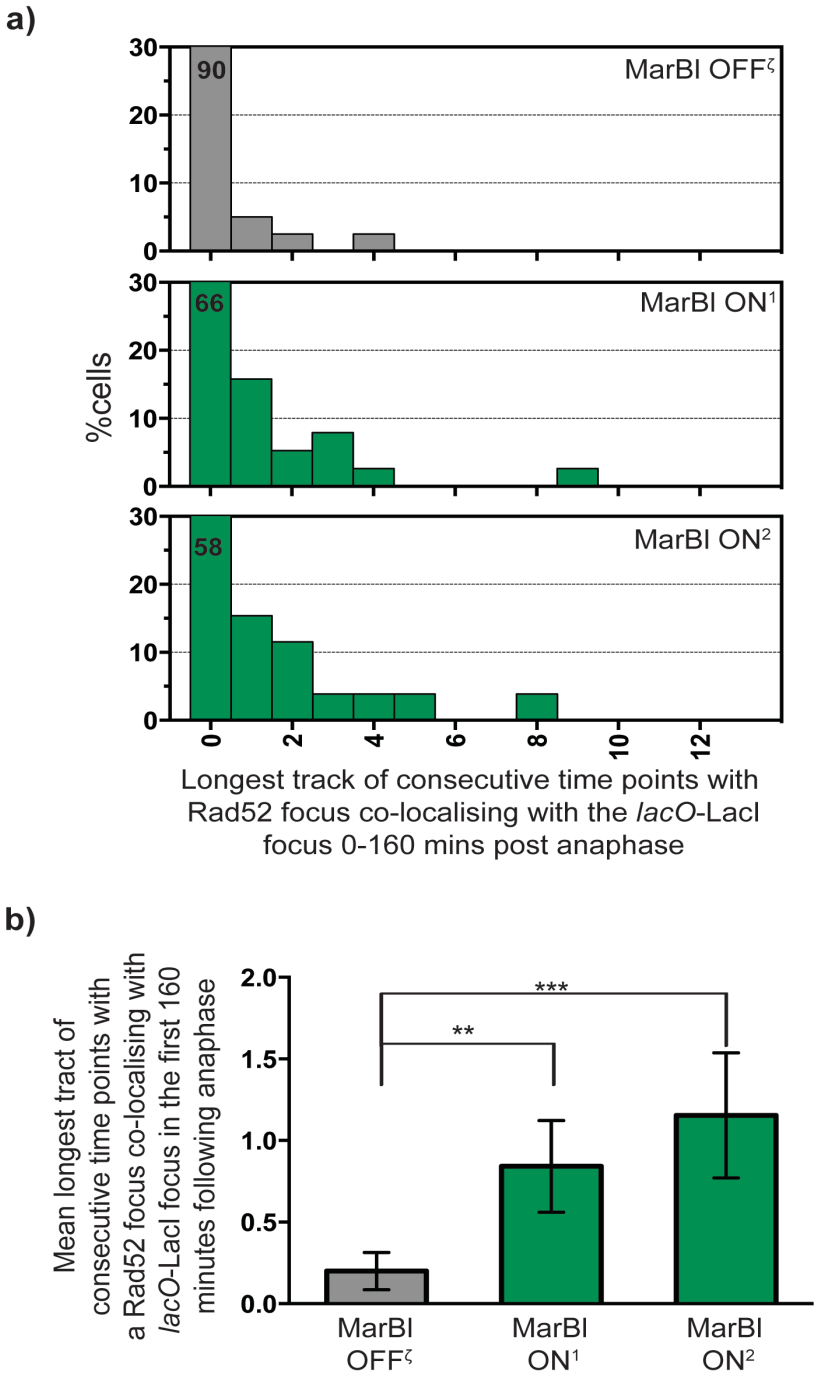


Fig. 8.iv Analysis of the track lengths of Rad52 co-localisation with MarBI.
a) Histograms showing the percentage of cells with the given number of uninterrupted time points in which a Rad52-YFP focus co-localises with *lacO*-LacI focus within the first 160 minutes following anaphase. The strains are MCW7578 (n=40), MCW7574 (n=38) and MCW7582 (n=26). MarBI OFF$^{\zeta}$ represents the system where the Mar^{D155A} protein is expressed but the transposon end is absent, MarBI ON^{1} where Mar^{D155A} is expressed and TO1 is present and MarBI ON^{2} where Mar^{D155A} is expressed and TO2 is present. Error bars represent ± standard error of the mean. P-values calculated using the Shapiro-Wilk normality test (ns $p>0.05$, *$p<0.05$, **$p<0.01$, ***$p<0.001$, ***$p<0.0001$). When the bar on the histogram extends beyond the scale of the Y-axis, the number in the bar indicates the value.

Table 8-1: Direct repeat recombinant frequencies (*RTS1*)

Genotype and Strain no.	*RTS1* presence and orientation[a]	Position of direct repeat relative to *RTS1*[b]	Number of colonies analysed	Ade$^+$ His$^+$ recombinant frequency (x 10^{-4})[c]		Ade$^+$ His$^-$ recombinant frequency (x 10^{-4})[c]		% gene conversion[c]
				Mean	*P* value[d]	Mean	*P* value[d]	Mean
wild-type MCW429	-	Flanking	20	1.10 (±0.37)	-	2.63 (±0.51)	-	29.4 (±5.9)
wild-type MCW4712	IO	Flanking	96	1.38 (±0.51)	0.020[e]	3.57 (±0.99)	<0.001[e]	28.0 (±7.3)
wild-type MCW4713	AO	Flanking	102	135.40 (±38.8)	<0.001[f]	107.90 (±45.7)	<0.001[f]	56.0 (±10.6)
wild-type MCW7131	IO	0.2 kb downstream	47	1.25 (±0.70)	0.186[f]	5.05 (±2.25)	<0.0001[f]	20.4 (±8.0)
wild-type MCW7133	AO	0.2 kb downstream	45	157.35 (±65.98)	<0.001[h]	682.35 (±286.54)	<0.001[h]	19.9 (±8.2)
*ori-1253*Δ MCW7414	IO	0.2 kb downstream	38	1.46 (±0.47)	0.106[h]	4.52 (±1.63)	0.230[h]	25.3 (±7.4)
*ori-1253*Δ MCW7416	AO	0.2 kb downstream	40	280.28 (±130.43)	<0.001[i]	465.35 (±166.99)	<0.001[i]	37.3 (±9.1)
wild-type MCW7229	-	12.4 kb downstream	17	0.77 (±0.29)	0.005[e]	1.14 (±1.07)	<0.001[e]	47.7 (±18.5)
wild-type MCW7257	IO	12.4 kb downstream	23	0.84 (±0.49)	0.617	2.01 (±0.77)	0.005[j]	29.4 (±13.5)
wild-type MCW7259	AO	12.4 kb downstream	104	4.95 (±2.54)	<0.001[k]	84.85 (±27.71)	<0.001[k]	5.9 (±3.2)
*ori-1253*Δ MCW7293	IO	12.4 kb downstream	22	1.83 (±0.84)	<0.001[k]	4.27 (±1.50)	<0.001[k]	29.8 (±9.5)
*ori-1253*Δ MCW7295	AO	12.4 kb downstream	26	103.45 (±39.48)	<0.001[l]	1006.41 (±429.81)	<0.001[l]	10.2 (±4.4)
wild-type MCW7429	-	35 kb downstream	17	4.25 (±2.41)	<0.001[e]	0.86 (±0.69)	<0.001[e]	82.0 (±13.3)
wild-type MCW7565	IO	35 kb downstream	13	3.75 (±2.21)	0.564[m]	0.69 (±0.54)	0.498[m]	84.3 (±9.1)

wild-type MCW7567	AO	35 kb downstream	17	61.39 (±30.77)	<0.001[n]	39.98 (±25.13)	<0.001[n]	61.5 (±15.4)
wild-type MCW7430	-	75 kb downstream	30	1.09 (±0.47)	0.944[e]	2.28 (±0.64)	0.042[e]	32.0 (±10.3)
wild-type MCW7614	IO	75 kb downstream	18	1.25 (±0.55)	0.284[p]	2.56 (±0.93)	0.217[p]	32.6 (±6.5)
wild-type MCW7616	AO	75 kb downstream	15	1.76 (±0.99)	0.071[q]	3.04 (±1.00)	0.161[q]	34.8 (±13.9)
*ori-1253*Δ MCW7987	-	75 kb downstream	16	1.19 (±0.49)	0.504[p]	2.97 (±1.66)	0.046[p]	30.7 (±10.7)
*ori-1253*Δ MCW7620	AO	75 kb downstream	15	2.35 (±0.82)	0.090[r]	16.34 (±8.85)	<0.001[r]	13.6 (±3.9)
wild-type MCW7297	-	140 kb downstream	9	0.87 (±0.22)	0.090[e]	2.09 (±0.75)	0.030[e]	30.3 (±6.5)
wild-type MCW7326	IO	140 kb downstream	13	1.05 (±0.61)	0.403[s]	2.58 (±1.22)	0.295[s]	29.6 (±12.2)
wild-type MCW7328	AO	140 kb downstream	12	1.19 (±0.62)	0.564[t]	2.69 (±1.01)	0.815[t]	31.2 (±11.15)
*ori-1253*Δ MCW7330	IO	140 kb downstream	13	0.86 (±0.24)	0.320[t]	2.24 (±1.27)	0.499[t]	30.2 (±10.2)
*ori-1253*Δ MCW7332	AO	140 kb downstream	13	1.13 (±0.66)	0.799[u]	3.14 (±1.55)	0.402[u]	27.38 (±12.91)
*rad51*Δ MCW1691	IO	Flanking	10	0.05 (±0.08)	<0.001[f]	15.40 (±2.87)	<0.001[f]	0.3 (±0.5)
*rad51*Δ MCW1692	AO	Flanking	48	1.12 (±1.24)	<0.001[g]	74.70 (±29.1)	<0.001[g]	1.5 (±1.5)
*rad51*Δ MCW7812	IO	12.4 kb downstream	17	0.09 (±0.16)	<0.001[k]	8.97 (±3.43)	<0.001[k]	0.9 (±1.3)
*rad51*Δ MCW7814	AO	12.4 kb downstream	15	1.28 (±0.68)	<0.001[l]	10.60 (±5.27)	<0.001[l]	12.4 (±6.53)
*rad51*Δ *52*Δ MCW1695	IO	Flanking	15	0.005 (±0.02)	<0.001[f]	1.09 (±0.52)	<0.001[f]	0.33 (±1.3)
*rad51*Δ *52*Δ MCW1696	AO	Flanking	15	0.03 (±0.057)	<0.001[g]	2.49 (±1.36)	<0.001[g]	1.75 (±3.36)

*rad51*Δ *52*Δ MCW7816	IO	12.4 kb downstream	17	0.00 (±0.00)	<0.001[k]	1.26 (±1.64)	0.061[k]	0.0 (±0.0)
*rad51*Δ *52*Δ MCW7818	AO	12.4 kb downstream	15	0.00 (±0.01)	<0.001[l]	1.20 (±0.83)	<0.001[l]	0.2 (±0.7)
pfh1-m21 MCW4934	-	Flanking	9	1.31 (±0.51)	0.212[e]	2.54 (±0.95)	0.723[e]	34.5 (±8.5)
pfh1-m21 MCW4940	IO	Flanking	9	1.41 (±0.39)	0.899[f]	3.57 (±0.62)	0.990[f]	28.4 (±7.2)
pfh1-m21 MCW4942	AO	Flanking	28	164.40 (±57.7)	0.002[g]	1778.90 (±359.3)	<0.001[g]	8.5 (±2.7)
*pfh1-mt** MCW4948	-	Flanking	9	1.27 (±0.48)	0.312[e]	4.36 (±0.48)	<0.001[e]	23.7 (±5.2)
*pfh1-mt** MCW4954	IO	Flanking	10	2.09 (±0.49)	<0.001[f]	14.40 (±4.65)	<0.001[f]	13.3 (±3.5)
*pfh1-mt** MCW4956	AO	Flanking	20	176.40 (±44.5)	0.586[g]	1610.50 (±257.0)	<0.001[g]	9.8 (±1.8)
pfh1-m21 MCW7599	IO	0.2 kb downstream	20	1.51 (±0.41)	0.124[h]	4.00 (±1.10)	0.052[h]	27.7 (±5.8)
pfh1-m21 MCW7601	AO	0.2 kb downstream	19	39.31 (±25.08)	<0.001[i]	779.20 (±168.2)	0.175[i]	4.8 (±2.7)
pfh1-m21 ori-1253Δ MCW7598	IO	0.2 kb downstream	20	2.82 (±1.79)	0.003[v]	8.00 (±3.70)	<0.001[v]	26.9 (±9.4)
pfh1-m21 *ori-1253*Δ MCW7600	AO	0.2 kb downstream	12	134.90 (±71.6)	<0.001[w]	1648.90 (±288.8)	<0.001[w]	7.5 (±3.1)
pfh1-mt* MCW7603	IO	0.2 kb downstream	18	2.58 (±0.88)	<0.001[h]	7.30 (±2.20)	0.001[h]	26.3 (±5.9)
*pfh1-mt** MCW7605	AO	0.2 kb downstream	20	4.85 (±2.19)	<0.001[i]	246.70 (±141.4)	<0.001[i]	2.3 (±1.3)
pfh1-mt* *ori-1253*Δ MCW7602	IO	0.2 kb downstream	21	4.34 (±2.09)	0.012[x]	10.80 (±4.63)	0.001[x]	28.76 (±7.23)

pfh1-mt* *ori-1253*Δ MCW7604	AO	0.2 kb downstream	20	16.69 (±10.53)	<0.001[y]	446.24 (±117.77)	<0.001[y]	3.55 (±1.95)
pfh1-m21 MCW7421	IO	12.4 kb downstream	18	2.14 (±1.23)	<0.001[k]	3.20 (±1.28)	0.001[k]	38.8 (±14.2)
pfh1-m21 MCW7422	AO	12.4 kb downstream	17	2.05 (±0.85)	<0.001[l]	10.4 (±3.07)	<0.001[l]	16.9 (±5.97)
pfh1-m21 *ori-1253*Δ MCW7423	IO	12.4 kb downstream	19	1.60 (±0.40)	0.081[z]	5.03 (±1.41)	<0.001[z]	24.7 (±5.9)
pfh1-m21 *ori-1253*Δ MCW7424	AO	12.4 kb downstream	20	9.15 (±2.38)	<0.001[aa]	121.70 (±55.3)	<0.001[aa]	8.2 (±3.0)
*pfh1-mt** MCW7425	IO	12.4 kb downstream	17	1.24 (±0.49)	0.014[k]	2.38 (±1.20)	0.242[k]	35.6 (±8.4)
*pfh1-mt** MCW7426	AO	12.4 kb downstream	18	1.49 (±0.64)	<0.001[l]	5.05 (±1.55)	<0.001[l]	23.4 (±8.7)
pfh1-mt* *ori-1253*Δ MCW7427	IO	12.4 kb downstream	15	1.71 (±0.52)	0.013[bb]	4.17 (±1.30)	<0.001[bb]	29.9 (±9.7)
pfh1-mt* *ori-1253*Δ MCW7428	AO	12.4 kb downstream	17	4.04 (±1.66)	<0.001[cc]	16.80 (±5.33)	<0.001[cc]	19.6 (±5.5)
*mus81*Δ MCW1451	IO	Flanking	21	1.29 (±0.78)	0.492[f]	3.00 (±1.57)	0.038[f]	31.83 (±13.5)
*mus81*Δ MCW1452	AO	Flanking	23	132.50 (±42.3)	0.750[g]	149.20 (±77.8)	0.001[g]	48.8 (±11.9)
*mus81*Δ MCW8195	AO	12.4 kb downstream	16	4.95 (±1.20)	0.999[l]	55.10 (±14.4)	<0.001[l]	8.6 (±2.5)
srs2Δ FO1748*	IO	Flanking	15	12.9 (±6.00)	<0.001[f]	17.0 (±9.20)	<0.001[f]	43.2 (±15.5
srs2Δ FO1750	AO	Flanking	16	1048.20 (±279.8)	<0.001[g]	548.20 (±148.2)	<0.001[g]	65.7 (±8.6)

srs2Δ MCW8200	AO	12.4 kb downstream	20	103.30 (±39.9)	<0.001[l]	462.30 (±144.7)	<0.001[l]	18.9 (±7.3)
rqh1Δ MCW1443	IO	Flanking	10	2.62 (±0.92)	<0.001[f]	14.7 (±3.29)	<0.001[f]	15.3 (±4.5
*rqh1*Δ MCW1447	AO	Flanking	11	357.60 (±209.5)	<0.001[g]	2167.30 (±848.9)	<0.001[g]	14.0 (±4.2)
*rqh1*Δ MCW8201	AO	12.4 kb downstream	19	11.10 (±3.98)	<0.001[l]	250.80 (±91.0)	<0.001[l]	4.6 (±2.0)
fbh1Δ FO1814	IO	Flanking	22	1.62 (±0.54)	0.0535[f]	3.35 (±0.82)	0.343[f]	32.5 (±7.4
fbh1Δ FO1836	AO	Flanking	15	916.70 (±455.5)	<0.001[g]	2165.50 (±662.2)	<0.001[g]	29.6 (±9.7)
fbh1Δ MCW8227	AO	12.4 kb downstream	15	63.90 (±33.5)	<0.001[l]	801.60 (±230.5)	<0.001[l]	8.0 (±4.9)
rad8Δ MCW3862	IO	Flanking	14	1.55 (±0.53)	0.257[f]	3.69 (±0.99)	0.649[f]	29.8 (±8.7)
*rad8*Δ MCW3864	AO	Flanking	15	312.10 (±58.1)	<0.001[g]	134.90 (±35.7)	0.030[g]	69.9 (±5.3)
*rad8*Δ MCW8197	AO	12.4 kb downstream	20	7.97 (±4.63)	<0.001[l]	113.40 (±41.9)	<0.001[l]	7.3 (±4.2)
exo1Δ FO949	-	Flanking	27	1.54 (±0.60)	0.006[e]	3.18 (±0.85)	0.015[e]	32.0 (±5.8
*exo1*Δ MCW1742	AO	Flanking	21	57.10 (±11.6)	<0.001[g]	51.80 (±23.3)	<0.001[g]	53.7 (±9.1)
*exo1*Δ MCW8219	AO	12.4 kb downstream	20	9.16 (±3.92)	<0.001[l]	163.0 (±86.4)	<0.001[l]	6.0 (±2.5)
Ter2X3 orientaion1 MCW7431	-	12.4 kb downstream	10	0.91 (±0.70)	0.473[j]	1.76 (±1.31)	0.191[j]	34.1 (±11.2)
Ter2X3 orientaion1 MCW7507	IO	12.4 kb downstream	10	0.95 (±0.50)	0.568[k]	2.91 (±1.20)	0.014[k]	26.3 (±13.6)

Ter2X3 orientaion1 MCW7509	AO	12.4 kb downstream	10	2.69 (±0.73)	0.006[l]	43.84 (±11.20)	<0.001[l]	6.0 (±2.1)
Ter2X3 orientaion2 MCW7432	-	12.4 kb downstream	9	1.70 (±1.38)	0.012[j]	1.32 (±0.61)	0.644[j]	53.9 (±17.0)
Ter2X3 orientaion2 MCW7511	IO	12.4 kb downstream	9	1.10 (±0.45)	0.175[k]	0.90 (±0.37)	<0.001[k]	55.5 (±10.4)
Ter2X3 orientaion2 MCW7513	AO	12.4 kb downstream	10	1.15 (±0.52)	<0.001[l]	1.30 (±0.41)	<0.001[l]	46.4 (±14.3)
tRNA co-directional MCW7434	-	12.4 kb downstream	16	0.75 (±0.27)	0.800[j]	1.07 (±0.48)	0.820[j]	42.2 (±11.7)
tRNA co-directional MCW7519	IO	12.4 kb downstream	18	0.70 (±0.24)	0.262[k]	0.89 (±0.56)	<0.001[k]	47.0 (±12.7)
tRNA co-directional MCW7521	AO	12.4 kb downstream	17	4.19 (±1.31)	0.228[l]	70.13 (±25.50)	0.042[l]	6.1 (±2.4)
tRNA contra-directional MCW7433	-	12.4 kb downstream	16	1.23 (±0.46)	0.002[j]	1.87 (±1.23)	0.077[j]	42.2 (±14.0)
tRNA contra-directional MCW7515	IO	12.4 kb downstream	16	1.56 (±0.71)	0.007[k]	1.58 (±0.71)	0.063[k]	48.5 (±12.0)
tRNA contra-directional MCW7517	AO	12.4 kb downstream	21	5.11 (±2.71)	0.801[l]	200.45 (±68.10)	<0.001[l]	2.5 (±1.2)
*elg1*Δ MCW7708	AO	Flanking	43	8.57 (±3.49)	<0.001[h]	31.79 (±11.48)	<0.001[h]	21.7 (±5.3)
elg1Δ MCW8191	AO	12.4 kb downstream	16	0.64 (±0.32)	<0.001[l]	13.90 (±7.12)	<0.001[l]	5.5 (±3.7)

elg1Δ *ori-1253*Δ MCW8290	AO	12.4 kb downstream	15	5.56 (±3.62)	<0.001[dd]	95.94 (±13.98)	<0.001[dd]	5.4 (±2.8)
*fml1*Δ MCW3061	AO	Flanking	22	17.24 (±8.86)	<0.001[g]	108.31 (±53.51)	0.971[g]	14.3 (±76.1)
fml1Δ MCW8193	AO	12.4 kb downstream	17	4.46 (±2.76)	0.468[l]	94.27 (±24.59)	0.189[l]	4.8 (±3.3)
*tid1*Δ MCW7704	AO	Flanking	7	166.46 (±51.62)	0.047[g]	132.21 (±128.83)	0.251[g]	60.9 (±25.9)
tid1Δ MCW8216	AO	12.4 kb downstream	10	6.03 (±2.77)	0.206[l]	73.59 (±28.30)	0.223[l]	8.1 (±3.6)
fen1Δ MCW1742	AO	Flanking	7	134.08 (±52.95)	0.933[g]	231.09 (±82.67)	<0.001[g]	37.1 (±11.1)
fen1Δ MCW8220	AO	12.4 kb downstream	17	7.01 (±2.87)	0.003[l]	73.57 (±25.67)	0.119[l]	9.4 (±4.7)
*rad54*Δ MCW2656	AO	Flanking	46	4.62 (±3.69)	<0.001[g]	197.19 (±86.65)	<0.001[g]	2.7 (±2.2)
*rad54*Δ MCW8223	AO	12.4 kb downstream	18	1.11 (±0.51)	<0.001[l]	14.63 (±6.17)	<0.001[l]	7.7 (±3.6)

a-*RTS1* is integrated at the *ade6* locus either between a direct repeat of *ade6*$^-$ alleles or replacing *ade6*. In strains without *RTS1*, the *ade6* gene is deleted from its normal locus; b-The different positions of the *ade6*$^-$ direct repeat recombination reporters are shown in Fig. 3.ii; c-The values in parentheses are the standard deviations about the mean; d-*P* values are derived from independent-sample *t*-tests comparing the mean values as indicated; e-Compared to the equivalent mean recombinant frequency of MCW429; f-Compared to the equivalent mean recombinant frequency of MCW4712; g-Compared to the equivalent mean recombinant frequency of MCW4713; h-Compared to the equivalent mean recombinant frequency of MCW7131; i-Compared to the equivalent mean recombinant frequency of MCW7133; j-Compared to the equivalent mean recombinant frequency of MCW7229; k-Compared to the equivalent mean recombinant frequency of MCW7257; l-Compared to the equivalent mean recombinant frequency of MCW7259; m-Compared to the equivalent mean recombinant frequency of MCW7429; n-Compared to the equivalent mean recombinant frequency of MCW7565; o-Compared to the equivalent mean recombinant frequency of MCW7567; p-Compared to the equivalent mean recombinant frequency of MCW7430; q-Compared to the equivalent mean recombinant frequency of MCW7614; r-Compared to the equivalent mean recombinant frequency of MCW7616; s-Compared to the equivalent mean recombinant frequency of MCW7297; t-Compared to the equivalent mean recombinant frequency of MCW7326; u-Compared to the equivalent mean recombinant frequency of MCW7328; v-Compared to the equivalent mean recombinant frequency of MCW7599; w-Compared to the equivalent mean recombinant frequency of MCW7601; x-Compared to the equivalent mean recombinant frequency of MCW7603; y-Compared to the equivalent mean recombinant frequency of MCW7605; z-Compared to the equivalent mean recombinant frequency of MCW7421; aa-Compared to the equivalent mean recombinant frequency of MCW7422; bb-Compared to the equivalent mean recombinant frequency of MCW7425; cc-Compared to the equivalent mean recombinant frequency of MCW7456; dd-Compared to the equivalent mean recombinant frequency of MCW8191.

Table 8-2: Direct repeat recombinant frequencies (MarBI)

Genotype and Strain no.	P_{nmt} strength[a]	MarBI Protein[b]	MarBI Site[c]	Position of direct repeat relative to MarBI[d]	Thiamine	Number of colonies analysed	$Ade^+ His^+$ recombinant frequency (x 10^{-4})[e]		$Ade^+ His^-$ recombinant frequency (x 10^{-4})[e]		% gene conversion[e]
							Mean	*P* value[f]	Mean	*P* value[f]	Mean
wild-type MCW39	-	-	-	Flanking	0μM	15	0.38 (±0.19)	-	1.30 (±0.55)	-	29.4 (±5.9)
wild-type MCW3118	-	-	TO1	Flanking	0μM	7	0.59 (±0.42)	0.062[g]	2.04 (±0.48)	0.006[g]	21.8 (±14.6)
wild-type MCW3258	-	-	TO2	Flanking	0μM	9	0.42 (±0.15)	0.573[g]	1.30 (±0.30)	0.090[g]	24.7 (±7.0)
wild-type MCW3119§	+	-	TO1	Flanking	0μM	6	0.88 (±0.68)	0.390[h]	3.21 (±1.62)	0.097[h]	21.0 (±15.4)
wild-type MCW3120§	+	Mar^{WT}	TO1	Flanking	0μM	4	301.92 (±149.72)	0.001[i]	279.19 (±130.14)	0.001[i]	51.9 (±8.5)
wild-type MCW3121§	+	Mar^{WT}-eGFP	TO1	Flanking	0μM	10	165.43 (±87.13)	<0.001[i]	92.98 (±28.47)	<0.001[i]	62.5 (±6.2)
wild-type MCW6630§	+	Mar^{D155A}-eGFP	TO1	Flanking	0μM	7	0.75 (±1.06)	0.816[i]	1.39 (±0.71)	0.021[i]	24.0 (±27.0)
wild-type MCW6631§	+	Mar^{V119G}-eGFP	TO1	Flanking	0μM	8	7.09 (±7.80)	0.078[i]	19.65 (±12.43)	0.008[i]	26.2 (±20.6)
wild-type MCW6480	+	Mar^{WT}	-	Flanking	0μM	14	0.38 (±0.21)	0.647[g]	0.75 (±0.37)	0.0004[g]	37.2 (±14.6)
wild-type MCW6483	+	Mar^{WT}	TO1	Flanking	0μM	8	214.11 (±135.53)	<0.001[j]	68.78 (±44.89)	<0.001[j]	75.6 (±4.1)
wild-type MCW6485	+	Mar^{WT}	TO2	Flanking	0μM	10	123.17 (±25.24)	<0.001[j]	30.52 (±6.78)	<0.001[j]	79.9 (±4.4)
wild-type MCW6481	++	Mar^{WT}	-	Flanking	0μM	43	0.44 (±0.32)	0.397[g]	0.91 (±0.43)	0.007[g]	32.7 (±16.2)
wild-type MCW6487	++	Mar^{WT}	TO1	Flanking	0μM	46	598.11 (±198.10)	<0.001[k]	575.09 (±241.39)	<0.001[k]	48.7 (±10.0)

wild-type MCW6487	++	Mar^{WT}	TO1	Flanking	0.01μM	6	5.98 (±3.61)	<0.001[l]	4.67 (±1.73)	<0.001[l]	51.6 (±20.9)
wild-type MCW6489	++	Mar^{WT}	TO2	Flanking	0μM	32	670.43 (±197.22)	<0.001[k]	1077.59 (±304.21)	<0.001[k]	38.5 (±7.3)
wild-type MCW6482	+	Mar^{WT}-eGFP	-	Flanking	0μM	11	0.37 (±0.36	0.913[g]	0.66 (±0.22)	0.001[g]	31.0 (±13.1)
wild-type MCW6492	+	Mar^{WT}-eGFP	TO1	Flanking	0μM	10	133.51) (±72.55	<0.001[n]	33.18 (±22.48)	<0.001[n]	80.2 (±5.0)
wild-type MCW6494	+	Mar^{WT}-eGFP	TO2	Flanking	0μM	14	13.66 (±3.85)	<0.001[n]	6.86 (±2.59)	<0.001[n]	66.6 (±10.3)
wild-type MCW7096	++	Mar^{WT}	-	Flanking	0μM	10	0.52 (±0.40)	0.499[k]	1.26 (±0.51)	0.028[k]	27.7 (±12.7)
wild-type MCW7096	++	Mar^{WT}	-	Flanking	1μM	5	0.30 (±0.03)	0.206[o]	0.90 (±0.13)	0.113[o]	25.3 (±4.3)
wild-type MCW7098	++	Mar^{WT}	TO1	Flanking	0μM	10	393.11 (±125.34)	0.003[l]	711.84 (±139.83)	0.091[l]	35.1 (±5.5)
wild-type MCW7098	++	Mar^{WT}	TO1	Flanking	1μM	5	0.36 (±0.13)	<0.001[p]	1.34 (±1.28)	<0.001[p]	29.3 (±15.6)
wild-type MCW7099	++	Mar^{WT}	TO2	Flanking	0μM	10	553.44 (±76.47)	0.076[m]	780.36 (±183.38)	0.006[m]	42.0 (±4.6)
wild-type MCW7099	++	Mar^{WT}	TO2	Flanking	1μM	5	0.35 (±0.12)	<0.001[q]	1.04 (±0.10)	<0.001[q]	24.9 (±7.7)
wild-type MCW8239	++	Mar^{D155A}	-	Flanking	0μM	15	0.27 (±0.11)	0.048[g]	0.73 (±0.25)	0.001[g]	27.8 (±12.6)
wild-type MCW7076	++	Mar^{D155A}	TO1	Flanking	0μM	75	644.57 (±216.03)	<0.001[r]	968.37 (±257.69)	<0.001[r]	39.9 (±8.0)
wild-type MCW7076	++	Mar^{D155A}	TO1	Flanking	0.005μM	6	433.74 (±98.77)	0.021[s]	586.41 (±233.01)	0.001[s]	43.4 (±5.2)
wild-type MCW7076	++	Mar^{D155A}	TO1	Flanking	0.01μM	6	211.27 (±88.16)	<0.001[s]	211.55 (±39.23)	<0.001[s]	48.5 (±12.5)
wild-type MCW7076	++	Mar^{D155A}	TO1	Flanking	1μM	11	1.20 (±0.61)	<0.001[s]	2.39 (±0.81)	<0.001[s]	33.1 (±15.2)
wild-type MCW7078	++	Mar^{D155A}	TO2	Flanking	0μM	23	745.68 (±267.87)	<0.001[r]	1337.72 (±405.50)	<0.001[r]	35.6 (±6.9)

*rad51*Δ MCW6847	++	Mar^{WT}	TO1	Flanking	0μM	10	0.00 (±0.00)	$<0.001^{l}$	744.38 (±225.33)	0.047^{l}	0.0 (±0.0)
*rad51*Δ MCW6849	++	Mar^{WT}	TO2	Flanking	0μM	10	0.00 (±0.00)	$<0.001^{m}$	1238.15 (±278.77)	0.146^{m}	0.0 (±0.0)
fml1Δ MCW6851	++	Mar^{WT}	TO1	Flanking	0μM	10	164.56 (±69.25)	$<0.001^{l}$	533.18 (±117.17)	0.596^{l}	23.4 (±8.6)
fml1Δ MCW6853	++	Mar^{WT}	TO2	Flanking	0μM	10	138.35 (±34.31)	$<0.001^{m}$	794.52 (±178.27)	0.008^{m}	15.3 (±4.6)
*rad51*Δ MCW8156	++	Mar^{D155A}	TO1	Flanking	0μM	13	0.00 (±0.00)	$<0.001^{s}$	594.18 (±144.52)	$<0.001^{s}$	0.0 (±0.0)
*rad51*Δ *52*Δ MCW8160	++	Mar^{D155A}	TO1	Flanking	0μM	33	0.00 (±0.00)	$<0.001^{s}$	155.53 (±72.28)	$<0.001^{s}$	0.0 (±0.0)
*rad54*Δ MCW8165	++	Mar^{D155A}	TO1	Flanking	0μM	31	8.57 (±16.01)	$<0.001^{s}$	1054.26 (±259.51)	0.970^{s}	0.8 (±1.4)
*mus81*Δ MCW8308	++	Mar^{D155A}	TO1	Flanking	0μM	15	484.69 (±100.07)	0.010^{s}	1105.60 (±261.10)	0.079^{s}	30.8 (±5.9)
fml1Δ MCW8304	++	Mar^{D155A}	TO1	Flanking	0μM	14	99.45 (±31.95)	$<0.001^{s}$	599.05 (±115.85)	$<0.001^{s}$	14.5 (±4.6)
*swi1*Δ MCW7753	++	Mar^{D155A}	-	Flanking	0μM	6	5.85 (±2.51)	$<0.001^{r}$	15.24 (±4.40)	$<0.001^{r}$	27.8 (±11.2)
*swi1*Δ MCW7755	++	Mar^{D155A}	TO1	Flanking	0μM	21	596.25 (±169.80)	0.347^{s}	625.31 (±156.24)	$<0.001^{s}$	48.5 (±6.9)
*swi1*Δ MCW7757	++	Mar^{D155A}	TO2	Flanking	0μM	6	410.51 (±112.82)	0.006^{t}	873.05 (±201.26)	0.012^{t}	31.7 (±3.0)
pfh1-m21 MCW7762	++	Mar^{D155A}	-	Flanking	0μM	6	0.97 (±0.73)	0.129^{r}	1.86 (±0.86)	0.122^{r}	33.4 (±17.1)
pfh1-m21 MCW7763	++	Mar^{D155A}	TO1	Flanking	0μM	21	554.71 (±86.26)	0.066^{s}	2110.00 (±412.65)	$<0.001^{s}$	21.2 (±3.2)
pfh1-m21 MCW7766	++	Mar^{D155A}	TO2	Flanking	0μM	6	803.88 (±137.82)	0.614^{t}	2308.37 (±537.21)	$<0.001^{t}$	26.4 (±5.9)
elg1Δ MCW8038	++	Mar^{D155A}	-	Flanking	0μM	17	2.17 (±0.67)	0.012^{r}	3.24 (±1.01)	0.010^{r}	40.3 (±9.1)
elg1Δ MCW8040	++	Mar^{D155A}	TO1	Flanking	0μM	34	272.24 (±124.09)	$<0.001^{s}$	524.07 (±163.04)	$<0.001^{s}$	34.0 (±10.6)

wild-type MCW7500	-	-	TO1	0.2 kb downstream	0μM	8	0.42 (±0.15)	0.592[g]	1.76 (±0.44)	0.055[g]	19.5 (±6.0)
wild-type MCW7444	-	-	TO2	0.2 kb downstream	0μM	12	0.71 (±0.28)	<0.001[g]	1.54 (±0.24)	0.173[g]	30.8 (±8.3)
wild-type MCW7624	++	Mar^{D155A}	TO1	0.2 kb downstream	0μM	20	5.94 (±3.62)	<0.001[u]	34.24 (±12.32)	<0.001[u]	15.3 (±7.4)
wild-type MCW7622	++	Mar^{D155A}	TO2	0.2 kb downstream	0μM	12	8.31 (±5.80)	<0.001[v]	42.88 (±9.53)	<0.001[v]	15.4 (±8.1)
swi1Δ MCW8282	-	-	TO1	0.2 kb downstream	0μM	18	5.24 (±2.54)	<0.001[u]	21.96 (±5.33)	<0.001[u]	19.5 (±9.5)
swi1Δ MCW8284	++	Mar^{D155A}	TO1	0.2 kb downstream	0μM	25	15.78 (±11.70)	0.001[w]	167.35 (±59.59)	<0.001[w]	8.5 (±4.7)
swi1Δ ori-1253Δ MCW8496	-	-	TO1	0.2 kb downstream	0μM	16	22.35 (±12.73)	<0.001[u]	34.23 (±11.51)	<0.001[u]	38.7 (±13.9)
swi1Δ ori-1253Δ MCW8498	++	Mar^{D155A}	TO1	0.2 kb downstream	0μM	15	43.36 (±24.80)	<0.001[w]	128.49 (±38.39)	<0.001[w]	24.6 (±9.6)
wild-type MCW7229	-	-	-	12.4 kb downstream	0μM	11	0.37 (±0.29)	0.903[g]	0.49 (±0.22)	<0.001[g]	40.0 (±16.2)
wild-type MCW7733	++	Mar^{D155A}	TO1	12.4 kb downstream	0μM	11	7.22 (±6.01)	<0.001[x]	3.65 (±3.88)	<0.001[x]	60.1 (±35.9)
wild-type MCW7731	++	Mar^{D155A}	TO2	12.4 kb downstream	0μM	19	2.04 (±1.30)	0.001[x]	3.00 (±1.68)	0.014[x]	40.8 (±23.2)
wild-type ori-1253Δ MCW7737	++	Mar^{D155A}	TO1	12.4 kb downstream	0μM	19	0.43 (±0.27)	<0.001[y]	0.52 (±0.27)	0.001[y]	44.3 (±15.0)
wild-type ori-1253Δ MCW7736	++	Mar^{D155A}	TO2	12.4 kb downstream	0μM	15	0.73 (±0.41)	0.001[z]	1.00 (±0.49)	<0.001[z]	41.5 (±13.2)

§-Strain containing either the empty pREP41 plasmid or a pREP41 plasmid expressing the Mar protein as indicated; a-MarBl is expressed either from the *nmt41* (+) or *nmt1* (++) promoter; b-The strain contains Mar^{WT}, Mar^{D155A} or Mar^{V119G} protein generally expressed from an integrated copy unless otherwise indicated in the table; c-MarBl site is integrated at the *ade6* locus either between a direct repeat of *ade6*$^-$ alleles or replacing *ade6*. In strains without the binding site, the *ade6* gene is deleted from its normal locus. The binding site is integrated in either TO1 or TO2; d-The different positions of the *ade6*$^-$ direct repeat recombination reporters are

shown in Fig. 3.ii.; e-The values in parentheses are the standard deviations about the mean; f-*P* values are derived from independent-sample *t*-tests comparing the mean values as indicated; g-Compared to the equivalent mean recombinant frequency of MCW39; h-Compared to the equivalent mean recombinant frequency of MCW3118; i-Compared to the equivalent mean recombinant frequency of MCW3119; j-Compared to the equivalent mean recombinant frequency of MCW6480; k-Compared to the equivalent mean recombinant frequency of MCW6481; l-Compared to the equivalent mean recombinant frequency of MCW6487; m-Compared to the equivalent mean recombinant frequency of MCW6489; n-Compared to the equivalent mean recombinant frequency of MCW6482.
o-Compared to the equivalent mean recombinant frequency of MCW7096; p-Compared to the equivalent mean recombinant frequency of MCW7098; q-Compared to the equivalent mean recombinant frequency of MCW7099; r-Compared to the equivalent mean recombinant frequency of MCW8239; s-Compared to the equivalent mean recombinant frequency of MCW7076; t-Compared to the equivalent mean recombinant frequency of MCW7078; u-Compared to the equivalent mean recombinant frequency of MCW7500; v-Compared to the equivalent mean recombinant frequency of MCW7444; w-Compared to the equivalent mean recombinant frequency of MCW7624; x-Compared to the equivalent mean recombinant frequency of MCW7229; y-Compared to the equivalent mean recombinant frequency of MCW7733; z-Compared to the equivalent mean recombinant frequency of MCW7731.

Table 8-3: Direct repeat recombinant frequencies (MarBI live-cell imaging)

Genotype and Strain no.	P_{nmt} strength[a]	MarBI Protein[b]	MarBI Site[c]	$lacO^{115}$ Array[d]	LacI[e]	Rad52-YFP	Thiamine	Number of colonies analysed	$Ade^+ His^+$ recombinant frequency (x 10^{-4})[f]		$Ade^+ His^-$ recombinant frequency (x 10^{-4})[f]		% gene conversion[f]
									Mean	*P* value[g]	Mean	*P* value[g]	Mean
wild-type MCW39	-	-	-	-	-	-	0μM	20	0.38 (±0.19)		1.30 (±0.55)		29.4 (±5.9)
wild-type MCW3118	-	-	TO1				0μM	7	0.59 (±0.42)	0.062[h]	2.04 (±0.48)	0.006[h]	21.8 (±14.6)
wild-type MCW7226	-	-	TO1	+	-	-	0μM	11	0.29 (±0.14)	0.056[i]	5.01 (±0.69)	<0.001[i]	5.5 (±2.6)
wild-type MCW7470	-	-	TO1	+	+	-	0μM	9	0.14 (±0.12)	0.025[j]	6.00 (±1.36)	0.048[j]	2.4 (±2.2)
wild-type MCW7476	++	Mar^{WT}	TO1	+	-	-	0μM	24	354.16 (±99.13)	<0.001[k]	374.10 (±114.12)	<0.001[k]	48.8 (±9.1)
wild-type MCW7482	++	Mar^{WT}	TO1	+	+	-	0μM	11	307.14 (±28.63)	0.103[l]	357.26 (±73.11)	0.135[l]	46.6 (±5.4)
wild-type MCW7492	++	Mar^{WT}	-	+	+	+	0μM	11	0.57 (±0.38)	0.266[n]	1.34 (±0.72)	0.014[n]	30.4 (±14.1)
wild-type MCW7488	++	Mar^{WT}	TO1	+	+	+	0μM	12	273.31 (±79.16)	0.402[m]	296.55 (±105.49)	0.584[m]	48.6 (±8.9)
wild-type MCW7496	++	Mar^{WT}	TO2	+	+	+	0μM	12	318.35 (±91.34)	<0.001[o]	517.37 (±86.67)	<0.001[o]	37.8 (±7.2)
wild-type MCW7577	++	Mar^{D155A}	-	+	+	+	0μM	11	0.37 (±0.21)	0.040[p]	1.61 (±0.58)	0.037[p]	18.7 (±7.5)
wild-type MCW7573	++	Mar^{D155A}	TO1	+	+	+	0μM	10	254.55 (±63.37)	<0.001[q]	381.70 (±71.67)	<0.001[q]	39.9 (±7.8)
wild-type MCW7581	++	Mar^{D155A}	TO2	+	+	+	0μM	11	357.14 (±115.38)	<0.001[r]	369.67 (±122.68)	<0.001[r]	49.2 (±10.1)

a-MarBI is expressed from the *nmt1*(++) promoter integrated in the yeast genome; b-Strains contain either MarBI catalytically active (Mar^{WT}) or MarBI catalytically dead-D155A (Mar^{D155A}) protein as mentioned in the table; c-MarBI binding site is integrated at the *ade6* locus either between a direct repeat of *ade6*$^-$ alleles or replacing *ade6*. It is integrated in either TO1 or TO2; d-Strains with and without the 115 repeat *lacO* array positioned after the MarBI binding site; e-NLS-LacI-tdKatushka2 is expressed from the *nmt81* promoter integrated in the yeast genome; f-The values in parentheses are the standard deviations about the mean.

g-*P* values are derived from independent-sample *t*-tests comparing the mean values as indicated; h-Compared to the equivalent mean recombinant frequency of MCW39; i-Compared to the equivalent mean recombinant frequency of MCW3118; j-Compared to the equivalent mean recombinant frequency of MCW7226.
k-Compared to the equivalent mean recombinant frequency of MCW7470; l-Compared to the equivalent mean recombinant frequency of MCW7476; m-Compared to the equivalent mean recombinant frequency of MCW7482; n-Compared to the equivalent mean recombinant frequency of MCW6481; o-Compared to the equivalent mean recombinant frequency of MCW6489; p-Compared to the equivalent mean recombinant frequency of MCW8239; q-Compared to the equivalent mean recombinant frequency of MCW7076; r-Compared to the equivalent mean recombinant frequency of MCW7078.

Table 8-4: Direct repeat recombinant frequencies (TusB-TerB)

Genotype and Strain no.	P_{nmt} strength[a]	TusB Protein	TerB Site[b]	Thiamine	Number of colonies analysed	$Ade^+ His^+$ recombinant frequency (x 10^{-4})[c]		$Ade^+ His^-$ recombinant frequency (x 10^{-4})[c]		% gene conversion[c]
						Mean	*P* value[d]	Mean	*P* value[d]	Mean
wild-type MCW39	-	-	-	0μM	15	0.38 (±0.19)	-	1.30 (±0.55)	-	29.4 (±5.9)
wild-type MCW7528	++	+	-	0μM	10	0.24 (±0.12)	0.039[e]	1.19 (±0.39)	0.590[e]	17.5 (±8.9)
wild-type MCW7530	++	+	Orientation1	0μM	12	137.48 (±52.67)	<0.001[f]	237.55 (±69.70)	<0.001[f]	36.6 (±11.2)
wild-type MCW7532	++	+	Orientation2	0μM	15	319.10 (±78.06)	<0.001[f]	680.47 (±113.25)	<0.001[f]	31.8 (±4.5)

a-TusB is expressed from the nmt1(++) promoter integrated at the Lys1 locus in the yeast genome; b-TerB binding site is integrated at the ade6 locus between a direct repeat of ade6- alleles. It is integrated in either orientation1 or orientation2; c-The values in parentheses are the standard deviations about the mean; d-P values are derived from independent-sample t-tests comparing the mean values as indicated; e-Compared to the equivalent mean recombinant frequency of MCW39; f-Compared to the equivalent mean recombinant frequency of MCW7528.

Table 8-5: Direct repeat recombinant frequencies (origin deletion leading to spontaneous hyper-recombination)

Genotype/ Strain no.	Position of direct repeat relative to origin deleted[a]	direct- repeat reporter positioned on	Number of colonies analysed	$Ade^+ His^+$ recombinant frequency ($x 10^{-4}$)[b]		$Ade^+ His^-$ recombinant frequency ($x 10^{-4}$)[b]		% gene conversion[b]
				Mean	P value[c]	Mean	P value[c]	Mean
wild-type MCW8044	15.9 kb centromere proximal	ChrI (site VII)	16	2.10 (±1.17)	0.001[d]	13.81 (±5.35)	<0.001[d]	13.8 (±7.3)
*oril-4739*Δ MCW8238	15.9 kb centromere proximal	ChrI (site VII)	29	2.97 (±1.46)	0.048[g]	12.50 (±4.90)	0.412[g]	20.3 (±10.0)
wild-type MCW8045	20.8 kb centromere proximal	ChrII (site VI)	23	1.44 (±0.73)	0.064[d]	3.93 (±1.24)	<0.001[d]	27.1 (±10.8)
oriII-2319Δ MCW8057	20.8 kb centromere proximal	ChrII (site VI)	16	6.38 (±3.78)	<0.001[h]	27.70 (±9.59)	<0.001[h]	18.8 (±9.4)
oriIII-1253Δ MCW8243	20.8 kb centromere proximal	ChrII (site VI)	9	0.69 (±0.36)	0.006[h]	3.56 (±1.12)	0.453[h]	15.9 (±6.1)
wild-type MCW429	63.7 kb telomere proximal	ChrIII (site I)	20	1.10 (±0.37)	-	2.63 (±0.51)	-	29.4 (±5.9)
oriIII-1253Δ MCW7377	63.7 kb telomere proximal	ChrIII (site I)	11	1.23 (±0.58)	0.471[d]	2.80 (±0.59)	0.412[d]	29.81 (±9.32)
wild-type MCW7229	53.2 kb telomere proximal	ChrIII (site II)	22	0.90 (±0.53)	0.157[d]	1.17 (±0.95)	<0.001[d]	47.3 (±17.9)

oriIII-1253Δ MCW8241	53.2 kb telomere proximal	ChrIII (site II)	11	1.46 (±0.64)	0.012[e]	2.34 (±1.19)	0.004[e]	39.91 (±14.12)
wild-type MCW7430	9.9 kb centromere proximal	ChrIII (site IV)	30	1.09 (±0.47)	0.944[d]	2.28 (±0.64)	0.042[d]	32.0 (±10.3)
oriIII-1253Δ MCW7987	9.9 kb centromere proximal	ChrIII (site IV)	16	1.40 (±0.78)	0.064[f]	3.02 (±1.45)	0.014[f]	32.2 (±11.6)

a-The different positions of the *ade6*$^-$ direct repeat recombination reporter in relation to the origin with a strong firing efficiency that is deleted; b-The values in parentheses are the standard deviations about the mean; c-*P* values are derived from independent-sample *t*-tests comparing the mean values as indicated; d-Compared to the equivalent mean recombinant frequency of MCW429; e-Compared to the equivalent mean recombinant frequency of MCW7229; f-Compared to the equivalent mean recombinant frequency of MCW7430; g-Compared to the equivalent mean recombinant frequency of MCW8044; h-Compared to the equivalent mean recombinant frequency of MCW8045.

Table 8-6: List of *S. pombe* strains used in this study.

Strain number	Mating type	Genotype	Source	Method of construction
FO652	$h^{-\ smt0}$	ura4-D18 leu1-32 his3-D1 arg3-D4	Lab Strain	N.A.
FO656	h^{+}	ura4-D18 leu1-32 his3-D1 arg3-D4	Lab Strain	N.A.
FO672	$h^{-\ smt0}$	rad54Δ::ura4^{+} ura4-D18 leu1-32 his3-D1 arg3-D4	Lab Strain	N.A.
FO1237	h+	ade6-M375 ura4-D18 leu1-32 his3-D1 arg3^{+}	Lab Strain	N.A.
FO1236	$h^{-\ smt0}$	ade6-M375 ura4-D18 leu1-32 his3-D1 arg3^{+}	Lab Strain	N.A.
FO1457	$h^{-\ smt0}$	rad51Δ::arg3^{+} rad52Δ::ura4^{+} ura4-D18 leu1-32 his3-D1 arg3-D4	Lab Strain	N.A.
FO1458	h^{+}	rad51Δ::arg3^{+} rad52Δ::ura4 ura4-D18 leu1-32 his3-D1 arg3-D4	Lab Strain	N.A.
FO1470	$h^{-\ smt0}$	rad52Δ::kanMX6 ura4-D18 leu1-32 his3-D1 arg3-D4	Lab Strain	N.A.
FO1750	h+	srs2Δ::ura4^{+} ade6-M375 int::puc8/his3^{+}/RTS1-AO/ade6-L469 ura4-D18 leu1-32 his3-D1 arg3-D4	Lab Strain	N.A.
FO1836	$h^{-\ smt0}$	fbh1Δ::arg3^{+} ade6-M375 int::puc8/his3^{+}/RTS1-AO/ade6-L469 ura4-D18 leu1-32 his3-D1 arg3-D4	Lab Strain	N.A.
MCW39	$h^{-\ smt0}$	ade6-M375 int::puc8/his3^{+}/ade6-L469 ura4-D18 leu1-32 his3-D1 arg3-D4	Lab Strain	N.A.
MCW44	$h^{-\ smt0}$	leu1-32 his3-D1	Lab Strain	N.A.
MCW45	h^{+}	leu1-32 his3-D1	Lab Strain	N.A.
MCW428	$h^{-\ smt0}$	ade6-M375 int::puc8/his3^{+}/ade6-L469 ura4-D18 leu1-32 his3-D1 arg3-D4	Lab Strain	N.A.
MCW429	h^{+}	ade6-M375 int::puc8/his3^{+}/ade6-L469 ura4-D18 leu1-32 his3-D1 arg3-D4	Lab Strain	N.A.
MCW328	$h^{-\ smt0?}$	rad50Δ:: kanMX6 ura4-D18 leu1-32 his3-D1 arg3^{+}	Lab Strain	N.A.
MCW1016	$h^{-\ smt0}$	srs2Δ::ura4^{+} ura4D-18 leu1-32 his3-D1 arg3-D4	Lab Strain	N.A.
MCW1088	h^{+}	rad51Δ::arg3^{+} ura4-D18 leu1-32 his3-D1 arg3-D4	Lab Strain	N.A.
MCW1239	$h^{-\ smt0}$	rqh1Δ::ura4^{+} ura4-D18 leu1-32 his3-D1 arg3-D4	Lab Strain	N.A.
MCW1447	h^{+}	rqh1Δ::KanMX6 ade6-M375 int::puc8/his3^{+}/RTS1-AO/ade6-L469 ura4-D18 leu1-32 his3-D1 arg3-D4	Lab Strain	N.A.

MCW1452	$h^{?}$	mus81Δ::KanMX6 ade6-M375 int::puc8/his3^{+}/RTS1-AO/ade6-L469 ura4-D18 leu1-32 his3-D1 arg3-D4	Lab Strain	N.A.
MCW1691	h^{+}	rad51Δ::arg3^{+} ade6-M375 int::puc8/his3^{+}/RTS1-IO/ade6-L469 ura4-D18 leu1-32 his3-D1 arg3-D4	Lab Strain	N.A.
MCW1692	h^{+}	rad51Δ::arg3^{+} ade6-M375 int::puc8/his3^{+}/RTS1-AO/ade6-L469 ura4-D18 leu1-32 his3-D1 arg3-D4	Lab Strain	N.A.
MCW1695	h^{+}	rad52Δ::ura4^{+} rad51Δ::arg3+ ade6-M375 int::puc8/his3^{+}/RTS1-IO/ade6-L469 ura4-D18 leu1-32 his3-D1 arg3-D4	Lab Strain	N.A.
MCW1696	h^{+}	rad52Δ::ura4^{+} rad51Δ::arg3+ ade6-M375 int::puc8/his3^{+}/RTS1-AO/ade6-L469 ura4-D18 leu1-32 his3-D1 arg3-D4	Lab Strain	N.A.
MCW1714	h^{+}	ura4-D18 leu1-32 his3-D1 ade6-D1 arg3-D4	Lab Strain	N.A.
MCW2226	h^{+}	rad2Δ::leu2^{+} ade6-M375 int::puc8/his3^{+}/RTS1-AO/ade6-L469 ura4-D18 leu1-32 his3-D1 arg3-D4	Lab Strain	N.A.
MCW2429	$h^{-\ smt0}$	fml1Δ::natMX4 mus81Darg3+ ura4-D18 his3-D1 leu1-32 arg3-D4	Lab Strain	N.A.
MCW2656	h^{+}	rad54Δ::ura4^{+} ade6-M375 int::puc8/his3^{+}/RTS1-AO/ade6-L469 ura4-D18 leu1-32 his3-D1 arg3-D4	Lab Strain	N.A.
MCW2668	$h^{-\ smt0}$	swi1Δ::ura4^{+} ura4-D18 leu1-32 his3-D1 arg3-D4	Lab Strain	N.A.
MCW3061	h^{+}	fml1Δ::natMX4 ade6-M375 int::puc8/his3^{+}/RTS1-AO/ade6-L469 ura4-D18 leu1-32 his3-D1 arg3-D4	Lab Strain	N.A.
MCW3118	$h^{-\ smt0}$	ade6-M375 int::puc8/his3^{+}/TO1/ade6-L469 ura4-D18 leu1-32 his3-D1 arg3-D4	Lab Strain	N.A.
MCW3119	$h^{-\ smt0}$	pREP41+ ade6-M375 int::puc8/his3^{+}/TO1/ade6-L469 ura4-D18 leu1-32 his3-D1 arg3-D4	Lab Strain	N.A.
MCW3120	$h^{-\ smt0}$	pMW841+ ade6-M375 int::puc8/his3^{+}/TO1/ade6-L469 ura4-D18 leu1-32 his3-D1 arg3-D4	Lab Strain	N.A.
MCW3121	$h^{-\ smt0}$	pMW842+ ade6-M375 int::puc8/his3^{+}/TO1/ade6-L469 ura4-D18 leu1-32 his3-D1 arg3-D4	Lab Strain	N.A.
MCW3258	$h^{-\ smt0}$	ade6-M375 int::puc8/his3^{+}/TO2/ade6-L469 ura4-D18 leu1-32 his3-D1 arg3-D4	Lab Strain	N.A.
MCW3780	$h^{-\ smt0}$	rad8Δ::ura4+ ura4-D18 leu1-32 his3-D1 arg3-D4	Lab Strain	N.A.

MCW3864	h+	rad8Δ::ura4^{+} ade6-M375 int::puc8/his3^{+}/RTS1-AO/ade6-L469 ura4-D18 leu1-32 his3-D1 arg3-D4	Lab Strain	N.A.
MCW4712	h^{+}	ade6-M375 int::puc8/his3^{+}/RTS1-IO/ade6-L469 ura4-D18 leu1-32 his3-D1 arg3-D4	Lab Strain	N.A.
MCW4713	h^{+}	ade6-M375 int::puc8/his3^{+}/RTS1-AO/ade6-L469 ura4-D18 leu1-32 his3-D1 arg3-D4	Lab Strain	N.A.
MCW4934	h^{+}	leu1Δ::pJK148-leu1^{+}-pfh1-m21 pfh1Δ::KanMX6 ade6-M375 int::puc8/his3^{+}/ade6-L469 ura4-D18 leu1-32 his3-D1 arg3-D4	Lab Strain	N.A.
MCW4940	h^{+}	leu1Δ::pJK148-leu1^{+}-pfh1-m21 pfh1Δ::KanMX6 ade6-M375 int::puc8/his3^{+}/RTS1-IO/ade6-L469 ura4-D18 leu1-32 his3-D1 arg3-D4	Lab Strain	N.A.
MCW4942	h^{+}	leu1Δ::pJK148-leu1^{+}-pfh1-m21 pfh1Δ::KanMX6 ade6-M375 int::puc8/his3^{+}/RTS1-AO/ade6-L469 ura4-D18 leu1-32 his3-D1 arg3-D4	Lab Strain	N.A.
MCW4948	h^{+}	leu1Δ::pJK148-leu1^{+}-pfh1-mt* pfh1Δ::KanMX6 ade6-M375 int::puc8/his3^{+}/ade6-L469 ura4-D18 leu1-32 his3-D1 arg3-D4	Lab Strain	N.A.
MCW4954	h^{+}	leu1Δ::pJK148-leu1^{+}-pfh1-mt* pfh1Δ::KanMX6 ade6-M375 int::puc8/his3^{+}/RTS1-IO/ade6-L469 ura4-D18 leu1-32 his3-D1 arg3-D4	Lab Strain	N.A.
MCW4956	h^{+}	leu1Δ::pJK148-leu1^{+}-pfh1-mt* pfh1Δ::KanMX6 ade6-M375 int::puc8/his3^{+}/RTS1-AO/ade6-L469 ura4-D18 leu1-32 his3-D1 arg3-D4	Lab Strain	N.A.
MCW6370	h^{+}	lys1Δ::P$_{nmt41}$-NLS-MAR^{WT}-hphMX4 ura4-D18 leu1-32 his3-D1 arg3-D4	This study	AvrII linearised fragment from pMJ2 was integrated into FO656. Progeny was screened by auxotrophy and drug selection.
MCW6371	h^{+}	lys1Δ::P$_{nmt1}$-NLS-MAR^{WT}-hphMX4 ura4-D18 leu1-32 his3-D1 arg3-D4	This study	AvrII linearised fragment from pMJ5 was integrated into FO656. Progeny was screened by auxotrophy and drug selection.
MCW6372	h^{+}	lys1Δ::P$_{nmt41}$-NLS-MAR^{WT}-GFP-hphMX4 ura4-D18 leu1-32 his3-D1 arg3-D4	This study	AvrII linearised fragment from pMJ3 was integrated into FO656. Progeny was screened by auxotrophy and drug selection.

MCW6395	h^+	lys1Δ::P_{nmt41}-NLS-lacI-tdKatushka2-hphMX4 rad52Δ::rad52-YFP-kanMX6 ade6-M375 int::puc8/lacO^{115}/his3$^+$/RTS1-IO/ade6-L469 ura4-D18 leu1-32 his3-D1 arg3-D4	Lab Strain	N.A.
MCW6480	h^+	lys1Δ::P_{nmt41}-NLS-MAR^{WT}-hphMX4 ade6-M375 int::puc8/his3$^+$/ade6-L469 ura4-D18 leu1-32 his3-D1 arg3-D4	This study	MCW6370 X MCW429. Progeny was screened by auxotrophy and drug selection.
MCW6481	h^+	lys1Δ::P_{nmt1}-NLS-MAR^{WT}-hphMX4 ade6-M375 int::puc8/his3$^+$/ade6-L469 ura4-D18 leu1-32 his3-D1 arg3-D4	This study	MCW6371 X MCW429. Progeny was screened by auxotrophy and drug selection.
MCW6482	h^+	lys1Δ::P_{nmt41}-NLS-MAR^{WT}-GFP-hphMX4ade6-M375 int::puc8/his3$^+$/ade6-L469 ura4-D18 leu1-32 his3-D1 arg3-D4	This study	MCW6372 X MCW429. Progeny was screened by auxotrophy and drug selection.
MCW6483	h^+	lys1Δ::P_{nmt41}-NLS-MAR^{WT}-hphMX4 ade6-M375 int::puc8/his3$^+$/TO1/ade6-L469 ura4-D18 leu1-32 his3-D1 arg3-D4	This study	MCW6370 X MCW3118. Progeny was screened by auxotrophy and drug selection.
MCW6485	h^+	lys1Δ::P_{nmt41}-NLS-MAR^{WT}-hphMX4 ade6-M375 int::puc8/his3$^+$/TO2/ade6-L469 ura4-D18 leu1-32 his3-D1 arg3-D4	This study	MCW6370 X MCW3258. Progeny was screened by auxotrophy and drug selection.
MCW6487	h^+	lys1Δ::P_{nmt1}-NLS-MAR^{WT}-hphMX4 ade6-M375 int::puc8/his3$^+$/TO1/ade6-L469 ura4-D18 leu1-32 his3-D1 arg3-D4	This study	MCW6371 X MCW3118. Progeny was screened by auxotrophy and drug selection.
MCW6489	h^+	lys1Δ::P_{nmt1}-NLS-MAR^{WT}-hphMX4 ade6-M375 int::puc8/his3$^+$/TO2/ade6-L469 ura4-D18 leu1-32 his3-D1 arg3-D4	This study	MCW6371 X MCW3258. Progeny was screened by auxotrophy and drug selection.
MCW6492	$h^{-\ smt0}$	lys1Δ::P_{nmt41}-NLS-MAR^{WT}-GFP-hphMX4 ade6-M375 int::puc8/his3$^+$/TO1/ade6-L469 ura4-D18 leu1-32 his3-D1 arg3-D4	This study	MCW6372 X MCW3118. Progeny was screened by auxotrophy and drug selection.
MCW6494	$h^{-\ smt0}$	lys1Δ::P_{nmt41}-NLS-MAR^{WT}-GFP-hphMX4 ade6-M375 int::puc8/his3$^+$/TO2/ade6-L469 ura4-D18 leu1-32 his3-D1 arg3-D4	This study	MCW6372 X MCW3258. Progeny was screened by auxotrophy and drug selection.

MCW6556	h^+	lys1Δ::P_{nmt41}-NLS-lacI-tdKatushka2-hphMX4 rad52Δ::rad52-YFP-kanMX6 ade6-M375 int::puc8/lacO^{115}/his3$^+$/RTS1-AO/ade6-L469 ura4-D18 leu1-32 his3-D1 arg3-D4	Lab Strain	N.A.
MCW6626	h^+	lys1Δ::P_{nmt1}-NLS-MAR^{D155A}-hphMX4 ura4-D18 leu1-32 his3-D1 arg3-D4	This study	AvrII linearised fragment from pMJ13 was integrated into FO656. Progeny was screened by auxotrophy and drug selection.
MCW6627	h^+	lys1Δ::P_{nmt1}-NLS-MAR^{V119G}-hphMX4 ura4-D18 leu1-32 his3-D1 arg3-D4	This study	AvrII linearised fragment from pMJ14 was integrated into FO656. Progeny was screened by auxotrophy and drug selection.
MCW6630	$h^{-\ smt0}$	pMJ9+ ade6-M375 int::puc8/his3$^+$/TO1/ade6-L469 ura4-D18 leu1-32 his3-D1 arg3-D4	This study	MCW3118 transiently transformed with pMJ9. Progeny was screened by auxotrophy selection.
MCW6631	$h^{-\ smt0}$	pMJ10+ ade6-M375 int::puc8/his3$^+$/TO1/ade6-L469 ura4-D18 leu1-32 his3-D1 arg3-D4	This study	MCW3118 transiently transformed with pMJ10. Progeny was screened by auxotrophy selection.
MCW6775	$h^{-\ smt0}$	oriIII-1253Δ::natMX4 ura4-D18 leu1-32 his3-D1 arg3-D4	Lab Strain	N.A.
MCW6778	h^+	oriIII-1253Δ::natMX4 ade6-M375 int::puc8/his3$^+$/RTS1-AO/ade6-L469 ura4-D18 leu1-32 his3-D1 arg3-D4	Lab Strain	N.A.
MCW6847	h^+	rad51Δ::arg3$^+$ lys1Δ::P_{nmt1}-NLS-MAR^{WT}-hphMX4 ade6-M375 int::puc8/his3$^+$/TO1/ade6-L469 ura4-D18 leu1-32 his3-D1 arg3-D4	This study	MCW 6487 X FO1541. Progeny was screened by auxotrophy and drug selection. Confirmed by spot-assays to check for sensitivity to genotoxic stress.
MCW6849	h^+	rad51Δ::arg3$^+$ lys1Δ::P_{nmt1}-NLS-MAR^{WT}-hphMX4 ade6-M375 int::puc8/his3$^+$/TO2/ade6-L469 ura4-D18 leu1-32 his3-D1 arg3-D4	This study	MCW 6489 X FO1541. Progeny was screened by auxotrophy and drug selection. Confirmed by spot-assays to check for sensitivity to genotoxic stress.
MCW6851	h^+	fml1Δ::natMX4 lys1Δ::P_{nmt1}-NLS-MAR^{WT}-hphMX4 ade6-M375 int::puc8/his3$^+$/TO1/ade6-L469 ura4-D18 leu1-32 his3-D1 arg3-D4	This study	MCW 6487 X MCW 4172. Progeny was screened by auxotrophy and drug selection. Confirmed by spot-assays to check for sensitivity to genotoxic stress.
MCW6853	h^+	fml1Δ::natMX4 lys1Δ::P_{nmt1}-NLS-MAR^{WT}-hphMX4 ade6-M375 int::puc8/his3$^+$/TO2/ade6-L469 ura4-D18 leu1-32 his3-D1 arg3-D4	This study	MCW 6489 X MCW 4172. Progeny was screened by auxotrophy and drug selection. Confirmed by spot-assays to check for sensitivity to genotoxic stress.
MCW6928	$h^{-\ smt0}$	lys1Δ::P_{nmt81}-NLS-lacI-tdKatushka2-hphMX4 rad52Δ::rad52-YFP-kanMX6 ura4-D18 leu1-32 his3-D1 arg3-D4	This study	AvrII linearised fragment from pMJ22 was integrated into FO1751. Progeny was screened by auxotrophy and drug selection. LacI-tdKatushka2 expression confirmed by western blot.

MCW6929	h^+	ura4Δ:: P_{nmt1}-NLS-MAR^{WT} leu1-32 his3-D1	This study	AvrII-BlpI linearised fragment from pMJ23 was integrated into MCW45. Progeny was screened by auxotrophy selection. Confirmed by colony PCR using oMW757-oMW994.
MCW7075	h^+	lys1Δ::P_{nmt1}-NLS-MAR^{D155A}-hphMX4 ade6-M375 int::puc8/$his3^+$/ade6-L469 ura4-D18 leu1-32 his3-D1 arg3-D4	This study	MCW6626 X MCW429. Progeny was screened by auxotrophy and drug selection.
MCW7076	h^+	lys1Δ::P_{nmt1}-NLS-MAR^{D155A}-hphMX4 ade6-M375 int::puc8/$his3^+$/TO1/ade6-L469 ura4-D18 leu1-32 his3-D1 arg3-D4	This study	MCW6626 X MCW3118. Progeny was screened by auxotrophy and drug selection.
MCW7078	h^+	lys1Δ::P_{nmt1}-NLS-MAR^{D155A}-hphMX4 ade6-M375 int::puc8/$his3^+$/TO2/ade6-L469 ura4-D18 leu1-32 his3-D1 arg3-D4	This study	MCW6626 X MCW3258. Progeny was screened by auxotrophy and drug selection.
MCW7096	$h^{-\ smt0}$	ura4Δ:: P_{nmt1}-NLS-MAR^{WT} ade6-M375 int::puc8/$his3^+$/ade6-L469 leu1-32 his3-D1 arg3-D4	This study	MCW6929 X MCW428. Progeny was screened by auxotrophy selection and by colony PCR using oMW758- oMW1606 (~0.9 kb product).
MCW7098	$h^{-\ smt0}$	ura4Δ:: P_{nmt1}-NLS-MAR^{WT} ade6-M375 int::puc8/his3/ade6-L469 leu1-32 his3-D1 arg3-D4	This study	MCW6929 X MCW3118. Progeny was screened by auxotrophy selection and by colony PCR using oMW758- oMW1606 (~0.9 kb product).
MCW7099	$h^{-\ smt0}$	ura4Δ:: P_{nmt1}-NLS-MAR^{WT} ade6-M375 int::puc8/$his3^+$/TO2/ade6-L469 leu1-32 his3-D1 arg3-D4	This study	MCW6929 X MCW3258. Progeny was screened by auxotrophy selection and by colony PCR using oMW758- oMW1606 (~0.9 kb product).
MCW7129	h^+	rtf1Δ::$ura4^+$ ade6-M375 int::puc8/$his3^+$/ade6-L469 int::RTS1-IO-hphMX4(0.2 kb from ade6-M375) ura4-D18 leu1-32 his3-D1 arg3-D4	This study	SpeI-HindIII linearised fragment from pMJ20 was integrated into MCW6576. Progeny was screened by auxotrophy selection. Confirmed by colony PCR using oMW1603-oMW285.
MCW7130	h+	rtf1Δ::$ura4^+$ ade6-M375 int::puc8/$his3^+$/ade6-L469 int::RTS1-AO-hphMX4(0.2 kb from ade6-M375) ura4-D18 leu1-32 his3-D1 arg3-D4	This study	SpeI-HindIII linearised fragment from pMJ21 was integrated into MCW6576. Progeny was screened by auxotrophy selection. Confirmed by colony PCR using oMW1603-oMW285.
MCW7131	h^+	ade6-M375 int::puc8/$his3^+$/ade6-L469 int::RTS1-IO-hphMX4(0.2 kb from ade6-M375) ura4-D18 leu1-32 his3-D1 arg3-D4	This study	MCW7129 X FO652. Progeny was screened by auxotrophy and drug selection.

MCW7133	h^+	ade6-M375 int::puc8/his3$^+$/ade6-L469 int::RTS1-AO-hphMX4(0.2 kb from ade6-M375) ura4-D18 leu1-32 his3-D1 arg3-D4	This study	MCW7130 X FO652. Progeny was screened by auxotrophy and drug selection.
MCW7215	h^{-} smt0	rad54-GFP-kanMX6 ura4-D18 leu1-32 his3-D1 arg3-D4	Lab Strain	N.A.
MCW7223	h^{-} smt0	ade6Δ::RTS1-AO-hphMX4 ura4-D18 leu1-32 his3-D1 arg3-D4	This study	SpeI-HindIII linearised fragment from pMW921 was integrated into FO652. Progeny was screened by auxotrophy and drug selection. Confirmed by colony PCR using oMW1635-oMW285.
MCW7224	h^{-} smt0	ade6Δ::RTS1-IO-hphMX4 ura4-D18 leu1-32 his3-D1 arg3-D4	This study	SpeI-HindIII linearised fragment from pMW922 was integrated into FO652. Progeny was screened by auxotrophy and drug selection. Confirmed by colony PCR using oMW1635-oMW285.
MCW7225	h^+	(12.4 kb from ade6) int::adeM375-kanMX6 ura4-D18 leu1-32 his3-D1 arg3-D4 ade6D-1	This study	SpeI-PvuII linearised fragment from pMW923 was integrated into MCW1714. Progeny was screened by auxotrophy and drug selection. Confirmed by colony PCR using oMW1633-oMW285.
MCW7226	h^+	ade6-M375 int::puc8/lacO^{115}/his3$^+$/TO1/ade6-L469 ura4-D18 leu1-32 his3-D1 arg3-D4	This study	BlpI linearised fragment from pMJ25 was integrated into FO1237. Progeny was screened by auxotrophy selection.
MCW7227	h^+	ade6-M375 int::puc8/lacO^{115}/his3$^+$/ade6-L469 ura4-D18 leu1-32 his3-D1 arg3-D4	This study	BlpI linearised fragment from pMJ24 was integrated into FO1237. Progeny was screened by auxotrophy selection.
MCW7228	h^+	ade6-M375 int::puc8/lacO^{115}/his3$^+$/TO1/ade6-L469 ura4-D18 leu1-32 his3-D1 arg3-D4	This study	BlpI linearised fragment from pMJ26 was integrated into FO1237. Progeny was screened by auxotrophy selection.
MCW7229	h^+	(12.4 kb from ade6) int::ade6-L469/puc8/his3$^+$/ade6-M375/kanMX6 ura4-D18 leu1-32 his3-D1 arg3-D4 ade6D-1	This study	BlpI linearised fragment from pFOX2 was integrated into MCW7225. Progeny was screened by auxotrophy selection.
MCW7257	h^+	ade6Δ::RTS1-IO-hphMX4 (12.4 kb from ade6) int::ade6-L469/puc8/his3$^+$/ade6-M375/kanMX6 ura4-D18 leu1-32 his3-D1 arg3-D4	This study	MCW7229 X MCW7224. Progeny was screened by auxotrophy and drug selection. *RTS1* orientation confirmed by colony PCR using oMW1635-oMW721 and oMW1635-oMW722.
MCW7259	h^+	ade6Δ::RTS1-AO-hphMX4 (12.4 kb from ade6) int::ade6-L469/puc8/his3$^+$/ade6-M375/kanMX6 ura4-D18 leu1-32 his3-D1 arg3-D4	This study	MCW7229 X MCW7223. Progeny was screened by auxotrophy and drug selection. *RTS1* orientation confirmed by colony PCR using oMW1635-oMW721 and oMW1635-oMW722.

MCW7263	h^+	lys1Δ::P_{nmt81}-NLS-lacI-tdKatushka2-hphMX4 rad52Δ::rad52-YFP-kanMX6 ade6-M375 int::puc8/lacO^{115}/his3$^+$/TO1/ade6-L469 ura4-D18 leu1-32 his3-D1 arg3-D4	This study	MCW 7226 X MCW6928. Progeny was screened by auxotrophy and drug selection.
MCW7265	h^- smt0	lys1Δ::P_{nmt81}-NLS-lacI-tdKatushka2-hphMX4 rad52Δ::rad52-YFP-kanMX6 ade6-M375 int::puc8/lacO^{115}/his3$^+$/TO1/ade6-L469 ura4-D18 leu1-32 his3-D1 arg3-D4	This study	MCW7226 X MCW6928. Progeny was screened by auxotrophy and drug selection.
MCW7267	h^+	lys1Δ::P_{nmt81}-NLS-lacI-tdKatushka2-hphMX4 rad52Δ::rad52-YFP-kanMX6 ade6-M375 int::puc8/lacO^{115}/his3$^+$/ade6-L469 ura4-D18 leu1-32 his3-D1 arg3-D4	This study	MCW7227 X MCW6928. Progeny was screened by auxotrophy and drug selection.
MCW7270	h^- smt0	lys1Δ::P_{nmt81}-NLS-lacI-tdKatushka2-hphMX4 rad52Δ::rad52-YFP-kanMX6 ade6-M375 int::puc8/lacO^{115}/his3$^+$/ade6-L469 ura4-D18 leu1-32 his3-D1 arg3-D4	This study	MCW7227 X MCW6928. Progeny was screened by auxotrophy and drug selection.
MCW7271	h^+	lys1Δ::P_{nmt81}-NLS-lacI-tdKatushka2-hphMX4 rad52Δ::rad52-YFP-kanMX6 ade6-M375 int::puc8/lacO^{115}/his3$^+$/TO2/ade6-L469 ura4-D8 leu1-32 his3-D1 arg3-D4	This study	MCW7228 X MCW6928. Progeny was screened by auxotrophy and drug selection.
MCW7274	h^- smt0	lys1Δ::P_{nmt81}-NLS-lacI-tdKatushka2-hphMX4 rad52Δ::rad52-YFP-kanMX6 ade6-M375 int::puc8/lacO^{115}/his3$^+$/TO2/ade6-L469 ura4-D8 leu1-32 his3-D1 arg3-D4	This study	MCW7228 X MCW6928. Progeny was screened by auxotrophy and drug selection.
MCW7275	h^+	(140 kb from ade6) int::ade6-M375-kanMX6 ura4-D18 leu1-32 his3-D1 arg3-D4 ade6D-1	This study	SpeI-PvuII linearised fragment from pCB44 was integrated into MCW1714. Progeny was screened by auxotrophy and drug selection. Confirmed by colony PCR using oMW1634-oMW285.
MCW7277	h^- smt0	oriIII-1253Δ::natMX4 ade6:: RTS1-IO-hphMX4 ura4-D8 leu1-32 his3-D1 arg3-D4	This study	MCW6778 X MCW7224. Progeny was screened by auxotrophy and drug selection.
MCW7279	h^- smt0	oriIII-1253Δ::natMX4 ade6:: RTS1-AO-hphMX4 ura4-D8 leu1-32 his3-D1 arg3-D4	This study	MCW6778 X MCW7223. Progeny was screened by auxotrophy and drug selection.

MCW7293	h^+	oriIII-1253Δ::natMX4 ade6:: RTS1-IO-hphMX4 (12.4 kb from ade6) int::ade6-L469/puc8/his3$^+$/ade6-M375/kanMX6 ura4-D18 leu1-32 his3-D1 arg3-D4	This study	MCW7229 X MCW7257. Progeny was screened by auxotrophy and drug selection.
MCW7295	h^+	oriIII-1253Δ::natMX4 ade6:: RTS1-AO- hphMX4 (12.4 kb from ade6) int::ade6-L469/puc8/his3$^+$/ade6-M375/kanMX6 ura4-D18 leu1-32 his3-D1 arg3-D4	This study	MCW7229 X MCW7259. Progeny was screened by auxotrophy and drug selection.
MCW7297	h^+	(140 kb from ade6) int::ade6-L469/puc8/his3$^+$/ade6-M375/kanMX6 ura4-D18 leu1-32 his3-D1 arg3-D4 ade6D-1	This study	BlpI linearised fragment from pFOX2 was integrated into MCW7275. Progeny was screened by auxotrophy selection.
MCW7322	h^+	leu1Δ::pJK148-leu1$^+$-pfh1-m21 pfh1Δ::arg3$^+$ ura4-D18 leu1-32 his3-D1 arg3-D4	This study	Constructed by CAM.
MCW7324	h^+	leu1Δ::pJK148-leu1$^+$-pfh1-mt* pfh1Δ::arg3$^+$ ura4-D18 leu1-32 his3-D1 arg3-D4	This study	Constructed by CAM.
MCW7326	h^+	ade6Δ::RTS1-IO-hphMX4 (140 kb from ade6) int::ade6-L469/puc8/his3$^+$/ade6-M375/kanMX6 ura4-D18 leu1-32 his3-D1 arg3-D4	This study	MCW7297 X MCW7277. Progeny was screened by auxotrophy and drug selection.
MCW7328	h^+	ade6Δ::RTS1-AO-hphMX4 (140 kb from ade6) int::ade6-L469/puc8/his3$^+$/ade6-M375/kanMX6 ura4-D18 leu1-32 his3-D1 arg3-D4	This study	MCW7297 X MCW7279. Progeny was screened by auxotrophy and drug selection.
MCW7330	h^+	oriIII-1253Δ::natMX4 ade6Δ::RTS1-IO-hphMX4 (140 kb from ade6) int::ade6-L469/puc8/his3$^+$/ade6-M375/kanMX6 ura4-D18 leu1-32 his3-D1 arg3-D4	This study	MCW7297 X MCW7277. Progeny was screened by auxotrophy and drug selection.
MCW7332	h^+	oriIII-1253Δ::natMX4 ade6Δ::RTS1-AO-hphMX4 (140 kb from ade6) int::ade6-L469/puc8/his3$^+$/ade6-M375/kanMX6 ura4-D18 leu1-32 his3-D1 arg3-D4	This study	MCW7297 X MCW7279. Progeny was screened by auxotrophy and drug selection.
MCW7360	$h^{-\ smt0}$	rad51Δ::arg3$^+$ ade6Δ::RTS1-IO-hphMX4 ura4-D18 leu1-32 his3-D1 arg3-D4	This study	MCW7277 X MCW1088. Progeny was screened by auxotrophy and drug selection. Confirmed by spot-assays to check for sensitivity to genotoxic stress.
MCW7362	$h^{-\ smt0}$	rad51Δ::arg3$^+$ ade6Δ::RTS1-AO-hphMX4 ura4-D18 leu1-32 his3-D1 arg3-D4	This study	MCW7279 X MCW1088. Progeny was screened by auxotrophy and drug selection. Confirmed by spot-assays to check for sensitivity to genotoxic stress.
MCW7364	$h^{-\ smt0}$	rad51Δ::arg3$^+$ oriIII-1253Δ::natMX4 ade6Δ::RTS1-IO-hphMX4 ura4-D8 leu1-32 his3-D1 arg3-D4	This study	MCW7277 X MCW1088. Progeny was screened by auxotrophy and drug selection. Confirmed by spot-assays to check for sensitivity to genotoxic stress.

MCW7366	h$^{-\ smt0}$	rad51Δ::arg3^{+} oriIII-1253Δ::natMX4 ade6Δ::RTS1-AO-hphMX4 ura4-D8 leu1-32 his3-D1 arg3-D4	This study	MCW7279 X MCW1088. Progeny was screened by auxotrophy and drug selection. Confirmed by spot-assays to check for sensitivity to genotoxic stress.
MCW7368	h$^{-\ smt0}$	rad51Δ::arg3^{+} rad52Δ::ura4^{+} ade6Δ::RTS1-IO-hphMX4 ura4-D18 leu1-32 his3-D1 arg3-D4	This study	MCW7277 X FO1458. Progeny was screened by auxotrophy and drug selection. Confirmed by spot-assays to check for sensitivity to genotoxic stress.
MCW7370	h$^{-\ smt0}$	rad51Δ::arg3^{+} rad52Δ::ura4^{+} ade6Δ::RTS1-AO-hphMX4 ura4-D18 leu1-32 his3-D1 arg3-D4	This study	MCW7279 X FO1458. Progeny was screened by auxotrophy and drug selection. Confirmed by spot-assays to check for sensitivity to genotoxic stress.
MCW7372	h$^{-\ smt0}$	rad51Δ::arg3^{+} rad52Δ::ura4^{+} oriIII-1253Δ::natMX4 ade6Δ::RTS1-IO-hphMX4 ura4-D8 leu1-32 his3-D1 arg3-D4	This study	MCW7277 X FO1458. Progeny was screened by auxotrophy and drug selection. Confirmed by spot-assays to check for sensitivity to genotoxic stress.
MCW7374	h$^{-\ smt0}$	rad51Δ::arg3^{+} rad52Δ::ura4^{+} oriIII-1253Δ::natMX4 ade6Δ::RTS1-AO-hphMX4 ura4-D8 leu1-32 his3-D1 arg3-D4	This study	MCW7279 X FO1458. Progeny was screened by auxotrophy and drug selection. Confirmed by spot-assays to check for sensitivity to genotoxic stress.
MCW7377	h^{+}	oriIII-1253Δ::natMX4 ade6-M375 int::puc8/his3^{+}/ade6-L469 ura4-D18 leu1-32 his3-D1 arg3-D4	This study	MCW6775 X MCW429. Progeny was screened by auxotrophy and drug selection.
MCW7409	h^{+}	(35 kb from ade6) int::ade6-M375-kanMX6 ura4-D18 leu1-32 his3-D1 arg3-D4 ade6D-1	This study	SpeI-PvuII linearised fragment from pMJ33 was integrated into MCW1714. Progeny was screened by auxotrophy and drug selection. Confirmed by colony PCR using oMW1679-oMW716.
MCW7410	h^{+}	(75 kb from ade6) int::ade6-M375-kanMX6 ura4-D18 leu1-32 his3-D1 arg3-D4	This study	SpeI-PvuII linearised fragment from pMJ34 was integrated into MCW1714. Progeny was screened by auxotrophy and drug selection. Confirmed by colony PCR using oMW1677-oMW716.
MCW7414	h^{+}	oriIII-1253Δ::natMX4 ade6-M375 int::puc8/his3^{+}/ade6-L469 int::RTS1-IO-hphMX4(0.2 kb from ade6-M375) ura4-D18 leu1-32 his3-D1 arg3-D4	This study	MCW7131 X MCW6775. Progeny was screened by auxotrophy and drug selection.
MCW7415	h$^{-\ smt0}$	oriIII-1253Δ::natMX4 ade6-M375 int::puc8/his3^{+}/ade6-L469 int::RTS1-IO-hphMX4(0.2 kb from ade6-M375) ura4-D18 leu1-32 his3-D1 arg3-D4	This study	MCW7131 X MCW6775. Progeny was screened by auxotrophy and drug selection.
MCW7416	h^{+}	oriIII-1253Δ::natMX4 ade6-M375 int::puc8/his3^{+}/ade6-L469 int::RTS1-AO-hphMX4(0.2 kb from ade6-M375) ura4-D18 leu1-32 his3-D1 arg3-D4	This study	MCW7133 X MCW6775. Progeny was screened by auxotrophy and drug selection.

MCW7417	h$^{-\ smt0}$	oriIII-1253Δ::natMX4 ade6-M375 int::puc8/his3^{+}/ade6-L469 int::RTS1-AO-hphMX4(0.2 kb from ade6-M375) ura4-D18 leu1-32 his3-D1 arg3-D4	This study	MCW7133 X MCW6775. Progeny was screened by auxotrophy and drug selection.
MCW7418	h^{+}	lys1Δ::P$_{nmt1}$-NLS-TusB-hphMX4 ura4-D18 leu1-32 his3-D1 arg3-D4	This study	Constructed by MJK. AvrII linearised fragment from pMJK6 was integrated into FO656. Progeny was screened by auxotrophy and drug selection.
MCW7419	h$^{-\ smt0}$	ade6-M375 int::puc8/his3^{+}/6XTerB orientation1/ade6-L469 ura4-D18 leu1-32 his3-D1 arg3-D4	This study	Constructed by MJK. BlpI linearised fragment from pMJK1 was integrated into FO1236. Progeny was screened by auxotrophy selection.
MCW7420	h$^{-\ smt0}$	ura4Δ:: P$_{nmt1}$-NLS-MAR^{D155A} leu1-32 his3-D1	This study	Constructed by AF. AvrII-BlpI linearised fragment from pAF1 was integrated into MCW44. Progeny was screened by auxotrophy selection. Confirmed by colony PCR using oMW757-oMW994.
MCW7421	h^{+}	pfh1Δ::arg3^{+} leu1Δ::pJK148-leu1^{+}-pfh1-m21 ade6Δ::RTS1-IO-hphMX4 (12.4 kb from ade6) int::ade6-L469/puc8/his3^{+}/ade6-M375/kanMX6 ura4-D18 leu1-32 his3-D1 arg3-D4	This study	MCW7322 X MCW7293. Progeny was screened by auxotrophy and drug selection. Confirmed by spot-assays to check for sensitivity to genotoxic stress.
MCW7422	h^{+}	pfh1Δ::arg3^{+} leu1Δ::pJK148-leu1^{+}-pfh1-m21 ade6Δ::RTS1-AO-hphMX4 (12.4 kb from ade6) int::ade6-L469/puc8/his3^{+}/ade6-M375/kanMX6 ura4-D18 leu1-32 his3-D1 arg3-D4	This study	MCW7322 X MCW7293. Progeny was screened by auxotrophy and drug selection. Confirmed by spot-assays to check for sensitivity to genotoxic stress.
MCW7423	h^{+}	pfh1Δ::arg3^{+} leu1Δ::pJK148-leu1^{+}-pfh1-m21 oriIII-1253Δ::natMX4 ade6Δ::RTS1-IO-hphMX4 (12.4 kb from ade6) int::ade6-L469/puc8/his3^{+}/ade6-M375/kanMX6 ura4-D18 leu1-32 his3-D1 arg3-D4	This study	MCW7322 X MCW7295. Progeny was screened by auxotrophy and drug selection. Confirmed by spot-assays to check for sensitivity to genotoxic stress.
MCW7424	h^{+}	pfh1Δ::arg3^{+} leu1Δ::pJK148-leu1^{+}-pfh1-m21 oriIII-1253Δ::natMX4 ade6Δ::RTS1-AO-hphMX4 (12.4 kb from ade6) int::ade6-L469/puc8/his3^{+}/ade6-M375/kanMX6 ura4-D18 leu1-32 his3-D1 arg3-D4	This study	MCW7322 X MCW7295. Progeny was screened by auxotrophy and drug selection. Confirmed by spot-assays to check for sensitivity to genotoxic stress.
MCW7425	h^{+}	pfh1Δ::arg3^{+} leu1Δ::pJK148-leu1^{+}-pfh1-mt* ade6Δ::RTS1-IO-hphMX4 (12.4 kb from ade6) int::ade6-L469/puc8/his3^{+}/ade6-M375/kanMX6 ura4-D18 leu1-32 his3-D1 arg3-D4	This study	MCW7324 X MCW7293. Progeny was screened by auxotrophy and drug selection. Confirmed by spot-assays to check for sensitivity to genotoxic stress.

MCW7426	h^+	pfh1Δ::arg3$^+$ leu1Δ::pJK148-leu1$^+$-pfh1-mt* ade6Δ::RTS1-AO-hphMX4 (12.4 kb from ade6) int::ade6-L469/puc8/his3$^+$/ade6-M375/kanMX6 ura4-D18 leu1-32 his3-D1 arg3-D4	This study	MCW7324 X MCW7293. Progeny was screened by auxotrophy and drug selection. Confirmed by spot-assays to check for sensitivity to genotoxic stress.
MCW7427	$h^{-\ smt0}$	pfh1Δ::arg3$^+$ leu1Δ::pJK148-leu1$^+$-pfh1-mt* oriIII-1253Δ::natMX4 ade6Δ::RTS1-IO-hphMX4 (12.4 kb from ade6) int::ade6-L469/puc8/his3$^+$/ade6-M375/kanMX6 ura4-D18 leu1-32 his3-D1 arg3-D4	This study	MCW7324 X MCW7295. Progeny was screened by auxotrophy and drug selection. Confirmed by spot-assays to check for sensitivity to genotoxic stress.
MCW7428	$h^{-\ smt0}$	pfh1Δ::arg3$^+$ leu1Δ::pJK148-leu1$^+$-pfh1-mt* oriIII-1253Δ::natMX4 ade6Δ::RTS1-AO-hphMX4 (12.4 kb from ade6) int::ade6-L469/puc8/his3$^+$/ade6-M375/kanMX6 ura4-D18 leu1-32 his3-D1 arg3-D4	This study	MCW7324 X MCW7295. Progeny was screened by auxotrophy and drug selection. Confirmed by spot-assays to check for sensitivity to genotoxic stress.
MCW7429	h^+	(35 kb from ade6) int::ade6-L469/puc8/his3$^+$/ade6-M375/kanMX6 ura4-D18 leu1-32 his3-D1 arg3-D4 ade6D-1	This study	BlpI linearised fragment from pFOX2 was integrated into MCW7409. Progeny was screened by auxotrophy selection.
MCW7430	h^+	(75 kb from ade6) int::ade6-L469/puc8/his3$^+$/ade6-M375/kanMX6 ura4-D18 leu1-32 his3-D1 arg3-D4 ade6D-1	This study	BlpI linearised fragment from pFOX2 was integrated into MCW7410. Progeny was screened by auxotrophy selection.
MCW7431	h^+	(12.4 kb from ade6) int::ade6-L469/puc8/his3$^+$/Ter2X3 orientation1/ade6-M375/kanMX6 ura4-D18 leu1-32 his3-D1 arg3-D4 ade6D-1	This study	BlpI linearised fragment from pBU5 was integrated into MCW7225. Progeny was screened by auxotrophy selection.
MCW7432	h^+	(12.4 kb from ade6) int::ade6-L469/puc8/his3$^+$/Ter2X3 orientation2/ade6-M375/kanMX6 ura4-D18 leu1-32 his3-D1 arg3-D4 ade6D-1	This study	BlpI linearised fragment from pBU6 was integrated into MCW7225. Progeny was screened by auxotrophy selection.
MCW7433	h^+	(12.4 kb from ade6) int::ade6-L469/puc8/his3$^+$/tRNA^{GLU80}replication contra-directional orientation/ade6-M375/kanMX6 ura4-D18 leu1-32 his3-D1 arg3-D4 ade6D-1	This study	BlpI linearised fragment from pMW899 was integrated into MCW7225. Progeny was screened by auxotrophy selection.
MCW7434	h^+	(12.4 kb from ade6) int::ade6-L469/puc8/his3$^+$/tRNA^{GLU80}replication co-directional orientation/ade6-M375/kanMX6 ura4-D18 leu1-32 his3-D1 arg3-D4 ade6D-1	This study	BlpI linearised fragment from pMW905 was integrated into MCW7225. Progeny was screened by auxotrophy selection.

MCW7439	$h^{-\ smt0}$	ade6Δ::TO2-hphMX4 ura4-D18 leu1-32 his3-D1 arg3-D4	This study	Constructed by AF. SpeI-HindIII linearised fragment from pAF2 was integrated into FO652. Progeny was screened by auxotrophy and drug selection. Confirmed by colony PCR using oMW1635-oMW285.
MCW7440	$h^{-\ smt0}$	ade6Δ::TO1-hphMX4 ura4-D18 leu1-32 his3-D1 arg3-D4	This study	Constructed by AF. SpeI-HindIII linearised fragment from pAF3 was integrated into FO652. Progeny was screened by auxotrophy and drug selection. Confirmed by colony PCR using oMW1635-oMW285.
MCW7444	h^+	ade6-M375 int::puc8/his3$^+$/ade6-L469 int::TO2-hphMX4(0.2 kb from ade6-M375) ura4-D18 leu1-32 his3-D1 arg3-D4	This study	Constructed by AF. SpeI-HindIII linearised fragment from pAF4 was integrated into MCW429. Progeny was screened by auxotrophy selection. Confirmed by colony PCR using oMW1603- oMW285.
MCW7470	h^+	lys1Δ::P_{nmt81}-NLS-lacI-tdKatushka2-hphMX4 ade6-M375 int::puc8/lacO^{115}/his3$^+$/TO1/ade6-L469 ura4-D18 leu1-32 his3-D1 arg3-D4	This study	MCW7226 X MCW6928. Progeny was screened by auxotrophy and drug selection.
MCW7476	h^+	ura4Δ:: P_{nmt1}-NLS-MAR^{WT} ade6-M375 int::puc8/lacO^{115}/his3$^+$/TO1/ade6-L469 leu1-32 his3-D1 arg3-D4	This study	MCW7265 X MCW6929. Progeny was screened by auxotrophy and drug selection as well as by colony PCR for screening for *MAR^{WT}* using oMW758- oMW1606 (~0.9 kb product).
MCW7482	$h^{-\ smt0}$	ura4Δ:: P_{nmt1}-NLS-MAR^{WT} lys1Δ::P_{nmt81}-NLS-lacI-tdKatushka2-hphMX4 ade6-M375 int::puc8/lacO^{115}/his3$^+$/TO1/ade6-L469 leu1-32 his3-D1 arg3-D4	This study	MCW7265 X MCW6929. Progeny was screened by auxotrophy and drug selection as well as by colony PCR for screening for *MAR^{WT}* using oMW758- oMW1606 (~0.9 kb product).
MCW7488	h^+	ura4Δ:: P_{nmt1}-NLS-MAR^{WT} lys1Δ::P_{nmt81}-NLS-lacI-tdKatushka2-hphMX4 rad52Δ::rad52-YFP-KanMX6 ade6-M375 int::puc8/lacO^{115}/his3$^+$/TO1/ade6-L469 leu1-32 his3-D1 arg3-D4	This study	MCW7265 X MCW6929. Progeny was screened by auxotrophy and drug selection as well as by colony PCR for screening for *MAR^{WT}* using oMW758- oMW1606 (~0.9 kb product).
MCW7492	h^+	ura4Δ:: P_{nmt1}-NLS-MAR^{WT} lys1Δ::P_{nmt81}-NLS-lacI-tdKatushka2-hphMX4 rad52Δ::rad52-YFP-kanMX6 ade6-M375 int::puc8/lacO^{115}/his3$^+$/ade6-L469 leu1-32 his3-D1 arg3-D4	This study	MCW7270 X MCW6929. Progeny was screened by auxotrophy and drug selection as well as by colony PCR for screening for *MAR^{WT}* using oMW758- oMW1606 (~0.9 kb product).

MCW7496	h^+	ura4Δ:: P_{nmt1}-NLS-MAR^{WT} lys1Δ::P_{nmt81}-NLS-lacI-tdKatushka2-hphMX4 rad52Δ::rad52-YFP-kanMX6 ade6-M375 int::puc8/lacO^{115}/his3$^+$/TO2/ade6-L469 ura4-D8 leu1-32 his3-D1 arg3-D4	This study	MCW7274 X MCW6929. Progeny was screened by auxotrophy and drug selection as well as by colony PCR for screening for *MAR^{WT}* using oMW758- oMW1606 (~0.9 kb product).
MCW7500	h^+	ade6-M375 int::puc8/his3$^+$/ade6-L469 int::TO1-hphMX4(0.2 kb from ade6-M375) ura4-D18 leu1-32 his3-D1 arg3-D4	This study	Constructed by AF. SpeI-HindIII linearised fragment from pAF5 was integrated into MCW429. Progeny was screened by auxotrophy selection. Confirmed by colony PCR using oMW1603- oMW285.
MCW7507	h^+	ade6Δ::RTS1-IO-hphMX4 (12.4 kb from ade6) int::ade6-L469/puc8/his3$^+$/Ter2X3 orientation1/ade6-M375/kanMX6 ura4-D18 leu1-32 his3-D1 arg3-D4	This study	MCW7431 X MCW7224. Progeny was screened by auxotrophy and drug selection.
MCW7509	h^+	ade6Δ::RTS1-AO-hphMX4 (12.4 kb from ade6) int::ade6-L469/puc8/his3$^+$/Ter2X3 orientation1/ade6-M375/kanMX6 ura4-D18 leu1-32 his3-D1 arg3-D4	This study	MCW7431 X MCW7223. Progeny was screened by auxotrophy and drug selection.
MCW7511	h^+	ade6Δ::RTS1-IO-hphMX4 (12.4 kb from ade6) int::ade6-L469/puc8/his3$^+$/Ter2X3 orientation2/ade6-M375/kanMX6 ura4-D18 leu1-32 his3-D1 arg3-D4	This study	MCW7432 X MCW7224. Progeny was screened by auxotrophy and drug selection.
MCW7513	h^+	ade6Δ::RTS1-AO-hphMX4 (12.4 kb from ade6) int::ade6-L469/puc8/his3$^+$/Ter2X3 orientation2/ade6-M375/kanMX6 ura4-D18 leu1-32 his3-D1 arg3-D4	This study	MCW7432 X MCW7223. Progeny was screened by auxotrophy and drug selection.
MCW7515	h^+	ade6Δ::RTS1-IO-hphMX4 (12.4 kb from ade6) int::ade6-L469/puc8/his3$^+$/tRNA^{GLU80}replication contra-directional orientation/ade6-M375/kanMX6 ura4-D18 leu1-32 his3-D1 arg3-D4	This study	MCW7433 X MCW7224. Progeny was screened by auxotrophy and drug selection.
MCW7517	h^+	ade6Δ::RTS1-AO-hphMX4 (12.4 kb from ade6) int::ade6-L469/puc8/his3$^+$/tRNA^{GLU80}replication contra-directional orientation/ade6-M375/kanMX6 ura4-D18 leu1-32 his3-D1 arg3-D4	This study	MCW7433 X MCW7223. Progeny was screened by auxotrophy and drug selection.
MCW7519	h^+	ade6Δ::RTS1-IO-hphMX4 (12.4 kb from ade6) int::ade6-L469/puc8/his3$^+$/tRNA^{GLU80}replication co-directional orientation/ade6-M375/kanMX6 ura4-D18 leu1-32 his3-D1 arg3-D4	This study	MCW7434 X MCW7224. Progeny was screened by auxotrophy and drug selection.

MCW7521	h^+	ade6Δ::RTS1-AO-hphMX4 (12.4 kb from ade6) int::ade6-L469/puc8/his3$^+$/tRNA^{GLU80}replication co-directional orientation/ade6-M375/kanMX6 ura4-D18 leu1-32 his3-D1 arg3-D4	This study	MCW7434 X MCW7223. Progeny was screened by auxotrophy and drug selection.
MCW7523	h^+	lys1Δ::P$_{nmt1}$-NLS-MAR^{D155A}-ura4$^+$ ura4-D18 leu1-32 his3-D1 arg3-D4	This study	BamHI-EcoRI linearised fragment from pALO67 was used to marker swap the hphMX4 cassette in MCW6626. Progeny was screened by auxotrophy and drug selection.
MCW7524	h^{-} smt0	lys1Δ::P$_{nmt1}$-NLS-MAR^{D155A}-ura4$^+$ura4-D18 leu1-32 his3-D1 arg3-D4	This study	MCW7523 X MCW6775. Progeny was screened by auxotrophy and drug selection.
MCW7527	h^{-} smt0	ade6-M375 int::puc8/his3$^+$/6XTerB orientation2/ade6-L469 ura4-D18 leu1-32 his3-D1 arg3-D4	This study	Constructed by MJK. BlpI linearised fragment from pMJK2 was integrated into FO1236. Progeny was screened by auxotrophy selection.
MCW7528	h^+	lys1Δ::P$_{nmt1}$-NLS-TusB-hphMX4 ade6-M375 int::puc8/his3$^+$/ade6-L469 ura4-D18 leu1-32 his3-D1 arg3-D4	This study	MCW428 X MCW7418. Progeny was screened by auxotrophy and drug selection.
MCW7530	h^+	lys1Δ::P$_{nmt1}$-NLS-TusB-hphMX4 ade6-M375 int::puc8/his3$^+$/6XTerB orientation1/ade6-L469 ura4-D18 leu1-32 his3-D1 arg3-D4	This study	MCW7419 X MCW7418. Progeny was screened by auxotrophy and drug selection.
MCW7532	h^+	lys1Δ::P$_{nmt1}$-NLS-TusB-hphMX4 ade6-M375 int::puc8/his3$^+$/6XTerB orientation2/ade6-L469 ura4-D18 leu1-32 his3-D1 arg3-D4	This study	MCW7527 X MCW7418. Progeny was screened by auxotrophy and drug selection.
MCW7540	h^+	ade6Δ::TO1-hphMX4 lys1Δ::P$_{nmt1}$-NLS-MAR^{D155A}-ura4$^+$ ura4-D18 leu1-32 his3-D1 arg3-D4	This study	MCW7440 X MCW7525. Progeny was screened by auxotrophy and drug selection.
MCW7541	h^{-} smt0	ade6Δ::TO1-hphMX4 lys1Δ::P$_{nmt1}$-NLS-MAR^{D155A}-ura4$^+$ ura4-D18 leu1-32 his3-D1 arg3-D4	This study	MCW7440 X MCW7525. Progeny was screened by auxotrophy and drug selection.
MCW7543	h^{-} smt0	oriIII-1253Δ::natMX4 ade6Δ::TO2-hphMX4 lys1Δ::P$_{nmt1}$-NLS-MAR^{D155A}-ura4$^+$ ura4-D18 leu1-32 his3-D1 arg3-D4	This study	MCW7439 X MCW7525. Progeny was screened by auxotrophy and drug selection.
MCW7545	h^{-} smt0	oriIII-1253Δ::natMX4 ade6Δ::TO1-hphMX4 lys1Δ::P$_{nmt1}$-NLS-MAR^{D155A}-ura4$^+$ ura4-D18 leu1-32 his3-D1 arg3-D4	This study	MCW7440 X MCW7525. Progeny was screened by auxotrophy and drug selection.
MCW7565	h^+	ade6Δ::RTS1-IO-hphMX4 (35 kb from ade6) int::ade6-L469/puc8/his3$^+$/ade6-M375/kanMX6 ura4-D18 leu1-32 his3-D1 arg3-D4	This study	MCW7429 X MCW7277. Progeny was screened by auxotrophy and drug selection.

MCW7567	h^+	ade6Δ::RTS1-AO-hphMX4 (35 kb from ade6) int::ade6-L469/puc8/his3$^+$/ade6-M375/kanMX6 ura4-D18 leu1-32 his3-D1 arg3-D4	This study	MCW7429 X MCW7279. Progeny was screened by auxotrophy and drug selection.
MCW7573	h^+	ura4Δ:: P_{nmt1}-NLS-MAR^{D155A} lys1Δ::P_{nmt81}-NLS-lacI-tdKatushka2-hphMX4 rad52Δ::rad52-YFP-kanMX6 ade6-M375 int::puc8/lacO^{115}/his3$^+$/TO1/ade6-L469 leu1-32 his3-D1 arg3-D4	This study	MCW7263 X MCW7420. Progeny was screened by auxotrophy and drug selection as well as by colony PCR for screening for *MAR^{D155A}* using oMW758- oMW1606 (~0.9 kb product).
MCW7574	h^+	ura4Δ:: P_{nmt1}-NLS-MAR^{D155A} lys1Δ::P_{nmt81}-NLS-lacI-tdKatushka2-hphMX4 rad52Δ::rad52-YFP-kanMX6 ade6-M375 int::puc8/lacO^{115}/his3$^+$/TO1/ade6-L469 leu1-32 his3-D1 arg3-D4	This study	MCW7263 X MCW7420. Progeny was screened by auxotrophy and drug selection as well as by colony PCR for screening for *MAR^{D155A}* using oMW758- oMW1606 (~0.9 kb product).
MCW7577	h^+	ura4Δ:: P_{nmt1}-NLS-MAR^{D155A} lys1Δ::P_{nmt81}-NLS-lacI-tdKatushka2-hphMX4 rad52Δ::rad52-YFP-kanMX6 ade6-M375 int::puc8/lacO^{115}/his3$^+$/ade6-L469 leu1-32 his3-D1 arg3-D4	This study	MCW7267 X MCW7420. Progeny was screened by auxotrophy and drug selection as well as by colony PCR for screening for *MAR^{D155A}* using oMW758- oMW1606 (~0.9 kb product).
MCW7578	h^+	ura4Δ:: P_{nmt1}-NLS-MAR^{D155A} lys1Δ::P_{nmt81}-NLS-lacI-tdKatushka2-hphMX4 rad52Δ::rad52-YFP-kanMX6 ade6-M375 int::puc8/lacO^{115}/his3$^+$/ade6-L469 leu1-32 his3-D1 arg3-D4	This study	MCW7267 X MCW7420. Progeny was screened by auxotrophy and drug selection as well as by colony PCR for screening for *MAR^{D155A}* using oMW758- oMW1606 (~0.9 kb product).
MCW7581	h^+	ura4Δ:: P_{nmt1}-NLS-MAR^{D155A} lys1Δ::P_{nmt81}-NLS-lacI-tdKatushka2-hphMX4 rad52Δ::rad52-YFP-kanMX6 ade6-M375 int::puc8/lacO^{115}/his3$^+$/TO2/ade6-L469 leu1-32 his3-D1 arg3-D4	This study	MCW7271 X MCW7420. Progeny was screened by auxotrophy and drug selection as well as by colony PCR for screening for *MAR^{D155A}* using oMW758- oMW1606 (~0.9 kb product).
MCW7582	h^+	ura4Δ:: P_{nmt1}-NLS-MAR^{D155A} lys1Δ::P_{nmt81}-NLS-lacI-tdKatushka2-hphMX4 rad52Δ::rad52-YFP-kanMX6 ade6-M375 int::puc8/lacO^{115}/his3$^+$/TO2/ade6-L469 leu1-32 his3-D1 arg3-D4	This study	MCW7271 X MCW7420. Progeny was screened by auxotrophy and drug selection as well as by colony PCR for screening for *MAR^{D155A}* using oMW758- oMW1606 (~0.9 kb product).
MCW7585	$h^{-\ smt0}$	elg1Δ::natMX4 ura4-D18 leu1-32 his3-D1 arg3-D4	Lab Strain	N.A.
MCW7598	h^+	pfh1Δ::arg3$^+$ leu1Δ::pJK148-leu1$^+$-pfh1-m21 oriIII-1253Δ::natMX4 ade6-M375 int::puc8/his3$^+$/ade6-L469 int::RTS1-IO-hphMX4(0.2 kb from ade6-M375) ura4-D18 leu1-32 his3-D1 arg3-D4	This study	Constructed by FK and FO. MCW7322 X MCW7415. Progeny was screened by auxotrophy and drug selection. Confirmed by spot-assays to check for sensitivity to genotoxic stress.

MCW7599	h$^{-\ smt0}$	pfh1Δ::arg3^{+} leu1Δ::pJK148-leu1^{+}-pfh1-m21 ade6-M375 int::puc8/his3^{+}/ade6-L469 int::RTS1-IO-hphMX4(0.2 kb from ade6-M375) ura4-D18 leu1-32 his3-D1 arg3-D4	This study	Constructed by FK and FO. MCW7322 X MCW7415. Progeny was screened by auxotrophy and drug selection. Confirmed by spot-assays to check for sensitivity to genotoxic stress.
MCW7600	h^{+}	pfh1Δ::arg3^{+} leu1Δ::pJK148-leu1^{+}-pfh1-m21 oriIII-1253Δ::natMX4 ade6-M375 int::puc8/his3^{+}/ade6-L469 int::RTS1-AO-hphMX4(0.2 kb from ade6-M375) ura4-D18 leu1-32 his3-D1 arg3-D4	This study	Constructed by FK and FO. MCW7322 X MCW7417. Progeny was screened by auxotrophy and drug selection. Confirmed by spot-assays to check for sensitivity to genotoxic stress.
MCW7601	h^{+}	pfh1Δ::arg3^{+} leu1Δ::pJK148-leu1^{+}-pfh1-m21 ade6-M375 int::puc8/his3^{+}/ade6-L469 int::RTS1-AO-hphMX4(0.2 kb from ade6-M375) ura4-D18 leu1-32 his3-D1 arg3-D4	This study	Constructed by FK and FO. MCW7322 X MCW7417. Progeny was screened by auxotrophy and drug selection. Confirmed by spot-assays to check for sensitivity to genotoxic stress.
MCW7602	h^{+}	pfh1Δ::arg3^{+} leu1Δ::pJK148-leu1^{+}-pfh1-mt* oriIII-1253Δ::natMX4 ade6-M375 int::puc8/his3^{+}/ade6-L469 int::RTS1-IO-hphMX4(0.2 kb from ade6-M375) ura4-D18 leu1-32 his3-D1 arg3-D4	This study	Constructed by FK and FO. MCW7325 X MCW7415. Progeny was screened by auxotrophy and drug selection. Confirmed by spot-assays to check for sensitivity to genotoxic stress.
MCW7603	h^{+}	pfh1Δ::arg3^{+} leu1Δ::pJK148-leu1^{+}-pfh1-mt* ade6-M375 int::puc8/his3^{+}/ade6-L469 int::RTS1-IO-hphMX4(0.2 kb from ade6-M375) ura4-D18 leu1-32 his3-D1 arg3-D4	This study	Constructed by FK and FO. MCW7325 X MCW7415. Progeny was screened by auxotrophy and drug selection. Confirmed by spot-assays to check for sensitivity to genotoxic stress.
MCW7604	h^{+}	pfh1Δ::arg3^{+} leu1Δ::pJK148-leu1^{+}-pfh1-mt* oriIII-1253Δ::natMX4 ade6-M375 int::puc8/his3^{+}/ade6-L469 int::RTS1-AO-hphMX4(0.2 kb from ade6-M375) ura4-D18 leu1-32 his3-D1 arg3-D4	This study	Constructed by FK and FO. MCW7325 X MCW7417. Progeny was screened by auxotrophy and drug selection. Confirmed by spot-assays to check for sensitivity to genotoxic stress.
MCW7605	h^{+}	pfh1Δ::arg3^{+} leu1Δ::pJK148-leu1^{+}-pfh1-mt* ade6-M375 int::puc8/his3^{+}/ade6-L469 int::RTS1-AO-hphMX4(0.2 kb from ade6-M375) ura4-D18 leu1-32 his3-D1 arg3-D4	This study	Constructed by FK and FO. MCW7325 X MCW7417. Progeny was screened by auxotrophy and drug selection. Confirmed by spot-assays to check for sensitivity to genotoxic stress.
MCW7614	h^{+}	ade6Δ::RTS1-IO-hphMX4 (75 kb from ade6) int::ade6-L469/puc8/his3^{+}/ade6-M375/kanMX6 ura4-D18 leu1-32 his3-D1 arg3-D4	This study	MCW7430 X MCW7277. Progeny was screened by auxotrophy and drug selection.
MCW7616	h^{+}	ade6Δ::RTS1-AO-hphMX4 (75 kb from ade6) int::ade6-L469/puc8/his3^{+}/ade6-M375/kanMX6 ura4-D18 leu1-32 his3-D1 arg3-D4	This study	MCW7430 X MCW7279. Progeny was screened by auxotrophy and drug selection.

MCW7620	h^+	oriIII-1253Δ::natMX4 ade6Δ::RTS1-AO-hphMX4 (75 kb from ade6) int::ade6-L469/puc8/his3$^+$/ade6-M375/kanMX6 ura4-D18 leu1-32 his3-D1 arg3-D4	This study	MCW7430 X MCW7279. Progeny was screened by auxotrophy and drug selection.
MCW7622	h+	lys1Δ::P_{nmt1}-NLS-MAR^{D155A}-ura4$^+$ ade6-M375 int::puc8/his3$^+$/ade6-L469 int::TO2-hphMX4(0.2 kb from ade6-M375) ura4-D18 leu1-32 his3-D1 arg3-D4	This study	MCW7444 X MCW7524. Progeny was screened by auxotrophy and drug selection.
MCW7624	h^+	lys1Δ::P_{nmt1}-NLS-MAR^{D155A}-ura4$^+$ ade6-M375 int::puc8/his3$^+$/ade6-L469 int::TO1-hphMX4(0.2 kb from ade6-M375) ura4-D18 leu1-32 his3-D1 arg3-D4	This study	MCW7500 X MCW7524. Progeny was screened by auxotrophy and drug selection.
MCW7704	h^+	tid1Δ::ura4$^+$ ade6-M375 int::puc8/his3$^+$/RTS1-AO/ade6-L469 ura4-D18 leu1-32 his3-D1 arg3-D4	Lab Strain	Constructed by FK
MCW7708	h^+	elg1Δ::natMX4 ade6-M375 int::puc8/his3$^+$/RTS1-AO/ade6-L469 ura4-D18 leu1-32 his3-D1 arg3-D4	Lab Strain	Constructed by FO
MCW7731	h^+	ade6Δ::TO2-hphMX4 lys1Δ::P_{nmt1}-NLS-MAR^{D155A}-ura4$^+$ (12.4 kb from ade6) int::ade6-L469/puc8/his3$^+$/ade6-M375/kanMX6 ura4-D18 leu1-32 his3-D1 arg3-D4	This study	MCW7543 X MCW7229. Progeny was screened by auxotrophy and drug selection.
MCW7733	h^+	ade6Δ::TO1-hphMX4 lys1Δ::P_{nmt1}-NLS-MAR^{D155A}-ura4$^+$ (12.4 kb from ade6) int::ade6-L469/puc8/his3$^+$/ade6-M375/kanMX6 ura4-D18 leu1-32 his3-D1 arg3-D4	This study	MCW7545 X MCW7229. Progeny was screened by auxotrophy and drug selection.
MCW7735	h^+	oriIII-1253Δ::natMX4 ade6Δ::TO2-hphMX4 lys1Δ::P_{nmt1}-NLS-MAR^{D155A}-ura4$^+$ (12.4 kb from ade6) int::ade6-L469/puc8/his3$^+$/ade6-M375/kanMX6 ura4-D18 leu1-32 his3-D1 arg3-D4	This study	MCW7543 X MCW7229. Progeny was screened by auxotrophy and drug selection.
MCW7737	h^+	oriIII-1253Δ::natMX4 ade6Δ::TO1-hphMX4 lys1Δ::P_{nmt1}-NLS-MAR^{D155A}-ura4$^+$ (12.4 kb from ade6) int::ade6-L469/puc8/his3$^+$/ade6-M375/kanMX6 ura4-D18 leu1-32 his3-D1 arg3-D4	This study	MCW7545 X MCW7229. Progeny was screened by auxotrophy and drug selection.
MCW7751	h^+	rnh201Δ::KanMX6 cdc20-M603F::lox ade6-704 leu1-32 ura4-D18	Daigaku et al., 2015	N.A.
MCW7752	h^+	rnh201Δ::KanMX6 cdc6-L591G::lox ade6-704 leu1-32 ura4-D18	Daigaku et al., 2015	N.A.
MCW7753	h^+	swi1Δ::ura4$^+$ lys1Δ::P_{nmt1}-NLS-MAR^{D155A}-hphMX4 ade6-M375 int::puc8/his3$^+$/ade6-L469 ura4-D18 leu1-32 his3-D1 arg3-D4	This study	MCW2668 X MCW7075. Progeny was screened by auxotrophy and drug selection. Confirmed by spot-assays to check for sensitivity to genotoxic stress.

MCW7755	h^+	swi1Δ::ura4$^+$ lys1Δ::P_{nmt1}-NLS-MAR^{D155A}-hphMX4 ade6-M375 int::puc8/his3$^+$/TO1/ade6-L469 ura4-D18 leu1-32 his3-D1 arg3-D4	This study	MCW2668 X MCW7076. Progeny was screened by auxotrophy and drug selection. Confirmed by spot-assays to check for sensitivity to genotoxic stress.
MCW7757	h^+	swi1Δ::ura4$^+$ lys1Δ::P_{nmt1}-NLS-MAR^{D155A}-hphMX4 ade6-M375 int::puc8/his3$^+$/TO2/ade6-L469 ura4-D18 leu1-32 his3-D1 arg3-D4	This study	MCW2668 X MCW7078. Progeny was screened by auxotrophy and drug selection. Confirmed by spot-assays to check for sensitivity to genotoxic stress.
MCW7761	h^+	pfh1Δ::arg3$^+$ leu1Δ::pJK148-leu1$^+$-pfh1- lys1Δ::P_{nmt1}-NLS-MAR^{D155A}-hphMX4 ade6-M375 int::puc8/his3$^+$/ade6-L469 ura4-D18 leu1-32 his3-D1 arg3-D4	This study	MCW7322 X MCW3118. Progeny was screened by auxotrophy and drug selection. Confirmed by spot-assays to check for sensitivity to genotoxic stress.
MCW7762	h^+	pfh1Δ::arg3$^+$ leu1Δ::pJK148-leu1$^+$-pfh1-m21 lys1Δ::P_{nmt1}-NLS-MAR^{D155A}-hphMX4 ade6-M375 int::puc8/his3$^+$/ade6-L469 ura4-D18 leu1-32 his3-D1 arg3-D4	This study	MCW7322 X MCW3118. Progeny was screened by auxotrophy and drug selection. Confirmed by spot-assays to check for sensitivity to genotoxic stress.
MCW7763	h^+	pfh1Δ::arg3$^+$ leu1Δ::pJK148-leu1$^+$-pfh1- lys1Δ::P_{nmt1}-NLS-MAR^{D155A}-hphMX4 ade6-M375 int::puc8/his3$^+$/TO1/ade6-L469 ura4-D18 leu1-32 his3-D1 arg3-D4	This study	MCW7322 X MCW7077. Progeny was screened by auxotrophy and drug selection. Confirmed by spot-assays to check for sensitivity to genotoxic stress.
MCW7764	h^+	pfh1Δ::arg3$^+$ leu1Δ::pJK148-leu1$^+$-pfh1-m21 lys1Δ::P_{nmt1}-NLS-MAR^{D155A}-hphMX4 ade6-M375 int::puc8/his3$^+$/TO1/ade6-L469 ura4-D18 leu1-32 his3-D1 arg3-D4	This study	MCW7322 X MCW7077. Progeny was screened by auxotrophy and drug selection. Confirmed by spot-assays to check for sensitivity to genotoxic stress.
MCW7766	h^+	pfh1Δ::arg3$^+$ leu1Δ::pJK148-leu1$^+$-pfh1-m21 lys1Δ::P_{nmt1}-NLS-MAR^{D155A}-hphMX4 ade6-M375 int::puc8/his3$^+$/TO2/ade6-L469 ura4-D18 leu1-32 his3-D1 arg3-D4	This study	MCW7322 X MCW7079. Progeny was screened by auxotrophy and drug selection. Confirmed by spot-assays to check for sensitivity to genotoxic stress.
MCW7812	h^+	rad51Δ::arg3$^+$ ade6Δ::RTS1-IO-hphMX4 (12.4 kb from ade6) int::ade6-L469/puc8/his3$^+$/ade6-M375/kanMX6 ura4-D18 leu1-32 his3-D1 arg3-D4	This study	MCW7372 X MCW7229. Progeny was screened by auxotrophy and drug selection. Confirmed by spot-assays to check for sensitivity to genotoxic stress.
MCW7814	h^+	rad51Δ::arg3$^+$ ade6Δ::RTS1-AO-hphMX4 (12.4 kb from ade6) int::ade6-L469/puc8/his3$^+$/ade6-M375/kanMX6 ura4-D18 leu1-32 his3-D1 arg3-D4	This study	MCW7374 X MCW7229. Progeny was screened by auxotrophy and drug selection. Confirmed by spot-assays to check for sensitivity to genotoxic stress.
MCW7816	h^+	rad51Δ::arg3$^+$ rad52Δ::ura4$^+$ ade6Δ::RTS1-IO-hphMX4 (12.4 kb from ade6) int::ade6-L469/puc8/his3$^+$/ade6-M375/kanMX6 ura4-D18 leu1-32 his3-D1 arg3-D4	This study	MCW7372 X MCW7229. Progeny was screened by auxotrophy and drug selection. Confirmed by spot-assays to check for sensitivity to genotoxic stress.

MCW7818	h^+	rad51Δ::arg3$^+$ rad52Δ::ura4$^+$ ade6Δ::RTS1-AO-hphMX4 (12.4 kb from ade6) int::ade6-L469/puc8/his3$^+$/ade6-M375/kanMX6 ura4-D18 leu1-32 his3-D1 arg3-D4	This study	MCW7374 X MCW7229. Progeny was screened by auxotrophy and drug selection. Confirmed by spot-assays to check for sensitivity to genotoxic stress.
MCW7821	h^{-} smt0	oriIII-1253Δ::arg3$^+$ ura4-D18 leu1-32 his3-D1 arg3-D4	This study	BamHI-EcoRI linearised fragment from pCB37 was used to marker swap the natMX4 cassette in MCW6775. Progeny was screened by auxotrophy and drug selection.
MCW7922	h^+	rad54Δ::rad54-GFP-kanMX6 lys1Δ::P$_{nmt81}$-NLS-lacI-tdKatushka2-hphMX4 ade6-M375 int::puc8/lacO^{115}/his3$^+$/TO1/ade6-L469 ura4-D18 leu1-32 his3-D1 arg3-D4?	This study	MCW7215 X MCW7470. Progeny was screened by auxotrophy and drug selection.
MCW7924	h^{-} smt0	rad54Δ::rad54-GFP-kanMX6 lys1Δ::P$_{nmt81}$-NLS-lacI-tdKatushka2-hphMX4 ade6-M375 int::puc8/lacO^{115}/his3$^+$/TO1/ade6-L469 ura4-D18 leu1-32 his3-D1 arg3-D4?	This study	MCW7215 X MCW7470. Progeny was screened by auxotrophy and drug selection.
MCW7979	h^+	(15 kb away from oriI-4739 on ChrI) int::ade6-M375-kanMX6 ura4-D18 leu1-32 his3-D1 arg3-D4 ade6D-1	This study	NotI linearised fragment from pMJ42 was integrated into MCW1714. Progeny was screened by auxotrophy and drug selection. Confirmed by colony PCR using oMW1771-oMW707.
MCW7980	h^+	(20 kb away from oriII-2319 on ChrII) int::ade6-M375-kanMX6 ura4-D18 leu1-32 his3-D1 arg3-D4 ade6D-1	This study	NotI linearised fragment from pMJ43 was integrated into MCW1714. Progeny was screened by auxotrophy and drug selection. Confirmed by colony PCR using oMW1773-oMW707.
MCW7987	h^+	oriIII-1253Δ::arg3$^+$ (75 kb from ade6) int::ade6-L469/puc8/his3$^+$/ade6-M375/kanMX6 ura4-D18 leu1-32 his3-D1 arg3-D4	This study	MCW7430 x MCW7821. Progeny was screened by auxotrophy and drug selection.
MCW8030	h^+	rnh201Δ::KanMX6 cdc20-M603F::lox ade6Δ::RTS1-AO-hphMX4 ura4-D18 leu1-32	This study	MCW7223 X MCW7751. Progeny was screened by auxotrophy and drug selection. *Cdc20-M603F* mutation confirmed by colony PCR using oMW1777- oMW1778 and sequencing of the product.
MCW8031	$h^?$	rnh201Δ::KanMX6 cdc20-M603F::lox ade6Δ::RTS1-IO-hphMX4 ura4-D18 leu1-32 his3-D1	This study	MCW7224 X MCW7751. Progeny was screened by auxotrophy and drug selection. *Cdc20-M603F* mutation confirmed by colony PCR using oMW1777- oMW1778 and sequencing of the product.

MCW8032	$h^{?}$	rnh201Δ::KanMX6 cdc6-L591G::lox ade6Δ::RTS1-AO-hphMX4 ura4-D18 leu1-32 his3-D1	This study	MCW7223 X MCW7752. Progeny was screened by auxotrophy and drug selection. *Cdc6-L591G* mutation confirmed by colony PCR using oMW1779- oMW1780 and sequencing of the product.
MCW8033	$h^{-\ smt0}$	rnh201Δ::KanMX6 cdc6-L591G::lox ade6Δ::RTS1-IO-hphMX4 ura4-D18 leu1-32	This study	MCW7224 X MCW7752. Progeny was screened by auxotrophy and drug selection. *Cdc6-L591G* mutation confirmed by colony PCR using oMW1779- oMW1780 and sequencing of the product.
MCW8038	$h^{-\ smt0}$	elg1Δ::natMX4 lys1Δ::P_{nmt1}-NLS-MAR^{D155A}-hphMX4 ade6-M375 int::puc8/$his3^{+}$/ade6-L469 ura4-D18 leu1-32 his3-D1 arg3-D4	This study	MCW7585 X MCW7075. Progeny was screened by auxotrophy and drug selection. Confirmed by spot-assays to check for sensitivity to genotoxic stress.
MCW8040	$h^{-\ smt0}$	elg1Δ::natMX4 lys1Δ::P_{nmt1}-NLS-MAR^{D155A}-hphMX4 ade6-M375 int::puc8/$his3^{+}$/TO1/ade6-L469 ura4-D18 leu1-32 his3-D1 arg3-D4	This study	MCW7585 X MCW7076. Progeny was screened by auxotrophy and drug selection. Confirmed by spot-assays to check for sensitivity to genotoxic stress.
MCW8044	h^{+}	(15 kb away from oriI-4739 on ChrI) int::ade6-L469/puc8/$his3^{+}$/ade6-M375/kanMX6 ura4-D18 leu1-32 his3-D1 arg3-D4 ade6D-1	This study	BlpI linearised fragment from pFOX2 was integrated into MCW7979. Progeny was screened by auxotrophy selection.
MCW8045	h^{+}	(20 kb away from oriII-2319 on ChrII) int::ade6-L469/puc8/$his3^{+}$/ade6-M375/kanMX6 ura4-D18 leu1-32 his3-D1 arg3-D4 ade6D-1	This study	BlpI linearised fragment from pFOX2 was integrated into MCW7980. Progeny was screened by auxotrophy selection.
MCW8057	h^{+}	oriII-2319Δ::arg3+ (20 kb away from oriII-2319 on ChrII) int::ade6-L469/puc8/$his3^{+}$/ade6-M375/kanMX6 ura4-D18 leu1-32 his3-D1 arg3-D4 ade6D-1	This study	NotI linearised fragment from pMJ45 was integrated into MCW8045. Progeny was screened by auxotrophy and drug selection. Confirmed by colony PCR using oMW1772-oMW285.
MCW8106	h^{+}	rad51Δ::$arg3^{+}$ ade6Δ::TO1-hphMX4 lys1Δ::P_{nmt1}-NLS-MAR^{D155A}-$ura4^{+}$ ura4-D18 leu1-32 his3-D1 arg3-D4	This study	MCW7541 X MCW1088. Progeny was screened by auxotrophy and drug selection. Confirmed by spot-assays to check for sensitivity to genotoxic stress.
MCW8152	h^{+}	rad51Δ::$arg3^{+}$ rad52Δ:::KanMX6 ade6Δ::TO1-hphMX4 lys1Δ::P_{nmt1}-NLS-MAR^{D155A}-$ura4^{+}$ ura4-D18 leu1-32 his3-D1 arg3-D4	This study	MCW8016 X FO1470. Progeny was screened by auxotrophy and drug selection. Confirmed by spot-assays to check for sensitivity to genotoxic stress.
MCW8156	$h^{-\ smt0}$	rad51Δ::$arg3^{+}$ lys1Δ::P_{nmt1}-NLS-MAR^{D155A}-hphMX4 ade6-M375 int::puc8/$his3^{+}$/TO1/ade6-L469 ura4-D18 leu1-32 his3-D1 arg3-D4	This study	MCW7076 X FO1457. Progeny was screened by auxotrophy and drug selection. Confirmed by spot-assays to check for sensitivity to genotoxic stress.

MCW8160	h^+	rad51Δ::arg3$^+$ rad52Δ::ura4 lys1Δ::P_{nmt1}-NLS-MAR^{D155A}-hphMX4 ade6-M375 int::puc8/his3$^+$/TO1/ade6-L469 ura4-D18 leu1-32 his3-D1 arg3-D4	This study	MCW7076 X FO1457. Progeny was screened by auxotrophy and drug selection. Confirmed by spot-assays to check for sensitivity to genotoxic stress.
MCW8165	h^{-} smt0	rad54Δ::ura4$^+$ lys1Δ::P_{nmt1}-NLS-MAR^{D155A}-hphMX4 ade6-M375 int::puc8/his3$^+$/TO1/ade6-L469 ura4-D18 leu1-32 his3-D1 arg3-D4	This study	MCW7076 X FO672. Progeny was screened by auxotrophy and drug selection. Confirmed by spot-assays to check for sensitivity to genotoxic stress.
MCW8167	h^+	rad54Δ::rad54-GFP-KanMX6 ura4Δ:: P_{nmt1}-NLS-MAR^{D155A} lys1Δ::P_{nmt81}-NLS-lacI-tdKatushka2-hphMX4 ade6-M375 int::puc8/lacO^{115}/his3$^+$/TO1/ade6-L469 leu1-32 his3-D1 arg3-D4?	This study	MCW7420 X MCW7922. Progeny was screened by auxotrophy and drug selection as well as by colony PCR for screening for *MAR^{D155A}* using oMW758- oMW1606 (~0.9 kb product).
MCW8174	h^+	swi1Δ::ura4+ lys1Δ::P_{nmt1}-NLS-MAR^{D155A}-arg3$^+$ ura4-D18 leu1-32 his3-D1 arg3-D4	This study	BamHI-EcoRI linearised fragment from pCB37 was used to marker swap the hphMX4 cassette in MCW8125. Progeny was screened by auxotrophy and drug selection.
MCW8191	h^+	elg1Δ::natMX4 ade6Δ::RTS1-AO-hphMX4 (12.4 kb from ade6) int::ade6-L469/puc8/his3$^+$/ade6-M375/kanMX6 ura4-D18 leu1-32 his3-D1 arg3-D4	This study	MCW7259 X MCW7585. Progeny was screened by auxotrophy and drug selection. Confirmed by spot-assays to check for sensitivity to genotoxic stress.
MCW8193	h^+	fml1Δ::NatMX4 ade6Δ::RTS1-AO-hphMX4 (12.4 kb from ade6) int::ade6-L469/puc8/his3$^+$/ade6-M375/kanMX6 ura4-D18 leu1-32 his3-D1 arg3-D4	This study	MCW7259 X MCW2429. Progeny was screened by auxotrophy and drug selection. Confirmed by spot-assays to check for sensitivity to genotoxic stress.
MCW8195	h^+	mus81Δ::arg3$^+$ ade6Δ::RTS1-AO-hphMX4 (12.4 kb from ade6) int::ade6-L469/puc8/his3$^+$/ade6-M375/kanMX6 ura4-D18 leu1-32 his3-D1 arg3-D4	This study	MCW7259 X MCW2429. Progeny was screened by auxotrophy and drug selection. Confirmed by spot-assays to check for sensitivity to genotoxic stress.
MCW8197	h^+	rad8Δ::ura4$^+$ ade6Δ::RTS1-AO-hphMX4 (12.4 kb from ade6) int::ade6-L469/puc8/his3$^+$/ade6-M375/kanMX6 ura4-D18 leu1-32 his3-D1 arg3-D4	This study	MCW7259 X MCW3780. Progeny was screened by auxotrophy and drug selection. Confirmed by spot-assays to check for sensitivity to genotoxic stress.
MCW8200	h^{-} smt0	srs2Δ::ura4$^+$ ade6Δ::RTS1-AO-hphMX4 (12.4 kb from ade6) int::ade6-L469/puc8/his3$^+$/ade6-M375/kanMX6 ura4-D18 leu1-32 his3-D1 arg3-D4	This study	MCW7259 X MCW1016. Progeny was screened by auxotrophy and drug selection. Confirmed by spot-assays to check for sensitivity to genotoxic stress.
MCW8201	h^+	rqh1Δ::ura4$^+$ ade6Δ::RTS1-AO-hphMX4 (12.4 kb from ade6) int::ade6-L469/puc8/his3$^+$/ade6-M375/kanMX6 ura4-D18 leu1-32 his3-D1 arg3-D4	This study	MCW7259 X MCW1239. Progeny was screened by auxotrophy and drug selection. Confirmed by spot-assays to check for sensitivity to genotoxic stress.

MCW8202	$h^{?}$	pMJ46+ ori1253Δ::natMX4 rad52Δ::rad52-YFP-kanMX6 lys1Δ::P_{nmt41}-NLS-lacI-tdKatushka2-hphMX4 ade6-M375 int::puc8/lacO^{115}/his3^{+}/RTS1-AO/ade6-L469 (35 kb from ade6) int::tetO^{112}-arg3^{+} ura4-D18 leu1-32 his3-D1 arg3-D4	This study	Constructed by CAM
MCW8216	h^{+}	tid1Δ::ura4^{+} ade6Δ::RTS1-AO-hphMX4 (12.4 kb from ade6) int::ade6-L469/puc8/his3^{+}/ade6-M375/kanMX6 ura4-D18 leu1-32 his3-D1 arg3-D4	This study	Constructed by CAM
MCW8218	$h^{-\ smt0}$	exo1Δ::ura4^{+} ade6Δ::RTS1-AO-hphMX4 (12.4 kb from ade6) int::ade6-L469/puc8/his3^{+}/ade6-M375/kanMX6 ura4-D18 leu1-32 his3-D1 arg3-D4	This study	Constructed by CAM
MCW8220	$h^{-\ smt0}$	fen1Δ::leu1^{+} ade6Δ::RTS1-AO-hphMX4 (12.4 kb from ade6) int::ade6-L469/puc8/his3^{+}/ade6-M375/kanMX6 ura4-D18 leu1-32 his3-D1 arg3-D4	This study	Constructed by CAM
MCW8222	$h^{-\ smt0}$	rad54Δ::ura4^{+} ade6Δ::RTS1-AO-hphMX4 (12.4 kb from ade6) int::ade6-L469/puc8/his3^{+}/ade6-M375/kanMX6 ura4-D18 leu1-32 his3-D1 arg3-D4	This study	Constructed by CAM
MCW8227	$h^{-\ smt0}$	fbh1Δ::arg3^{+} ade6Δ::RTS1-AO-hphMX4 (12.4 kb from ade6) int::ade6-L469/puc8/his3^{+}/ade6-M375/kanMX6 ura4-D18 leu1-32 his3-D1 arg3-D4	This study	Constructed by CAM
MCW8229	h^{+}	rad51Δ::arg3^{+} lys1Δ::P_{nmt1}-NLS-MAR^{D155A}-hphMX4 ura4-D18 leu1-32 his3-D1 arg3-D4	This study	*ade6*$^{+}$ *his3*$^{-}$ recombinant from MCW8155. Confirmed by spot-assays to check for sensitivity to genotoxic stress.
MCW8232	h^{+}	rad51Δ::arg3^{+} rad52Δ::ura4^{+} lys1Δ::P_{nmt1}-NLS-MAR^{D155A}-hphMX4 ura4-D18 leu1-32 his3-D1 arg3-D4	This study	*ade6*$^{+}$ *his3*$^{-}$ recombinant from MCW8159. Confirmed by spot-assays to check for sensitivity to genotoxic stress.
MCW8233	h^{+}	swi1Δ::ura4^{+} ura4Δ:: P_{nmt1}-NLS-MAR^{D155A} lys1Δ::P_{nmt81}-NLS-lacI-tdKatushka2-hphMX4 rad52Δ::rad52-YFP-kanMX6 ade6-M375 int::puc8/lacO^{115}/his3^{+}/TO1/ade6-L469 leu1-32 his3-D1 arg3-D4	This study	MCW7574 X MCW2668. Progeny was screened by auxotrophy and drug selection as well as by colony PCR for screening for *MAR*^{D155A} using oMW758- oMW1606 (~0.9 kb product). Confirmed by spot-assays to check for sensitivity to genotoxic stress.
MCW8238	h^{+}	oriI-4739Δ::arg3^{+} (15 kb away from oriI-4739 on ChrI) int::ade6-L469/puc8/his3^{+}/ade6-M375/kanMX6 ura4-D18 leu1-32 his3-D1 arg3-D4 ade6D-1	This study	NotI linearised fragment from pMJ47 was integrated into MCW8045. Progeny was screened by auxotrophy and drug selection. Confirmed by colony PCR using oMW1770-oMW285.

MCW8239	h^+	lys1Δ::P_{nmt1}-NLS-MAR^{D155A}-hphMX4 ade6-M375 int::puc8/his3$^+$/ade6-L469 ura4-D18 leu1-32 his3-D1 arg3-D4	This study	MCW6626 X MCW428. Progeny was screened by auxotrophy and drug selection.
MCW8241	h^+	oriIII-1253Δ::arg3$^+$ (12.4 kb from ade6) int::ade6-L469/puc8/his3$^+$/ade6-M375/kanMX6 ura4-D18 leu1-32 his3-D1 arg3-D4	This study	MCW7229 X MCW7821. Progeny was screened by auxotrophy and drug selection.
MCW8243	h^+	oriIII-1253Δ::arg3$^+$ (20 kb away from oriII-2319 on ChrII) int::ade6-L469/puc8/his3$^+$/ade6-M375/kanMX6 ura4-D18 leu1-32 his3-D1 arg3-D4 ade6D-1	This study	MCW8045 X MCW7821. Progeny was screened by auxotrophy and drug selection.
MCW8275	$h^{-\ smt0}$	rad50Δ:: kanMX6 lys1Δ::P_{nmt1}-NLS-MAR^{D155A}-hphMX4 ade6-M375 int::puc8/his3$^+$/TO1/ade6-L469 ura4-D18 leu1-32 his3-D1 arg3?	This study	MCW 7076 X MCW328. Progeny was screened by auxotrophy and drug selection. Confirmed by spot-assays to check for sensitivity to genotoxic stress.
MCW8282	h^+	swi1Δ::ura4$^+$ ade6-M375 int::puc8/his3$^+$/ade6-L469 int::TO1-hphMX4(0.2 kb from ade6-M375) ura4-D18 leu1-32 his3-D1 arg3-D4	This study	MCW8174 X MCW7500. Progeny was screened by auxotrophy and drug selection. Confirmed by spot-assays to check for sensitivity to genotoxic stress.
MCW8283	h^+	swi1Δ::ura4$^+$ ade6-M375 int::puc8/his3$^+$/ade6-L469 int::TO1-hphMX4(0.2 kb from ade6-M375) ura4-D18 leu1-32 his3-D1 arg3-D4	This study	MCW8174 X MCW7500. Progeny was screened by auxotrophy and drug selection. Confirmed by spot-assays to check for sensitivity to genotoxic stress.
MCW8284	h^+	swi1Δ::ura4$^+$ lys1Δ::P_{nmt1}-NLS-MAR^{D155A}-arg3$^+$ ade6-M375 int::puc8/his3$^+$/ade6-L469 int::TO1-hphMX4(0.2 kb from ade6-M375) ura4-D18 leu1-32 his3-D1 arg3-D4	This study	MCW8174 X MCW7500. Progeny was screened by auxotrophy and drug selection. Confirmed by spot-assays to check for sensitivity to genotoxic stress.
MCW8290	h^+	oriIII-1253Δ::arg3$^+$ elg1Δ::natMX4 ade6Δ::RTS1-AO-hphMX4 (12.4 kb from ade6) int::ade6-L469/puc8/his3$^+$/ade6-M375/kanMX6 ura4-D18 leu1-32 his3-D1 arg3-D4	This study	MCW8191 X MCW7821. Progeny was screened by auxotrophy and drug selection. Confirmed by spot-assays to check for sensitivity to genotoxic stress.
MCW8304	h^+	fml1Δ::natMX4 lys1Δ::P_{nmt1}-NLS-MAR^{D155A}-hphMX4 ade6-M375 int::puc8/his3$^+$/TO1/ade6-L469 ura4-D18 leu1-32 his3-D1 arg3-D4	This study	MCW2429 X MCW7076. Progeny was screened by auxotrophy and drug selection. Confirmed by spot-assays to check for sensitivity to genotoxic stress.
MCW8308	h^+	mus81Δ::arg3$^+$ lys1Δ::P_{nmt1}-NLS-MAR^{D155A}-hphMX4 ade6-M375 int::puc8/his3$^+$/TO1/ade6-L469 ura4-D18 leu1-32 his3-D1 arg3-D4	This study	MCW2429 X MCW7076. Progeny was screened by auxotrophy and drug selection. Confirmed by spot-assays to check for sensitivity to genotoxic stress.

MCW8312	h^+	swi1Δ::ura4$^+$ lys1Δ::P_{nmt81}-NLS-lacI-tdKatushka2-hphMX4 rad52Δ::rad52-YFP-KanMX6 ade6-M375 int::puc8/lacO^{115}/his3$^+$/TO1/ade6-L469 ura4-D18 leu1-32 his3-D1 arg3-D4	This study	MCW7263 X MCW2668. Progeny was screened by auxotrophy and drug selection. Confirmed by spot-assays to check for sensitivity to genotoxic stress.
MCW8496	h^+	oriIII-1253Δ::natMX4 swi1Δ::ura4$^+$ ade6-M375 int::puc8/his3$^+$/ade6-L469 int::TO1-hphMX4(0.2 kb from ade6-M375) ura4-D18 leu1-32 his3-D1 arg3-D4	This study	MCW8284 X MCW6775. Progeny was screened by auxotrophy and drug selection. Confirmed by spot-assays to check for sensitivity to genotoxic stress.
MCW8498	h^+	oriIII-1253Δ::natMX4 swi1Δ::ura4+ lys1Δ::P_{nmt1}-NLS-MAR^{D155A}-arg3$^+$ ade6-M375 int::puc8/his3$^+$/ade6-L469 int::TO1-hphMX4(0.2 kb from ade6-M375) ura4-D18 leu1-32 his3-D1 arg3-D4	This study	MCW8284 X MCW6775. Progeny was screened by auxotrophy and drug selection. Confirmed by spot-assays to check for sensitivity to genotoxic stress.

*AF: Andrew Fower; CAM: Carl Antony Morrow; FO: Fikret Osman; FK: Felix Kerstine; MJK: Min Ki Kim

Table 8-7: List of plasmids used in this study.

Bacterial strain number	*E. coli* strain background	Plasmid Name	Antibiotic resistance	Description of Plasmid
MW2057[§]	DH5α	pMW838	Ampicillin	Constructed by MCW. PCR amplified (oMW996, oMW999) *MarBI TO1* from pRC824 (from R. Chalmers); cloned as a SalI-EcoRV fragment into pFOX2; [pFOX2-puc8/his3^{+}/TO1/ade6-L469]
MW2058[§]	DH5α	pMW839	Ampicillin	Constructed by MCW.PCR amplified (oMW997, oMW998) *MarBI TO2* from pRC824 (from R. Chalmers); cloned as a SalI-EcoRV fragment into pFOX2; [pFOX2-puc8/his3^{+}/TO2/ade6-L469]
MW2060[§]	DH5α	pMW841	Ampicillin	Constructed by MCW. PCR amplified (oMW991, oMW992) *NLS-Mar^{WT}* mutant from pRC880 (from R. Chalmers); cloned as a BamHI-NdeI fragment into pREP41; [pREP41-NLS- Mar^{WT}- hphMX4]
MW2061[§]	DH5α	pMW842	Ampicillin	Constructed by MCW. PCR amplified (oMW991, oMW993) *NLS-Mar^{WT}* mutant from pRC880 (from R. Chalmers); cloned as a BamHI-NdeI fragment into pREP41-eGFP; [pREP41-NLS- Mar^{WT}eGFP-hphMX4]
MW2069[§]	DH5α	pMW850	Ampicillin	Constructed by MCW. NdeI-BamHI cleaved *NLS-Mar^{WT}* from pMW838 cloned into pREP1; [pREP1-NLS- Mar^{WT}- hphMX4]
MW2357[±]	DH5α	pALO67	Ampicillin	Targeting construct for the marker swapping of any chromosomal integrated gene marked with a natMX4, kanMX6 or hphMX4 into a *ura4^{+}* marker.
MW2392[±]	DH5α	pMW899[c]	Ampicillin	Targeting construct for generating a recombinant substrate with the tRNA^{GLU80} gene positioned between *his3* and *ade6* in the orientation in which a head on collision with replication will be generated.
MW2428[±]	DH5α	pMW905[c]	Ampicillin	Targeting construct for generating a recombinant substrate with the tRNA^{GLU80} gene positioned between *his3* and *ade6* in the orientation opposite to pMW899.
MW2558[§]	DH5α	pMJ2	Ampicillin	PCR amplified (oMW1418, oMW1477) *P$_{nmt41}$-NLS- Mar^{WT}* from pMW841; cloned as an Asc1 fragment into pSHA4. Confirmed by sequencing using oMW1172 and oMW1040; [pSHA4+ 5'*lys1*-P$_{nmt41}$-NLS-Mar^{WT}-hphMX4-3'*lys1*]
MW2559[§]	DH5α	pMJ3	Ampicillin	PCR amplified (oMW1418, oMW1477) *P$_{nmt41}$-NLS- Mar^{WT}eGFP* from pMW842; cloned as an Asc1 fragment into pSHA4. Confirmed by sequencing using oMW1172 and oMW1040; [pSHA4+ 5'*lys1*-P$_{nmt41}$-NLS-Mar^{WT}eGFP-hphMX4-3'*lys1*]
MW2561[§]	DH5α	pMJ5	Ampicillin	PCR amplified (oMW1418, oMW1477) *P$_{nmt1}$-NLS- Mar^{WT}* from pMW850; cloned as an Asc1 fragment into pSHA4. Confirmed by sequencing using oMW1172 and oMW1040; [pSHA4+ 5'*lys1*-P$_{nmt1}$-NLS-Mar^{WT}-hphMX4-3'*lys1*]

MW2579[§]	DH5α	pMJ9	Ampicillin	PCR amplified (oMW991, oMW993) *NLS-Mar^{D115A}* from pRC1113 (from R. Chalmers); cloned as a BamHI-NdeI fragment into pREP41-eGFP. Confirmed by sequencing using oMW994 and oMW995; [pREP41-NLS- Mar^{D155A}eGFP- hphMX4]
MW2580[§]	DH5α	pMJ10	Ampicillin	PCR amplified (oMW991, oMW993) *NLS-Mar^{V119G}* from pRC1220 (from R. Chalmers); cloned as a BamHI-NdeI fragment into pREP41-eGFP. Confirmed by sequencing using oMW994 and oMW995; [pREP1-NLS- Mar^{V119G}eGFP- hphMX4]
MW2581[§]	DH5α	pMJ11	Ampicillin	PCR amplified (oMW991, oMW992) *NLS-Mar^{V119G}* from pRC1220 (from R. Chalmers); cloned as a BamHI-NdeI fragment into pREP1; [pREP1-NLS- Mar^{V119G}- hphMX4]
MW2582[§]	DH5α	pMJ12	Ampicillin	PCR amplified (oMW991, oMW992) *NLS-Mar^{D155A}* from pRC1113 (from R. Chalmers); cloned as a BamHI-NdeI fragment into pREP1. Confirmed by sequencing using oMW994 and oMW995; [pREP1-NLS- Mar^{D155A}- hphMX4]
MW2583[§]	DH5α	pMJ13	Ampicillin	PCR amplified (oMW1418, oMW1477) *P_{nmt1}-NLS- Mar^{D155A}* from pMJ12; cloned as an Asc1 fragment into pSHA4. Confirmed by sequencing using oMW1172 and oMW1040; [pSHA4+ 5'*lys1*-P_{nmt1}-NLS-Mar^{D155A}-hphMX4-3'*lys1*]
MW2584[§]	DH5α	pMJ14	Ampicillin	PCR amplified (oMW1418, oMW1477) *P_{nmt1}-NLS- Mar^{V119G}* from pMJ11; cloned as an Asc1 fragment into pSHA4. Confirmed by sequencing using oMW1172 and oMW1040; [pSHA4+ 5'*lys1*-P_{nmt1}-NLS-Mar^{V119G}-hphMX4-3'*lys1]*
MW2594[§]	DH5α	pMJ17	Ampicillin	BamHI cleaved *RTS1* from pRS115 cloned into pAG32; [pAG32-*RTS1*-hphMX4]
MW2596[§]	DH5α	pMJ19	Ampicillin	PCR amplified (oMW1563, oMW1564) 3' UTR of *ade6* from *S. pombe* (FO656) gDNA; cloned as a HindIII-SalI fragment into pMJ17; [pAG32-3'UTR *ade6-RTS1-IO*-hphMX4]
MW2597[§]	DH5α	pMJ20	Ampicillin	PCR amplified (oMW1565, oMW1566) 3' UTR of *vct4* from *S. pombe* (FO656) gDNA; cloned as a SacI-SpeI fragment into pMJ19. Confirmed by sequencing using oMW1563, oMW1564, oMW1565 and oMW1566; [pAG32-3'UTR *ade6-RTS1-IO*-hphMX4-3'UTR *vct4*]
MW2598[§]	DH5α	pMJ21	Ampicillin	BamHI cleaved *RTS1* from pMJ20 cloned into pMJ20; [pAG32-3'UTR *ade6-RTS1-AO*-hphMX4-3'UTR *vct4*]
MW2615[±]	DH5α	pBU5	Ampicillin	Targeting construct for generating a recombinant substrate with the *TER2X3* positioned between *his3* and *ade6* in the orientation 1 (permissive orientation; Mizuno et al., 2013).
MW2616[±]	DH5α	pBU6	Ampicillin	Targeting construct for generating a recombinant substrate with the *TER2X3* positioned between *his3* and *ade6* in the orientation 1 (restrictive orientation; Mizuno et al., 2013).
MW2619[§]	DH5α	pMJ22	Ampicillin	XhoI-BamHI cleaved tdKatushka2 from pMN7cloned into pMN2; [pSHA4+ 5'*lys1*-P_{nmt81}-NLS-LacItdkatushka2-hphMX4-3'*lys1*]
MW2620[§]	DH5α	pMJ23	Ampicillin	PCR amplified (oMW1477, oMW1040) *P_{nmt1}-NLS- Mar^{WT}* from pMJ5; AscI cleaved and Klenow blunted; cloned into pREP42 at the EcoRV-StuI site; [pREP42+ 5'*ura4*-P_{nmt1}-NLS-Mar^{WT}-3'*ura4*]

MW2621[§]	DH5α	pMJ24	Ampicillin	2.4 kb fragment PCR amplified from pFOX2 (oMW1586, oMW1587); cloned as a PvuII- EcoRV fragment into pMN5. Confirmed by sequencing using oMW717; [pFOX2-pUC8/4.5 kb lacO/his3/ade6-L469]
MW2622[§]	MACH1	pMJ25	Ampicillin	SalI-EcoRV cleaved *MarBl TO1* from pMW838 cloned into pMJ24. Confirmed by sequencing using oMW717; [pFOX2-pUC8/4.5 kb lacO/his3/TO1/ade6-L469]
MW2623[§]	DH5α	pMJ26	Ampicillin	SalI-EcoRV cleaved *MarBl TO2* from pMW839 cloned into pMJ24. Confirmed by sequencing using oMW717; [pFOX2-pUC8/4.5 kb lacO/his3/TO2/ade6-L469]
MW2628[±]	DH5α	pCB37	Ampicillin	Targeting construct for the marker swapping of any chromosomal integrated gene marked with a natMX4, kanMX6 or hphMX4 into a *arg3*$^{+}$ marker.
MW2639[§]	DH5α	pMW921	Ampicillin	Constructed by MCW. Construct for replacing the endogenous *ade6* with *RTS1.* [pAG32-5'UTR *ade6-RTS1-AO*-hphMX4-3'UTR *ade6*]
MW2640[§]	DH5α	pMW922	Ampicillin	Constructed by MCW. Construct for replacing the endogenous *ade6* with *RTS1.* [pAG32-5'UTR *ade6-RTS1-IO*-hphMX4-3'UTR *ade6*]
MW2640[§]	DH5α	pMW923	Ampicillin	Constructed by MCW. Construct for targeting *ade6-M375* 12.4 kb downstream (Site II: ChrIII 1306145-1306146) of the endogenous *ade6.* [pFA6-5'flanking-*ade6-M375*-KanMX6-3'flanking]
MW2646[§]	MACH1	pCB44	Ampicillin	Constructed by CB. Construct for targeting *ade6-M375* 140 kb downstream (Site V: ChrIII 1173489-1175846) of the endogenous *ade6.* [pFA6-5'flanking-*ade6-M375*-KanMX6-3'flanking]
MW2659[§]	MACH1	pAF1	Ampicillin	Constructed by AF. AscI cleaved P_{nmt1}-*NLS-Mar*^{D155A} from pMJ13 cloned into pREP42 at the EcoRV-StuI site; [pREP42+ 5'*ura4*-P_{nmt1}-NLS-Mar^{D155A}-3'*ura4*]
MW2662[§]	MACH1	pMJ31	Ampicillin	Construct for targeting *ade6-M375* 35 kb downstream (Site III: ChrIII 1282755-1282757) of the endogenous *ade6.* PCR amplified (oMW1659, oMW1660) 5' flanking region from *S. pombe* (FO656) gDNA; cloned as a PvuII-SalI fragment into pMW923; [pFA6-5'flanking-*ade6-M375*-KanMX6 (Site III)]
MW2663[§]	MACH1	pMJ32	Ampicillin	Construct for targeting *ade6-M375* 75 kb downstream (Site IV: ChrIII 1244737-1244738) of the endogenous *ade6.* PCR amplified (oMW1663, oMW1664) 5' flanking region from *S. pombe* (FO656) gDNA; cloned as a PvuII-SalI fragment into pMW923; [pFA6-5'flanking-*ade6-M375*-KanMX6 (Site IV)]
MW2664[§]	MACH1	pMJ33	Ampicillin	Construct for targeting *ade6-M375* 35 kb downstream (Site III: ChrIII 1282755-1282757) of the endogenous *ade6.* PCR amplified (oMW1661, oMW1662) 3' flanking region from *S. pombe* (FO656) gDNA; cloned as a SacI-SpeI fragment into pMJ31; [pFA6-5'flanking-*ade6-M375*-KanMX6-3'flanking (Site III)]

MW2665§	MACH1	pMJ34	Ampicillin	Construct for targeting *ade6-M375* 75 kb downstream (Site IV: ChrIII 1244737-1244738) of the endogenous *ade6.* PCR amplified (oMW1665, oMW1666) 3' flanking region from *S. pombe* (FO656) gDNA; cloned as a SacI-SpeI fragment into pMW923; [pFA6-5'flanking-*ade6-M375*-KanMX6-3'flanking (Site IV)]
MW2666§	MACH1	pMJK1	Ampicillin	Constructed by MJK. SalI cleaved *6XTerB* from pJ241-6XTerB cloned into pFOX2; [pFOX2-pUC8/his3/*6XTerB* orientation1/ade6-L469](permissive orientation; Larsen et al., 2014)
MW2667§	RRL107 (DJS)	pMJK2	Ampicillin+ Chloramphenicol	Constructed by MJK. SalI-BamHI cleaved *6XTerB* from pJ241-6XTerB cloned into pFOX2; [pFOX2-pUC8/his3/*6XTerB* orientation2/ade6-L469](restrictive oriention; Larsen et al., 2014)
MW2668§	MACH1	pMJK3	Ampicillin	Constructed by MJK. PCR amplified (oMW1651, oMW1652) *NLS-TusB* from *E. coli* (DS841) gDNA; cloned as a BamHI-NdeI fragment into pREP1; [pREP1-NLS-TusB- hphMX4]
MW2693§	MACH1	pAF2	Ampicillin	Constructed by AF. SalI-EcoRV cleaved *MarBI TO1* from pMW838 cloned into pMW921; [pAG32-5'UTR *ade6-TO2*-hphMX4-3'UTR *ade6*]
MW2694§	MACH1	pAF3	Ampicillin	Constructed by AF. SalI-EcoRV cleaved *MarBI TO2* from pMW839 cloned into pMW921; [pAG32-5'UTR *ade6-TO1*-hphMX4-3'UTR *ade6*]
MW2695§	MACH1	pAF4	Ampicillin	Constructed by AF. SalI-EcoRV cleaved *MarBI TO1* from pMW838 cloned into pMJ20 at the SalI-SmaI site; [pAG32-3'UTR *ade6-TO2*-hphMX4-3'UTR *vct4*]
MW2696§	MACH1	pAF5	Ampicillin	Constructed by AF. SalI-EcoRV cleaved *MarBI TO2* from pMW839 cloned into pMJ20 at the SalI-SmaI site; [pAG32-3'UTR *ade6-TO1*-hphMX4-3'UTR *vct4*]
MW2698§	MACH1	pMJK6	Ampicillin	NdeI-BamHI cleaved TusB fragment from pMJK1 cloned into pMJ5; [pSHA4+ 5'*lys1*-P_{nmt1}-NLS-TusB-hphMX4-3'*lys1*
MW2705§	MACH2	pMJ35	Ampicillin	BamHI-XhoI cleaved eCFP cleaved from pMW868 inserted into pMW620 [pREP41-NLS-TetReCFP-hphMX4] (OUT-OFF FRAME)
MW2750§	MACH1	pMJ38	Ampicillin	PCR amplified (oMW1748, oMW1749) upstream region flanking *oriI-4739* from *S. pombe* (FO656) gDNA; cloned as a PvuII-SalI fragment into pCB37; [pAG25-5' flanking-*oriI-4739-arg3*$^{+}$MX4]
MW2751§	MACH1	pMJ39	Ampicillin	PCR amplified (oMW1756, oMW1757) upstream region flanking *oriII-2319* from *S. pombe* (FO656) gDNA; cloned as a PvuII-SalI fragment into pCB37; [pAG25-5' flanking-*oriII-2319-arg3*$^{+}$MX4]
MW2752§	MACH1	pMJ40	Ampicillin	Construct for targeting *ade6-M375* 15 kb downstream (Site VII: ChrI 4724696-4724697) of the *oriI-4739.* PCR amplified (oMW1752, oMW1753) 5' flanking region from *S. pombe* (FO656) gDNA; cloned as a PvuII-SalI fragment into pZN5; [pFA6-5'flanking-*ade6-M375*-KanMX6 (Site VII)]
MW2753§	MACH1	pMJ41	Ampicillin	Construct for targeting *ade6-M375* 20 kb downstream (Site VI: ChrII 2300586-2300587) of the *oriII-2319.* PCR amplified (oMW1760, oMW1761) 5' flanking region from *S. pombe* (FO656) gDNA; cloned as a PvuII-SalI fragment into pZN5; [pFA6-5'flanking-*ade6-M375*-KanMX6 (Site VI)]

MW2754§	MACH1	pMJ42	Ampicillin	Construct for targeting *ade6-M375* 15 kb downstream (Site VII: ChrI 4724696-4724697) of the *oriI-4739.* PCR amplified (oMW1754, oMW1755) 3' flanking region from *S. pombe* (FO656) gDNA; cloned as a SacI-SpeI fragment into pMJ40; [pFA6-5'flanking-*ade6-M375*-KanMX6-3'flanking (Site VII)]
MW2755§	MACH1	pMJ43	Ampicillin	Construct for targeting *ade6-M375* 20 kb downstream (Site VI: ChrII 2300586-2300587) of the *oriII-2319.* PCR amplified (oMW1762, oMW1763) 3' flanking region from *S. pombe* (FO656) gDNA; cloned as a SacI-SpeI fragment into pMJ41; [pFA6-5'flanking-*ade6-M375*-KanMX6-3'flanking (Site VI)]
MW2778§	MACH1	pMJ44	Ampicillin	PCR amplified (oMW1758, oMW1759) downstream region flanking *oriII-2319* from *S. pombe* (FO656) gDNA; cloned as a SacI-SpeI fragment into pCB37; [pAG25- *oriII-2319-arg3*$^{+}$MX4-3' flanking *oriII-2319*]
MW2779§	MACH1	pMJ45	Ampicillin	PvuII-PstI cleaved 5' upstream region flanking *oriII-2319* from pMJ39 cloned into pMJ44. [pAG25- 5' flanking *oriII-2319-arg3*$^{+}$MX4-3' flanking *oriII-2319*]
MW2780§	MACH1	pMJ46	Ampicillin	NcoI-BamHI cleaved TetR-eCFP from pMJ35 cloned into pMJK4. [pREP41-NLS-TetReCFP-hphMX4] (IN FRAME)
MW2781§	DH5α	pMJ47	Ampicillin	PCR amplified (oMW1750, oMW1751) downstream region flanking *oriI-4739* from *S. pombe* (FO656) gDNA; cloned as a SacI fragment into pCB37; [pAG25-5' flanking- *oriI-4739-arg3*$^{+}$MX4-3' flanking *oriI-4739*]
-	-	pREP41[a]	Ampicillin	Carrier plasmid with modified *nmt1* promoter leading to lower expression than pREP1
-	-	pFOX2[b]	Ampicillin	Targeting construct for generating a recombinant substrate consisting of nontandem direct- repeats of *ade6* heteroalleles, interspersed by a *his3*$^{+}$ gene.

±-Lab plasmid; §-Plasmid constructed for this study; *Constructed by- AF: Andrew Fower; MCW: Matthew Whitby; MJK: Min Ki Kim
a-Basi et al., 1993; b-Osman et al., 2000; c-Steinacher et al., 2012

Table 8-8: List of oligonucleotides used in this study.

Oligo Name	Oligo Sequence (5'>3')
oMW285	AATGTACGGGCGACAGTC
oMW706	AAAGGCCTCGCTTCTCGAG
oMW707	AGCAGCATACGCTAAAATC
oMW716	ATTTGATGTTTAAGCGATGG
oMW717	AGAAGAAAGCGATCGATGAG
oMW721	AGTTGGTTGCGTTATTCGAG
oMW722	AAAACATGTTGACAAACCTG
oMW757	CTCTGCATGCAGCTACAAATCCCAC
oMW758	CTCTGCATGCGTGATATTGACGAAAC
oMW991	TTTCATATGGGAAGTCCTAAGAAGAAACGAAAGGTGTTCACCATGGAAATGATGCTCGATAAG
oMW992	TTTGGATCCTTAATCGAAGTAGCTGCCGT
oMW993	TTTGGATCCATCGAAGTAGCTGCCGTTAC
oMW994	ATGCACCGTAAACTGCAG
oMW995	TTCAGGAAGGAATAGTGG
oMW996	TTGATATCTATTAGGTTGGTGCAAAAGTAATTGC
oMW997	TTTGTCGACTATTAGGTTGGTGCAAAAGTAATTGC
oMW998	TTGATATCAAATCAGCATCCATGTTGG
oMW999	TAAGTCGACAAATCAGCATCCATGTTGG
oMW1040	ATCCCGCACCCGTCTACG
oMW1172	GATAATGGACCTGTTAATCG
oMW1418	TATGGCGCGCCCTGCAGGTCGATCGACTC
oMW1477	TATGGCGCGCCCGAATTCGAGCTCGCATTAC

Oligo Name	Oligo Sequence (5'>3')
oMW1563	TATAAAGCTTGAAATTCTAGATTGTAAAATG
oMW1564	TATAGTCGACTTTCAACTGCTTCACAGCAC
oMW1565	TTAGAGCTCCAATATAATATGCTATAAAGC
oMW1566	TATACTAGTCATCTTTTAATAATTGAAGAC
oMW1586	CTAAGATGCAGGTGATATC
oMW1587	AATGCAGCTGGCACGACAG
oMW1603	AACCCTCCCTTTTGGCTG
oMW1606	CATGTCTGCAAGATTAATCCAGC
oMW1633	AAAGATGGAAACTAGTTATGC
oMW1634	TGGACGATGTCGTTTATTCCGAGTG
oMW1635	TCTGCACTTGGTTCGACGAC
oMW1651	TTTCATATGGGAAGTCCTAAGAAGAAACGAAAGGTGTTCACCATGGCGCGTTACGATCTCG
oMW1652	TTTGGATCCTTAATCTGCAACATACAGGTG
oMW1659	TATCAGCTGTATCCTTCTGCGTTAAT
oMW1660	AATGTCGACGACGATTTCAAAAATAGTAT
oMW1661	TATGAGCTCGCGACTCTTAATTTTCTCTCT
oMW1662	AATACTAGTGAAATACATGAAATCACAACC
oMW1663	TATCAGCTGTTTTTAAGGAGTTCAAGACTT
oMW1664	AATGTCGACTACAGCAGCAG AAACC
oMW1665	TATGAGCTCACAATTCTTCTGATATATTAA
oMW1666	AATACTAGTTCCAGAGTTGAATGTTT
oMW1679	CGTACCACAGTGAGGTGCAT
oMW1748	TCACAGCTGCCATAACAGATCCAATCCATG

Oligo Name	Oligo Sequence (5'>3')
oMW1749	TAAGTCGACGAGATCTGAACTTCGTCATCT
oMW1750	TATGAATTCTGTATGGTAAAAAGTGAAATT
oMW1751	TATACTAGTGTTCTAGTTCCAACGATGTTG
oMW1752	CATCAGCTGACGAAATGTTCGAACGCTCGG
oMW1753	ATAGTCGACGCATTAATATACAAGTCAAAG
oMW1754	CATGAGCTCGCTATTGTTTAGGAAATATAA
oMW1755	ATAACTAGTAAAGTGTGGACAATAGCTTGC
oMW1756	CATCAGCTGGCAAGGCATAAACACCGTTCT
oMW1757	ATAGTCGACTATGATCGCAACTAAGCACTT
oMW1758	CATGAGCTCGGCCGTTTGGTCTAGTGGTAT
oMW1759	ATACCGCGGCGCTATAAACGAAATCTTTTT
oMW1760	CATCAGCTGTTGTGATCAAGGAAATTTCTG
oMW1761	ATAGTCGACATTCGCGTTCTACGTATCTCA
oMW1762	CATGAGCTCGTCCGACTGCTTCCGCGATCC
oMW1763	ATAACTAGTTCCGTCTCTTCTTCTACTTTG
oMW1770	AGTGTCGTTCGCAAAAACTG
oMW1771	TCGTATGGTTTACACGGCCGAC
oMW1772	ACCTAGTTTTGACATAATACAG
oMW1773	AAGAGAACTCTTTTGTCCGCG
oMW1777	ACAGTTGGACAAAGCCTTAG
oMW1778	AGAAAGCTCTTGAAATGACC
oMW1779	CTTCTTGCTAGAGGCCAACAG
oMW1780	AAGCTAGCTGTCTACCATCC

Table 8-9: List of collaborative data in this study.

Strain Number	Source of Data
FO949	Ade^+ recombinant value published in Osman et al., 2016.
FO1748	Ade^+ recombinant value published in Lorenz et al., 2009.
FO1750	Ade^+ recombinant value published in Lorenz et al., 2009.
FO1814	Ade^+ recombinant value published in Lorenz et al., 2009.
FO1836	Ade^+ recombinant value published in Lorenz et al., 2009.
MCW39	Ade^+ recombinant value published in Osman et al., 2016.
MCW429	Ade^+ recombinant value provided by M.C. Whitby.
MCW1443	Ade^+ recombinant value published in Ahn et al., 2005
MCW1447	Ade^+ recombinant value published in Ahn et al., 2005
MCW1451	Ade^+ recombinant value provided by M.C. Whitby.
MCW1452	Ade^+ recombinant value provided by M.C. Whitby.
MCW1691	Ade^+ recombinant value published in Ahn et al., 2005.
MCW1692	Ade^+ recombinant value published in Ahn et al., 2005
MCW1695	Ade^+ recombinant value published in Ahn et al., 2005
MCW1696	Ade^+ recombinant value published in Ahn et al., 2005
MCW1742	Ade^+ recombinant value published in Osman et al., 2016.
MCW2226	Ade^+ recombinant value provided by M.C. Whitby.
MCW2656	Ade^+ recombinant value provided by M.C. Whitby.
MCW3061	Ade^+ recombinant value published in Steinacher et al., 2012.
MCW3862	Ade^+ recombinant value provided by M.C. Whitby.
MCW3864	Ade^+ recombinant value provided by M.C. Whitby.
MCW4712	Ade^+ recombinant value provided by M.C. Whitby.
MCW4713	Ade^+ recombinant value and 2D gel image provided by M.C. Whitby.
MCW4940	Ade^+ recombinant value provided by M.C. Whitby.
MCW4942	Ade^+ recombinant value provided by M.C. Whitby.
MCW4954	Ade^+ recombinant value provided by M.C. Whitby.
MCW4956	Ade^+ recombinant value published in Steinacher et al., 2012.
MCW6395	Data collected by M.O. Nguyen. Re-analysed for this study.
MCW6556	Data collected by M.O. Nguyen. Re-analysed for this study.

MCW7377	Strain assayed by A. Fowler.
MCW7598	Strain constructed and assayed by F. Kerstine and F. Osman.
MCW7599	Strain constructed and assayed by F. Kerstine and F. Osman.
MCW7600	Strain constructed and assayed by F. Kerstine and F. Osman.
MCW7601	Strain constructed and assayed by F. Kerstine and F. Osman.
MCW7602	Strain constructed and assayed by F. Kerstine and F. Osman.
MCW7603	Strain constructed and assayed by F. Kerstine and F. Osman.
MCW7604	Strain constructed and assayed by F. Kerstine and F. Osman.
MCW7605	Strain constructed and assayed by F. Kerstine and F. Osman.
MCW7708	Strain constructed by F. Osman and assayed by S. Tamang.
MCW7740	Strain constructed and assayed by F. Kerstine and F. Osman.
MCW8202	Strain construction and imaging in collaboration with C.A. Morrow.

Chapter 9

Bibliography

Ahn, J.S., Osman, F., and Whitby, M.C. (2005). Replication fork blockage by RTS1 at an ectopic site promotes recombination in fission yeast. EMBO J. *24*, 2011–2023.

Akamatsu, Y., Dziadkowiec, D., Ikeguchi, M., Shinagawa, H., and Iwasaki, H. (2003). Two different Swi5-containing protein complexes are involved in mating-type switching and recombination repair in fission yeast. Proc. Natl. Acad. Sci. U. S. A. *100*, 15770–15775.

Akamatsu, Y., Tsutsui, Y., Morishita, T., Siddique, M.S.P., Kurokawa, Y., Ikeguchi, M., Yamao, F., Arcangioli, B., and Iwasaki, H. (2007). Fission yeast Swi5/Sfr1 and Rhp55/Rhp57 differentially regulate Rhp51-dependent recombination outcomes. EMBO J. *26*, 1352–1362.

Alexeev, A., Mazin, A., and Kowalczykowski, S.C. (2003). Rad54 protein possesses chromatin-remodeling activity stimulated by the Rad51-ssDNA nucleoprotein filament. Nat. Struct. Biol. *10*, 182–186.

Alver, R.C., Chadha, G.S., and Blow, J.J. (2014). The contribution of dormant origins to genome stability: From cell biology to human genetics. DNA Repair (Amst). *19*, 182–189.

Amin, A.A., and Hurwitz, J. (1992). Polar arrest of the simian virus 40 tumor antigen-mediated replication fork movement in vitro by the tus protein-terB complex of Escherichia coli. J. Biol. Chem. *267*, 18612–18622.

Anand, R.P., Lovett, S.T., and Haber, J.E. (2013). Break-induced DNA replication. Cold Spring Harb. Perspect. Biol. *5*, 1–18.

Anand, R.P., Tsaponina, O., Greenwell, P.W., Lee, C.-S., Du, W., Petes, T.D., and Haber, J.E. (2014). Chromosome rearrangements via template switching between diverged repeated sequences. Genes Dev. *28*, 2394–2406.

Andersen, P.L., Xu, F., and Xiao, W. (2008). Eukaryotic DNA damage

tolerance and translesion synthesis through covalent modifications of PCNA. Cell Res. *18*, 162–173.

Atkinson, J., and McGlynn, P. (2009). Replication fork reversal and the maintenance of genome stability. Nucleic Acids Res. *37*, 3475–3492.

Azvolinsky, A., Dunaway, S., Torres, J.Z., Bessler, J.B., and Zakian, V.A. (2006). The S. cerevisiae Rrm3p DNA helicase moves with the replication fork and affects replication of all yeast chromosomes. Genes Dev. *20*, 3104–3116.

Bachrati, C.Z., Borts, R.H., and Hickson, I.D. (2006). Mobile D-loops are a preferred substrate for the Bloom's syndrome helicase. Nucleic Acids Res. *34*, 2269–2279.

Basi, G., Schmid, E., and Maundrell, K. (1993). TATA box mutations in the Schizosaccharomyces pombe nmt1 promoter affect transcription efficiency but not the transcription start point or thiamine repressibility. Gene *123*, 131–136.

Baumann, P., Benson, F.E., and West, S.C. (1996). Human Rad51 protein promotes ATP-dependent homologous pairing and strand transfer reactions in vitro. Cell *87*, 757–766.

Benson, F.E., Baumann, P., and West, S.C. (1998). Synergistic actions of Rad51 and Rad52 in recombination and DNA repair. Nature *391*, 401–404.

Bernstein, K.A., Gangloff, S., and Rothstein, R. (2010). The RecQ DNA helicases in DNA repair. Annu. Rev. Genet. *44*, 393–417.

Bernstein, K. a, Reid, R.J.D., Sunjevaric, I., Demuth, K., Burgess, R.C., and Rothstein, R. (2011). The Shu complex, which contains Rad51 paralogues, promotes DNA repair through inhibition of the Srs2 anti-recombinase. Mol. Biol. Cell *22*, 1599–1607.

Bethke, B.D., and Golin, J. (1994). Long-tract mitotic gene conversion in yeast: Evidence for a triparental contribution during spontaneous recombination.

Genetics *137*, 439–453.

Bidnenko, V., Ehrlich, S.D., and Michel, B. (2002). Replication fork collapse at replication terminator sequences. EMBO J. *21*, 3898–3907.

Blastyák, A., Pintér, L., Unk, I., Prakash, L., Prakash, S., and Haracska, L. (2007). Yeast Rad5 Protein Required for Postreplication Repair Has a DNA Helicase Activity Specific for Replication Fork Regression. Mol. Cell *28*, 167–175.

Boddy, M.N., Lopez-Girona, A., Shanahan, P., Interthal, H., Heyer, W.D., and Russell, P. (2000). Damage tolerance protein Mus81 associates with the FHA1 domain of checkpoint kinase Cds1. Mol. Cell. Biol. *20*, 8758–8766.

Boersma, V., Moatti, N., Segura-Bayona, S., Peuscher, M.H., van der Torre, J., Wevers, B.A., Orthwein, A., Durocher, D., and Jacobs, J.J.L. (2015). MAD2L2 controls DNA repair at telomeres and DNA breaks by inhibiting 5' end resection. Nature *521*, 537–540.

Bosco, G., and Haber, J.E. (1998). Chromosome break-induced DNA replication leads to nonreciprocal translocations and telomere capture. Genetics *150*, 1037–1047.

Branzei, D., and Foiani, M. (2010). Maintaining genome stability at the replication fork. Nat. Rev. Mol. Cell Biol. *11*, 208–219.

Branzei, D., and Psakhye, I. (2016). DNA damage tolerance. Curr. Opin. Cell Biol. *40*, 137–144.

Branzei, D., and Szakal, B. (2016). DNA damage tolerance by recombination: Molecular pathways and DNA structures. DNA Repair (Amst). *44*, 68–75.

Branzei, D., Seki, M., and Enomoto, T. (2004). Rad18/Rad5/Mms2-mediated polyubiquitination of PCNA is implicated in replication completion during replication stress. Genes to Cells *9*, 1031–1042.

Branzei, D., Vanoli, F., and Foiani, M. (2008). SUMOylation regulates Rad18-

mediated template switch. Nature *456*, 915–920.

Brewer, B.J., and Fangman, W.L. (1987). The localization of replication origins on ARS plasmids in S. cerevisiae. Cell *51*, 463–471.

Brewer, B.J., and Fangman, W.L. (1988). A replication fork barrier at the 3' end of yeast ribosomal RNA genes. Cell *55*, 637–643.

Bridges, B.A., Munson, R.J., and Munson R. J. (1968). Mutagenesis in Escherichia coli: Evidence for the Mechanism of Base Change Mutation by Ultraviolet Radiation in a Strain Deficient in Excision-Repair. Proc. R. Soc. London. Ser. B, Biol. Sci. *171*, 213–226.

Budworth, H., and McMurray, C.T. (2013). A brief history of triplet repeat diseases. Methods Mol. Biol. *1010*, 3–17.

Bugreev, D. V., Mazina, O.M., and Mazin, A. V. (2006). Rad54 protein promotes branch migration of Holliday junctions. Nature *442*, 590–593.

Bugreev, D. V., Yu, X., Egelman, E.H., and Mazin, A. V. (2007). Novel pro- and anti-recombination activities of the Bloom's syndrome helicase. Genes Dev. *21*, 3085–3094.

Bugreev, D. V., Rossi, M.J., and Mazin, A. V. (2011). Cooperation of RAD51 and RAD54 in regression of a model replication fork. Nucleic Acids Res. *39*, 2153–2164.

Burgess, R.C., Lisby, M., Altmannova, V., Krejci, L., Sung, P., and Rothstein, R. (2009). Localization of recombination proteins and Srs2 reveals anti-recombinase function in vivo. J. Cell Biol. *185*, 969–981.

Caldecott, K.W. (2008). Single-strand break repair and genetic disease. Nat. Rev. Genet. *9*, 619–631.

Calzada, A., Hodgson, B., Kanemaki, M., Bueno, A., and Labib, K. (2005). Molecular anatomy and regulation of a stable replisome eukaryotic DNA at a

paused replication fork. Genes Dev. *19*, 1905–1919.

Carr, A.M., and Lambert, S. (2013). Replication stress-induced genome instability: The dark side of replication maintenance by homologous recombination. J. Mol. Biol. *425*, 4733–4744.

Carr, A.M., Paek, A.L., and Weinert, T. (2011). DNA replication: failures and inverted fusions. Semin. Cell Dev. Biol. *22*, 866–874.

Cayrou, C., Coulombe, P., Vigneron, A., Stanojcic, S., Ganier, O., Peiffer, I., Rivals, E., Puy, A., Laurent-Chabalier, S., Desprat, R., et al. (2011). Genome-scale analysis of metazoan replication origins reveals their organization in specific but flexible sites defined by conserved features. Genome Res. *21*, 1438–1449.

Cayrou, C., Ballester, B., Peiffer, I., Fenouil, R., Coulombe, P., Andrau, J.-C., van Helden, J., and Méchali, M. (2015). The chromatin environment shapes DNA replication origin organization and defines origin classes. Genome Res. *25*, 1873–1885.

Cejka, P., Plank, J.L., Dombrowski, C.C., and Kowalczykowski, S.C. (2012). Decatenation of DNA by the S. cerevisiae Sgs1-Top3-Rmi1 and RPA Complex: A Mechanism for Disentangling Chromosomes. Mol. Cell *47*, 886–896.

Chan, K.-L., North, P.S., and Hickson, I.D. (2007). BLM is required for faithful chromosome segregation and its localization defines a class of ultrafine anaphase bridges. EMBO J. *26*, 3397–3409.

Chan, K.L., Palmai-Pallag, T., Ying, S., and Hickson, I.D. (2009). Replication stress induces sister-chromatid bridging at fragile site loci in mitosis. Nat. Cell Biol. *11*, 753–760.

Chen, J.M., Cooper, D.N., Férec, C., Kehrer-Sawatzki, H., and Patrinos, G.P. (2010). Genomic rearrangements in inherited disease and cancer. Semin. Cancer Biol. *20*, 222–233.

Chow, K.H., and Courcelle, J. (2004). RecO Acts with RecF and RecR to Protect and Maintain Replication Forks Blocked by UV-induced DNA Damage in Escherichia coli. J. Biol. Chem. *279*, 3492–3496.

Chu, W.K., and Hickson, I.D. (2009). RecQ helicases: multifunctional genome caretakers. Nat. Rev. Cancer *9*, 644–654.

Claeys Bouuaert, C., and Chalmers, R. (2009). Transposition of the human Hsmar1 transposon: Rate-limiting steps and the importance of the flanking TA dinucleotide in second strand cleavage. Nucleic Acids Res. *38*, 190–202.

Claeys Bouuaert, C., Chalmers, R.R., Aziz, R., Breitbart, M., Edwards, R., Feschotte, C., Pritham, E., Atkinson, H., Chalmers, R.R., Bouuaert, C.C., et al. (2013). Hsmar1 Transposition Is Sensitive to the Topology of the Transposon Donor and the Target. PLoS One *8*, e53690.

Cobb, J.A., Bjergbaek, L., Shimada, K., Frei, C., and Gasser, S.M. (2003). DNA polymerase stabilization at stalled replication forks requires Mec1 and the RecQ helicase Sgs1. EMBO J. *22*, 4325–4336.

Cobb, J.A., Schleker, T., Rojas, V., Bjergbaek, L., Tercero, J.A., and Gasser, S.M. (2005). Replisome instability, fork collapse, and gross chromosomal rearrangements arise synergistically from Mec1 kinase and RecQ helicase mutations. Genes Dev. *19*, 3055–3069.

Codlin, S., and Dalgaard, J.Z. (2003). Complex mechanism of site-specific DNA replication termination in fission yeast. EMBO J. *22*, 3431–3440.

Cordaux, R., Udit, S., Batzer, M.A., and Feschotte, C. (2006). Birth of a chimeric primate gene by capture of the transposase gene from a mobile element. Proc. Natl. Acad. Sci. U. S. A. *103*, 8101–8106.

Costantino, L., Sotiriou, S.K., Rantala, J.K., Magin, S., Mladenov, E., Helleday, T., Haber, J.E., Iliakis, G., Kallioniemi, O.P., and Halazonetis, T.D. (2014). Break-

induced replication repair of damaged forks induces genomic duplications in human cells. Science *343*, 88–91.

Cotta-Ramusino, C., Fachinetti, D., Lucca, C., Doksani, Y., Lopes, M., Sogo, J., and Foiani, M. (2005). Exo1 processes stalled replication forks and counteracts fork reversal in checkpoint-defective cells. Mol. Cell *17*, 153–159.

Coulon, S., Gaillard, P.-H.L., Chahwan, C., McDonald, W.H., Yates, J.R., and Russell, P. (2004). Slx1-Slx4 are subunits of a structure-specific endonuclease that maintains ribosomal DNA in fission yeast. Mol. Biol. Cell *15*, 71–80.

Coulon, S., Noguchi, E., Noguchi, C., Du, L.-L., Nakamura, T.M., and Russell, P. (2006). Rad22Rad52-dependent repair of ribosomal DNA repeats cleaved by Slx1-Slx4 endonuclease. Mol. Biol. Cell *17*, 2081–2090.

Crasta, K., Ganem, N.J., Dagher, R., Lantermann, A.B., Ivanova, E. V., Pan, Y., Nezi, L., Protopopov, A., Chowdhury, D., and Pellman, D. (2012). DNA breaks and chromosome pulverization from errors in mitosis. Nature *482*, 53–58.

Dai, J., Chuang, R.-Y., and Kelly, T.J. (2005). DNA replication origins in the Schizosaccharomyces pombe genome. Proc. Natl. Acad. Sci. U. S. A. *102*, 337–342.

Daigaku, Y., Keszthelyi, A., Müller, C.A., Miyabe, I., Brooks, T., Retkute, R., Hubank, M., Nieduszynski, C.A., and Carr, A.M. (2015). A global profile of replicative polymerase usage. Nat. Struct. Mol. Biol. *22*, 192–198.

Dalgaard, J.Z., and Klar, A.J. (1999). Orientation of DNA replication establishes mating-type switching pattern in S. pombe. Nature *400*, 181–184.

Dalgaard, J.Z., and Klar, A.J.S. (2001). A DNA replication-arrest site RTS1 regulates imprinting by determining the direction of replication at mat1 in S. pombe. Genes Dev. *15*, 2060–2068.

Dalgaard, J.Z., and Klar, a J. (2000). swi1 and swi3 perform imprinting,

pausing, and termination of DNA replication in S. pombe. Cell *102*, 745–751.

Deem, A., Keszthelyi, A., Blackgrove, T., Vayl, A., Coffey, B., Mathur, R., Chabes, A., and Malkova, A. (2011). Break-induced replication is highly inaccurate. PLoS Biol. *9*, e1000594.

Dershowitz, A., and Newlon, C.S. (1993). The effect on chromosome stability of deleting replication origins. Mol. Cell. Biol. *13*, 391.

Deshpande, A.M., and Newlon, C.S. (1996). DNA replication fork pause sites dependent on transcription. Science *272*, 1030–1033.

Dewar, J.M., Budzowska, M., and Walter, J.C. (2015). The mechanism of DNA replication termination in vertebrates. Nature *525*, 345–350.

Diffley, J.F.X. (2004). Regulation of early events in chromosome replication. Curr. Biol. *14*, R778-86.

DiNardo, S., Voelkel, K., and Sternglanz, R. (1984). DNA topoisomerase II mutant of Saccharomyces cerevisiae: topoisomerase II is required for segregation of daughter molecules at the termination of DNA replication. Proc. Natl. Acad. Sci. U. S. A. *81*, 2616–2620.

Ding, L., and Forsburg, S.L. (2014). Essential domains of Schizosaccharomyces pombe Rad8 required for DNA damage response. G3 (Bethesda). *4*, 1373–1384.

Doe, C.L., and Whitby, M.C. (2004). The involvement of Srs2 in post-replication repair and homologous recombination in fission yeast. Nucleic Acids Res. *32*, 1480–1491.

Doe, C.L., Ahn, J.S., Dixon, J., and Whitby, M.C. (2002). Mus81-Eme1 and Rqh1 involvement in processing stalled and collapsed replication forks. J. Biol. Chem. *277*, 32753–32759.

Doe, C.L., Osman, F., Dixon, J., and Whitby, M.C. (2004). DNA repair by a

Rad22-Mus81-dependent pathway that is independent of Rhp51. Nucleic Acids Res. *32*, 5570–5581.

Donley, N., and Thayer, M.J. (2013). DNA replication timing, genome stability and cancer: late and/or delayed DNA replication timing is associated with increased genomic instability. Semin. Cancer Biol. *23*, 80–89.

Donnianni, R.A., and Symington, L.S. (2013). Break-induced replication occurs by conservative DNA synthesis. Proc. Natl. Acad. Sci. U. S. A. *110*, 13475–13480.

Dungrawala, H., and Cortez, D. (2015). Purification of proteins on newly synthesized DNA using iPOND. Methods Mol. Biol. *1228*, 123–131.

Dupaigne, P., Le Breton, C., Fabre, F., Gangloff, S., Le Cam, E., and Veaute, X. (2008). The Srs2 Helicase Activity Is Stimulated by Rad51 Filaments on dsDNA: Implications for Crossover Incidence during Mitotic Recombination. Mol. Cell *29*, 243–254.

Durkin, S.G., and Glover, T.W. (2007). mageni. Annu. Rev. Genet. *41*, 169–192.

Egel, R. (2004). DNA replication: Stalling a fork for imprinting and switching. Curr. Biol. *14*, R915-7.

Errico, A., and Costanzo, V. (2010). Differences in the DNA replication of unicellular eukaryotes and metazoans: known unknowns. EMBO Rep. *11*, 270–278.

Errico, A., and Costanzo, V. (2012). Mechanisms of replication fork protection: a safeguard for genome stability. Crit. Rev. Biochem. Mol. Biol. *47*, 222–235.

Eydmann, T., Sommariva, E., Inagawa, T., Mian, S., Klar, A.J.S., and Dalgaard, J.Z. (2008). Rtf1-mediated eukaryotic site-specific replication termination. Genetics *180*, 27–39.

Fachinetti, D., Bermejo, R., Cocito, A., Minardi, S., Katou, Y., Kanoh, Y.,

Shirahige, K., Azvolinsky, A., Zakian, V.A., and Foiani, M. (2010). Replication Termination at Eukaryotic Chromosomes Is Mediated by Top2 and Occurs at Genomic Loci Containing Pausing Elements. Mol. Cell *39*, 595–605.

Forment, J. V., Blasius, M., Guerini, I., and Jackson, S.P. (2011). Structure-specific DNA endonuclease mus81/eme1 generates DNA damage caused by chk1 inactivation. PLoS One *6*, e23517.

Fraser, H.B. (2013). Cell-cycle regulated transcription associates with DNA replication timing in yeast and human. Genome Biol. *14*, R111.

Fricke, W.M., and Brill, S.J. (2003). Slx1 - Slx4 is a second structure-specific endonuclease functionally redundant with Sgs1 - Top3. Genes Dev. *17*, 1768–1778.

Froget, B., Blaisonneau, J., Lambert, S., and Baldacci, G. (2008). Cleavage of stalled forks by fission yeast Mus81/Eme1 in absence of DNA replication checkpoint. Mol. Biol. Cell *19*, 445–456.

Fugger, K., Mistrik, M., Neelsen, K.J., Yao, Q., Zellweger, R., Kousholt, A.N., Haahr, P., Chu, W.K., Bartek, J., Lopes, M., et al. (2015). FBH1 catalyzes regression of stalled replication forks. Cell Rep. *10*, 1749–1757.

Gaillard, H., Herrera-Moyano, E., and Aguilera, A. (2013). Transcription-associated genome instability. Chem. Rev. *113*, 8638–8661.

Gaillard, H., García-Muse, T., and Aguilera, A. (2015). Replication stress and cancer. Nat. Rev. Cancer *15*, 276–289.

Ganesan, A.K. (1974). Persistence of pyrimidine dimers during post-replication repair in ultraviolet light-irradiated Escherichia coli K12. J. Mol. Biol. *87*, 103–119.

Garg, P., and Burgers, P.M. (2005). Ubiquitinated proliferating cell nuclear antigen activates translesion DNA polymerases eta and REV1. Proc. Natl. Acad. Sci. U. S. A. *102*, 18361–18366.

Gari, K., Décaillet, C., Delannoy, M., Wu, L., and Constantinou, A. (2008). Remodeling of DNA replication structures by the branch point translocase FANCM. Proc. Natl. Acad. Sci. U. S. A. *105*, 16107–16112.

Gazy, I., Liefshitz, B., Parnas, O., and Kupiec, M. (2015). Elg1, a central player in genome stability. Mutat. Res. Mutat. Res. *763*, 267–279.

Ge, X.Q., Jackson, D.A., and Blow, J.J. (2007). Dormant origins licensed by excess Mcm2-7 are required for human cells to survive replicative stress. Genes Dev. *21*, 3331–3341.

Gelot, C., Magdalou, I., and Lopez, B.S. (2015). Replication stress in mammalian cells and its consequences for mitosis. Genes (Basel). *6*, 267–298.

Gerber, J.K., Gögel, E., Berger, C., Wallisch, M., Müller, F., Grummt, I., and Grumm, F. (1997). Termination of mammalian rDNA replication: Polar arrest of replication fork movement by transcription termination factor TTF-I. Cell *90*, 559–567.

Ghamrasni, S. El, Cardoso, R., Li, L., Guturi, K.K.N., Bjerregaard, V.A., Liu, Y., Venkatesan, S., Hande, M.P., Henderson, J.T., Sanchez, O., et al. (2016). Rad54 and Mus81 cooperation promotes DNA damage repair and restrains chromosome missegregation. Oncogene *35*, 4836–4845.

Hanada, K., Budzowska, M., Davies, S.L., van Drunen, E., Onizawa, H., Beverloo, H.B., Maas, A., Essers, J., Hickson, I.D., and Kanaar, R. (2007). The structure-specific endonuclease Mus81 contributes to replication restart by generating double-strand DNA breaks. Nat. Struct. Mol. Biol. *14*, 1096–1104.

Haracska, L., Torres-Ramos, C.A., Johnson, R.E., Prakash, S., and Prakash, L. (2004). Opposing effects of ubiquitin conjugation and SUMO modification of PCNA on replicational bypass of DNA lesions in Saccharomyces cerevisiae. Mol. Cell. Biol. *24*, 4267–4274.

Haruta, N., Akamatsu, Y., Tsutsui, Y., Kurokawa, Y., Murayama, Y., Arcangioli, B., and Iwasaki, H. (2008). Fission yeast Swi5 protein, a novel DNA recombination mediator. DNA Repair (Amst). *7*, 1–9.

Hashimoto, Y., Chaudhuri, A.R., Lopes, M., and Costanzo, V. (2010). Rad51 protects nascent DNA from Mre11-dependent degradation and promotes continuous DNA synthesis. Nat. Struct. Mol. Biol. *17*, 1305–1311.

Hayano, M., Kanoh, Y., Matsumoto, S., Renard-Guillet, C., Shirahige, K., and Masai, H. (2012). Rif1 is a global regulator of timing of replication origin firing in fission yeast. Genes Dev. *26*, 137–150.

Hayashi, M., Katou, Y., Itoh, T., Tazumi, A., Tazumi, M., Yamada, Y., Takahashi, T., Nakagawa, T., Shirahige, K., and Masukata, H. (2007). Genome-wide localization of pre-RC sites and identification of replication origins in fission yeast. EMBO J. *26*, 1327–1339.

Heichinger, C., Penkett, C.J., Bähler, J., Nurse, P., Bähler, J., Schuchert, P., Grimm, C., Kohli, J., Beach, D., Nurse, P., et al. (2006). Genome-wide characterization of fission yeast DNA replication origins. EMBO J. *25*, 5171–5179.

Helmrich, A., Ballarino, M., and Tora, L. (2011). Collisions between Replication and Transcription Complexes Cause Common Fragile Site Instability at the Longest Human Genes. Mol. Cell *44*, 966–977.

Helmrich, A., Ballarino, M., Nudler, E., and Tora, L. (2013). Transcription-replication encounters, consequences and genomic instability. Nat. Struct. Mol. Biol. *20*, 412–418.

Heyer, W.-D., Ehmsen, K.T., and Liu, J. (2010). Regulation of homologous recombination in eukaryotes. Annu. Rev. Genet. *44*, 113–139.

Heyer, W.D., Li, X., Rolfsmeier, M., and Zhang, X.P. (2006). Rad54: The Swiss Army knife of homologous recombination? Nucleic Acids Res. *34*, 4115–

4125.

Hiasa, H., and Marians, K.J. (1994). Tus prevents overreplication of oriC plasmid DNA. J. Biol. Chem. *269*, 26959–26968.

Hickson, I.D. (2003). RecQ helicases: caretakers of the genome. Nat. Rev. Cancer *3*, 169–178.

Hickson, I.D. (2014). The dissolution of double Holliday junctions. Cold Spring Harb. Perspect. Biol. *6*, a016477.

Higgins, N.P., Kato, K., and Strauss, B. (1976). A model for replication repair in mammalian cells. J. Mol. Biol. *101*, 417–425.

Higuchi, K., Katayama, T., Iwai, S., Hidaka, M., Horiuchi, T., and Maki, H. (2003). Fate of DNA replication fork encountering a single DNA lesion during oriC plasmid DNA replication in vitro. Genes to Cells *8*, 437–449.

Hill, T.M., and Marians, K.J. (1990). Escherichia coli Tus protein acts to arrest the progression of DNA replication forks in vitro. Proc. Natl. Acad. Sci. U. S. A. *87*, 2481–2485.

Hirano, Y., and Sugimoto, K. (2006). ATR homolog Mec1 controls association of DNA polymerase ζ-Rev1 complex with regions near a double-strand break. Curr. Biol. *16*, 586–590.

Hoege, C., Pfander, B., Moldovan, G.-L., Pyrowolakis, G., and Jentsch, S. (2002). RAD6-dependent DNA repair is linked to modification of PCNA by ubiquitin and SUMO. Nature *419*, 135–141.

Hoffelder, D.R., Luo, L., Burke, N.A., Watkins, S.C., Gollin, S.M., and Saunders, W.S. (2004). Resolution of anaphase bridges in cancer cells. Chromosoma *112*, 389–397.

Hofmann, R.M., and Pickart, C.M. (1999). Noncanonical MMS2-encoded ubiquitin-conjugating enzyme functions in assembly of novel polyubiquitin chains

for DNA repair. Cell *96*, 645–653.

Holmes, A.M., Kaykov, A., and Arcangioli, B. (2005). Molecular and cellular dissection of mating-type switching steps in Schizosaccharomyces pombe. Mol Cell Biol *25*, 303–311.

Hsiang, Y.H., Hertzberg, R., Hecht, S., and Liu, L.F. (1985). Camptothecin induces protein-linked DNA breaks via mammalian DNA topoisomerase I. J. Biol. Chem. *260*, 14873–14878.

Hu, J., Sun, L., Shen, F., Chen, Y., Hua, Y., Liu, Y., Zhang, M., Hu, Y., Wang, Q., Xu, W., et al. (2012). The intra-S phase checkpoint targets Dna2 to prevent stalled replication forks from reversing. Cell *149*, 1221–1232.

Hu, Y., Raynard, S., Sehorn, M.G., Lu, X., Bussen, W., Zheng, L., Stark, J.M., Barnes, E.L., Chi, P., Janscak, P., et al. (2007). RECQL5/Recql5 helicase regulates homologous recombination and suppresses tumor formation via disruption of Rad51 presynaptic filaments. Genes Dev. *21*, 3073–3084.

Hyppa, R.W., and Smith, G.R. (2009). Using Schizosaccharomyces pombe Meiosis to Analyze DNA Recombination Intermediates. Meiosis, Vol 1 Mol. Genet. Methods *557*, 235–252.

Ibarra, A., Schwob, E., and Méndez, J. (2008). Excess MCM proteins protect human cells from replicative stress by licensing backup origins of replication. Proc. Natl. Acad. Sci. U. S. A. *105*, 8956–8961.

Inagawa, T., Yamada-Inagawa, T., Eydmann, T., Mian, I.S., Wang, T.S., and Dalgaard, J.Z. (2009). Schizosaccharomyces pombe Rtf2 mediates site-specific replication termination by inhibiting replication restart. Proc. Natl. Acad. Sci. U. S. A. *106*, 7927–7932.

Ira, G., and Haber, J.E. (2002). Characterization of RAD51-independent break-induced replication that acts preferentially with short homologous

sequences. Mol. Cell. Biol. *22*, 6384–6392.

Ira, G., Malkova, A., Liberi, G., Foiani, M., and Haber, J.E. (2003). Srs2 and Sgs1-Top3 Suppress Crossovers during Double-Strand Break Repair in Yeast. Cell *115*, 401–411.

Iraqui, I., Chekkal, Y., Jmari, N., Pietrobon, V., Freon, K., Costes, A., Lambert, S.A.E., Fréon, K., Costes, A., Lambert, S.A.E., et al. (2012). Recovery of Arrested Replication Forks by Homologous Recombination Is Error-Prone. Plos Genet. *8*, e1002976.

Ishimi, Y., Sugasawa, K., Hanaoka, F., Eki, T., and Hurwitz, J. (1992). Topoisomerase II plays an essential role as a swivelase in the late stage of SV40 chromosome replication in vitro. J. Biol. Chem. *267*, 462–466.

Ivessa, A.S., Zhou, J.Q., and Zakian, V.A. (2000). The Saccharomyces Pif1p DNA helicase and the highly related Rrm3p have opposite effects on replication fork progression in ribosomal DNA. Cell *100*, 479–489.

Ivessa, A.S., Zhou, J.Q., Schulz, V.P., Monson, E.K., and Zakian, V.A. (2002). Saccharomyces Rrm3p, a 5' to 3' DNA helicase that promotes replication fork progression through telomeric and subtelomeric DNA. Genes Dev. *16*, 1383–1396.

Ivessa, A.S., Lenzmeier, B.A., Bessler, J.B., Goudsouzian, L.K., Schnakenberg, S.L., and Zakian, V.A. (2003). The Saccharomyces cerevisiae Helicase Rrm3p Facilitates Replication Past Nonhistone Protein-DNA Complexes. Mol. Cell *12*, 1525–1536.

Jacome, A., and Fernandez-Capetillo, O. (2011). Lac operator repeats generate a traceable fragile site in mammalian cells. EMBO Rep. *12*, 1032–1038.

Jain, S., Sugawara, N., Lydeard, J., Vaze, M., Gac, N.T. Le, and Haber, J.E. (2009). A recombination execution checkpoint regulates the choice of homologous recombination pathway during DNA double-strand break repair. Genes Dev. *23*,

291–303.

Jasin, M., and Rothstein, R. (2013). Repair of strand breaks by homologous recombination. Cold Spring Harb. Perspect. Biol. *5*, a012740–a012740.

Jentsch, S., McGrath, J.P., and Varshavsky, A. (1987). The yeast DNA repair gene RAD6 encodes a ubiquitin-conjugating enzyme. Nature *329*, 131–134.

Jin, Y.H., Obert, R., Burgers, P.M., Kunkel, T.A., Resnick, M.A., and Gordenin, D.A. (2001). The 3'-->5' exonuclease of DNA polymerase delta can substitute for the 5' flap endonuclease Rad27/Fen1 in processing Okazaki fragments and preventing genome instability. Proc. Natl. Acad. Sci. U. S. A. *98*, 5122–5127.

Jinek, M., Chylinski, K., Fonfara, I., Hauer, M., Doudna, J.A., and Charpentier, E. (2012). A programmable dual-RNA-guided DNA endonuclease in adaptive bacterial immunity. Science *337*, 816–821.

Johnson, C., Gali, V.K., Takahashi, T.S., and Kubota, T. (2016). PCNA Retention on DNA into G2/M Phase Causes Genome Instability in Cells Lacking Elg1. Cell Rep. *16*, 684–695.

Johnson, R.E., Klassen, R., Prakash, L., and Prakash, S. (2015). A Major Role of DNA Polymerase δ in Replication of Both the Leading and Lagging DNA Strands. Mol. Cell *59*, 163–175.

Jones, R.M., and Petermann, E. (2012). Replication fork dynamics and the DNA damage response. Biochem. J. *443*, 13–26.

Kai, M., Furuya, K., Paderi, F., Carr, A.M., and Wang, T.S.F.F. (2007). Rad3-dependent phosphorylation of the checkpoint clamp regulates repair-pathway choice. Nat. Cell Biol. *9*, 691–697.

Kang, H.Y., Choi, E., Bae, S.H., Lee, K.H., Gim, B.S., Kim, H.D., Park, C., MacNeill, S.A., and Seo, Y.S. (2000). Genetic analyses of Schizosaccharomyces pombe dna2(+) reveal that dna2 plays an essential role in Okazaki fragment

metabolism. Genetics *155*, 1055–1067.

Katou, Y., Kanoh, Y., Bando, M., Noguchi, H., Tanaka, H., Ashikari, T., Sugimoto, K., and Shirahige, K. (2003). S-phase checkpoint proteins Tof1 and Mrc1 form a stable replication-pausing complex. Nature *424*, 1078–1083.

Kawabata, T., Luebben, S.W., Yamaguchi, S., Ilves, I., Matise, I., Buske, T., Botchan, M.R.P., and Shima, N. (2011). Stalled fork rescue via dormant replication origins in unchallenged S phase promotes proper chromosome segregation and tumor suppression. Mol. Cell *41*, 543–553.

Kaykov, A., and Arcangioli, B. (2004). A programmed strand-specific and modified nick in S. pombe constitutes a novel type of chromosomal imprint. Curr. Biol. *14*, 1924–1928.

Kaykov, A., and Nurse, P. (2015). The spatial and temporal organization of origin firing during the S-phase of fission yeast. Genome Res.

Keijzers, G., Liu, D., and Rasmussen, L.J. (2016). Exonuclease 1 and its versatile roles in DNA repair. Crit. Rev. Biochem. Mol. Biol. *9238*, 1–12.

Kervrann, C., and Boulanger, J. (2006). Optimal spatial adaptation for patch-based image denoising. IEEE Trans. Image Process. *15*, 2866–2878.

Keszthelyi, A., Daigaku, Y., Ptasińska, K., Miyabe, I., and Carr, A.M. (2015). Mapping ribonucleotides in genomic DNA and exploring replication dynamics by polymerase usage sequencing (Pu-seq). Nat. Protoc. *10*, 1786–1801.

Khasanov, F.K., Salakhova, A.F., Chepurnaja, O. V, Korolev, V.G., and Bashkirov, V.I. (2004). Identification and characterization of the rlp1+, the novel Rad51 paralog in the fission yeast Schizosaccharomyces pombe. DNA Repair (Amst). *3*, 1363–1374.

Khatri, G.S., MacAllister, T., Sista, P.R., and Bastia, D. (1989). The replication terminator protein of E. coli is a DNA sequence-specific contra-helicase. Cell *59*,

667–674.

Kim, S.M., and Huberman, J.A. (2001). Regulation of replication timing in fission yeast. EMBO J. *20*, 6115–6126.

Kim, W.J., Park, E.J., Lee, H., Seong, R.H., and Park, S.D. (2002). Physical interaction between recombinational proteins Rhp51 and Rad22 in Schizosaccharomyces pombe. J. Biol. Chem. *277*, 30264–30270.

Kitamura, E., Blow, J.J., and Tanaka, T.U. (2006). Live-cell imaging reveals replication of individual replicons in eukaryotic replication factories. Cell *125*, 1297–1308.

Van Komen, S., Petukhova, G., Sigurdsson, S., Stratton, S., and Sung, P. (2000). Superhelicity-Driven Homologous DNA Pairing by Yeast Recombination Factors Rad51 and Rad54. Mol. Cell *6*, 563–572.

Krejci, L., Van Komen, S., Li, Y., Villemain, J., Reddy, M.S., Klein, H., Ellenberger, T., and Sung, P. (2003). DNA helicase Srs2 disrupts the Rad51 presynaptic filament. Nature *423*, 305–309.

Krings, G., and Bastia, D. (2004). swi1- and swi3-dependent and independent replication fork arrest at the ribosomal DNA of Schizosaccharomyces pombe. Proc. Natl. Acad. Sci. USA *101*, 14085–14090.

Kubota, T., Nishimura, K., Kanemaki, M.T., and Donaldson, A.D. (2013). The Elg1 Replication Factor C-like Complex Functions in PCNA Unloading during DNA Replication. Mol. Cell *50*, 273–280.

Kubota, T., Katou, Y., Nakato, R., Shirahige, K., and Donaldson, A.D. (2015). Replication-Coupled PCNA Unloading by the Elg1 Complex Occurs Genome-wide and Requires Okazaki Fragment Ligation. Cell Rep. *12*, 774–787.

Kucherlapati, M., Yang, K., Kuraguchi, M., Zhao, J., Lia, M., Heyer, J., Kane, M.F., Fan, K., Russell, R., Brown, A.M.C., et al. (2002). Haploinsufficiency of Flap

endonuclease (Fen1) leads to rapid tumor progression. Proc. Natl. Acad. Sci. U. S. A. *99*, 9924–9929.

Kuzminov, A. (2001). Single-strand interruptions in replicating chromosomes cause double-strand breaks. Proc. Natl. Acad. Sci. U. S. A. *98*, 8241–8246.

Labib, K., and Hodgson, B. (2007). Replication fork barriers: pausing for a break or stalling for time? EMBO Rep. *8*, 346–353.

Lambert, S., and Carr, A.M. (2013). Impediments to replication fork movement: Stabilisation, reactivation and genome instability. Chromosoma *122*, 33–45.

Lambert, S., Watson, A., Sheedy, D.M., Martin, B., and Carr, A.M. (2005). Gross chromosomal rearrangements and elevated recombination at an inducible site-specific replication fork barrier. Cell *121*, 689–702.

Lambert, S., Mizuno, K., Blaisonneau, J., Martineau, S., Chanet, R., Freon, K., Murray, J.M., Carr, A.M., and Baldacci, G. (2010). Homologous Recombination Restarts Blocked Replication Forks at the Expense of Genome Rearrangements by Template Exchange. Mol. Cell *39*, 346–359.

Lang, G.I., and Murray, A.W. (2011). Mutation rates across budding yeast chromosome VI Are correlated with replication timing. Genome Biol. Evol. *3*, 799–811.

Larsen, E., Gran, C., Saether, B.E., Seeberg, E., and Klungland, A. (2003). Proliferation failure and gamma radiation sensitivity of Fen1 null mutant mice at the blastocyst stage. Mol. Cell. Biol. *23*, 5346–5353.

Larsen, N.B., Sass, E., Suski, C., Mankouri, H.W., and Hickson, I.D. (2014). The Escherichia coli Tus-Ter replication fork barrier causes site-specific DNA replication perturbation in yeast. Nat. Commun. *5*, 3574.

Lee, B.I., and Wilson, D.M. (1999). The RAD2 domain of human exonuclease 1 exhibits 5’ to 3’ exonuclease and flap structure-specific endonuclease activities.

J. Biol. Chem. *274*, 37763–37769.

Lee, K., Fu, H., Aladjem, M.I., and Myung, K. (2013). ATAD5 regulates the lifespan of DNA replication factories by modulating PCNA level on the chromatin. J. Cell Biol. *200*, 31–44.

Lee, K.-Y., Yang, K., Cohn, M.A., Sikdar, N., D'Andrea, A.D., and Myung, K. (2010). Human ELG1 regulates the level of ubiquitinated proliferating cell nuclear antigen (PCNA) through Its interactions with PCNA and USP1. J. Biol. Chem. *285*, 10362–10369.

Leman, A.R., and Noguchi, E. (2012). Local and global functions of Timeless and Tipin in replication fork protection. Cell Cycle *11*, 3945–3955.

Leonard, A.C., and Méchali, M. (2013). DNA replication origins. Cold Spring Harb. Perspect. Biol. *5*, a010116–a010116.

Li, X., and Heyer, W.-D. (2009). RAD54 controls access to the invading 3'-OH end after RAD51-mediated DNA strand invasion in homologous recombination in Saccharomyces cerevisiae. Nucleic Acids Res. *37*, 638–646.

Limbo, O., Chahwan, C., Yamada, Y., de Bruin, R.A.M., Wittenberg, C., and Russell, P. (2007). Ctp1 Is a Cell-Cycle-Regulated Protein that Functions with Mre11 Complex to Control Double-Strand Break Repair by Homologous Recombination. Mol. Cell *28*, 134–146.

Lindsay, H.D., Griffiths, D.J.F., Edwards, R.J., Christensen, P.U., Murray, J.M., Osman, F., Walworth, N., and Carr, A.M. (1998). S-phase-specific activation of Cds1 kinase defines a subpathway of the checkpoint response in Schizosaccharomyces pombe. Genes Dev. *12*, 382–395.

Lisby, M., Rothstein, R., and Mortensen, U.H. (2001). Rad52 forms DNA repair and recombination centers during S phase. Proc. Natl. Acad. Sci. U. S. A. *98*, 8276–8282.

Lisby, M., Barlow, J.H., Burgess, R.C., and Rothstein, R. (2004). Choreography of the DNA damage response: Spatiotemporal relationships among checkpoint and repair proteins. Cell *118*, 699–713.

Liu, Y., Nielsen, C.F., Yao, Q., and Hickson, I.D. (2014). The origins and processing of ultra fine anaphase DNA bridges. Curr. Opin. Genet. Dev. *26*, 1–5.

Lomonosov, M., Anand, S., Sangrithi, M., Davies, R., and Venkitaraman, A.R. (2003). Stabilization of stalled DNA replication forks by the BRCA2 breast cancer susceptibility protein. Genes Dev. *17*, 3017–3022.

Long, D.T., Räschle, M., Joukov, V., and Walter, J.C. (2011). Mechanism of RAD51-dependent DNA interstrand cross-link repair. Science *333*, 84–87.

Lopes, M., Foiani, M., and Sogo, J.M. (2006). Multiple mechanisms control chromosome integrity after replication fork uncoupling and restart at irreparable UV lesions. Mol. Cell *21*, 15–27.

Lopez Castel, A., Cleary, J.D., and Pearson, C.E. (2010). Repeat instability as the basis for human diseases and as a potential target for therapy. Nat. Rev. Mol. Cell. Biol. *11*, 165–170.

Lorenz, A., Osman, F., Folkyte, V., Sofueva, S., and Whitby, M.C. (2009). Fbh1 limits Rad51-dependent recombination at blocked replication forks. Mol. Cell. Biol. *29*, 4742–4756.

Lorenz, A., Osman, F., Sun, W., Nandi, S., Steinacher, R., and Whitby, M.C. (2012). The fission yeast FANCM ortholog directs non-crossover recombination during meiosis. Science *336*, 1585–1588.

Lucca, C., Vanoli, F., Cotta-Ramusino, C., Pellicioli, A., Liberi, G., Haber, J., and Foiani, M. (2004). Checkpoint-mediated control of replisome-fork association and signalling in response to replication pausing. Oncogene *23*, 1206–1213.

Lydeard, J.R., Jain, S., Yamaguchi, M., and Haber, J.E. (2007). Break-induced

replication and telomerase-independent telomere maintenance require Pol32. Nature *448*, 820–823.

Lydeard, J.R., Lipkin-Moore, Z., Sheu, Y.-J.J., Stillman, B., Burgers, P.M., and Haber, J.E. (2010). Break-induced replication requires all essential DNA replication factors except those specific for pre-RC assembly. Genes Dev. *24*, 1133–1144.

MacAlpine, D.M., and Bell, S.P. (2005). A genomic view of eukaryotic DNA replication. Chromosome Res. *13*, 309–326.

Maiorano, D., Lutzmann, M., and Méchali, M. (2006). MCM proteins and DNA replication. Curr. Opin. Cell Biol. *18*, 130–136.

Majka, J., and Burgers, P.M.. (2004). The PCNA–RFC Families of DNA Clamps and Clamp Loaders. Prog. Nucleic Acid Res. Mol. Biol. *78*, 227–260.

Maki, K., Inoue, T., Onaka, A., Hashizume, H., Somete, N., Kobayashi, Y., Murakami, S., Shigaki, C., Takahashi, T.S., Masukata, H., et al. (2011). Abundance of prereplicative complexes (Pre-RCs) facilitates recombinational repair under replication stress in fission yeast. J. Biol. Chem. *286*, 41701–41710.

Malkova, A., Naylor, M.L., Yamaguchi, M., Ira, G., and Haber, J.E. (2005). RAD51-dependent break-induced replication differs in kinetics and checkpoint responses from RAD51-mediated gene conversion. Mol. Cell. Biol. *25*, 933–944.

Maric, M., Maculins, T., De Piccoli, G., and Labib, K. (2014). Cdc48 and a ubiquitin ligase drive disassembly of the CMG helicase at the end of DNA replication. Science *346*, 1253596.

Martín, V., Chahwan, C., Gao, H., Blais, V., Wohlschlegel, J., Yates, J.R., McGowan, C.H., and Russell, P. (2006). Sws1 is a conserved regulator of homologous recombination in eukaryotic cells. EMBO J. *25*, 2564–2574.

Matsumoto, S., Ogino, K., Noguchi, E., Russell, P., and Masai, H. (2005).

Hsk1-Dfp1/Him1, the Cdc7-Dbf4 kinase in Schizosaccharomyces pombe, associates with Swi1, a component of the replication fork protection complex. J. Biol. Chem. *280*, 42536–42542.

Matsuo, Y., Asakawa, K., Toda, T., and Katayama, S. (2006). A rapid method for protein extraction from fission yeast. Biosci. Biotechnol. Biochem. *70*, 1992–1994.

Mayle, R., Campbell, I.M., Beck, C.R., Yu, Y., Wilson, M., Shaw, C.A., Bjergbaek, L., Lupski, J.R., and Ira, G. (2015). DNA REPAIR. Mus81 and converging forks limit the mutagenicity of replication fork breakage. Science *349*, 742–747.

Mazin, A. V, Alexeev, A.A., and Kowalczykowski, S.C. (2003). A novel function of Rad54 protein. Stabilization of the Rad51 nucleoprotein filament. J. Biol. Chem. *278*, 14029–14036.

Mazin, A. V., Bornarth, C.J., Solinger, J.A., Heyer, W.-D., and Kowalczykowski, S.C. (2000). Rad54 Protein Is Targeted to Pairing Loci by the Rad51 Nucleoprotein Filament. Mol. Cell *6*, 583–592.

Mazin, A. V., Mazina, O.M., Bugreev, D. V., and Rossi, M.J. (2010). Rad54, the motor of homologous recombination. DNA Repair (Amst). *9*, 286–302.

McGlynn, P., and Lloyd, R.G. (2002). Genome stability and the processing of damaged replication forks by RecG. Trends Genet. *18*, 413–419.

Méchali, M., Yoshida, K., Coulombe, P., and Pasero, P. (2013). Genetic and epigenetic determinants of DNA replication origins, position and activation. Curr. Opin. Genet. Dev. *23*, 124–131.

Mehta, A., and Haber, J.E. (2014). Sources of DNA Double-Strand Breaks and Models of Recombinational DNA Repair. Cold Spring Harb. Perspect. Biol. *6*, a016428–a016428.

Meister, P., Poidevin, M., Francesconi, S., Tratner, I., Zarzov, P., and Baldacci, G. (2003). Nuclear factories for signalling and repairing DNA double strand breaks in living fission yeast. Nucleic Acids Res. *31*, 5064–5073.

Michel, B., Flores, M.J., Viguera, E., Grompone, G., Seigneur, M., and Bidnenko, V. (2001). Rescue of arrested replication forks by homologous recombination. Proc. Natl. Acad. Sci. U. S. A. *98*, 8181–8188.

Mimitou, E.P., and Symington, L.S. (2008). Sae2, Exo1 and Sgs1 collaborate in DNA double-strand break processing. Nature *455*, 770-U3.

Minocherhomji, S., and Hickson, I.D. (2014). Structure-specific endonucleases: Guardians of fragile site stability. Trends Cell Biol. *24*, 321–327.

Minocherhomji, S., Ying, S., Bjerregaard, V.A., Bursomanno, S., Aleliunaite, A., Wu, W., Mankouri, H.W., Shen, H., Liu, Y., and Hickson, I.D. (2015). Replication stress activates DNA repair synthesis in mitosis. Nature *528*, 286–290.

Mirkin, S.M. (2006). DNA structures, repeat expansions and human hereditary disorders. Curr. Opin. Struct. Biol. *16*, 351–358.

Mirkin, E. V, and Mirkin, S.M. (2007). Replication fork stalling at natural impediments. Microbiol. Mol. Biol. Rev. *71*, 13–35.

Miskey, C., Papp, B., Mátés, L., Sinzelle, L., Keller, H., Izsvák, Z., and Ivics, Z. (2007). The ancient mariner sails again: transposition of the human Hsmar1 element by a reconstructed transposase and activities of the SETMAR protein on transposon ends. Mol. Cell. Biol. *27*, 4589–4600.

Miyabe, I., Kunkel, T.A., and Carr, A.M. (2011). The major roles of DNA polymerases epsilon and delta at the eukaryotic replication fork are evolutionarily conserved. PLoS Genet. *7*, e1002407.

Miyabe, I., Mizuno, K., Keszthelyi, A., Daigaku, Y., Skouteri, M., Mohebi, S., Kunkel, T.A., Murray, J.M., and Carr, A.M. (2015). Polymerase δ replicates both

strands after homologous recombination–dependent fork restart. Nat. Struct. Mol. Biol. *22*, 1–8.

Mizuno, K., Lambert, S., Baldacci, G., Murray, J.M., and Carr, A.M. (2009). Nearby inverted repeats fuse to generate acentric and dicentric palindromic chromosomes by a replication template exchange mechanism. Genes Dev. *23*, 2876–2886.

Mizuno, K.K., Miyabe, I., Schalbetter, S.A., Carr, A.M., and Murray, J.M. (2013). Recombination-restarted replication makes inverted chromosome fusions at inverted repeats. Nature *493*, 246–249.

Moreno, A., Carrington, J.T., Albergante, L., Al Mamun, M., Haagensen, E.J., Komseli, E.-S., Gorgoulis, V.G., Newman, T.J., and Blow, J.J. (2016). Unreplicated DNA remaining from unperturbed S phases passes through mitosis for resolution in daughter cells. Proc. Natl. Acad. Sci. U. S. A. *113*, E5757-64.

Moreno, S.P., Bailey, R., Campion, N., Herron, S., and Gambus, A. (2014). Polyubiquitylation drives replisome disassembly at the termination of DNA replication. Science *346*, 477–481.

Moriel-Carretero, M., and Aguilera, A. (2010). A Postincision-Deficient TFIIH Causes Replication Fork Breakage and Uncovers Alternative Rad51- or Pol32-Mediated Restart Mechanisms. Mol. Cell *37*, 690–701.

Morrow, D.M., Connelly, C., and Hieter, P. (1997). 'Break copy' duplication: A model for chromosome fragment formation in saccharomyces cerevisiae. Genetics *147*, 371–382.

Mundbjerg, K., Jørgensen, S.W., Fredsøe, J., Nielsen, I., Pedersen, J.M., Bentsen, I.B., Lisby, M., Bjergbaek, L., and Andersen, A.H. (2015). Top2 and Sgs1-Top3 Act Redundantly to Ensure rDNA Replication Termination. PLoS Genet. *11*, e1005697.

Naim, V., Wilhelm, T., Debatisse, M., and Rosselli, F. (2013). ERCC1 and MUS81-EME1 promote sister chromatid separation by processing late replication intermediates at common fragile sites during mitosis. Nat. Cell Biol. *15*, 1008–1015.

Nandi, S., and Whitby, M.C. (2012). The ATPase activity of Fml1 is essential for its roles in homologous recombination and DNA repair. Nucleic Acids Res. *40*, 9584–9595.

Neelsen, K.J., and Lopes, M. (2015). Replication fork reversal in eukaryotes: from dead end to dynamic response. Nat. Rev. Mol. Cell Biol. *16*, 207–220.

Nguyen, M.O., Jalan, M., Morrow, C.A., Osman, F., and Whitby, M.C. (2015). Recombination occurs within minutes of replication blockage by RTS1 producing restarted forks that are prone to collapse. Elife *4*, e04539.

Nieduszynski, C.A., Knox, Y., and Donaldson, A.D. (2006). Genome-wide identification of replication origins in yeast by comparative genomics. Genes Dev. *20*, 1874–1879.

Nieduszynski, C.A., Hiraga, S., Ak, P., Benham, C.J., and Donaldson, A.D. (2007). OriDB: a DNA replication origin database. Nucleic Acids Res. *35*, D40-6.

Noguchi, E., Noguchi, C., Du, L.-L., and Russell, P. (2003). Swi1 Prevents Replication Fork Collapse and Controls Checkpoint Kinase Cds1. Mol. Cell. Biol. *23*, 7861–7874.

Noguchi, E., Noguchi, C., McDonald, W.H., Yates, J.R., and Russell, P. (2004). Swi1 and Swi3 are components of a replication fork protection complex in fission yeast. Mol. Cell. Biol. *24*, 8342–8355.

Okazaki, K., Okazaki, N., Kume, K., Jinno, S., Tanaka, K., and Okayama, H. (1990). High-frequency transformation method and library transducing vectors for cloning mammalian cDNAs by trans-complementation of Schizosaccharomyces

pombe. Nucleic Acids Res *18*, 6485–6489.

Osman, F., and Whitby, M.C. (2007). Exploring the roles of Mus81-Eme1/Mms4 at perturbed replication forks. DNA Repair (Amst). *6*, 1004–1017.

Osman, F., and Whitby, M.C. (2009). Monitoring homologous recombination following replication fork perturbation in the fission yeast schizosaccharomyces pombe. Methods Mol. Biol. *521*, 535–552.

Osman, F., Adriance, M., and McCready, S. (2000). The genetic control of spontaneous and UV-induced mitotic intrachromosomal recombination in the fission yeast Schizosaccharomyces pombe. Curr. Genet. *38*, 113–125.

Osman, F., Dixon, J., Barr, A.R., and Whitby, M.C. (2005). The F-Box DNA helicase Fbh1 prevents Rhp51-dependent recombination without mediator proteins. Mol. Cell. Biol. *25*, 8084–8096.

Osman, F., Ahn, J.S., Lorenz, A., and Whitby, M.C. (2016). The RecQ DNA helicase Rqh1 constrains Exonuclease 1-dependent recombination at stalled replication forks. Sci. Rep. *6*, 22837.

Papouli, E., Chen, S., Davies, A.A., Huttner, D., Krejci, L., Sung, P., and Ulrich, H.D. (2005). Crosstalk between SUMO and ubiquitin on PCNA is mediated by recruitment of the helicase Srs2p. Mol. Cell *19*, 123–133.

Pardo, B., and Aguilera, A. (2012). Complex Chromosomal Rearrangements Mediated by Break-Induced Replication Involve Structure-Selective Endonucleases. PLoS Genet. *8*, e1002979.

Pepe, A., West, S.C.S.C.C., Bayani, J., Squire, J.A., Blasco, M.A., Lee, H.W., Hande, M.P., Samper, E., Lansdorp, P.M., DePinho, R.A., et al. (2014). MUS81-EME2 promotes replication fork restart. Cell Rep. *7*, 1048–1055.

Petukhova, G., Van Komen, S., Vergano, S., Klein, H., and Sung, P. (1999). Yeast Rad54 promotes Rad51-dependent homologous DNA pairing via ATP

hydrolysis-driven change in DNA double helix conformation. J. Biol. Chem. *274*, 29453–29462.

Pfander, B., Moldovan, G.-L., Sacher, M., Hoege, C., and Jentsch, S. (2005). SUMO-modified PCNA recruits Srs2 to prevent recombination during S phase. Nature *436*, 428–433.

Pinter, S.F., Aubert, S.D., and Zakian, V.A. (2008). The Schizosaccharomyces pombe Pfh1p DNA Helicase Is Essential for the Maintenance of Nuclear and Mitochondrial DNA. Mol. Cell. Biol. *28*, 6594–6608.

Plasterk, R.H.A., Izsvák, Z., and Ivics, Z. (1999). Resident aliens the Tc1/mariner superfamily of transposable elements. Trends Genet. *15*, 326–332.

Postow, L., Ullsperger, C., Keller, R.W., Bustamante, C., Vologodskii, A. V, and Cozzarelli, N.R. (2001). Positive torsional strain causes the formation of a four-way junction at replication forks. J. Biol. Chem. *276*, 2790–2796.

Prakash, L. (1981). Characterization of postreplication repair in Saccharomyces cerevisiae and effects of rad6, rad18, rev3 and rad52 mutations. MGG Mol. Gen. Genet. *184*, 471–478.

Prakash, R., Satory, D., Dray, E., Papusha, A., Scheller, J., Kramer, W., Krejci, L., Klein, H., Haber, J.E., Sung, P., et al. (2009). Yeast Mph1 helicase dissociates Rad51-made D-loops: implications for crossover control in mitotic recombination. Genes Dev. *23*, 67–79.

Prioleau, M.-N., and MacAlpine, D.M. (2016). DNA replication origins—where do we begin? Genes Dev. *30*, 1683–1697.

Pryce, D.W., Ramayah, S., Jaendling, A., and McFarlane, R.J. (2009). Recombination at DNA replication fork barriers is not universal and is differentially regulated by Swi1. Proc. Natl. Acad. Sci. U. S. A. *106*, 4770–4775.

Qi, Z., Redding, S., Lee, J.Y., Gibb, B., Kwon, Y., Niu, H., Gaines, W.A., Sung,

P., and Greene, E.C. (2015). DNA Sequence Alignment by Microhomology Sampling during Homologous Recombination. Cell *160*, 856–869.

Ralf, C., Hickson, I.D., and Wu, L. (2006). The Bloom's syndrome helicase can promote the regression of a model replication fork. J. Biol. Chem. *281*, 22839–22846.

Raoul Tan, T.L., Kanaar, R., and Wyman, C. (2003). Rad54, a Jack of all trades in homologous recombination. DNA Repair (Amst). *2*, 787–794.

Regairaz, M., Zhang, Y.-W., Fu, H., Agama, K.K., Tata, N., Agrawal, S., Aladjem, M.I., and Pommier, Y. (2011). Mus81-mediated DNA cleavage resolves replication forks stalled by topoisomerase I-DNA complexes. J. Cell Biol. *195*, 739–749.

Renodon-Cornière, A., Weigel, P., Breton, M. Le, and Fleury, F. (2013). New Potential Therapeutic Approaches by Targeting Rad51-Dependent Homologous Recombination. In Chen, C., (Ed.), New Research Directions in DNA Repair, Chapter 17, (InTech), pp. 467–488.

Reyes-Lamothe, R., Possoz, C., Danilova, O., and Sherratt, D.J. (2008). Independent positioning and action of Escherichia coli replisomes in live cells. Cell *133*, 90–102.

Robertson, H.M., and Zumpano, K.L. (1997). Molecular evolution of an ancient mariner transposon, Hsmar1, in the human genome. Gene *205*.

Roseaulin, L., Yamada, Y., Tsutsui, Y., Russell, P., Iwasaki, H., Arcangioli, B., Abraham, J., Lemmers, B., Hande, M., Moynahan, M., et al. (2008). Mus81 is essential for sister chromatid recombination at broken replication forks. Embo J. *27*, 1378–1387.

Rothstein, R., Michel, B., and Gangloff, S. (2000). Replication fork pausing and recombination or 'gimme a break'. Genes Dev. *14*, 1–10.

Rupp, W.D., and Howard-Flanders, P. (1968). Discontinuities in the DNA synthesized in an excision-defective strain of Escherichia coli following ultraviolet irradiation. J. Mol. Biol. *31*, 291–304.

Sabatinos, S.A., and Forsburg, S.L. (2010). Molecular Genetics of Schizosaccharomyces Pombe. Methods Enzymol. Vol 470 Guid. to Yeast Genet. *470*, 759–795.

Sabouri, N., McDonald, K.R., Webb, C.J., Cristea, I.M., and Zakian, V.A. (2012). DNA replication through hard-to-replicate sites, including both highly transcribed RNA Pol II and Pol III genes, requires the S. pombe Pfh1 helicase. Genes Dev. *26*, 581–593.

Saini, N., Ramakrishnan, S., Elango, R., Ayyar, S., Zhang, Y., Deem, A., Ira, G., Haber, J.E., Lobachev, K.S., and Malkova, A. (2013). Migrating bubble during break-induced replication drives conservative DNA synthesis. Nature *502*, 389–392.

Sale, J.E. (2015). REV7/MAD2L2: the multitasking maestro emerges as a barrier to recombination. EMBO J. *34*, 1609–1611.

Sambrook, J., Fritsch, E.F., and Maniatis., T. (1989). Molecular Cloning: A Laboratory Manual (CSHL Press).

Sánchez-Gorostiaga, A., López-Estraño, C., Krimer, D.B., Schvartzman, J.B., and Hernández, P. (2004). Transcription termination factor reb1p causes two replication fork barriers at its cognate sites in fission yeast ribosomal DNA in vivo. Mol. Cell. Biol. *24*, 398–406.

Sandell, L.L., Zakian, V.A.A., Biessmann, H., Mason, J.M., Biessmann, H., Carter, S.B., Mason, J.M., Conrad, M.N., Wright, J.H., Wolf, A.J., et al. (1993). Loss of a yeast telomere: arrest, recovery, and chromosome loss. Cell *75*, 729–739.

Schlacher, K., Christ, N., Siaud, N., Egashira, A., Wu, H., and Jasin, M. (2011). Double-strand break repair-independent role for BRCA2 in blocking stalled replication fork degradation by MRE11. Cell *145*, 529–542.

Schmidt, K.H., Derry, K.L., and Kolodner, R.D. (2002). Saccharomyces cerevisiae RRM3, a 5' to 3' DNA helicase, physically interacts with proliferating cell nuclear antigen. J. Biol. Chem. *277*, 45331–45337.

Segurado, M. (2003). Genome-wide distribution of DNA replication origins at A T-rich\n\t\tislands in Schizosaccharomyces pombe. EMBO Rep. *4*, 1048–1053.

Sharma, S., Sommers, J.A., Choudhary, S., Faulkner, J.K., Cui, S., Andreoli, L., Muzzolini, L., Vindigni, A., and Brosh, R.M. (2005). Biochemical analysis of the DNA unwinding and strand annealing activities catalyzed by human RECQ1. J. Biol. Chem. *280*, 28072–28084.

Shiomi, Y., and Nishitani, H. (2013). Alternative replication factor C protein, Elg1, maintains chromosome stability by regulating PCNA levels on chromatin. Genes Cells *18*, 946–959.

Simandlova, J., Zagelbaum, J., Payne, M.J., Chu, W.K., Shevelev, I., Hanada, K., Chatterjee, S., Reid, D.A., Liu, Y., Janscak, P., et al. (2013). FBH1 helicase disrupts RAD51 filaments in vitro and modulates homologous recombination in mammalian cells. J. Biol. Chem. *288*, 34168–34180.

Singh, S.K., Sabatinos, S., Forsburg, S., and Bastia, D. (2010). Regulation of Replication Termination by Reb1 Protein-Mediated Action at a Distance. Cell *142*, 868–878.

Sirbu, B.M., Couch, F.B., and Cortez, D. (2012). Monitoring the spatiotemporal dynamics of proteins at replication forks and in assembled chromatin using isolation of proteins on nascent DNA. Nat. Protoc. *7*, 594–605.

Skipper, K.A., Andersen, P.R., Sharma, N., and Mikkelsen, J.G. (2013). DNA

transposon-based gene vehicles - scenes from an evolutionary drive. J. Biomed. Sci. *20*, 92.

Smith, O.K., and Aladjem, M.I. (2014). Chromatin structure and replication origins: Determinants of chromosome replication and nuclear organization. J. Mol. Biol. *426*, 3330–3341.

Smith, C.E., Llorente, B., and Symington, L.S. (2007). Template switching during break-induced replication. Nature *447*, 102–105.

Sofueva, S., Osman, F., Lorenz, A., Steinacher, R., Castagnetti, S., Ledesma, J., and Whitby, M.C. (2011). Ultrafine anaphase bridges, broken DNA and illegitimate recombination induced by a replication fork barrier. Nucleic Acids Res. *39*, 6568–6584.

Sogo, J.M., Lopes, M., and Foiani, M. (2002). Fork Reversal and ssDNA Accumulation at Stalled Replication Forks Owing to Checkpoint Defects. Sci. *297*, 599–602.

Solinger, J.A., Kiianitsa, K., and Heyer, W.-D. (2002). Rad54, a Swi2/Snf2-like Recombinational Repair Protein, Disassembles Rad51:dsDNA Filaments. Mol. Cell *10*, 1175–1188.

Sommariva, E., Pellny, T.K., Karahan, N., Kumar, S., Huberman, J.A., and Dalgaard, J.Z. (2005). Schizosaccharomyces pombe Swi1, Swi3, and Hsk1 are components of a novel S-phase response pathway to alkylation damage. Mol. Cell. Biol. *25*, 2770–2784.

Song, B.W., and Sung, P. (2000). Functional interactions among yeast Rad51 recombinase, Rad52 mediator, and replication protein A in DNA strand exchange. J. Biol. Chem. *275*, 15895–15904.

Stafa, A., Donnianni, R.A., Timashev, L.A., Lam, A.F., and Symington, L.S. (2014). Template switching during break-induced replication is promoted by the

mph1 helicase in Saccharomyces cerevisiae. Genetics *196*, 1017–1028.

Stamatoyannopoulos, J.A., Adzhubei, I., Thurman, R.E., Kryukov, G. V, Mirkin, S.M., and Sunyaev, S.R. (2009). Human mutation rate associated with DNA replication timing. Nat. Genet. *41*, 393–395.

Steinacher, R., Osman, F., Dalgaard, J.Z., Lorenz, A., and Whitby, M.C. (2012). The DNA helicase Pfh1 promotes fork merging at replication termination sites to ensure genome stability. Genes Dev. *26*, 594–602.

Stelter, P., and Ulrich, H.D. (2003). Control of spontaneous and damage-induced mutagenesis by SUMO and ubiquitin conjugation. Nature *425*, 188–191.

Stephens, P.J., Greenman, C.D., Fu, B., Yang, F., Bignell, G.R., Mudie, L.J., Pleasance, E.D., Lau, K.W., Beare, D., Stebbings, L.A., et al. (2011). Massive genomic rearrangement acquired in a single catastrophic event during cancer development. Cell *144*, 27–40.

Stewart, J.A., Miller, A.S., Campbell, J.L., and Bambara, R.A. (2008). Dynamic removal of replication protein A by Dna2 facilitates primer cleavage during Okazaki fragment processing in Saccharomyces cerevisiae. J. Biol. Chem. *283*, 31356–31365.

Stewart, J.A., Campbell, J.L., and Bambara, R.A. (2009). Significance of the dissociation of Dna2 by flap endonuclease 1 to Okazaki fragment processing in Saccharomyces cerevisiae. J. Biol. Chem. *284*, 8283–8291.

Stith, C.M., Sterling, J., Resnick, M.A., Gordenin, D.A., and Burgers, P.M. (2008). Flexibility of eukaryotic Okazaki fragment maturation through regulated strand displacement synthesis. J. Biol. Chem. *283*, 34129–34140.

Stodola, J.L., and Burgers, P.M. (2016). Resolving individual steps of Okazaki-fragment maturation at a millisecond timescale. Nat. Struct. Mol. Biol. *23*, 402–408.

Sugiyama, T., and Kowalczykowski, S.C. (2002). Rad52 protein associates with replication protein A (RPA)-single-stranded DNA to accelerate Rad51-mediated displacement of RPA and presynaptic complex formation. J. Biol. Chem. *277*, 31663–31672.

Sun, W., Nandi, S., Osman, F., Ahn, J.S., Jakovleska, J., Lorenz, A., and Whitby, M.C. (2008). The FANCM Ortholog Fml1 Promotes Recombination at Stalled Replication Forks and Limits Crossing Over during DNA Double-Strand Break Repair. Mol. Cell *32*, 118–128.

Sung, P. (1997). Yeast Rad55 and Rad57 proteins form a heterodimer that functions with replication protein A to promote DNA strand exchange by Rad51 recombinase. Genes Dev. *11*, 1111–1121.

Sung, P., Petukhova, G., and Stratton, S. (1998). Catalysis of homologous DNA pairing by yeast Rad51 and Rad54 proteins. Nature *393*, 91–94.

Sung, P., Krejci, L., Van Komen, S., and Sehorn, M.G. (2003). Rad51 Recombinase and Recombination Mediators. J. Biol. Chem. *278*, 42729–42732.

Szostak, J.W., Orr-Weaver, T.L., Rothstein, R.J., and Stahl, F.W. (1983). The double-strand-break repair model for recombination. Cell *33*, 25–35.

Tercero, J.A., Longhese, M.P., and Diffley, J.F.X. (2003). A central role for DNA replication forks in checkpoint activation and response. Mol. Cell *11*, 1323–1336.

Thomä, N.H., Czyzewski, B.K., Alexeev, A.A., Mazin, A. V, Kowalczykowski, S.C., and Pavletich, N.P. (2005). Structure of the SWI2/SNF2 chromatin-remodeling domain of eukaryotic Rad54. Nat. Struct. Mol. Biol. *12*, 350–356.

Tishkoff, D.X., Boerger, A.L., Bertrand, P., Filosi, N., Gaida, G.M., Kane, M.F., and Kolodner, R.D. (1997). Identification and characterization of Saccharomyces cerevisiae EXO1, a gene encoding an exonuclease that interacts with MSH2.

Proc. Natl. Acad. Sci. U. S. A. *94*, 7487–7492.

Torres, J.Z., Bessler, J.B., and Zakian, V.A. (2004). Local chromatin structure at the ribosomal DNA causes replication fork pausing and genome instability in the absence of the S. cerevisiae DNA helicase Rrm3p. Genes Dev. *18*, 498–503.

Torres-Ramos, C.A., Prakash, S., and Prakash, L. (2002). Requirement fo RAD5 and MMS2 for Postreplication Repair of UV-Damaged DNA in Saccharomyces cerevisiae. Mol. Cell. Biol. *22*, 2419–2426.

Trujillo, K.M., and Sung, P. (2001). DNA Structure-specific Nuclease Activities in the Saccharomyces cerevisiae Rad50-Mre11 Complex. J. Biol. Chem. *276*, 35458–35464.

Trujillo, K.M., Roh, D.H., Chen, L., Van Komen, S., Tomkinson, A., and Sung, P. (2003). Yeast xrs2 binds DNA and helps target rad50 and mre11 to DNA ends. J. Biol. Chem. *278*, 48957–48964.

Tsang, E., Miyabe, I., Iraqui, I., Zheng, J., Lambert, S.A.E., and Carr, A.M. (2014). The extent of error-prone replication restart by homologous recombination is controlled by Exo1 and checkpoint proteins. J. Cell Sci. *127*, 2983–2994.

Ulrich, H.D., Jentsch, S., Bailly, V., Lamb, J., Sung, P., Prakash, S., Prakash, L., Bailly, V., Lauder, S., Prakash, S., et al. (2000). Two RING finger proteins mediate cooperation between ubiquitin-conjugating enzymes in DNA repair. EMBO J. *19*, 3388–3397.

Veaute, X., Jeusset, J., Soustelle, C., Kowalczykowski, S.C., Le Cam, E., and Fabre, F. (2003). The Srs2 helicase prevents recombination by disrupting Rad51 nucleoprotein filaments. Nature *423*, 309–312.

Vengrova, S., and Dalgaard, J.Z. (2006). The wild-type Schizosaccharomyces pombe mat1 imprint consists of two ribonucleotides. EMBO Rep. *7*, 59–65.

Vujcic, M., Miller, C.A., and Kowalski, D. (1999). Activation of silent replication

origins at autonomously replicating sequence elements near the HML locus in budding yeast. Mol. Cell. Biol. *19*, 6098–6109.

West, S.C., Blanco, M.G., Chan, Y.W., Matos, J., Sarbajna, S., and Wyatt, H.D.M. (2016). Resolution of recombination intermediates: Mechanisms and regulation. Cold Spring Harb. Symp. Quant. Biol. *80*, 103–109.

Whitby, M.C. (2010). The FANCM family of DNA helicases/translocases. DNA Repair (Amst). *9*, 224–236.

Willis, N. a, Chandramouly, G., Huang, B., Kwok, A., Follonier, C., Deng, C., and Scully, R. (2014). BRCA1 controls homologous recombination at Tus/Ter-stalled mammalian replication forks. Nature *510*, 556–559.

Wilson, M.A., Kwon, Y., Xu, Y., Chung, W.H., Chi, P., Niu, H., Mayle, R., Chen, X., Malkova, A., Sung, P., et al. (2013). Pif1 helicase and Poldelta promote recombination-coupled DNA synthesis via bubble migration. Nature *502*, 393–396.

Woodward, A.M., Göhler, T., Luciani, M.G., Oehlmann, M., Ge, X., Gartner, A., Jackson, D.A., and Blow, J.J. (2006). Excess Mcm2-7 license dormant origins of replication that can be used under conditions of replicative stress. J. Cell Biol. *173*, 673–683.

Wu, L., and Hickson, I.D. (2003). The Bloom's syndrome helicase suppresses crossing over during homologous recombination. Nature *426*, 870–874.

Wyatt, H.D.M., and West, S.C. (2014). Holliday junction resolvases. Cold Spring Harb. Perspect. Biol. *6*, a023192–a023192.

Wyatt, M.D., and Pittman, D.L. (2006). Methylating agents and DNA repair responses: Methylated bases and sources of strand breaks. Chem. Res. Toxicol. *19*, 1580–1594.

Xu, G., Chapman, J.R., Brandsma, I., Yuan, J., Mistrik, M., Bouwman, P., Bartkova, J., Gogola, E., Warmerdam, D., Barazas, M., et al. (2015). REV7

counteracts DNA double-strand break resection and affects PARP inhibition. Nature *521*, 541–544.

Yang, W., and Woodgate, R. (2007). What a difference a decade makes: insights into translesion DNA synthesis. Proc. Natl. Acad. Sci. U. S. A. *104*, 15591–15598.

Yeeles, J.T.P., and Marians, K.J. (2011). The Escherichia coli Replisome Is Inherently DNA Damage Tolerant. Science *334*, 235–239.

Yeeles, J.T.P., Deegan, T.D., Janska, A., Early, A., and Diffley, J.F.X. (2015). Regulated eukaryotic DNA replication origin firing with purified proteins. Nature *519*, 431–435.

Ying, S., Minocherhomji, S., Chan, K.L., Palmai-Pallag, T., Chu, W.K., Wass, T., Mankouri, H.W., Liu, Y., and Hickson, I.D. (2013). MUS81 promotes common fragile site expression. Nat. Cell Biol. *15*, 1001–1007.

Yu, C., Gan, H., Han, J., Zhou, Z.X., Jia, S., Chabes, A., Farrugia, G., Ordog, T., and Zhang, Z. (2015). Strand-Specific Analysis Shows Protein Binding at Replication Forks and PCNA Unloading from Lagging Strands when Forks Stall. Mol. Cell *33*, 395–401.

Zellweger, R., Dalcher, D., Mutreja, K., Berti, M., Schmid, J.A., Herrador, R., Vindigni, A., and Lopes, M. (2015). Rad51-mediated replication fork reversal is a global response to genotoxic treatments in human cells. J. Cell Biol. *208*, 563–579.

Zhang, C.-Z., Spektor, A., Cornils, H., Francis, J.M., Jackson, E.K., Liu, S., Meyerson, M., and Pellman, D. (2015). Chromothripsis from DNA damage in micronuclei. Nature *522*, 179–184.

Zheng, L., and Shen, B. (2011). Okazaki fragment maturation: nucleases take centre stage. J. Mol. Cell Biol. *3*, 23–30.

Zheng, L., Dai, H., Qiu, J., Huang, Q., and Shen, B. (2007). Disruption of the FEN-1/PCNA interaction results in DNA replication defects, pulmonary hypoplasia, pancytopenia, and newborn lethality in mice. Mol. Cell. Biol. *27*, 3176–3186.

Zheng, X.F., Prakash, R., Saro, D., Longerich, S., Niu, H., and Sung, P. (2011). Processing of DNA structures via DNA unwinding and branch migration by the S. cerevisiae Mph1 protein. DNA Repair (Amst). *10*, 1034–1043.

Zhu, Z., Chung, W.H., Shim, E.Y., Lee, S.E., and Ira, G. (2008). Sgs1 helicase and two nucleases Dna2 and Exo1 resect DNA double-strand break ends. Cell *134*, 981–994.